ILMATIETEEN LAITOS
METEOROLOGISKA INSTITUTET
FINNISH METEOROLOGICAL INSTITUTE

119
CONTRIBUTIONS

MODELLING RADIATIVE AND CLIMATE EFFECTS OF AEROSOLS: FROM ANTHROPOGENIC EMISSIONS TO GEOENGINEERING

ANTON LAAKSO

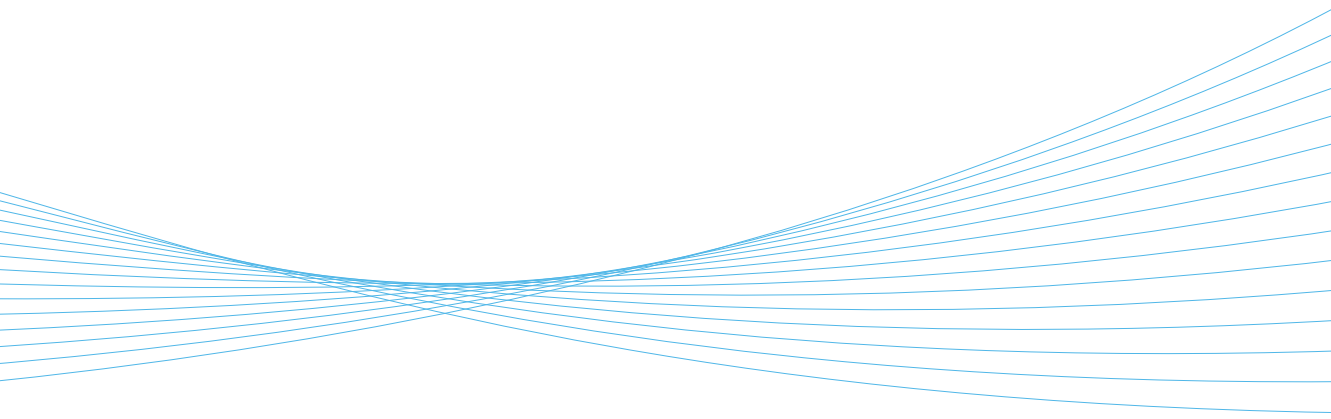

FINNISH METEOROLOGICAL INSTITUTE
CONTRIBUTIONS

No. 119

MODELLING RADIATIVE AND CLIMATE EFFECTS OF AEROSOLS: FROM ANTHROPOGENIC EMISSIONS TO GEOENGINEERING

Anton Laakso

Finnish Meteorological Institute
Kuopio, Finland

Doctoral dissertation

To be presented, with the permission of the Faculty of Science and Forestry of the University of Eastern Finland for public examination in Auditorium SN201, Snellmania building, University of Eastern Finland, on April 9th, 2016, at 12 o clock noon.

Finnish Meteorological Institute

Kuopio, 2016

Author s address: Finnish Meteorological Institute
Atmospheric Research Centre of Eastern Finland
P.O. Box 1627
70211, Kuopio, Finland
anton.laakso@fmi.

Supervisors: Research Professor Hannele Korhonen, Ph.D.
Climate Research
Finnish Meteorological Institute, Helsinki, Finland

Docent Harri Kokkola, Ph.D.
Atmospheric Research Centre of Eastern Finland
Finnish Meteorological Institute, Kuopio, Finland

Professor Kari Lehtinen, Ph.D.
Department of Applied Physics
University of Eastern Finland, Kuopio, Finland

Preliminary examiners: Researcher Risto Makkonen, Ph.D.
Department of Physics
University of Helsinki, Helsinki, Finland

Researcher Helene Muri, Ph.D.
Department of Geosciences
University of Oslo, Oslo, Norway

Opponent: Associate Professor Ilona Riipinen, Ph.D.
Department of Environmental Science
and Analytical Chemistry
Stockholm University, Stockholm, Sweden

Custos: Research Professor Hannele Korhonen, Ph.D.
Climate Research
Finnish Meteorological Institute, Helsinki, Finland

ISBN 978-951-697-870-6 (paperback)
ISSN 0782-6117
Erweko Oy
Helsinki 2016

ISBN 978-951-697-871-3 (pdf)
UEF Electronic Publications
http://epublications.uef. /
Kuopio 2016

FINNISH METEOROLOGICAL INSTITUTE

Published by
Finnish Meteorological Institute
(Erik Palménin aukio 1) , P.O. Box 503
FIN-00101 Helsinki, Finland

Series title, number and report code of publication
Finnish Meteorological Institute
Contributions No. 119, FMI-CONT-119

Date
April 2016

Author
Anton Laakso

Title
Modelling radiative and climate effects of aerosols: from Anthropogenic emissions to geoengineering

Abstract

Atmospheric aerosols have been shown to exert a cooling effect on climate by scattering incoming solar radiation back to space or increasing cloud albedo by increasing the cloud droplet number concentration in the clouds. If greenhouse gas emissions cannot be reduced to slow down climate warming, it has been postulated that climate could be artificially cooled by increasing atmospheric aerosol concentrations. These methods are called solar radiation management or geoengineering. This work evaluated two potential solar radiation management techniques; 1) where marine aerosol concentrations would be elevated to enhance marine cloud albedo and 2) a technique where stratospheric sulphur concentration would be increased. The key objectives of this thesis were to: 1) Investigate the potential of aerosols to cool the climate at the global scale, 2) Evaluate the role of the simulation of the aerosol microphysics in the global climate models and 3) Identify the possible limits in the effectiveness of the Solar Radiation Management techniques as well as the risks related to these techniques. Climate is already being affected by our current aerosols emissions. This work also examined how the geographical change in aerosol emissions has affected the climate and evaluated how the climate would change due to aerosols if all electrical energy were to be generated by nuclear power is instead of by coal combustion.

The global aerosol-climate model ECHAM-HAMMOZ was used to study radiation and the climatic effects of aerosols. The model simulates the formation, growth, transportation and deposition of aerosols and their interactions with clouds. In addition, the effects on the climate, assessed as temperature changes, were studied using a mixed layer ocean model coupled to the atmospheric model ECHAM and Max Planck Institute's Earth System Model (MPI-ESM).

The results revealed that the geoengineering techniques which were studied in this work, have the potential to significantly cool climate and thus slow down global warming. However, the cooling effect has limitations. Stratospheric sulphur injections would lead to relatively less cooling, should the amount of injected sulphur need to be increased. Thus for example, a large volcanic eruption would also lead to a clearly smaller and shorter period cooling if the volcano were to erupt during the stratospheric sulphur injections than if the eruption took place in an unperturbed atmosphere. This work also studied if ship or air traffic were to be used for geoengineering by increasing sulphur concentration in fuel. This would lead to a significant cooling effect but would require changes in current legislation. Even if this were to occur, the cooling effect would be concentrated around the vicinity of routes of the traffic and would thus lead to a regionally uneven cooling effect. Furthermore, the cooling effect would be clearly smaller compared to injection strategies which were intended to maximize the cooling effect of aerosols. The global mean cooling effect attributable to aerosols would be rather small due to the geographical change in tropospheric aerosol emissions or change in energy production studied here when compared to the warming due to the increased greenhouse gas emissions.

This work shows the necessity of including aerosol microphysics into climate modelling since most of the conclusions in this work could not be obtained without aerosol microphysics or taking into account the interactions between clouds and aerosols. Thus, micrometer scale physical phenomena would influence the climatic impact on a global scale. Simulating aerosol microphysics led also to many unpredictable results.

Publishing unit
Atmospheric Research Centre of Eastern Finland

Classification (UDC)
551.58

Keywords
Geoengineering, aerosol radiative effects, global climate modelling

ISSN and series title
0782-6117 Finnish Meteorological Insitute Contributions

ISBN
978-951-697-870-6 (paperback), 978-951-697-871-3 (pdf)

Language
English

Pages
153

ILMATIETEEN LAITOS

Julkaisun sarja, numero ja raporttikoodi
Finnish Meteorological Institute
Contributions No. 119, FMI-CONT-119

Julkaisija Ilmatieteen laitos, (Erik Palménin aukio 1)
PL 503, 00101 Helsinki

Tekijä Anton Laakso

Julkaisuaika
Huhtikuu 2016

Nimeke

Aerosolien säteily- ja ilmastovaikutusten mallintaminen: Antropogeenisista emissioista ilmastonmuokkaukseen

Tiivistelmä

Ilmakehässä olevien aerosolien on osoitettu viilentävän ilmastoa sirottamalla maahan tulevaa auringon säteilyä takaisin avaruuteen tai epäsuorasti tekemällä pilvistä heijastavampia kasvattamalla niiden pilvipisaroiden lukumäärää. Jos kasvihuonekaasupäästöjä ei saada vähennettyä ja ilmaston lämpenemistä siten pysäytettyä, on ehdotettu, että ilmastoa voitaisiin viilentää keinotekoisesti lisäämällä ilmakehän aerosolien määrää kontrolloidusti. Näitä menetelmiä kutsutaan ilmastonmuokkaukseksi. Tässä työssä tarkastellaan kahta potentiaalista ilmastonmuokkausmenetelmää, merellisiä aerosoli-injektioita pilvien heijastavuuden lisäämiseksi sekä rikki-injektioita stratosfääriin. Työn tavoitteena oli selvittää: 1) aerosolien potentiaalia viilentää ilmastoa globaalisti, 2) aerosolien mikrofysiikan roolia globaaleissa ilmastomalleissa sekä 3) tunnistaa auringon valon heijastamiseen perustuvien ilmastonmuokkaustekniikoiden mahdollisia rajoitteita ja riskejä. Myös ihmiskunnan nykyiset aerosolipäästöt ovat vaikuttavat ilmastoon. Siten tässä työssä tarkasteltiin myös kuinka aerosolipäästöjen alueellisessa jakaumassa viime vuosikymmeninä tapahtuneet muutokset ovat muuttaneet ilmaston lämpötilaa, sekä miten muutokset energian tuotannossa ydinvoiman ja hiilienergian välillä vaikuttaisivat ilmastoon.

Tässä työssä on käytetty globaalia aerosoli-ilmastomallia, ECHAM-HAMMOZ:a, aerosolien säteily ja ilmastovaikutuksien tutkimiseen. Mallilla voidaan kuvata ilmakehään tuotettujen aerosolihiukkasten koko elinkaari; niiden muodostuminen, kasvu, kulkeutuminen ja poistuminen sekä vuorovaikutukset pilvien kanssa. Tämän lisäksi aerosolien vaikutuksia ilmaston lämpötilaan on tarkasteltu kytkemällä ECHAM ilmastomalli sekoituskerrosmerimalliin, sekä käyttämällä maasysteemimallia MPI-ESM.

Tulokset osoittavat, että tässä työssä tutkituilla ilmastonmuokkausmenetelmillä on mahdollista viilentää merkittävästi ilmastoa ja siten aerosoleilla on potentiaalia hidastaa ilmastonlämpenemistä. Kuitenkin menetelmien viilennysvaikutukset ovat rajallisia. Stratosfäärin injektoitujen hiukkasten kyky viilentää ilmastoa heikkenee suhteellisesti kun injektoitavan rikin määrää kasvatetaan. Tästä syystä myös suurista tulivuorenpurkauksista seuranneet viilenemisjaksot ovat vähemmän viileämpiä ja lyhytkestoisempia jos stratosfäärin hiukkaspitoisuutta on purkauksen sattuessa kasvatettu ilmastonmuokkaustarkoituksessa. Lisäksi työ osoitti, että muutokset aerosolipäästöissä viimeisenä kahtena vuosikymmenenä ovat vaikuttaneet vain vähän ilmaston lämpötilaan. Energia tuotannon siirtyminen ydinvoimasta hiilienergiaan johtaisi taas ilmanlaadun huononemiseen ja kuolleisuuden kasvuun. Tämän lisäksi työssä tarkasteltiin laiva ja lentoliikenteen hyödyntämistä ilmastonmuokkauksessa kasvattamalla polttoaineiden rikkipitoisuutta. Kuitenkin viilennysvaikutus keskittyisi tällöin liikennereittien läheisyyteen ja johtaisi siten epätasaisesti jakautuneeseen viilennysvaikutukseen maapallolla. Päästöjen lisäys olisi lisäksi kansainvälisten sopimusten vastaista sekä johtaisi selvästi heikompaan viilennykseen verrattuna aerosolien injektointistrategioihin, joilla pyritään saamaan maksimi viilennysvaikutus.

Työ osoitti aerosolien mikrofysiikan mallintamisen merkityksen myös käytettäessä globaaleja ilmastomalleja. Mitään tämän työn johtopäätöksistä ei olisi voinut tehdä ellei aerosolien mikrofysiikkaa tai vuorovaikutuksia pilvien ei olisi otettu huomioon. Siten globaalin mittakaavan ilmastovaikutukset ovat riippuvaisia mikrometrin skaalalla tapahtuvista fysiikan ilmiöistä. Aerosolien simuloiminen johti myös moniin ennalta arvaamattomiin tuloksiin.

Julkaisijayksikkö
Itä-Suomen ilmatieteellinen tutkimuskeskus

Luokitus (UDK)
551.58

Asiasanat
Ilmastonmuokkaus, aerosolien säteilyvaikutukset, globaali ilmastonmallinnus

ISSN ja avainnimike
0782-6117 Finnish Meteorological Institute Contributions

ISBN
978-951-697-870-6 (nidottu), 978-951-697-871-3 (pdf)

Kieli
Englanti

Sivumäärä
153

Acknowledgements

The research presented in this thesis was conducted in the Atmospheric Research Centre of Eastern Finland of the Finnish Meteorological Institute. I am very grateful to Prof. Kari Lehtinen and Doc. Sami Romakkaniemi for the opportunity to work in the greatest unit in the world and the possibility to tackle this challenge, which I have really enjoyed (with the exception of some speci c moments with tuning, noticing bug in the model after the seventh resimulations or when adding space between word and *-mark when performing rm- command in the model output-folder). I also want to thank my supervisors Prof. Hannele Korhonen and Doc. Harri Kokkola for their exceptional commitment to providing guidance and warm support throughout these years. I also appreciate the fact that you had trust in me and allowed me to make my own mistakes (and learn from them) which may have also made possible my few own successes. I also thank Dr. Risto Makkonen and Dr. Helene Muri for reviewing this thesis and Dr. Ewen MacDonald for revision in English. I would also like to thank all of the people who have participated in writing papers included in this work.

There are many other people who have helped and supported me in this work. I want thank my o cemate Dr. Tommi Bergman. Without your (instantly received) help with the model and support I would not be here, or would be much later, and thank you also for conversations about many topics other than work. Thank you also to Dr. Antti-Ilari Partanen. These years would have been much more di cult if I could not share all the joy and sorrow related to geoengineering and modelling with you. Thank you, Dr. Tero Mielonen, for the time both in work and outside of o ce. I also want to give special thanks for rest of our group, Dr. Eimear Dunne, Dr. Thomas Kuhn and Dr. Juha Tonttila and the whole unit in Kuopio. It has been really nice to work with all of you!

I would also like to thank all of my friends and relatives, especially Miika Talvasto for the support when most needed. The warmest and deepest thanks have to go to the most loving and caring person, my soon-to-be wife Hanne. Your love and support has been invaluable. Because of you, I have been the happiest man in the world even during all the frustration and pain this work has caused at times.

Kuopio, March 2016

Anton Laakso

Contents

List of publications

Paper I: T. Kuhn, A.-I. Partanen, A. Laakso, Z. Lu, T. Bergman, S. Mikkonen, H. Kokkola, H. Korhonen, P. Raisanen, D. G. Streets, S. Romakkaniemi, and A. Laaksonen Climate impacts of changing aerosol emissions since 1996. *Geophys. Res. Lett. 41*, 13, 4711-4718, doi:10.1002/2014GL060349, 2014.

Paper II: T. Mielonen, A. Laakso, A. Karhunen, H. Kokkola, A.-I. Partanen, H. Korhonen, S. Romakkaniemi and K. E.J. Lehtinen From nuclear power to coal power: Aerosol-induced health and radiative e ects *J. Geophys. Res. Atmos., 120,* 12,631-12,643, 2015.

Paper III: A.-I. Partanen, A. Laakso, A. Schmidt, H. Kokkola, T. Kuokkanen, J.-P. Pietikainen, V.-M. Kerminen, K. E. J. Lehtinen, L. Laakso, and H. Korhonen Climate and air quality trade-o s in altering ship fuel sulfur content. *Atmospheric Chemistry and Physics 13*,12059-12071, doi:10.5194/acp-13-12059-2013, 2013.

Paper IV: A. Laakso, A.-I. Partanen, H. Kokkola, A. Laaksonen, K.E.J. Lehtinen and H. Korhonen. Stratospheric passenger ights are likely an ine cient geoengineering strategy. *Environ. Res. Lett. 7*, 034021, doi:10.1088/1748-9326/7/3/034021, 2012.

Paper V: A. Laakso, A.-I. Partanen, U. Niemeier, C. Timmreck, H. Kokkola, K. E. J. Lehtinen, H. Hakkarainen and H. Korhonen E ects of concurrent stratospheric sulfur geoengineering and large volcanic eruption, *Atmospheric Chemistry and Physics 16*, 305-323, doi:10.5194/acp-16-305-2016, 2016.

1 Introduction

Throughout their existence, humans have modi ed their environment, one could say that they have moulded the Earth to enjoy a better quality of life and to create better conditions for survival. Unfortunately, these e orts have occasionally had devastating consequences such as the unintended destruction of an environment and habitat, threatening the very existence of human and other forms of life. For example, this happened to the citizens of Eastern Island approximately 400 years ago who destroyed their civilization by over-harvesting the trees on their island so that ultimately the residents were no longer able to build boats and use them for shing. We should not view these kinds of events as simply colourful aspects of history or think that they only concern far-o speci c regions; today the impact of human activities is so enormous that we are no longer simply changing our local environment, instead the negative e ects are global. Currently one of the largest threats to the environment originates from the industry and tra c since these are activities which emit huge amounts of gases and particles into the atmosphere. This is changing the Earth s radiative balance and a ecting the whole climate system.

Currently, the climate is changing due to increased concentrations of greenhouse gases (GHG) in the atmosphere. Greenhouse gases are important in maintaining the current forms of life, because without them, the global mean surface temperature would be approximately -18 C (Seinfeld and Pandis, 2005) which is not compatible with the survival of almost all current life-forms on this planet. Greenhouse gases absorb most of the outgoing longwave radiation and emit some of this back to the surface (Seinfeld and Pandis, 2005) increasing the temperature of the surface thus creating more suitable conditions for life. However, because of human actions, the atmospheric concentration of carbon dioxide, which is one of the most signi cant greenhouse gases, has increased by approximately 40 % since the early days of the industrial revolution (Hartmann *et al.*, 2013). At the same time, the globally averaged surface temperature has undergone warming of 0.85 C from pre-industrial times (Hartmann *et al.*, 2013). This is mostly due to the increased GHG concentrations.

Even though the climate change due to the human actions is widely recognized, we are still emitting large amounts of GHG into the atmosphere and there is a risk that the climate will warm up by several degrees before the end of this century (Stocker *et al.*, 2013). If we are to prevent this from happening, strict reduction limits in global emissions will be required. At the end of the year

2015, the Paris Climate Change Conference negotiated the new agreement to hold the increase in the global average temperature to below 2 C above pre-industrial levels and to pursue e orts to limit the temperature increase to 1.5 C above pre-industrial levels (UNFCCC, 2015). However, this is not only challenging but also it is most unlikely to be achieved unless the demand for energy will decline in the future or some form of Carbon Capture and Storage technology would become available (Rogelj *et al.*, 2014). So far, the global e orts to reduce emissions have not been adequately successful. The other problem is that CO_2 is a long-living greenhouse gas and once released into the atmosphere, it remains there for decades, even longer in the overall circulation of the Earth system (CO_2 exchange between atmosphere and soil or sea) where its lifespan is not in years but in centuries (Sonnemann and Grygalashvyly, 2013). Thus, even if we were to stop all of our emissions immediately, the already emitted GHG would still remain for a long time in the atmosphere and warm the climate.

There are also anthropogenic emissions which are cooling the climate. Burning and combustion processes release aerosols and precursor gases into the atmosphere. These aerosols scatter radiation back to space or change the optical properties of clouds making them more re ective. Depending on the size and optical properties of particles, some aerosols might also absorb the radiation and thus warm the atmosphere. Aerosols from anthropogenic sources have been estimated to reduce radiation directly by -0.27 (-0.77 to 0.23) W/m^2 and thus cool the climate (Myhre *et al.*, 2013a). Indirectly via clouds, anthropogenic aerosols have been claimed to have changed the Earths radiation balance by -0.55 (-1.33 to -0.06) W/m^2 (Myhre *et al.*, 2013a). However, the total radiative e ect from aerosols is less than half of the estimated radiative e ect from anthropogenic CO_2 emissions (1.68 W/m^2).

Temporally the cooling radiative e ect from aerosols has been of the same magnitude as the warming e ect from the anthropogenic GHG emissions. This has happened, for example, after a large volcanic eruption such as the Mt. Pinatubo eruption in 1990s. It has been shown that the Earths surface was approximately 0.5 K cooler two years after the eruption (Hansen *et al.*, 1992). After the eruption, large amounts of sulphur dioxide (SO_2) were released into the stratosphere. In the stratosphere, SO_2 becomes oxidized and forms sulphate (H_2SO_4) particles. These particles e ectively scatter solar radiation back to space so that less radiation reaches the Earths surface (Robock, 2000). Since there are no e cient removal mechanisms in the stratosphere, the lifetime of particles might be years and the cooling e ect will last signi cantly longer than if particles had been emitted or formed in troposphere (Hamill *et al.*, 1997).

Cooling after the large volcanic eruptions is a temporary phenomenon, lasting only a few years before the sulphate aerosols are removed from the atmosphere. However there have been proposals that a high stratospheric sulphate concentration could be sustained by delivering continuous injections of sulphur into the stratosphere (Crutzen *et al.*, 2006). This might be an alternative method to prevent climate warming were the emissions of greenhouse gases to continue to increase. Several other methods have also been proposed to cool the climate; these aim to increase the Earth s re ectivity or decrease the absorption of longwave radiation emitted from the surface by removing greenhouse gas from atmosphere or modifying cirrus clouds (Rickels *et al.*, 2011; Royal Society, 2009; Mitchell *et al.*, 2009). These methods are known as geoengineering or climate engineering.

Though the methods which aim to increase re ectivity of the Earth have been claimed to be fast, e cient and cheap, they may well possess many negative and dangerous side-e ects. This group of methods is called solar radiation management (SRM) and it includes diverse methods from coating deserts with re ective material to mirrors in the space (Royal Society, 2009). Currently the most extensively studied, and probably the most cost e cient SRM method is injection of sulphur into the stratosphere (Crutzen 2006; Royal Society 2009; Rasch *et al.*, 2008b; Kravitz *et al.*, 2013a). However it has been shown that sulphur injections might a ect the ozone layer or change monsoon precipitations (Tilmes *et al.*, 2008; Robock *et al.*, 2008). Marine cloud brightening is another widely studied method which aims to increase the re ectivity of clouds over the sea areas by increasing cloud droplet number concentrations (Latham, 2008; Latham *et al.*, 2012). This thesis concentrates on these two methods.

Even though geoengineering has been studied extensively in the last decade (Oldham *et al.*, 2014), there are still huge uncertainties in the estimations of the e ectiveness and the risks associated with geoengineering techniques. Experimental testing of the methods in the atmosphere is challenging and includes many risks in itself. In addition, obtaining a signi cant climate signal would require large scale implementation of the studied method. Climate models can be used to test di erent scenarios in a simulated climate and thus they are valuable tools with which to study geoengineering. Even though perhaps the two most cost-e ective SRM methods are based on aerosols, many of the previous SRM studies have been conducted with very simpli ed assumptions such as simulating the aerosol radiative e ect via a reduction in the solar constant (Govindasamy and Caldeira, 2000; Govindasamy *et al.*, 2002, 2003; Matthews and Caldeira, 2007; Bala *et al.*, 2008; Caldeira and Wood, 2009; Schmidt *et al.*, 2012; Kravitz *et al.*, 2013b) or assuming that the stratospheric aerosol elds consist of particles with a xed size (Rasch *et al.*, 2008a; Modak and Bala,

2013; Kalidindi *et al.*, 2014). These above studies did not take into account aerosol microphysics which de nes the size and thus the optical properties and lifetime of the stratospheric aerosols.

In this thesis, an aerosol-climate model has been used to study radiative and climate e ects on the global scale from current aerosol emissions and to evaluate possible future scenarios which might also include geoengineering. The key objectives of this thesis were to:

Investigate the potential of aerosols to cool the climate at the global scale

Evaluate the role of the simulation of the aerosol microphysics in the global climate models

Identify the possible limits in the e ectiveness of the Solar Radiation Management techniques as well as risks related to these techniques.

The core of this thesis consists of ve research papers. Paper I investigated how the emissions have a ected the global climate after 1996. The sulphate and carbonaceous aerosol emissions in China and India have increased and there have been proposals that this could explain the currently-seen slowdown in the global warming. Our choices in the near future could also a ect the aerosol emissions and thus, the climate. For example, energy production is one of the largest contributors to the current emissions and our choices in how we will generate energy in the future could dramatically a ect how our climate will change in the future (Edenhofer *et al.*, 2011; Jacobson, 2016). The risks associated with the nuclear power have changed the energy production in many countries such as Germany or Japan, where the energy generated in nuclear power plants has decreased dramatically. This might lead to an increase in coal-derived power. Paper II revealed what will happen if all the worlds nuclear power were to be replaced by coal-derived power. In addition to exerting a signi cant impact on climate due to the increased emissions, there would also be negative health e ects.

Decreased air quality due to aerosols was one of the reason for signing treaties which aim to reduce the air pollution. During the current decade, the reductions have targeted also the sulphur emissions from ship tra c. However this simultaneously will decrease the cooling e ect from the ship emissions. Paper III evaluated whether it would be possible to retain current or even increase the climate cooling e ect but still decrease mortality by increasing sulphur concentration fuel used by ships while they are sailing in open seas but decreasing

it while in coastal areas. Paper IV investigated how increasing the fuel sulphur concentration in commercial stratospheric air tra c would a ect the climate and could it be feasible to use commercial air tra c to stratospheric sulphur injections.

Under certain circumstances, stratospheric aerosols concentration could rise to very high levels, especially if stratospheric sulphur injections have been implemented. As has been seen throughout history, large volcanic eruptions cause an increase in stratospheric aerosol concentrations and there is a temporary cooling of the climate. This might also happen when the climate has been already cooled arti cially by deliberate use of stratospheric aerosols which would lead to a very high aerosol concentration in the stratosphere. This scenario was examined in Paper V.

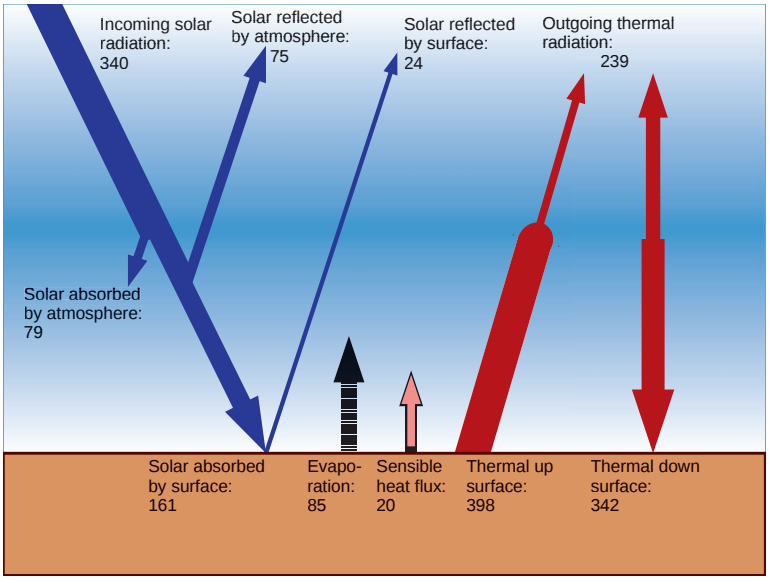

Figure 1: Present day global mean radiation in the climate (Wild *et al.*, 2013). The unit of the radiative fluxes is W/m^2.

2 Aerosols and climate

2.1 The Earth's radiation budget

The Earth can be thought of as a closed system which does not change mass (except for some incoming meteorites and exiting space rockets) between its surrounding and the only energy change occurs via radiation (Pierrehumbert, 2009). The Earths climate system is powered by solar radiation. At the distance from the Earth, the Sun radiates approx. 1370 W for every square meter (Seinfeld and Pandis, 2005). This value is referred to as the solar constant. Due to the spherical shape of the Earth, this radiation is distributed to a relatively larger area when moving from low to high latitudes and the average energy value for every square meter at the Earth's surface is 340 W (Wild *et al.*, 2013). Approximately 30 % of this energy is reflected back to space by aerosols, clouds or the Earths surface, 23 % is absorbed by the atmosphere (Wild *et al.*, 2013) and the rest is absorbed by the Earths surface. If the surface temperature does not change, the same amount of energy that reaches the surface has to be transferred out from the surface. Some of the energy is transferred through evaporation (latent heat needed for phase change from water to vapour) and sensible heat which cover only a small fraction of total

energy transferred. All matter with a temperature greater than absolute zero emits radiation at wavelengths which depend on the temperature of the matter (Young and Freedman 2004). The surface of the Sun has a temperature of approximately 5800 K and thus the incoming radiation from the Sun is mostly shortwave radiation. The surface of the Earth is much cooler (290 K) and most of the energy of the surface is transferred as longwave radiation. Earths surface emits an average of 398 W/m^2 radiation (Wild *et al.*, 2013). Some of this energy passes through the atmosphere back to space (atmospheric window) but most is absorbed by the atmosphere. The absorbed energy stays in the Earths system and although some of it is transferred back to the surface, eventually it will also be emitted back to space.

In order to maintain radiative balance, the incoming solar radiation that is not re ected back to space has to be in balance with an equal amount of outgoing longwave (LW) radiation emitted by the surface and the atmosphere. If this is not true, more energy is either stored in or released from the Earths system. Generally this energy is stored in or released from the kinetic energies of the molecules of a material which means that the temperature of the Earth will change. In addition, the amount of emitted longwave radiation will be altered due to the changed temperature until the energy balance is restored. Most of the LW radiation emitted from the surface is absorbed and re-emitted by the optically active gases such as water vapour, carbon dioxide, methane and ozone (Schneider 1990). Some of the radiation absorbed by these gases is re-emitted back to the surface which is generally known as the greenhouse e ect. If one were to estimate the surface temperature from outside the Earth without knowing anything about the Earths atmosphere, and simply calculate the temperature based on the outgoing LW radiation and Stefan-Boltzmann law, the average temperature would be -18 C (Seinfeld and Pandis, 2005). However, due the greenhouse gases, the surface temperature is +15 C which is suitable for the current forms of life. Radiation is also absorbed and scattered by aerosols and clouds. If the optical properties of clouds or the Earth s surface, or the concentrations of atmospheric gases or aerosols were to change, this would alter the energy transfer in the atmosphere. If the changes in the radiation transfer do not compensate for each other, then there will be an imbalance in the radiation which will cause a temperature change.

Currently the Earth is not in radiative balance. The atmospheric composition has been changed due to human activities. The atmospheric concentration of the major greenhouse gases i.e. CO_2, methane and nitrous oxide have exceeded the pre-industrial levels by approximately 40 %, 150 %, and 20 %, respectively (Stocker *et al.*, 2013). This has created an imbalance in the climate system which has been partly compensated by temperature changes on the surface

(land and sea) and the atmosphere. It has been estimated that the surface, has warmed by 0.85 C over the period from 1880 to 2012 (Stocker *et al.*, 2013). Even though the temperature has been increased, there is still an imbalance of 0.58 W/m^2 in the climate system (Hansen *et al.*, 2011). Thus the climate system is still recovering from this imbalance and warming further (Murphy *et al.*, 2009). Since we are emitting greenhouse gases into the atmosphere and the GHG concentration in the atmosphere continues to increase, the climate system cannot reach the radiative balance even though the temperature is increasing. Thus, the climate will keep on warming if GHG emissions are not reduced or if the radiation is not balanced by some alternative technique (Murphy *et al.*, 2009).

2.2 Aerosol radiative e ect

As mentioned, the gases are not the only materials in the atmosphere that a ect the radiation. There are a large number of particles of di erent sizes with their own distinctive compositions due to the di erent species in the atmosphere. The term aerosol means a composition of particles in liquid or solid form in a gas ranging in size from the nanometer scale to tens or even hundreds of micrometers (Baron and Willeke 2011, Seinfeld and Pandis 2005). The major species in the atmosphere are sulphate, organic matter (or organic carbon (OC)), black carbon (BC), nitrates, mineral dust and sea salt (Jacobson, 2005). Aerosols are often divided into natural and anthropogenic aerosols according to their origins. Natural sources include soil dust, wind uplift of sea spray, natural biomass res and volcanic eruptions. Major anthropogenic sources are fossil fuel combustion, biofuel and biomass burning and also soil dust over eroded land (Jacobson, 2005). In global terms, the emissions from natural sources are greater than from their anthropogenic counterparts but in urban areas, the anthropogenic emissions can exceed the natural emissions (Jacobson, 2005).

In this thesis, the sulphate particles have a major role in all of the papers. Sulphur is emitted from both anthropogenic and natural sources. The average mass mixing ratio of sulphur is less than 500 parts per million but it has a signi cant in uence on the atmospheric chemistry (Seinfeld and Pandis, 2005). The major naturals sources of sulphur are oceans, where dimethyl sulphide (DMS) is produced by marine phytoplankton and volcanic eruptions, which can temporally emit a large amount of sulphur dioxide (SO_2) to the atmosphere. Global anthropogenic SO_2 emissions have increased dramatically from 20 MT yearly emissions at the beginning of the last century to approximately 130 MT

in the middle of the 1970s. Since then, the emissions slowly declined to 100 MT/yr until global emission began again to increase after the year 2000. The latest increase is a result from increased emissions from China and India even though the emissions have decreased in other regions e.g. in Europe and USA (Smith *et al.*, 2011). However, it has been assumed that the global sulphur emissions will decrease signi cantly before the end of this century (Riahi *et al.*, 2011).

Aerosols a ect the climate by scattering the radiation, which increases the atmospheres re ectivity, and by absorbing radiation which also cause warming of the climate (Ramanathan *et al.*, 2001). Generally those particles which have a diameter of 0.2 - 1 m and contain sulphate, nitrate and organic carbon scatter light e ciently. Those aerosols smaller than 1 m and which consist of black carbon absorb radiation e ciently (Jacobson 2005). When radiation is absorbed, it warms the surrounding atmosphere, which can then a ect convection and this can lead to the formation of cloud droplets and cloud cover. Clouds re ect e ectively the radiation and changes in the clouds have an impact on radiation. This is known as an aerosol semi-direct e ect (Lohmann and Feicher 2005, Kock and Del Genio, 2010).

The Fifth Assessment report (AR5) of the Intergovernmental Panel on Climate Change (IPCC) estimated that the total direct radiative forcing (a measure of the in uence a factor has in altering the balance of incoming and outgoing energy in the Earth-atmosphere system (IPCC 2007)) from anthropogenic aerosols is currently -0.27 (-0.77 to 0.23) W/m^2 (Stocker *et al.*, 2013). In temporal terms, aerosols direct radiative forcing can be larger due to the occasional increases in anthropogenic or natural emissions. Fig 2 shows how global mean temperature changed in the last century. In general terms, the global temperature is a ected by many di erent factors and the temperature changes are rarely straightforwardly connected with changes in the aerosol burden in the atmosphere. However, in some situations, for example a sudden strong increase in aerosol burden, this parameter can be connected to global mean temperature change. Figure 2 shows the timings of the four largest volcanic eruptions after the year of 1880. After these large volcanic eruptions, there have been periods of a few years when the climate was clearly cooler and this cooling has been attributable to the particles in the stratosphere. Since there is no e ective removal mechanism in the stratosphere, the lifetime of the particles is 1-2 years and this leads to a clear response in the temperature and the surface of the Earth will be cooled for the next few years after a major eruption (Robock 2000). The last clear response was after the Mount Pinatubo eruption in year 1991 (Hansen *et al.*, 1992). After the eruption, 18-20 MT sulphur dioxide was emitted into the stratosphere (Guo *et al.*, 2004b). In the

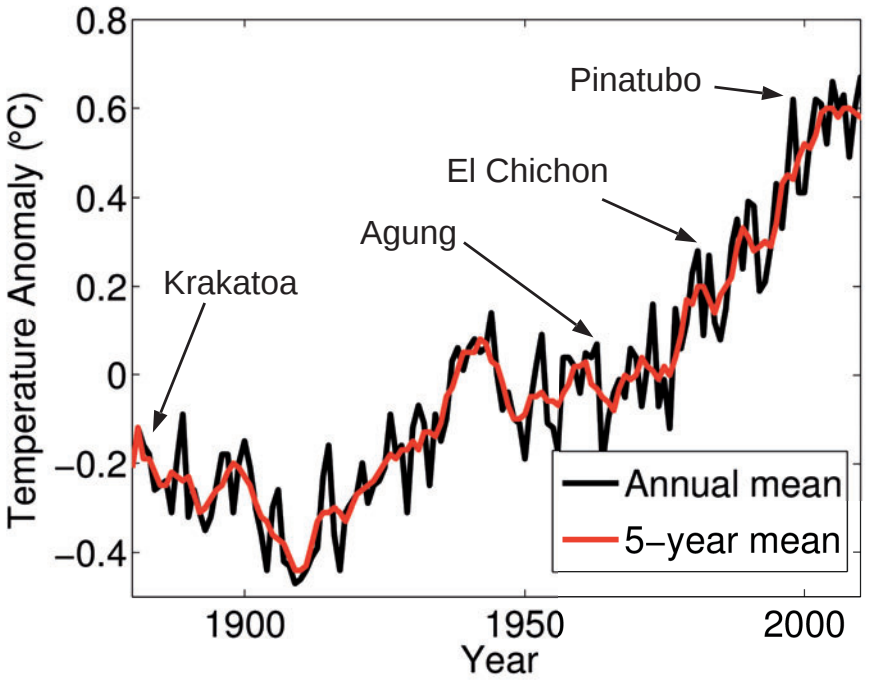

Figure 2: Global mean temperature anomaly after year 1880 (Hansen *et al.*, 2010, GISTEMP Team 2015). Time of the large volcanic eruption is shown by arrows.

stratosphere, SO_2 reacts with hydroxyl radical (OH) and forms sulphate particles. After the particles have grown large enough, they are able to scatter solar radiation efficiently back into space.

The impact of the particles on radiation depends on the optical properties of particles (composition/species) but also on the size of the particle. Figure 3 shows the size dependence of factors that determine the direct radiative effect of stratospheric sulphate particles according to Pierce *et al.* (2010). The solar radiation scattered back to space depends strongly on the size of the particles e.g. the optimal diameter for the particles to scatter solar radiation is in the range of 100-300 nm. When particles become larger, they are less effective at scattering the solar radiation back to space and their gravitational settling velocity increases which further decreases their lifetime in the stratosphere. Thus the radiative effects and climate effect depend also on the size of the particles in the stratosphere, in addition to the particles mass in the atmosphere. This has been observed also in this thesis and especially in Papers IV and V.

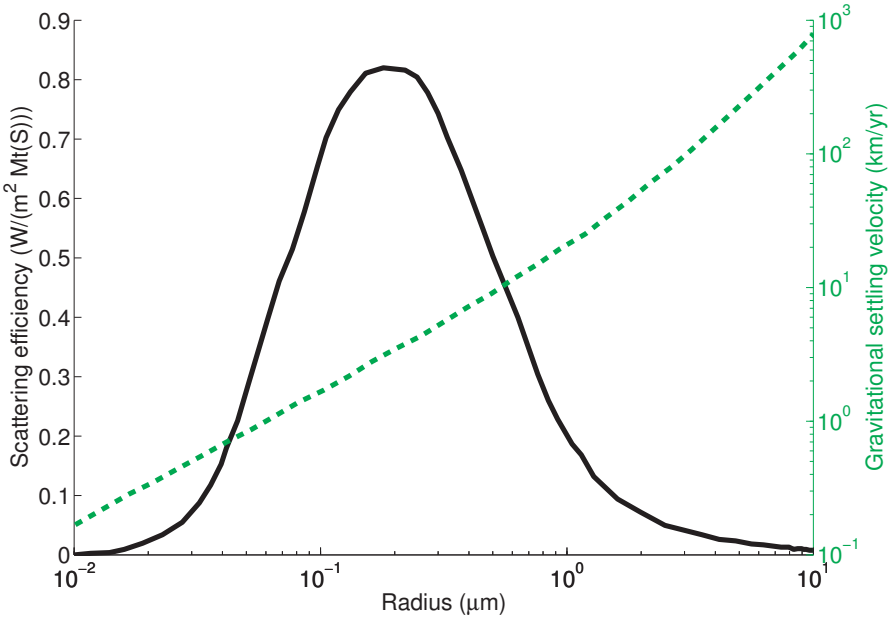

Figure 3: Size dependence of scattering e ciency (black line) and gravitational settling velocity (green dashed line) according to Pierce *et al.* (2010). The black line shows how much radiation is scattered back to space (direct radiative forcing) per mass of monodisperse sulphate aerosol eld. The green line shows the gravitational settling velocity at a height of 25 km.

Particles can also a ect radiation indirectly by in uencing cloud properties. Clouds consist of cloud droplets (also ice crystals in mixed-phase clouds and ice clouds). The formation of cloud droplets requires aerosols that have suitable properties to allow the condensation of water vapour (or a very high relative humidity which does not occur in atmosphere) (Seinfeld and Pandis, 2006). These particles have to be large enough and consist of a water soluble material so that water can condense on the surface of the particle. The vapour pressure of a curved surface of a particle is higher than that of a non-curved surface. Thus smaller particles cannot become activated into cloud droplets (Kelvin effect, Seinfeld and Pandis, 2006). However, if particles at least partially consist of a water soluble material, this decreases the vapour pressure at the surface of particle (Raoults law). If particles have these properties, then the water can condense on the surfaces and particles can act as Cloud Condensation Nuclei

(CCN) and grow into cloud droplets.

The cloud Droplet Number Concentration (CDNC) is related to cloud radiative properties. If the liquid water content (LWC) remains constant and CDNC increases, then the cloud albedo increases and more radiation is re ected. This is known as the Twomey e ect or the rst indirect e ect (Twomey, 1974). A higher CDNC also generally means a relatively smaller size of the cloud droplets. Further this has been theorized to a ect the precipitation e ciency which then increases the liquid water content. For these reasons, the lifetime of clouds and cloud thickness are increased (Albrecht, 1989) (Pincus and Baker, 1994). This is called the second indirect e ect. The latest IPCC report estimates that total e ective radiative forcing due to the aerosol-cloud interactions is currently -0.45 W/m^2 compared to the preindustrial level (Boucher *et al.*, 2013). Even though the knowledge about aerosol-cloud interactions has increased during the past years, there is still considerable uncertainty about how aerosols have a ected radiative balance after industrial times (from -1.2 to 0.0 W/m^2) (Boucher *et al.*, 2013).

3 Modelling aerosols, climate and health effects

Many of our estimates about future climate are based on simulations emerging from three dimensional global climate models. These models describe atmospheric (and the ocean in coupled models and Earth System Models) properties in three dimensional grid and they simulate main atmospheric (and oceanic) physical properties (McGu e and Henderson-Sellers, 2005). Thus, models can be useful for testing scenarios and processes in simulated climate, which would be impossible to investigate by any other means. Unfortunately, climate models always provide an incomplete description of the climate. Every process in the atmosphere cannot be modelled and if one wished to build a perfect climate model, one would require perfect theory about the entire multitude of physical and chemical phenomena in the atmosphere and everything that interacts with the atmosphere. Even with the perfect theory and knowledge, computational resources have a restricted capability to simulate climate. Nonetheless, despite their limitations, climate models are valuable tools with which to evaluate and investigate climate in the past, present and the future.

Several climate models are used in this thesis. The general circulation model (GCM) ECHAM5 and ECHAM6 (Roeckner *et al.*, 2003; Stevens *et al.*, 2013) make up the core of all of the simulations presented here. This general circulation model has been coupled with the second generation aerosol module HAM2 (Zhang *et al.*, 2012). This aerosol-climate model (ECHAM-HAMMOZ) has been used in all papers which are included in this work. The model system includes also the atmospheric chemistry model MOZART, which is not used in the studies of this work (Emmons *et al.*, 2010). In addition, in Paper I the ECHAM-HAMMOZ is coupled with the slab ocean model. Paper V includes also simulations by Max Planck Institutes Earth System Model (MPI-ESM, Chapter 3.4; Giorgetta *et al.*, 2013) where ECHAM is coupled with the Max Planck Institutes Ocean model (MPIOM), a land model (JSBACH) and the ocean biochemistry model (HAMOCC). However MPI-ESM does not include an aerosol module.

3.1 General Circulation Model - ECHAM

In the simulations in this thesis, the global atmosphere is described by The European Centre Hamburg Model (ECHAM) (Roeckner *et al.*, 2003; Stevens *et al.*, 2013). This was developed in the Max Planck Institute for Meteorology. The ECHAM development originated from an early version of the global

numerical weather prediction model developed at the European Centre for Medium-Range Weather Forecasts (ECMWF) and currently is in its sixth version. The model describes the main relevant atmospheric processes and variables. The dynamical part of ECHAM is formulated in spherical harmonics. Thus, atmospheric circulation (vorticity and divergence) temperature, pressure and humidity are solved in a spectral grid. Radiation, clouds, convection and precipitation are solved in a regular Gaussian grid. The fth generation of ECHAM was used in Papers I, III, IV and V. In Paper II, ECHAM6 was used and Paper V includes also simulations by MPI-ESM where the atmosphere is modelled by ECHAM6.

A horizontal resolution of T63 (which corresponds to a 1.9 x 1.9 sized grid box) was used in all of the simulations presented in this work, excluding Paper I where a lower, T42 (which corresponds to a 2.8 x 2.8 sized grid box), resolution was used. The vertically model uses a hybrid-sigma coordinate system. The model then applies the terrain following sigma coordinate (Phillips, 1957) at lower height levels and a hybrid coordinate in upper-levels, where the model levels are planar even when the levels are representing steep terrain (Simmons and Burridge, 1981, Simmons and Strung, 1981).

Two di erent vertical resolutions were applied in this study. In papers I, II, and III, the atmosphere was divided into 31 vertical levels (L31) up to 10 hPa pressure level (which correspond roughly to a height of 30 km). In papers IV and V stratospheric aerosols were studied. The stratosphere is described only by few model levels in L31 and in order to simulate the stratosphere in more detail L47 was used instead in these two studies. This increases the vertical resolution above the tropopause (approximately from 8 to 22 levels) and model levels reach 1 hPa (80km).

3.2 Aerosol module HAM, M7 and SALSA

Aerosols are simulated by the Hamburg Aerosol Model (HAM) (Stier *et al.*, 2005; Zhang *et al.*, 2012). HAM takes into account the following aerosol processes; emissions, wet and dry depositions, cloud processes, aerosol cloud interaction and sulphur chemistry. In this thesis, both submodels M7 (Vignati *et al.*, 2004) and a Sectional Aerosol module for Large Scale Applications (SALSA) (Kokkola *et al.*, 2008; Bergman *et al.*, 2012) were applied to simulate aerosol microphysical processes and both models calculate the main aerosol processes such as nucleation, condensation, coagulation and hydration. Nucleation is calculated by considering it as binary nucleation (Vehkamaki *et al.*, 2002) except in boundary layer where nucleation is calculated by the activation nucleation

(Sihto *et al.*, 2006; Riipinen *et al.*, 2007; Makkonen *et al.*, 2009). The modelled aerosol species are sulphate, organic and black carbon, dust and sea salt. These species are divided into water soluble and insoluble materials.

SO_2 is the main precursor gas of the particles in the model; this is emitted from several sources. Most of the SO_2 emissions come from anthropogenic sources such as industrial and transportation but some of emissions originate from forest res and volcanic eruptions. SO_2 is also produced in a reaction between dimethyl sulphide (DMS) and OH. DMS emissions from marine sources (produced by phytoplanktons) are calculated based on DMS sea water concentration using air-sea exchange rate and a 10 m wind speed. Over the land, o ine DMS emissions are used. In the model, sulphate aerosol chemistry module is described according to the work devised by Feichter *et al.* (1996). In the module, SO_2 is oxidized with hydroxyl (OH), hydrogen peroxide (H_2O_2), ozone (O_3) and nitrogen dioxide (NO_2), which are described by three dimensional monthly mean elds. Due to its photochemical reactions with ozone, more OH is produced during the daytime and also during the summer (Seinfeld and Pandis, 2006). In the model, the diurnal variation of OH is accounted for by multiplying monthly mean values by a diurnal coe cient which follows the cosine peak between a sunrise and a sunset. This approach has some disadvantages, for example it does not take account of decreased solar radiation below clouds. One viable alternative is to use solar radiation based on an OH-proxy but this was not used in this work (Pietikainen *et al.*, 2014). Sulphate is also produced in cloud droplets, where condensed SO_2 reacts with trace gases.

The sea spray emissions are estimated by formulation of Schulz *et al.* (2004) which combines the wind-speed-dependent source functions proposed by Monahan *et al.* (1986) and Smith and Harrison (1998). Dust emissions were also calculated online as a function of wind speed and hydrological parameters according to the Tegen *et al.* (2002) scheme. Anthropogenic and wild re OC, BC and SO_2 emission were based on the AEROCOM emission inventory (Dentener *et al.*, 2006).

Aerosols are coupled interactively with clouds. The cloudiness or the cloud fraction of the model grid cell is calculated as a function of relative humidity (Sundquist *et al.*, 1989). The e ect of aerosols on cloud properties are implemented as follows. Aerosol activation to the cloud droplets are calculated with either the semi-empirical scheme of Lin and Leaitch (1997) (Paper II, Paper IV and Paper V) or with the physically based parameterization by Abdul-Razzak and Ghan (2000) (Paper I, Paper III), which takes into account also the chemical composition and size distribution of particles. Autoconversion of cloud droplets to rain is parameterized according to the work of Khairoutdinov and Kogan (2000).

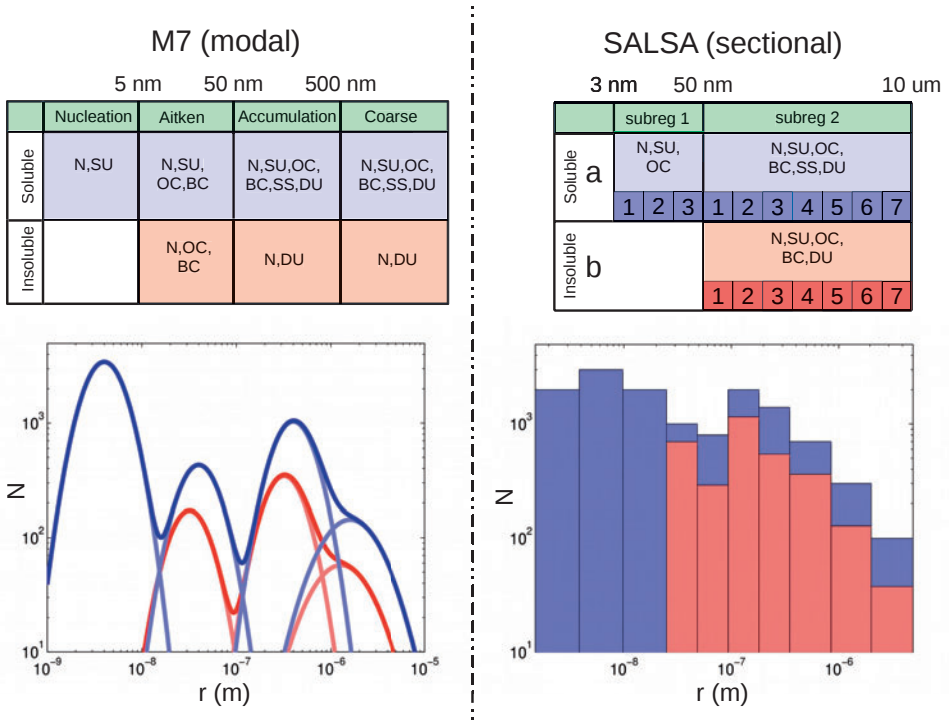

Figure 4: Aerosol size distributions in the modal M7 and the sectional SALSA microphysical models. SU refers to sulphate, OC and BC to organic and black carbon, SS to sea salt and DU to dust mass concentrations. N refers to number concentration.

Figure 4 illustrates how an aerosol size distribution is described in the M7 and SALSA microphysical models. In M7, the aerosol size distribution is described by a superposition of seven log-normal modes. Four modes cover the size range from the nucleation mode to the coarse mode for soluble materials. Nucleation mode describes new particles formed by nucleation. Coarse mode particles are usually mechanically produced (sea salt and dust) particles. Between these modes, there are Aitken and Accumulation modes which describe particles that are growth via coagulation and condensation (Baron and Willeke, 2011). Insoluble materials are described by three modes from the Aitken mode to the coarse mode. The model calculates the number concentration of all modes and the mass of one or more of the major aerosols components for each mode (Figure 4).

The modal approach is a computationally efficient and accurate way to model and simulate particle size distribution but it has also some defects. In the

modal approach used in M7, the model reallocates numerically particles between modes, the size of which is restricted by the xed mode width and the position by prede ned boundary values. This might lead to an arti cial change in the particle size distribution, when particles are moved from one mode to another. This has been shown for example to lead to an overestimation of CDNC and light extinction (Korhola *et al.*, 2012). Calculations of various particle properties, such as rates of coagulation and condensation are done on the basis of the average number mode radius. The average mode radius can vary but it is restricted between speci c values and the widths of the modes are xed. Nucleation, Aitken and Accumulation modes are described by the same value for the standard deviation (= 1 59) while the coarse modes are described by a wider mode in the basic model setup (= 2 0). This is suitable for tropospheric conditions, but it may lead to some problems in speci c cases such as volcanic eruptions and stratospheric sulphur geoengineering, where the sulphur concentration may become high in the stratosphere (Kokkola *et al.*, 2009). In the troposphere, the lifetime of particles is only several days and the role of the coarse mode is to represent mainly dust and sea salt particles which are relatively large when emitted to the atmosphere. The sea salt and dust particles described by wide coarse mode display a good agreement with the measurements (Stier *et al.*, 2005). However in the stratosphere, the lifetime of particles is long which allows particles to grow to a relatively larger size than in the troposphere, if particle or condensable gas concentrations are high. In this case, describing particles by the wide coarse mode would lead to excessively large particles due to the numerical reasons. Thus these particles are better represented by the narrow mode. Previous studies with M7 where the volcanic eruption or stratospheric sulphur geoengineering had applied only three modes (no coarse mode) and a smaller standard deviation for the accumulation mode (= 1 2) (Niemeier *et al.*, 2009, 2011, Niemeier and Timmreck, 2015, Toohey *et al.*, 2012). This mode setup better represents particles in stratospheric conditions with a high sulphur concentration but it does not represent tropospheric sea salt and dust aerosols as well as the wider mode. Thus in these studies, only stratospheric aerosols have been simulated. In this thesis, M7 was used in Papers I, III and IV. In Paper I and Paper III, only tropospheric aerosols were simulated. Even though the stratospheric aerosols were simulated in Paper IV, the stratospheric sulphur concentrations were signi cantly smaller than in the studies conducted by Niemeier *et al.* (2009, 2011) and Toohey *et al.* (2012) and the standard mode width was used. This also made it possible to simulate tropospheric aerosols.

By using the sectional method for the aerosol size distribution, the abovementioned problems achieved a smaller numerical error than if the modal

method is used. However this required describing aerosols by several sections which means that more variables had to be simulated (compared to modal approach) and the calculation of aerosol microphysics was then computationally heavier. In this work, the sectional aerosol module SALSA was used in Paper II and Paper V. SALSA simulates aerosols by categorizing them into 10 size sections which are grouped according to subsize ranges or subregions. These subregions di er from each other according to which chemical compounds and microphysical processes are simulated. In the earlier version of SALSA, three subregions were used (Kokkola *et al.*, 2008; Bergman *et al.*, 2012). In this earlier version, the third (the largest three size sections) subregion included only information about a number concentration of sea salt and dust and a mass fraction of water soluble material and interactions within a subregion and with the other size sections was reduced. In this thesis work, the third subregion was excluded and second subregion was extended to cover the largest size sections (Paper V). The rst and second subregions di er from each other only according to which chemical compounds are simulated and the volume ratio between the adjacent bins is narrower in the second subregion (Figure 4). Similar to M7, aerosols are divided into soluble and insoluble sections. Soluble materials are described by all 10 size sections. These sections are divided into two subregions where the rst subregion encompasses the 3 smallest size section for particles size of 3 nm - 50 nm. The smallest subregion includes information about a soluble material number concentration and mass concentrations of sulphate and organic carbon but instead, the second covers both soluble and insoluble materials. In addition to sulphate and organic carbon, mass concentration for black carbon, sea salt (only soluble) and dust were tracked. In total, SALSA covers the size range of particles up to 10 micrometer. SALSA with this modi ed setup is used in Paper V and modi cations was also included in later standard version ECHAM-HAMMOZ and used in ECHAM6.1-HAM2.3 and in Paper II.

3.3 Calculating aerosol radiative e ects from global aerosol climate model simulations

In this work, the aerosol radiative e ect has been evaluated by using two definitions, aerosol direct radiative forcing and e ective radiative forcing (ERF) (or Radiative Flux Perturbation (RFP)). The aerosol direct e ect has been diagnosed in ECHAM-HAMMOZ by a double radiation call, where radiative uxes were determined with and without aerosols and it has been calculated in a clear sky (neglecting clouds) and all-sky/total-sky (taking account of the in uence of clouds on radiation) conditions. Direct radiative forcing due to

the studied aerosols has been calculated as the di erence of the aerosols direct e ect in a simulation, which includes changes in emissions, and a control run. Thus, the radiative forcing in this work di ers from the IPCC AR5 report de nition where radiative forcing is de ned as the change in net downward radiative ux at the tropopause after allowing for stratospheric temperatures to readjust to radiative equilibrium, while holding surface and tropospheric temperatures and state variables such as water vapour and cloud cover xed at the unperturbed values. (Stocker *et al.*, 2013).

As was mentioned in the previous chapter, aerosols a ect radiation also indirectly by changing the properties of clouds. This is a rapid adjustment which is not included in the de nition of direct radiative forcing, but is instead included in the de nition of e ective radiative forcing (ERF). ERF is de ned as a change in net TOA downward radiative ux when the surface temperature has been kept unchanged but allowing for atmospheric temperatures, water vapour and clouds to adjust to changed conditions resulting from the presence of the aerosols. All papers in this thesis included simulations with xed sea surface temperature (SST) and sea ice cover. Thus ERF can be calculated by comparing a change in the radiation between studied scenario and the control simulation.

The use of a xed SST facilitates evaluating the radiative e ect and also decreases computational costs compared to one applying the sea model which simulates changes in the oceans. However, the ocean has a major role in determining how energy is transferred in the Earth and especially in modulating the temperature at the surface level. Thus, it is not totally feasible to study climate e ects as temperature changes at the surface and changes in the precipitation if temperature or energy ux changes in ocean are not taken into account.

3.4 Mixed layer ocean model

The mixed-layer ocean model is a simple way to estimate the energy change between the ocean and atmosphere. In this work, a 50m slab ocean model was used in Paper I as described in Raisanen *et al.* 2008. In this model, the heat budget of the constant-depth mixed layer is described as:

$$ {}_w c_w h \frac{T_m}{t} = F \quad Q_{clim} \tag{1} $$

where $_w$ is the density, c_w speci c heat capacity of the sea water, h is a globally uniform mixed layer depth, T_m is the mixed layer temperature (SST) and F

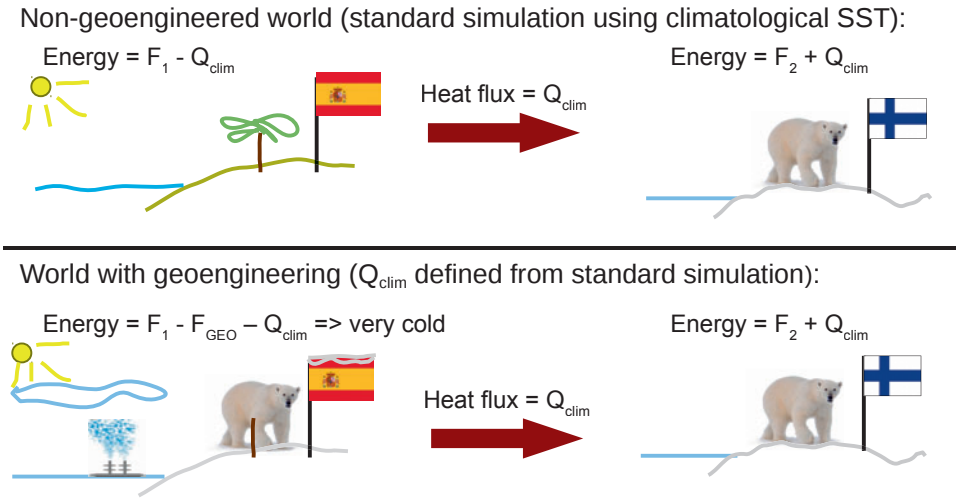

Figure 5: Energy fluxes in localized radiative flux changes are simulated by the slab ocean model. F_1 and F_2 shows the energy fluxes in the grid box excluding the ocean heat-flux (Q_{clim}). The climatological ocean heat-flux used in the mixed layer ocean is defined from standard simulations without geoengineering. The defined Q_{clim} is used also in simulations with geoengineering which might lead to situation where an unrealistic amount of energy is transferred out from the grid box where solar radiation is reduced (by F_{GEO}).

is the net surface heat flux. The variable Q_{clim} is the climatological ocean heat-flux divergence and is derived using surface-flux data from a simulation with a standard version of the atmospheric model (ECHAM), and by applying climatological SSTs. The value of Q_{clim} from this simulation is then used in all of the simulated scenarios and indicates how much energy in the surface grid box is transferred via the ocean. The simulations with the mixed layer ocean are computationally faster than the simulations with a full ocean model. They are also appropriate in those cases where changes in the ocean-atmospheric fluxes are relatively small. Then the fixed value of Q_{clim} is representative also in the case where atmospheric energy fluxes are changed due to the studied experiment. This is the case in Paper I, where changes in the radiative fluxes over the ocean are relatively small.

Using mixed layer ocean model might lead to unrealistic changes in the climate if used to model situations where flux changes are large. This is the case for example after volcanic eruptions or if there has been geoengineering. Problems arise especially when a fairly local geoengineering method (e.g. sea

spray geoengineering (chapter 5.1.2)) is being studied (Partanen *et al.*, 2012a). Figure 5 shows the situation in a non-geoengineered climate condition and in a geoengineered world. Q_{clim} is de ned by calculating climatological ocean ux without geoengineering in unperturbed climate conditions and then this is used also in geoengineering simulations. In the world of geoengineering, solar radiation and energy which reaches the surface grid box over the ocean is reduced (F_{GEO} in gure), and thus the surface temperature is decreased. Simultaneously this should also decrease heat energy which is transported out of the grid box, but the model still assumes that the same amount of heat energy (Q_{clim}) is being transported from this area as was the case before the geoengineering. This might lead to signi cant overcooling in the areas where radiative ux has been reduced. For this reason, the mixed layer ocean is not well suited for many geoengineering studies and climate e ects have to be studied with more sophisticated ocean models.

3.5 Earth System Model - MPI-ESM

Climate models are valuable tools for estimating future climate conditions and investigating the response of a climate system to various forcings. The results and projections of future climate in the latest IPCC report were based on simulations of 39 climate models (Myhre *et al.*, 2013a). All of these models include atmospheric and ocean models which are coupled together. These Atmosphere-Ocean General Circulation Models can be used to make projections of future scenarios for example, to evaluate temperature and precipitations changes. Some of the models include also a sea-ice and vegetation models, variety of biogeochemical cycles such as those involved in the carbon cycle or the sulphur cycle. These models are called Earth System Models (ESM). One of these models is the Max Planck Institutes Earth System Model (MPI-ESM, Figure 6) which was also used here in Paper V.

The MPI-ESM consists of the atmospheric model ECHAM6 (Stevens *et al.*, 2013) which was presented earlier in chapter 3.1. The ECHAM6 is coupled to the Max Planck Institutes Ocean Model (MPIOM) (Jungclaus *et al.*, 2013) by using the Oasis coupler. The model also includes subsystem models for land and vegetation JSBACH (Reick *et al.*, 2013) and a HAMMOC marine biochemistry model (Ilyina *et al.*, 2013). The current version of MPI-ESM does not include a microphysical aerosol model and aerosol elds are described o ine. In the troposphere the model uses spectrally resolved aerosol optical properties (Kinne *et al.*, 2013). In the standard version, stratospheric aerosols are provided for the historical period (Stenchikov *et al.*, 1998). In the future

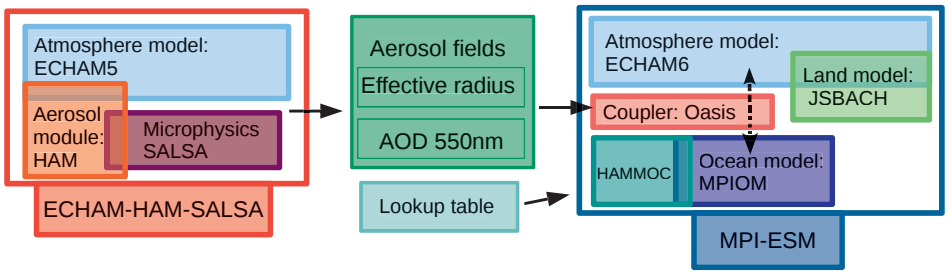

Figure 6: In Paper V, aerosol fields and optical properties are first simulated by global aerosol-climate model. Then these fields are described as effective radius and by AOD for 550 nm wavelength in MPI-ESM. Other relevant optical properties are read from a look-up table by using effective radius and 550nm AOD.

scenarios, the extinction due to the volcanic stratospheric aerosols is set to zero (Giorgetta *et al.*, 2005).

If one wishes to study the climate effects of stratospheric sulphur injections and marine cloud brightening, or some other scenarios related to aerosols by MPI-ESM, it is necessary to implement an aerosol model into MPI-ESM or describing aerosols offline. The aerosol module HAM is already implemented into ECHAM, but coupling ECHAM-HAM with the ocean models requires model tuning (chapter 3.5) (Mauritsen *et al.*, 2012) which is not done in the model's current state. Another major issue is that running the aerosol model is computationally heavy. Earth System Models are used to study climate effect which usually means that the simulations have to take account of changes lasting for several decades. Furthermore natural variation is large in the model and statistically significant results require the ensemble of several simulations. Thus simulating the climate effects by MPI-ESM requires several simulations over several decades and this cannot be done with the coupled aerosol model since it would require clearly more computational resources than needed for describing aerosols offline.

Paper V deals with stratospheric aerosols. The conditions in the stratosphere are relatively stable and the lifetime of particles is long (1-2 years). The particles consist mainly sulphate and water. Since the particles reside at an altitude of over 15 km, the ocean does not exert any significant direct influence on the stratospheric aerosol field, meaning that the offline aerosol fields can be used in the MPI-ESM. In Paper V, the modelling of the climate effects was done in two steps. Aerosol fields and optical properties from the studied emission/geoengineering scenario were first simulated by ECHAM-HAM-SALSA

which takes account of aerosol microphysics. These aerosol elds were then described by e ective radius and aerosol optical depths at 550 nm wavelength (AOD550). In the second step, these elds were used as the input in MPI-ESM and utilized in the climate simulations. MPI-ESM reads in AOD, single scattering albedo and the asymmetry factor of the aerosol particles were obtained from a look-up table, where these parameters are described as a function of wavelength, e ective radius and AOD550. In this table, radiation properties are calculated assuming a single modal (= 1 2) size distribution and chemical composition of particles which consist of 75 % sulphate and 25 % water.

3.6 Tuning of the model

Model tuning is an integral part of the model development process. It is the last step of the model development process (Mauritsen *et al.*, 2012). Models are always an incomplete description of the real atmosphere and many of the physical subgrid processes are parametrized to lessen the computational burden. The model also includes some parameters which are set between some boundaries, but their values display great uncertainties, because of the lack of any exact theory behind the parameter. Many of these parameters are related to clouds and thus changing these parameters will change radiation uxes in the atmosphere. By tuning these parameters, it is possible to e ectively change radiative values in the model and adjust the model radiation values so that they exhibit a better agreement with actual observations. This has to be done in all model versions and con gurations. In this work, the model was tuned in Paper I, Paper III, Paper IV and Paper V before proceeding to the actual simulations.

3.7 Health e ects from the Global Climate Model

In this work, health e ects are calculated from the mass concentration of particulate matter with a dry diameter less than 2.5 m ($PM_{2\,5}$) which is simulated by ECHAM-HAMMOZ. The long term health e ects were studied in Papers II and III. Five-year-mean values were used for surface level PM2.5 concentration which is calculated in the control simulation with standard emissions, and used as a reference, and for the studied scenarios with additional emissions. The methods devised by Ostro (2004) were used to calculate premature mortality from cardiopulmonary disease and lung cancer due to the decreased air-quality. Annual excess mortality rates E were calculated from

the simulated $PM_{2\,5}$ concentration with the following concentration-response function:

$$E = \quad 1 \qquad \frac{PM_{2\,5\,c} + 1}{PM_{2\,5} + 1} \qquad B_y \quad P_{30+} \tag{2}$$

where $PM_{2\,5\,c}$ is the reference concentration (m/m^3) from the control run and $PM_{2\,5}$ from the simulations with additional emissions.; is a cause-speci c coe cient with a value of 0.23218 (95% con dence interval: 0.08563-0.37873) for lung cancer and 0.15515 (95 % con dence interval: 0.0562- 0.2541) for cardiopulmonary diseases (Ostro, 2004). B_y is the baseline mortality rate (e.g. deaths per year per 1000 people) for lung cancer and cardiopulmonary diseases (diseases related to hearth and lungs) in the exposed population with age over 30 years (P_{30+}) which are calculated based on data provided by the World Health Organisation (WHO, 2008). Population density data is for the year 2010 and obtained from the Socioeconomic Data and Application Center at Columbia University (SEDAC, 2005). Population data, B_y and P_{30+} are gridded into the used model grid resolution (T63).

4 Climate response due to anthropogenic aerosol emissions

Current climate warming is a result of the increased greenhouse gas emissions. At the same time, we have emitted more aerosols into the atmosphere which have re ected more solar radiation back to space and compensated to some extent for the warming e ect from the increased GHG emissions. One interesting question is would it be possible to signi cantly slow down global warming by emitting more aerosols into the atmosphere; another important question is how our decisions about energy production can a ect the aerosol concentration at the atmosphere and the climate warming. However, in general aerosol emissions simultaneously decrease air quality which means that there should be a reduction in the particulate emissions.

4.1 Aerosol emissions in last two decades and impacts to the climate

Substantial changes have taken place in the geographical distribution of aerosol emissions in the last decades. Together with the changes in the amount of global emissions, this might have changed the global radiative e ects of aerosols. Simultaneously there appears to have been a slow-down in global warming since the beginning of 21st century which might be caused by the geographical change in the emissions (Santer *et al.*, 2015). Due to air quality legislation, between the years from 1990 to 2005, SO_2 emissions have decreased in North America from 24 000 Gt SO_2 by 38% and in Western and Central Europe from 30 522 Gt SO_2 by 64 % (Smith *et al.*, 2011). However, during the same time, the yearly SO_2 emissions from China and India have increased after the year 1990 respectively by 90 % 17 194 and 3 302 Gt SO_2. SO_2 emissions in China and India have continued to grow since 2005. Thus, even though there have been no large changes in the total global emissions, the emissions are located di erently. After the year 1998, the percentual contribution of China and India to the global SO_2 emissions has increased from under 30 % to over 40 %. In addition, also BC emissions have increased substantially. Solar intensity is greater at low latitudes and since the emission areas have moved towards countries in the low latitudes, it is expected that emissions will now make a larger contribution to radiation in these regions. Murphy (2013) studied the direct e ects of aerosols and observed that the regional redistribution of aerosols had little e ect on global average clear-sky direct radiative forcing

from 2000 to 2012. However, aerosols also a ect radiation indirectly and this fact was not taken into account in the study of Murphy (2013).

Paper I evaluated climate impacts of the changing aerosol emissions in the period from 1996 to 2010 and investigated if this could be the reason for the slowdown in global warming which has been postulated to have occurred at the beginning of this current century. The simulations with xed SST show that clear-sky aerosol direct forcing has clearly increased in China and India and decreased in Europe and North America as expected. Surprisingly, there has also been a decrease in the all-sky direct aerosol forcing in China and the e ect on all-sky forcing is opposite to the clear-sky aerosol direct forcing. However, if the aerosol indirect e ect is also taken into account, there has been total cooling e ect attributable to the increased emissions also in China. Nevertheless in global terms, ERF has increased by 0.42 W/m^2 due to the changes in emissions between the years 1996 and 2010. Paper I presented also transient simulations by a slab ocean model instead of applying the xed SST. These simulations indicated that there was an 0.25 C global annual-mean 2-meter temperature change due to shifts in aerosol emission regions between the years 1996 and 2010 and the warming was concentrated in the northern hemisphere. However, the slab ocean model reacts rapidly to any changes in the radiation because heat uxes in the deeper ocean have not been taken into account and thus the transient trend is overestimated. Even though the results indicated that the increased aerosol emissions from China have not led to global cooling, emissions have made a substantial contribution on the climate temperature and for example full elimination of SO_2 emissions in China might lead to a 0.05-0.4 C increase in the global mean temperature and this warming would be felt especially in the northern hemisphere (Kasoar *et al.*, 2016).

Paper I showed that all-sky direct aerosol forcing may have di erent sign than total radiative forcing from aerosols. In Paper I, the total cloud fraction was very high over China and in simulations this has even increased by roughly about 5 % from the year 1996 to 2010 due to increased aerosol emissions. Under speci c conditions, clouds can also a ect aerosol direct e ect as illustrated in gure 7. In comparison with cloud-free regions, in cloudy areas, shortwave radiation is re ected e ciently by clouds and less radiation penetrates through to be able to interact with aerosols under the cloud. In Paper I, aerosol emissions were increased over China since the year 1996. As a consequence, the clear-sky direct forcing increased as expected. However, simultaneously the cloud cover in the year 2010 also increased, and it now covered areas which in 1996 had been considered as cloud free areas. Particles in these areas cannot re ect as much radiation as before, because some of the radiation is re ected

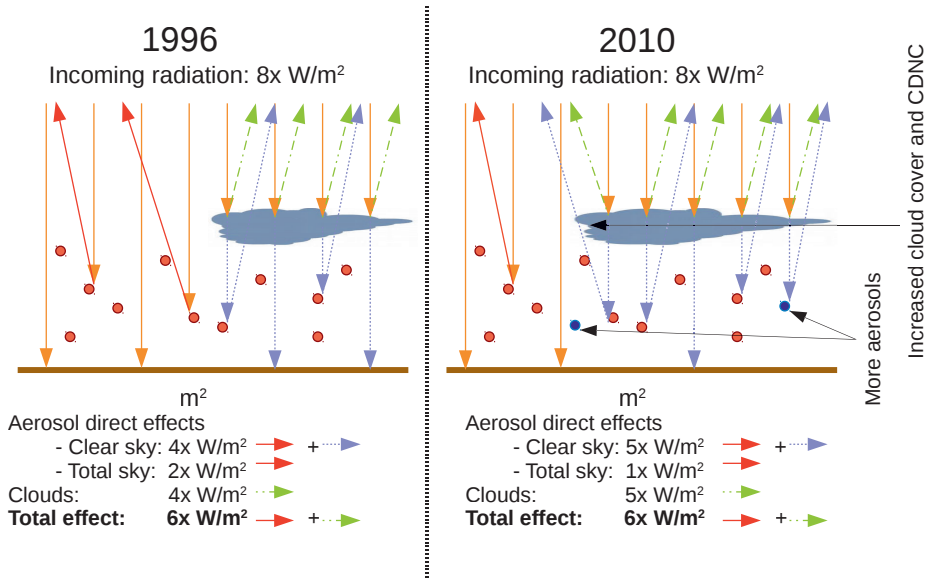

Figure 7: Illustrated aerosol radiative effects when aerosols clear-sky direct effect and indirect effect are increased, but the aerosol all-sky direct effect is decreased. Single arrow in the figure represents an arbitrary value x for radiation, which is reflected by aerosols (red), clouds (green) or would be reflected by aerosols without the existence of clouds (light blue). Note that the fractions of reflected radiation are chosen only to simplify the figure and do not represent any actual values from simulations.

now by clouds. In addition, the cloud optical depth is increased which affects aerosol direct forcing basically in a similar manner as an increase in the cloud cover, such that less radiation reaches the under cloud layers.

Aerosols also absorb radiation and the aerosol absorption optical depth (AAOD) becomes larger, especially if BC emissions are increased. Shindell *et al.* (2013) reported a strong positive all-sky forcing over East Asia due to BC emissions between the years 1980 and 2000 and Tsay *et al.* (2013) found that the occurrence of absorbing aerosols was rather frequent in this area. In Paper I, the increase in AAOD in China and India is much larger than the decrease in Europe and North America. In addition, the BC concentration and AAOD have increased above the clouds and thus these BC particles interact with incoming radiation also in cloudy areas. Due to these reasons, the all-sky direct radiative forcing is decreased. However, as was seen, the total radiative effect (ERF) of clouds and aerosols is increased.

It is possible to make two general conclusions from the study. First, the pres-

ence of clouds could also a ect the aerosols abilities to scatter radiation and the geographical change of the aerosol emissions to the lower latitudes, where solar intensity is higher, will not necessarily increase global mean radiative forcing, if emissions are located in more cloudy areas. Second, based on this study, the slowdown of the global warming occurring at the beginning of this century is not due to the changes in aerosol emissions. Instead, these changes would tend to accelerate global warming.

There have been many suggestions to explain what may be causing the apparent slowing down of global warming if it is not the geographical change in emissions. One explanation would be that it is due to the sulphate particles from volcanic activity (Santer *et al.*, 2014; Ridley *et al.*, 2014). As already discussed, the aerosols from volcanic eruption are known to lead to cooling of the climate and changes in volcanic activity could therefore cause a temporal change in surface temperature. Recent volcanic activity after the year 2000 has been estimated to be the reason for the global cooling of 0.05-0.12 C (Ridley *et al.*, 2014). Another reason for the slowdown of global warming might be the natural variability of the Earths climatic system and this is related to the decadal cooling attributable to the La Nia phase of the El Nino-Southern Oscillation (ENSO) in the eastern equatorial Paci c (Kosaka and Xie 2013). Strengthening of the Paci c trade winds over the past two decades has increased subsurface ocean heat uptake which may explain the slowdown of global warming (England *et al.*, 2014). This also indicates that natural variability of global temperature could be relatively large compared to the change due to external driving factors for example, aerosols. This also creates challenges for the climate models and future predictions. Furthermore, measuring and calculating global mean temperature is far from straightforward and it might be that the increase in global mean temperature in the last decades has been underestimated (Karl *et al.*, 2015).

4.2 Emissions from industry and energy production

Climate in the near future is in a close relationship with our choices in energy production. How energy production will change depends strongly not only on our long term plans and targets (via emission reduction agreements) but also short term choices with might be related some speci c event which are shaping public and governmental opinions. One of these kinds of events which shaped public opinions about energy production in some countries, happened in 2011 when there was a nuclear accident in Fukushima, Japan. Subsequently, several countries reassessed the question of whether the economic and environmental

bene ts of nuclear energy outweighed the risk associated with nuclear power and problems related to radioactive material. The hardest a ected country was Japan, where the nuclear power plants were progressively shut down. Germany is also planning to abandon nuclear power before the year 2022. However this has created a gap in energy production which will have to be replaced by some alternative source of energy. Coal power is an economically attractive option. Resources are widely available and easy to store and the production of energy is cost e cient. Paper II shows an extreme case, where all nuclear power plants would be shut down everywhere in the world and the energy they produced would be replaced by coal power. In a world where the energy production was derived from coal power would increase CO_2 emissions on the climate but also to air quality would deteriorate when hazardous emissions from coal-burning power stations would increase. In fact, this can be considered as the worst case scenario if all nuclear plants were to be shut down all around the world.

Based on the IPCC AR5 report, 40.4 10^6 GWh/yr of energy is produced by coal power (Bruckner *et al.*, 2014). Energy produced by nuclear plants is clearly smaller (2.6 10^6 GWh/yr). Even though nuclear power is in global terms a relatively small fraction of the whole energy production, most of the nuclear power is produced in the western countries, where the nuclear power has the large role. Fission based nuclear power can be considered as a relatively clean energy source not only in terms in climate (Lenzen *et al.*, 2008) but also in air quality and thus replacing nuclear power by coal power would have major local air quality consequences, especially in Europe. Paper II simulated the increased emissions from SO_2, BC and OC. Since the nuclear plants to be replaced are located primarily in western countries, the average emissions from coal power plants in US from the year 2009 were used in study. We also used locations of operational nuclear reactors in the year 2012 which also includes nuclear reactors from Japan which were closed later.

In the year 2012, most of the nuclear plants were located in Western Europe, Eastern US and also in Japan. Figure 8 shows all-sky direct forcing from increased emissions globally and the change in ERF over Europe should nuclear power be replaced by coal power. As can be seen, the radiative e ect would be concentrated on regions where the nuclear plants were located. In the eastern US, ERF is -0.46 W/m^2, in Europe -0.64 W/m^2 and Japan ERF: -0.94 W/m^2. However there is also the impact on the air quality. Based on the simulations in Paper II, the highest increase in the premature mortality would occur in Europe where there would be almost 100 000 premature deaths. The global mortality would increase by almost 150 000 premature deaths per year.

The global mean direct radiative e ect is -0.016 W/m^2. Together with the indirect e ect from increased emissions this would lead globally to -0.062 W/m^2

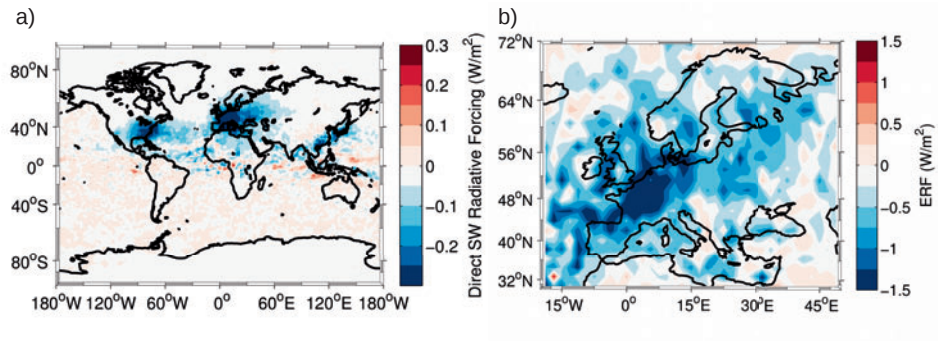

Figure 8: a) Global direct all-sky shortwave radiative forcing and b) effective radiative forcing in Europe if all nuclear power were to be replaced by coal power.

effective radiative forcing. Thus radiative effects due to the emissions are approximately 10 times higher near to the emission sources than the global averages. Increase of the energy produced by coal would also lead to an increase in GHG emissions. It has been estimated that GHG emissions from full life cycle of hard coal and natural gas technologies are 410-950 g/kWhel (Bruckner *et al.*, 2014). There are also some GHG emissions from nuclear energy which originate mainly from mining, milling, enrichment etc. By doing simple calculations (as in Paper II), it was estimated that replacing nuclear power by coal power would lead to 0.00168 to 0.00171 W/m^2 increase in the CO_2 radiative forcing every year for several decades. Since approximately half of the emitted CO_2 accumulates in the atmosphere, the positive radiative forcing from CO_2 would cancel out the negative (more instantaneous) aerosol forcing in 37 years, and thereafter accelerate climate warming. After 50 years, radiative forcing because of the increased GHG emissions would be increased by 0.085 W/m^2.

5 Solar radiation management

Paper I and Paper II reveal that aerosols have potential to cool climate, but the radiative forcing from current or near future anthropogenic emissions are small compared to the warming effect from GHG emissions. The indirect radiative effect also exceeded the direct effect from aerosols in both of the studies. Thus aerosols might prevent or significantly slow down climate warming, if aerosols were to be intentionally used to target the properties of clouds. The aerosol direct effect would also be a feasible way to cool climate if the aerosols had longer lifetimes which would be possible by emitting aerosols to the stratosphere.

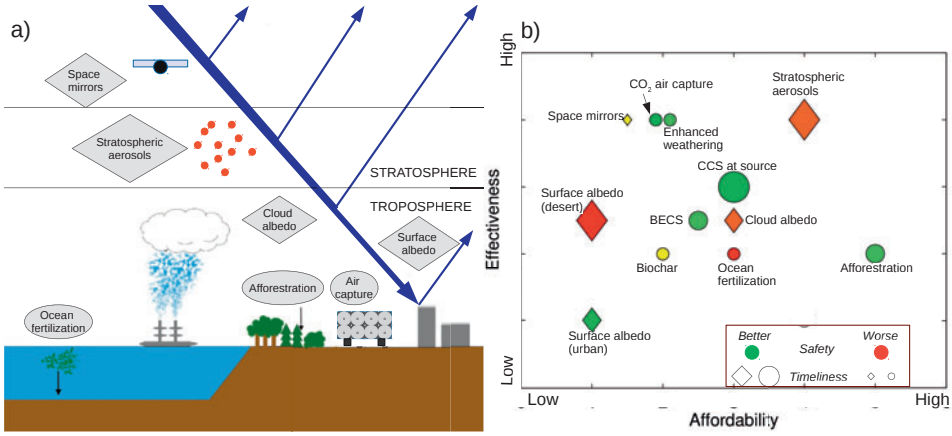

Figure 9: a) Figure of different geoengineering techniques at the different heights of the atmosphere. Figure is adapted from Lenton and Vaughan (2009). b) Evaluation of the geoengineering techniques. Figure is amended version of the Figure 5.1 in Royal Society (2009). SRM techniques are shown as diamonds and CDR techniques as circles.

Because reductions of GHG emissions have not been sufficiently successful, the idea has been put forward that it might be possible to cool the climate with aerosols (Crutzen 2006, Keith 2000). These kinds of actions are called geoengineering or climate engineering. The Royal Society has defined geoengineering as "the deliberate large-scale intervention in the Earth's climate system, in order to moderate global warming" (Royal Society, 2009). Thus it includes all the methods that aim to cool the climate, but excludes mitigation and carbon capture and storage (CCS). Generally geoengineering methods are divided into two groups. Methods that aim to increase the Earths reflectivity and shortwave radiation (blue arrows in Figure 1.) are called Solar Radiation

Management (SRM); these include techniques to add aerosols to the atmosphere and covering deserts with some kind of re ective material or placing mirrors in the space (Figure 9). Another group is referred to as Carbon Dioxide Removal (CDR). These techniques aim to remove carbon dioxide from the atmosphere and thus increasing of outgoing longwave radiation (red arrows in Figure 1.).

Both CDR and SRM include many innovative techniques. CDR techniques remove greenhouse gases from the atmosphere. Thus CDR techniques target the root cause of climate. This would decrease the probability of unpredictable risks. The aim in CDR methods is to enhance natural CO_2 sequestration through a modi cation of the physical, chemical, and biological processes that control the carbon cycle (Rickels *et al.*, 2011). Many of these methods aim to accelerate the rate of oceanic CO_2 uptake, for example by fertilizing marine phytoplankton. More CO_2 would also be captured from the atmosphere by a orestation. However capturing CO_2 from atmosphere is not very e cient with existing technologies and CDR methods only slowly exert any in uence on the climate system. Even though the climate risks are relatively small, CDR methods could impact on other natural systems of the Earth (Royal Society, 2009).

While CDR directly in uences the root cause of GHG-induced radiative forcing, SRM methods aim to compensate for the warming caused by GHG-induced radiative forcing by reducing solar radiation. Thus SRM methods do not prevent other consequences resulting from GHG for example, acidi cation of seas which is caused by high CO_2 concentration in the atmosphere and ocean. Methods also hardly a ect directly the altered LW radiation due to the increased GHG but instead would change SW radiation uxes. This would lead to a totally new state of climate where both LW and SW radiation uxes would be changed compared to the pre-industrial climate. When incoming SW radiation is reduced at the surface, plants would receive either less or more di used radiation (depending on which SRM method would be used) and this in turn would a ect their productivity (Kalidindi *et al.*, 2014). In addition, any reduction in the amount of radiation reaching the surface would have also impacts for example on solar energy production. Unlike CDR methods, many of SRM methods are generally rapid to implement and suspend and are usually cost ef- cient at least when compared with mitigation (Royal Society, 2009). However, the negative side e ects and risks are often larger than encountered with CDR methods. Figure 9b) shows evaluation of di erent geoengineering techniques based on the Royal Society (2009). Stratospheric aerosols have been speculated to be bene cial due to the e ectiveness, a ordability and the method would be fast to implement, but using would include many risks (section 5.4).

Similarly to stratospheric aerosols, modifying cloud albedo would also be relatively cost e ective but also has many negative side e ects. Since SRM does not a ect the root cause of climate warming (CO_2), SRM methods should be used only together with mitigation (or CDR).

There is also a third kind of group of geoengineering, thermal radiation management (TRM), which (similar to CDR methods) aims to increase outgoing LW radiation instead of decreasing incoming SW radiation (as SRM). High altitude ice clouds (cirrus clouds) obstruct both LW and SW radiation, but unlike low-level clouds, more outgoing LW radiation is blocked and this causes them to have a warming e ect (Lee *et al.* 2009). The magnitude of this e ect depends on the latitude of the clouds, their altitude, particle size, and the crystal structure of the ice (Zhang *et al.*, 1999). Mitchell *et al.* (2009) suggested that injecting certain types of ice nuclei would increase heterogeneous nucleation (nucleation on the surface of particle) in preference to the homogeneous nucleation which would lead to the production of larger ice particles. This would cause these ice particles to sediment more rapidly and would decrease the lifetime of cirrus clouds. Cirrus clouds could also be modi ed as a side e ect of stratospheric sulphur geoengineering (Kuebbeler *et al.*, 2012, Cirisan *et al.*, 2013). Thinning of cirrus clouds target mainly LW radiation, and thus the part of the radiation budget which is being changed by greenhouse gases, but not SW radiation, like SRM methods. One of the results is that cirrus cloud modi cation would manage to cool global temperatures, without reducing global annual mean precipitation rates, which is a phenomenon encountered in many SRM techniques (Chapter 5.4) (Muri *et al.*, 2014). However, Penner *et al* (2015) showed that the balance between homogeneous and heterogeneous ice nucleation is uncertain and therefore viability of cirrus cloud seeding is being debated.

A fast and su ciently large impact on climate temperature more likely could be achieved by SRM methods than CDR methods or cirrus cloud seeding. Depending on the method, the full implementation would take anything from one year to several decades (space mirrors). When a method is implemented, it is likely that the climate system would respond quickly and the surface temperatures return towards pre-industrial conditions (Royal Society, 2009). This work concentrates on to two SRM method, marine cloud brightening and stratospheric sulphur geoengineering.

5.1 Marine cloud brightening

It was observed in Papers I and II that an increase in aerosols emissions leads to more re ective clouds by increasing CDNC in the atmosphere. Most of the

Earths surface is covered by oceans. The albedo of the oceans is naturally low. This means that only a small fraction of radiation is re ected back to space over the oceans but also that the radiative e ects of aerosols and clouds are relative larger above the seas than above more re ective surfaces e.g. sea ice or snow. Approximately 23% of the oceans are covered by stratocumulus clouds (Wood, 2012) and CDNC is generally low in these areas. Thus these clouds are ideal for being subjected to cloud modi cation since increasing CCN concentration over these areas would lead to a relatively larger radiative e ect than increasing CCN in over some less re ective area.

5.1.1 Manipulating ship emissions

Clouds over the oceans are already modi ed by human actions, even though it has been done unintentionally. Approximately 90% of world trade is transported by the international shipping (ICS, 2014). Large numbers of vessels are sailing over the seas at any given time and all of these ships emit aerosols to the atmosphere. These aerosols change cloud properties and optically thicker clouds on the ship tracks compared to surrounding clouds can be seen, for example in satellite images (Campmany *et al.*, 2009).

There have been many estimations on how shipping emissions a ect clouds and the radiation. Calpaldo *et al.* (1999) estimated that aerosol indirect forcing would be -0.11 W/m^2, Lauer *et al.* (2007) assessed the value to be between -0.19 W/m^2 to -0.6 W/m^2 and Lauer *et al.* (2009) from -0.27 to -0.58 W/m^2. Fuglestvedt *et al.* (2007) estimated a clearly smaller value, -0.066 W/m^2. There are large uncertainties in the values, which depends on how the clouds, aerosols and emissions are calculated in the model. Peters *et al.* (2012) studied how the uncertainty in the size distributions of emitted aerosols, the amount of emissions and reducing carbonaceous emissions would a ect the estimates of the indirect e ect from the shipping emissions and end up estimations of global mean from -0.08 to -0.45 W/m^2. Despite the wide range of values, it is worth noting that all studies do seem to agree that present day indirect radiative forcing due to the shipping emissions is negative.

In the near future, aerosol-induced climate e ects from ship tra c will be decreased due to treaties to reduce the emission. Particulate emissions from internationals shipping are estimated to be responsible for 18 900 - 90 600 premature deaths per year (Corbett *et al.*, 2007; Winebrake *et al.*, 2009). In order to reduce the risk of premature mortality, treaties have been negotiated that will reduce shipping emissions in the future, especially the sulphur emissions. From the climate point of view, sulphate particles are e ective scatterers and

they have high hydroscopicity and their size is large enough that they can act as a cloud nucleus. Pollution of ships is regulated by the International Maritime Organization (IMO). This treaty determined that the global cap of fuel sulphur content would be 3.5% after the beginning of 2012 with clearly stricter restriction of 0.1 % in some areas of Europe and Northern America and progressive global cap reduction to 0.5 % until the year 2020 (Paper III). This would reduce premature mortality by several tens of thousands per year (Winebrake et 2009) but it has also estimated that it would halve the radiative forcing of shipping emissions (Lauer *et al.*, 2009).

Most of the shipping emissions originate around the coastal areas (Eyring *et al.*, 2010.). These areas are also close to populations and thus they exert a large e ect on mortality. In order to avoid negative health e ects, it is necessary that there will be a reduction of the emissions around the coastal areas. On the other hand, the emissions in the open oceans do not contribute substantially to the health e ects, because emissions are far away from population, but they could exert a signi cant e ect on the climate. Paper III evaluated the scenarios where shipping emissions would be regulated in areas near to the coast in order to improve air quality, but fuel with a higher sulphur concentration could be used in the open sea for cloud modi cation and bene cial climate e ects.

Figure 10 illustrates the main results from Paper III. Based on these simulations, the present-day ship emissions (2010, in gure 10) lead to approx. 50 000 premature deaths per year which is similar to the estimates in other studies (Corbett *et al.*, 2007; Winebrake *et al.*, 2009). Global mean e ective radiative forcing due to the shipping emissions is -0.39 W/m^2. After the restrictions, fuel sulphur content is reduced to 0.1 % and 0.5 % in coastal and open sea area respectively (2020 in Figure 10), almost all of the radiation e ect has disappeared and ship emissions lead to only -0.06 W/m^2 radiative cooling. However, mortality is reduced to only 4 % of the 2010 emission level. If the fuel sulphur content were to be restricted to 0.5% over a 400-600 km wide area (two grid cells of the model) in the coastal areas but the fuel sulphur content increased to 5.4 % over open oceans (GEO wide), then premature mortality would decline by almost 70% compared the present day ship emissions (2010). Since emissions are increased in the open seas, global mean e ective radiative forcing would be increased by 10%. Although emissions are reduced in a more narrow coastal area (200-300 km in GEO - narrow) and increased elsewhere, the mortality would be reduced by 30% from the present day and e ective radiative forcing due to the ship emissions would be -0.53 W/m^2.

The results in Paper III demonstrated both the climate and air quality bene ts that could be achieved if ship fuel sulphur content and the emissions were

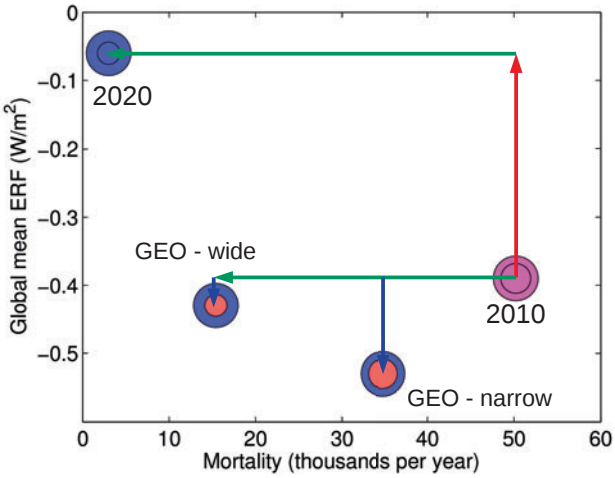

Figure 10: Global mean effective radiative forcing and yearly premature mortality due to the emissions from shipping. The value for 2010 represents the scenario where the sulphur content of marine fuel is 2.7 % in both coastal and open sea; in 2020, the sulphur content is reduced to 0.1 % and 0.5 % in coastal and open sea area respectively. GEO displays the scenario where sulphur content is increased to 5.4 % in open seas but reduced in wide (GEO - wide) or narrow (GEO - narrow) coastal areas to 0.1 %.

to be modified appropriately. However even if the fuel sulphur content is considerably increased, the total radiative effect would be only a small fraction of radiative warming effect due to the increased GHG concentration, if GHG emissions are not reduced significantly.

5.1.2 Sea spray injections

Latham (1990, 2008) proposed a method that uses sea salt particles to increase aerosol concentrations as a means of changing the albedo in marine boundary layer clouds. Salter *et al.* (2008) hypothesized that unmanned wind-powered vessels could operate open sea and inject seawater into the atmosphere. These sea water droplets/sea salt particles could act as additional CCNs and increase cloud albedo. Latham *et al.* (2008) calculated the global mean forcing to be -8 W/m^2 when a CDNC of 375 $cm^{-}3$ in all marine clouds below approximately 3 km was assumed; this value was compared to no seeding conditions, where global average CDNC was approximately 100 $cm^{-}3$. The radiative effects were

very di erent between the di erent regions. Regionally the largest forcing (over (30-50) W/m^2) was seen in three stratocumulus areas in the west coast of Africa and the west coasts of North and South America. Based on the publication of Latham *et al.* (2008), this kind of geoengineering would compensate for even the radiative forcing from a doubled CO_2 concentration (+3.7 W/m^2 (Forster *et al.*, 2007)). Jones *et al.* (2009) estimated that if injections were made in all stratocumulus regions (3.3 % of the Earth s Surface), the injection would lead to -1 W/m^2 global mean radiative forcing. If very high water droplet concentrations in stratocumulus region could be achieved, then global mean forcing could be somewhere between -2.5 and -3.9 W/m^2 (Rasch *et al.* 2009).

All of the studies mentioned above assumed that CDNC in the modi ed clouds would be uniformly set to a constant value and hence these models do not take account of aerosol microphysics, the emissions, wet and dry deposition and transport of arti cially produced sea salt particles. Korhonen *et al.* 2010 included these features in the chemical transport model mean and studied CDNC concentration when a wind speed dependent baseline geoengineering ux was applied over three persistent stratocumulus regions. That study revealed that the relative increase in CDNC over the stratocumulus regions would be increased by less than 20 % and even decreased (-2 %) in the North Paci c stratocumulus region (Korhonen *et al.*, 2010). The median background CDNC in the study was below 175 cm 3 and the authors concluded that it would be extremely di cult to achieve the previously assumed uniform distribution of high CDNC as proposed by Latham (2008). For example, large sea salt particles prevent smaller background particles from becoming activated by acting as a coagulation sink for the smaller particles but also lowering the maximum supersaturation in clouds (Korhonen *et al.*, 2010; Alterskj r and Kristjansson, 2013a; Partanen *et al.*, 2014).

Partanen *et al.* (2012) studied radiative e ects by using the global aerosol-climate model ECHAM5.5-HAM2 and similar sea spray uxes than Korhonen *et al.* (2010). This resulted in a clearly higher CDNC concentration (70 %-80 %) over the stratocumulus regions and -0.8 W/m^2 global mean e ective radiative forcing. They also revealed that the sea spray injections would exert also a considerable direct e ect, adding to the indirect e ect mediated via clouds. There are also many uncertainties related to size of the injected particles, background aerosol concentration, updraft velocity and cloud altitude which was seen in Partanen *et al.* (2012). Injected sea salt particles could a ect also other cloud properties in addition to CDNC. A high injection ux of small particles (Aitken mode) could lead to a decline in the Liquid Water Path (LWP) and eventually lead to positive forcing (Alterskj r and Kristjansson 2013a).

Based on these results, it is concluded that sea spray geoengineering would be probably less e cient than thought earlier.

5.2 Stratospheric aerosols

The previous chapters have examined four major problems or restrictions related to climate cooling with tropospheric aerosols:

Lifetime of emitted particles is short

Some particles also absorb the radiation and cause a warming e ect

Negative air quality e ects

Injected particles might decrease the cooling e ect of existing particles via clouds or act as a condensational sink

In the troposphere, particles are e ciently removed by wet and dry deposition and their lifetime is only a few days (Textor *et al.*, 2006). In the stratosphere, these mechanisms play no major role and particles are removed mainly by sedimentation (Rasch *et al.*, 2008). For this reason, for example the lifetime of sulphate particles from volcanic eruptions can be as long as one or two years (Robock, 2000). Because of the long lifetime, large volcanic eruptions are known to exert a signi cant e ect on the climate. From the geoengineering point of view, less particles would have to be injected into the stratosphere in order to obtain a similar radiative e ect than if they were delivered to the troposphere. Since the amount of injected aerosols would be small and the particles would be located in the stratosphere, the particles would not have any signi cant e ect on human health, even though health impacts would need to be considered in the cost-bene t analysis of SRM (E ong and Neitzel, 2016). At present, there is only a low concentration of stratospheric aerosols (in the Junge layer) with occasionally higher concentration of aerosols after volcanic eruptions. Thus aerosols originating from stratospheric injections would have a very limited probability of interacting with existing particles.

5.2.1 Volcanic eruptions

In Chapter 2.3, Figure 2 showed that there were several periods in the last century where major volcanic eruptions have led to climate cooling for the next 1-2 years after the eruption. This has been seen also much earlier; as many as

2000 years ago, it was observed that the Sun had dimmed after an eruption of Mount Etna (Forsyth, 1988). After industrialization (i.e. after the year 1850) there have been four eruptions (Krakatau 1883, Santa Maria 1902, Katmai 1912 and Pinatubo 1991) which have a volcanic explosivity index of over 5 and several smaller eruptions which have temporally cooled the climate (Robock, 2000). During a volcanic eruption, large amounts of sulphur and volcanic ash are blasted into the atmosphere and sulphur and ne ash particles reach the stratosphere. Larger particles stay in the troposphere where they have an impact on aviation and health. The resulting ash cloud is typically fairly local and short-lived. Guo *et al.* (2004a) have shown that volcanic ash was sedimented within the rst days after the Mt. Pinatubo eruption. Less than 5 % of the erupted ash was detected in the stratosphere after 5 days. However, a large fraction of sulphur reaches the stratosphere and once there it has an e ect on the climate. The sulphur is erupted as SO_2. In the stratosphere, this will oxidize into H_2SO_4 gas in a reaction with hydroxyl radical (OH). The oxidation time is dependent on the availability of OH in the atmosphere, which is further dependent on solar radiation and thus on the season, especially in high latitudes (Paper IV, Paper V). Based on Paper V, 80 % of SO_2 had been oxidized at three months after Mt. Pinatubo eruption. Gas phase sulphate either condenses to the existing particles or forms new particles by nucleation. When the sulphate particles have grown large enough, they scatter some of the solar radiation back to space and cool the climate. Because of Brewer-Dobson circulation, sulphur is prominently transported from the equator to the mid-latitudes and poles and is mainly removed from the stratosphere at high latitudes (Paper V; Rasch *et al.*, 2008; Kravitz *et al.*, 2009). Thus, the location of the eruption site has a major in uence on the lifetime of the erupted sulphur i.e. sulphur from the Arctic eruption has a clearly shorter lifetime than sulphur from a tropical eruption (Paper V). Model simulations of Pinatubo eruption (located at 15 N) have shown that over half of the erupted sulphur would still be in the atmosphere one year after the eruption (Paper V; English *et al.*, 2013; Dhomse *et al.*, 2014; Niemeier *et al.*, 2009; Toohey *et al.*, 2011).

Due to the seasonality of stratospheric circulation, sulphur transportation in the atmosphere is strongly related at the time of the year. For example, most of the sulphur from a Pinatubo like event (15 N) stays in the northern hemisphere if a volcano erupts in the boreal autumn or winter months whereas if the eruption occurs in spring or summer, this leads to a more even distribution of the sulphate cloud between hemispheres (Paper V; Toohey *et al.*, 2011). Paper V also shows that distribution of the sulphate cloud is dependent on the local winds over the eruption site at the time of the eruption.

5.2.2 Stratospheric sulphur injections and delivery methods

Based on measurements and the model simulations, stratospheric aerosols from large volcanic eruptions have been shown to cool the climate. This has been the source of the idea that climate could be intentionally cooled by mimicking volcanic eruptions and injecting sulphur into the stratosphere. By using Pinatubo as an analogue, Crutzen (2006) estimated that a source of 5 Tg (S)/yr would su ce to balance the warming associated with a doubling of CO_2. The rst model studies showed that this would require 1.5 - 5 Tg(S)/yr (Rasch *et al.*, 2008a; Robock *et al.*, 2008). However these models did not take into account aerosol microphysics and assumed that the aerosol elds consisted of sulphate particles with a xed size distribution. Even some of the latest studies have used this kind of idealized sulphate distribution where xed sized sulphate particles are distributed uniformly to all latitudes (Modak and Bala, 2013; Kalidindi *et al.*, 2014). The climate impacts of stratospheric sulphur emissions are also often assessed as decreasing the solar constant (Kravitz *et al.*, 2013b). This corresponds more closely to space-based SRM than stratospheric sulphur geoengineering where sulphur injection leads to a non-uniform distribution of both particles and radiation uxes reductions. Studies where aerosol microphysics have been simulated have indicated that the particles size utilized in the rst studies was too small, which then overestimated radiative forcing from particles and, in reality, larger sulphur injections would be required.

The idea of injecting sulphur into the stratosphere to cool the climate is not new. In the 1970s, Budyko (1974) suggested that sulphur from the jet fuel of civil aircraft could cause climate cooling. However this would require that the planes were Concorde-type supersonic aircraft ying at a stratospheric altitude. Even although supersonic planes are no longer in commercial use, in the future this kind of aircraft might again become a reality. Similarly to the enhancement of fuel sulphur concentration examined in Paper III, also aircraft fuel sulphur concentration could be enhanced and geoengineering could be done as a by-product of normal civil air tra c.

Paper IV investigated the cooling potential of civil air tra c in scenarios where most long-distance ights would be own in the stratosphere and the fuel sulphur concentration would be enhanced. The study assumed that the fuel would contain the current the average sulphur concentration i.e. 0.06% (Barret *et al.*, 2010). If all air tra c ew in the stratosphere instead of the troposphere only 0.06 Tg (S) would be injected yearly into the stratosphere. For example, this would be a small amount compared to sulphur from a large volcanic eruption and the e ect to the all-sky radiation at the surface would be only -0.05 W/m^2. Thus, the fuel sulphur concentration would have to be increased signi cantly

in order to achieve a substantial cooling effect. The current legal limit for sulphur concentration in the fuel used in aviation is 0.3% (Penner *et al.*, 1990). This means that within the legal limits, five times enhanced sulphur concentration could be legally used. However based on simulations, all-sky radiation at the surface would still be only -0.1 W/m^2. This means that sulphur concentrations would need to be enhanced clearly over the current limits if they are to have any substantial climate impact. Were the sulphur concentration to be enhanced by a factor 50, cooling from the stratospheric air traffic would be -0.85 W/m^2 which is high enough that it could be considered to exert a significant effect on temperature at the surface of the Earth.

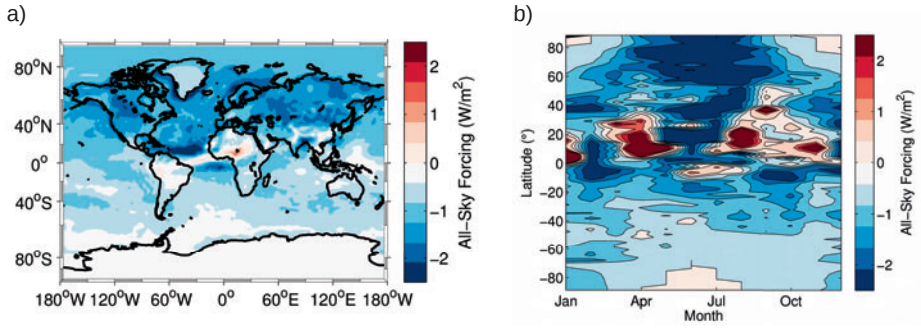

Figure 11: a) The five year mean and b) the seasonal variation of the zonal mean of all-sky SW direct radiative forcing if 50 times current fuel sulphur concentration is used in the air traffic.

The cooling due to the increased sulphur emissions from the air traffic is unevenly distributed between different regions. Most of the air traffic is concentrated in the northern mid-latitudes and thus yearly mean radiative forcing is concentrated on the northern hemisphere and the boreal summer months, when solar intensity is higher (Figure 11). Yearly average solar intensity is highest at the equator, thus injections at the lower latitudes would be more effective for geoengineering purposes. Based on RCP8.5, by 2050 it is estimated that air traffic will increase in the lower latitudes of Asia, Africa and South America. Based on the simulations conducted in Paper IV, five times enhanced fuel sulphur concentration would lead to -0.38 W/m^2 global mean direct radiative forcing. This means that the relation of forcing/injected sulphur is 70% larger with 2050 routes than by current flight routes with maximum legal limit of fuels sulphur. If the same amount of sulphur were to be injected continuously over the equator (thus not by using commercial air traffic) than was resulted if fuel sulphur concentration is enhanced by a factor of 50, global mean radiative direct forcing would be 55% larger (Paper IV).

Since current civil air tra c is concentrated in the northern hemisphere, if one wishes to have a more uniform radiative e ect between the hemispheres, then some other delivery method would be required for the injections. Delivering sulphur to the stratosphere is very challenging due to the high altitude and amount of required sulphur. However several methods have been suggested, in addition to commercial supersonic aircrafts. In the future, the development of lighter and stronger materials could make it possible to build very high towers for the injections and furthermore guns, rockets and tethered balloons could perhaps be used (Robock *et al.* 2009). McClellan *et al.* 2012 estimated that custom aircraft specially designed for geoengineering would be the most cost e cient option. Generally, the direct costs of injecting sulphur to the stratosphere have been considered to be low compared to the costs of climate changes or the mitigation of greenhouse gas emissions (Barrett 2008, Royal Society 2009).

5.2.3 Climate cooling due to the high sulphur concentration in the stratosphere

If stratospheric sulphur injection is ever going to be used, there might temporally be the situation when the aerosol concentration in the stratosphere would be very high. Stratospheric sulphur injection would most likely be ongoing for decades and it is highly possible that a large eruption similar to Mt. Pinatubo would happen during this time. If this is happened, there would be a cooling e ect from both aerosols from the volcanic eruption and from the stratospheric sulphur injections. However, the cooling e ect from the volcanic eruption cannot be straightforwardly estimated based on an eruption occurring in current background atmospheric conditions, when the stratosphere is relatively clean of particles. During SRM, there would already be a large amount of sulphate in the stratosphere prior to the eruption, and these particles would interact with the sulphur from the eruption.

Paper V studied radiative e ect and climate impacts after a volcanic eruption in a scenario where there was geoengineering. Figure 12 shows the global mean direct radiative forcing (solid lines) after the Pinatubo-like eruption compared to the pre-eruption level. The black line shows the radiative forcing in unperturbed atmospheric conditions and the red line during the stratospheric sulphur injections. As the gure shows, peak forcing is 32% smaller and additional radiative forcing disappears clearly faster if the volcano erupts concurrently with the stratospheric sulphur injections. This means that cooling is signi cantly smaller (dashed lines). The simulations with a volcanic eruption

in background atmospheric conditions lead on average to -0.27 K cooling in the three years following the eruption. In the case of an eruption occurring during the SRM, cooling would be only 2/3 of this value. In reality, due to safety and economic considerations, it might be that SRM would be suspended at some point after the eruption. If SRM injection is suspended immediately after the eruption, there will be only minor cooling (blue lines) and the climate would start to warm at about 10 months after the eruption.

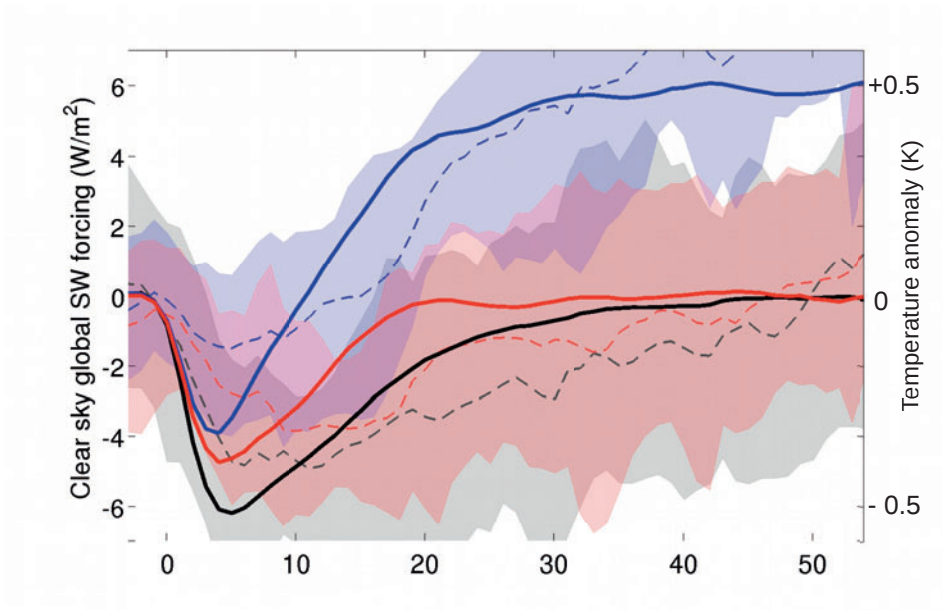

Figure 12: 5-months' running global mean of all-sky radiative forcing (solid lines, left axis) and ensemble mean temperature (dashed lines, right axes) compared to pre-eruption level. Shaded area shows values between the maximum and minimum global mean temperatures of the 10 simulations ensemble. Black line shows radiative forcing and 2-m temperature after volcanic eruption in unperturbed stratospheric conditions, red and blue during SRM when sulphur injections are continued (red) and suspended immediately after eruption (blue).

As the results are very different if one simulates the outcome of a volcanic eruption in normal unperturbed conditions in comparison with one happening during SRM, it is concluded that the stratospheric sulphur injections must have affected the fate of sulphur from the eruption. Were the volcano to erupt when there had been stratospheric sulphur injection, some of the sulphur from the eruption would condense with the existing particles. If new particles are

formed, these would coagulate e ectively with the existing large particles in the stratosphere. This same phenomenon would happen to the sulphur which would be injected into the stratosphere after the eruption, if SRM injections still continued. This leads to a larger size and smaller amount of particles compared to particles from the eruption in unperturbed stratospheric conditions. Then there are relatively less particles in the atmosphere and these particles have also smaller scattering e ciency and larger gravitational settling velocity (Figure 3). The larger gravitational settling velocity leads to a lower lifetime of sulphur in the stratosphere (Paper V) which explains why the cooling effect would disappear faster if a volcanic eruption takes place at a time when there have been stratospheric sulphur injections (Figure 12). In addition, this sulphur from SRM would absorb radiation and thus warm the stratosphere which may have minor e ect on the transportation properties of the particles originating from the eruption.

The high sulphur concentration might result from stratospheric sulphur injections only and does not necessarily require a large concurrent volcanic eruption. For example, this could be the case if GHG emissions are not reduced, and stratospheric sulphur injection is the only approach taken to keep the temperature of the climate at the current level. Thus, compensating for the warming e ect from continually increased GHG concentration would require that more and more sulphur would have to be injected into the stratosphere. Similarly to a volcanic eruption during the sulphur injections, this would lead to relatively larger and larger particles and the global mean radiative forcing would not increase linearly with the amount of injected.

Niemeier and Timmreck 2015 have studied how radiative forcing would increase if the amount of injected sulphur was increased much more than the values currently being considered. Their results showed that the LW radiative forcing of aerosols increases rather linearly with the amount of injected sulphur but the ratio between sulphate aerosol SW forcing and injection rate decays exponentially. Thus the ratio of total forcing and injection rate also decays exponentially and stratospheric sulphur injections would not be so e ective if GHG emissions are not reduced i.e. attempts are made to prevent the temperature increase exclusively by stratospheric sulphur injections. These results also imply that the amount of injected sulphur required to keep temperatures constant after 2020, without reduction to GHG emission (RCP8.5), would be roughly 45 Tg(S)/yr at the end of this century. Based on RCP8.5 scenario, the global SO_2 emissions would be slightly over 10 Tg(S)/yr (Riahi *et al.*, 2011) before the end of this century. Thus compensating for warming only by stratospheric sulphur injections would have increased global emission of SO_2 by 450 % by the year 2100.

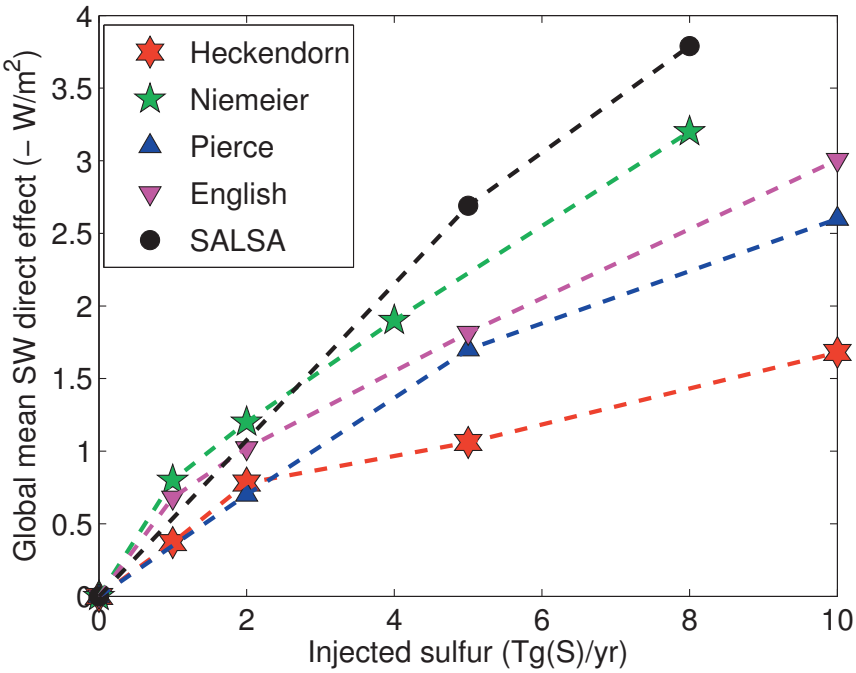

Figure 13: Top of the atmosphere SW radiative uxes for di erent injection rates. Note that injection areas and height is not necessarily the same between the models. SALSA shows results from ECHAM6.1-HAM2.2-SALSA when sulphur is injected between 10 N and 10 S latitudes and the 21 km height (Laakso *et al.*, 2015). Radiative forcing was not calculated in English *et al.* (2013), and the values are calculated from sulphate burden and relation of forcing to burden in SALSA.

The results of direct radiative forcing due to the high sulphur concentration depend on how and where sulphate is injected and also details of the model used in simulation (Figure 13). A higher injection height increases the lifetime of particles and leads to larger global mean forcing (Niemeier *et al.*, 2011). Niemeier *et al.* (2011) also suggested that sulphur injections into a narrow band along the equator would lead to larger global mean radiation than distributing sulphur injections over a wider area. (Niemeier *et al.*, 2011). However Niemeier *et al.* (2011) used the modal aerosol model (see chapter 3.2) and simulations in sectional aerosol models instead of the modal (English *et al.*, 2012 or ECHAM with sectional microphysics SALSA (not shown)) indicate the opposite. Pierce *et al.* (2011) and Heckendorn *et al.* (2009) have used a used

a 3D chemistry climate model, where aerosol elds and size distributions are prede ned by a zonal mean aerosol model. Niemeier *et al.* (2011) used 3D aerosol-climate model ECHAM with the modal aerosol schema. The curve denoted as SALSA in Figure 13 shows the results from same climate model (ECHAM) but where the aerosol size distribution is described sectionally. The global mean radiative forcing from the results simulated by SALSA are larger than those reported by English et al. (2011), where a sectional aerosol microphysics model was also used with a 3D climate model. However even though the variations in the results between the models are large, all of the models demonstrate the saturation of the forcing while increasing the amount of injected sulphur. This also demonstrates that aerosol microphysics makes a signi cant contribution to the resulting radiative e ect and therefore it should be included in geoengineering studies.

5.2.4 Alternatives to injection of SO_2

All of the studies presented above concern injections of SO_2. However there are alternative sulphur components in addition to SO_2. One option would be injections of hydrogen sulphide (H_2S) (Crutzen *et al.*, 2006; Volodin *et al.*, 2011; Izrael *et al.*, 2013). Bene t from using H_2S compared to SO_2 is that its sulphur content is larger. Thus less mass would be required to be injected in order to acquire the same amount of sulphate particles because there is already available hydrogen and oxygen in the atmosphere. H_2S is oxidized to SO_2 within one or two days (Rasch *et al.*, 2008). Thus sulphur would exist for a longer time in the gas phase compared to the situation when sulphur is injected as SO_2 and it would be dispersed better after the injections. This would reduce self-coagulation and achieve a higher particle concentration (Volodin *et al.*, 2011). One of the problems in using H_2S instead of SO_2 is that H_2S is more corrosive than SO_2 (Kleber *et al.*, 2008; Robock *et al.*, 2008a). It is also lethal at fairly low concentrations (Kilburn and Warshaw, 1995) for example, it was used as a chemical weapon in World War I (Croddy *et al.*, 2001).

Since injections by SO_2 or H_2S tend to produce large particles (that are sedimented quickly) when the amount of injected sulphur is increased, Pierce *et al.* (2010) suggested injections by H_2SO_4 gas. A high initial H_2SO_4 concentration favours nucleation over condensation; this results from its smaller size and larger number of particles compared to injections by SO_2 (Pierce *et al.*, 2010; Niemeier *et al.*, 2011). It was predicted that this would produce more and smaller particles compared to injections by SO_2 or H_2S. Pierce *et al.* (2010)

hypothesized that this might increase global mean radiative forcing by up to 77 % if 10 Tg(S)/yr were to be injected. However, with a smaller injection rate, this di erence attributable to the injected species, became smaller. This can be seen in Paper IV where the scenario where current fuel sulphur concentration in aircraft fuels was enhanced by a factor 50 was repeated by injecting sulphur as H_2SO_4 (corresponds to the immediately oxidation of SO_2 in the aircraft plume) instead of SO_2. Global mean forcing was increased by 33%. However in the southern hemisphere, where there is clearly less air tra c and the emitted sulphur concentration was low, the extent of forcing was rather similar regardless of which chemical form of sulphur compound was being injected. In the northern mid-latitudes, where air tra c is concentrated, injection of H_2SO_4 leads to radiative forcing which was roughly 60% higher at some latitudes than could be achieved from injections by SO_2. However, it should be noted that the simulations are done by global model where size of the grid box is several thousand square kilometers and model assumes instant mixing after the injections. Thus model does not take account of the sub-grid particle formations in injection plume which is crucial factor for particle formation and the resulting size distribution of sulphate particles. Overall, the injection as H_2SO_4 might be the more e ective for geoengineering than injection by SO_2 if a large amount of sulphur had to be injected. However, a problem arises from the need to transport sulphur to the stratosphere, because the sulphur content is much smaller in H_2SO_4 than in the SO_2 molecule.

It has also been proposed than di erent substances other than sulphur could be used. Fujii (2010) proposed that limestone powder instead of sulphur compounds. Sulphate would cause some environmental problems such as acid rain. In contrast to sulphur, limestone would mitigate acidi cation of lakes (Guhren *et al.*, 2006). In addition, black carbon injection has been studied but this would result in extensive warming in the stratosphere (Ferraro *et al.*, 2011; Kravitz *et al.*, 2012; Jones *et al.*, 2015) because black carbon e ectively absorbs radiation. There are also many other alternatives, such as titanium dioxide which is a good scatterer, but would not a ect the ozone layer in the same way as sulphur compounds (Pope *et al.*, 2012; Jones *et al.*, 2015). Keith *et al.* (2010) proposed speci cally engineered particles levitating by photophoretic forces. Weisenstein *et al.* (2015) suggested also solid particles as alumina or diamond particles which would be coated with liquid sulphate when injected into the atmosphere. Their presence would result in similar forcing as obtained with sulphur injections but produce less extensive ozone loss, less stratospheric heating, and less forward scattering.

5.2.5 Termination e ect

Stratospheric aerosols injection would lead to a signi cant cooling within a few months (depending on the injected aerosols or precursor gases) after implementation. However the lifetime of sulphur in the stratosphere is roughly one year. Thus if injections were abruptly suspended, the sulphate particles would be removed from the atmosphere after a relatively short time. This type of fast disappearance of the cooling e ect after the suspension of the method was seen regardless of the SRM method used (excluding levitating particles which would stay several years in the atmosphere). If the CO_2 concentration in the atmosphere is not decreased by reducing emissions or CDR methods, and if warming is compensated by SRM, the temperature would increase very rapidly in the years following suspension and within a few decades, the level would be back to where it would have been without SRM (Jones *et al.*, 2013; Alterskjr *et al.*, 2013b; Aswathy *et al.*, 2015). However, the warming rate would be clearly faster than if it were attributable to the increased GHG concentration and without the SRM. In addition, the suspension of solar radiation management would also be followed by increases in global-mean precipitation rate and a decrease in the sea-ice cover. It would be much more di cult for humans, animals and ecosystem to adapt to this kind of rapid global change, especially the regional changes, in the climate conditions than to a lower rate warming because of increased GHG concentration (Davis and Shaw, 2001; Jones *et al.*, 2013).

However, in some situations, the rapid recovery from SRM could be bene cial. As was discussed earlier, volcanic eruptions will always occur, but their size and timing cannot be predicted. Volcanic eruptions do a ect the climate and sometimes they lead to substantial disruption to human civilization (Self 2006; Fuglestvedt *et al.*, 2014). In a world with SRM, it would be possible compensate for cooling from an eruption by quickly suspending SRM. For example, in gure 12, the blue solid line shows the radiative forcing compared to the pre-eruption level in the scenario where stratospheric sulphur injection are suspended immediately after the eruption. As the gure shows, radiative forcing in the simulated scenario returns back to the pre-eruption level within 10 months. Peak forcing also would be only 60% from the eruption in normal unperturbed atmospheric conditions. This would lead to only 0.1 K global mean temperature cooling for the year after the eruption. After that, the climate would start to warm rapidly and thus stratospheric sulphur injection would need to be restarted rather soon after its suspension in order to prevent the climate from warming.

5.3 Risks of Solar Radiation Management

Solar radiation management includes many risks and undesired consequences. As discussed in the previous chapter, the termination e ect (5.3) would be one possible risk. Furthermore, an increase in surface area of sulphate particles in the atmosphere together with cold temperatures would enhance the destruction of the ozone layer (Tilmes *et al.*, 2008, 2009). In addition, a change in the atmospheric temperature pro le due to the absorption of particles and the subsequent increase of stratospheric H_2O could decrease the stratospheric ozone level (Heckendorn *et al.*, 2009). Another consequence related to the use of sulphur, is acid rain and acidi cation of lakes and forests. However, the sulphur mass injected into the stratosphere would be relatively small compared to the current anthropogenic emissions and acidi cation would not be a larger threat than it is today (Kravitz, 2009). Nevertheless stratospheric sulphur injections have been shown to aggravate acidi cation of the deep ocean (Tjiputra *et al.*, 2016).

One fundamental problem related to solar radiation management is that it a ects the incoming shortwave radiation in the atmosphere (blue arrows in Figure 1) whereas GHG absorbs the outgoing longwave radiation (red arrows). The rst consequence of this phenomenon would be di erent geographical distributions of the solar and greenhouse gas forcings. As seen in the previous chapters, SRM a ects the radiation more in the areas where solar intensity is stronger. This is dependent of latitude and the season, but the annual average of solar intensity is the largest in the equator and clearly smaller near the poles. Thus a uniform percentage reduction in solar radiation a ects mainly the latitudes closer to the equator while the largest warming is encountered at the higher latitudes (Royal Society, 2009). Outgoing longwave radiation, which is absorbed by GHG, is related to the temperature of the surface. Thus the intensity of outgoing LW radiation is also stronger at the lower latitudes than at higher latitudes, but the di erence in the intensity of radiation between these latitudes is not as large as for incoming solar radiation (Jacobsen, 2005). Thus compensating change in the global mean radiation ux caused by increased GHG concentration with a uniform percentage reduction in solar radiation leading to a situation, where the low latitudes would cool whereas high latitudes would warm even though the global mean temperature change is being compensated (Kravitz *et al.*, 2013b; Schmidt *et al.*, 2012). It should be noted that a uniform percentage reduction of the solar constant corresponds to the situation envisaged with space mirrors but not for example, stratospheric sulphur injections where solar reduction would be zonally quite di erent. The same fundamental problem of uneven latitudinal temperature changes exists

also in the case of the sulphur injections and might be even worse since the sulphur burden would be more concentrated in the low than in the high latitudes (Paper IV, V). However, an unrealistic scenario where stratospheric sulphur injections have been done without climate warming would lead to a larger cooling at the high latitudes than low latitudes, even though the reduction in radiation is larger at high latitudes (Paper V). This Arctic ampli cation is also seen in climate warming and it is not only due to a reduction of snow and ice cover but also to the temperature feedbacks (Pithan and Mauritsen, 2014). Overall, the compensating increase in LW radiation zonally by reducing SW radiation would be very challenging, especially in the polar areas where the intensity of SW radiation is low especially in the winter season.

Another consequence is related to the hydrological system and precipitation (Kravitz *et al.*, 2013c). Greenhouse warming increases speci c humidity and the global mean precipitation. However solar radiation management would decrease the global mean evaporation and precipitation (Paper V; Kravitz *et al.*, 2013c). If GHG warming is compensated by SRM, the decrease in the precipitation due to SRM would be larger than any increase due to GHG (Laakso *et al.*, 2015; Ricke *et al.*, 2010; Kravitz *et al.*, 2013b). In global terms, this would lead to a drier world. Locally the consequences might be much more devastating than evident from the global mean. For example, Robock *et al.* 2008 have shown that SRM would in uence the monsoons and reduce precipitation due to the decreased temperature gradient between Asia and Europe and the Indian and Atlantic Oceans (Oman *et al.*, 2006) and thus it would exert a signi cant e ect in many highly populated areas.

Reducing shortwave radiation might also a ect the atmospheric circulation. The stratospheric sulphate a ects precipitation via two climate system responses. The rst one is the rapid adjustment (fast response) due to atmospheric forcing (change in solar irradiance and absorption of radiation) and this occurs in a short time scale (Huneeus *et al.*, 2014). For example, this e ect is seen immediately after the volcanic eruption (Paper V). The second one is the feedback response (slow response) which is due to temperature changes (Paper V; Bony *et al.*, 2013; Ferraro *et al.*, 2014; Fuglestvedt *et al.*, 2014; Kravitz *et al.*, 2013c). The tropical circulation is weakening due to the climate warming (Held *et al.*, 2006; Vecchi *et al.*, 2007), because mid-troposphere is warmed more than the surface due to the increased GHG concentration (Knutson and Manabe, 1995). Compensating warming by stratospheric sulphur geoengineering does not prevent this, because of the radiative heating (fast response) from the aerosol layer (Ferraro *et al.*, 2014). This suppressing convection and further reducing precipitation.

As mentioned earlier, due to the reduction in incoming SW radiation, plants would receive either less or more di used radiation, which would then a ect their productivity. In addition, plants would be a ected not only by changes in precipitation and evaporation, surface temperature, and carbon and nitrogen cycle due the solar radiation management but also by fertilisation due to the increase in atmospheric CO_2 concentration which has caused the warming of the climate. Solar radiation management together with increased CO_2 concentration might a ect agricultural productivity (Xia *et al.*, 2015) and also increase the terrestrial photosynthesis rate (Xia *et al.*, 2016). However, as vegetation is dependent on many di erent factors, the estimates about vegetation response remain uncertain until all main processes, that a ect the vegetation, can be properly simulated (Glienke *et al.*, 2015).

The consequences of SRM depend strongly on where SRM is implemented. Large asymmetric radiative forcing between the hemispheres has been shown to a ect the zonal temperature gradient, Hadley circulation and intertropical convergence zone (ITCZ). This would cause a shifting of the monsoon circulation and would have further impacts of Sahelian rainfall (Haywood *et al.*, 2013). Paper V revealed that solar radiation management and a volcanic eruption would lead to altered precipitation patterns. According to the simulations, temperature gradients between the tropics and mid-latitudes are di erent in the case of a volcanic eruption, stratospheric sulphur injection and also for a volcanic eruption occurring during a time of stratospheric sulphur injections. Thus precipitation changes due to the stratospheric sulphur injection are dif- cult to predict, for example if based on the present observations after Mt. Pinatubo.

Overall compensating for changed climate due to GHG with SRM would be very di cult. Even if globally SRM would bring the world closer to current conditions, the regional impacts on the climate might be even worse than without SRM and the optimal magnitude of geoengineering would be dependent on the region (Irvine *et al.*, 2010; Ricke *et al.*, 2010; Kravitz *et al.*, 2014). This would give rise to other problems which are not related to the climate science, for example who would decide when and where climate engineering should be deployed. It would be very challenging to nd a geoengineering strategy that would be bene cial for all nations, but there might be coalitions of nations who could be happy to desire certain climate outcomes and powerful enough to deploy solar geoengineering (Ricke *et al.*, 2013). One concern related to geoengineering is the concept of geoengineering itself, which has been called a moral hazard. The willingness of people and governments to reduce emissions might be lost if there were thought to be alternative ways to cool the climate (Lin, 2013). However, as has been shown in this work and in several

other studies, the SRM cannot compensate for the e ects from increased GHG emissions and thus it cannot be viewed as an alternative to emission reduction (Kravitz *et al.*, 2013b; Niemeier and Timmreck, 2015)

6 Review of papers and the author s contribution

The author alone is responsible for writing this introductory part of thesis

Paper I

T. Kuhn, A.-I. Partanen, A. Laakso, Z. Lu, T. Bergman, S. Mikkonen, H. Kokkola, H. Korhonen, P. Raisanen, D. G. Streets, S. Romakkaniemi, and A. Laaksonen Climate impacts of changing aerosol emissions since 1996. *Geophys. Res. Lett. 41*, 13, 4711-4718, doi:10.1002/2014GL060349, 2014.

Overview: Paper I studies the radiative forcing and climate responses caused by anthropogenic sulphur, black and organic carbon emission change between the years 1996 and 2010. Simulations are conducted by the aerosol-climate model ECHAM5.5-HAM2. The aerosols radiative forcings are de ned by using xed sea surface temperature and climate e ects by using a slab ocean model. The results show that increased Asian emissions have very little regional or global climate e ects, but reductions of emission in Europe and U.S have caused a small positive radiative forcing. Globally this led to 0.42 W/m^2 e ective radiative forcing and thus to climate warming. The geographical change of emissions does not explain the slowing down of global warming which has been seen in the beginning of this millennia.

Author contribution: The author was responsible for tuning the model and participated in interpreting the results.

Paper II

T. Mielonen, A. Laakso, A. Karhunen, H. Kokkola, A.-I. Partanen, H. Korhonen, S. Romakkaniemi and K. E.J. Lehtinen From nuclear power to coal power: Aerosol-induced health and radiative e ects *J. Geophys. Res. Atmos., 120,* 12,631-12,643, 2015.

Overview: ECHAM6.1-HAM2.3-SALSA is used to investigate the climate and PM-induced air quality e ects should all nuclear reactors worldwide be replaced by coal power. This would cause 150 000 premature deaths per year, two-thirds of which would occur in Europe. Increased particulate emissions would also cause a small climate cooling e ect which would be compensated after 37 years by the accumulated CO_2 emissions from the coal plants.

Author contribution: The author participated in implementing SALSA to ECHAM6.1-HAM2.3, carried out the model runs and participated in

analysing the results and writing of the paper.

Paper III

A.-I. Partanen, A. Laakso, A. Schmidt, H. Kokkola, T. Kuokkanen, J.-P. Pietikainen, V.-M. Kerminen, K. E. J. Lehtinen, L. Laakso, and H. Korhonen Climate and air quality trade-o s in altering ship fuel sulfur content. *Atmospheric Chemistry and Physics 13*,12059-12071, doi:10.5194/acp-13-12059-2013, 2013.

Overview: Paper III presents the climate and air quality trade-o s in the alternative shipping emission scenarios. Simulations are conducted by the aerosol-climate model ECHAM5.5-HAM2. The scenario is one where strict emission limits for fuel sulphur content would be applied in the coastal areas butemissions would be increased in the open sea and this is compared to current emissions and the reduced emission in the future. With this kind of scenario, it would be possible to retain the current climate cooling e ect but signi cantly decrease premature deaths caused by shipping emissions.

Author contribution: The author analysed the results from the preliminary model runs, performed the model-observation comparison for particulate matter and participated in analysing the results and writing of the paper.

Paper IV

A. Laakso, A.-I. Partanen, H. Kokkola, A. Laaksonen, K.E.J. Lehtinen and H. Korhonen. Stratospheric passenger ights are likely an ine cient geoengineering strategy. *Environ. Res. Lett.* *7*, 034021, doi:10.1088/1748-9326/7/3/034021, 2012.

Overview: Paper IV investigates geoengineering by stratospheric sulphur injections where the injections are carried out by enhancing fuel sulphur concentration of commercial air tra c ying at a higher ight altitude. The results show that a moderate climate e ect would be achieved only if the fuel sulphur concentration would be allowed to be increased clearly over the current legal limits. Nonetheless, the cooling e ect is concentrated mainly in the northern hemisphere. Simulations are carried out with the aerosol-climate model ECHAM5.5-HAM2.

Author contribution: The author designed the experiments, implemented stratospheric emissions to the models, and carried out the simulations. The author is also responsible for the data analysis and the writing of the paper

with help from the co-authors.

Paper V

A. Laakso, A.-I. Partanen, U. Niemeier, C. Timmreck, H. Kokkola, K. E. J. Lehtinen, H. Hakkarainen and H. Korhonen E ects of concurrent stratospheric sulfur geoengineering and large volcanic eruption, *Atmospheric Chemistry and Physics 16*, 305-323, doi:10.5194/acp-16-305-2016, 2016.

Overview: Climate impacts of large volcanic eruption during the stratospheric sulphur injections are studied. Aerosol elds and radiative properties are rst de ned by aerosol-climate model ECHAM5-HAM-SALSA. These elds are then included into the climate simulations by Max Planck Institutes Earth System Model (MPI-ESM). Results showed that an eruption during stratospheric sulphur injections leads to a smaller amount but larger sulphate particles in the stratosphere, and therefore cooling is smaller than in the case of volcanic eruption in the unperturbed stratospheric conditions. It was also found that an explosive eruption could lead to signi cantly di erent regional climate responses depending on whether or not it takes place during geoengineering or into an unperturbed background atmosphere. This implies that observations from previous large eruptions are not directly applicable when estimating the potential consequences of a volcanic eruption during stratospheric geoengineering.

Author contribution: The experiments were designed by author. The author implemented the aerosol elds from the ECHAM-HAMMOZ to MPI-ESM. The author is responsible for the simulations, the data analysis and the writing of the paper with help from co-authors.

7 Discussion and conclusions

This work has investigated the potential of exploiting aerosols to compensate for global warming. This has been done mainly by using the global aerosol climate-model ECHAM-HAMMOZ and with Max Planck Institutes Earth System Model in Paper V. The aims of this work were to:

Investigate the potential of aerosols to cool the climate at the global scale

Evaluate the role of the simulation of the aerosol microphysics in the global climate models

Identify the possible limits in the e ectiveness of the Solar Radiation Management techniques as well as risks related to these techniques.

The work presented here supports the earlier estimations and research that aerosols have a signi cant e ect on the climate. Anthropogenic emissions from shipping (Paper III), air tra c (Paper IV), industry (Paper I), and energy production (Paper II) have been shown to cool climate directly by scattering solar radiation back to space and indirectly by changing the properties of clouds. However, currently our warming e ect from GHG emissions exceeds the cooling e ect from aerosol emissions and even large scale changes in geographical distribution of emissions (Paper I) have not been able to slow down the global warming. This work investigates also large changes in energy production i.e. a scenario where global energy production by nuclear power would be replaced by coal power. Based on the outcomes of the simulations, this would lead to a temporal cooling e ect due to the increased aerosol emissions but after several years, the warming e ect from simultaneously increased GHG emission would exceed the cooling e ect (Paper II). Furthermore, as was shown in Papers II and III, the cooling from aerosols is often achieved at the cost of air quality. An increase in these kinds of emissions could lead to an increase in premature mortality (Paper II). This is the reason why aerosol emissions should be reduced. However, the reduction in the emissions from shipping would lead to a loss of the cooling e ect due to the aerosols and accelerate global warming (Paper III). Papers II and III showed that air quality and premature mortality are most a ected by the emissions from continents and near coastal area. Thus, it could be possible to retain current cooling e ect from shipping emissions, for example by reducing emissions from near to the coastal area but increasing it in the open sea (Paper III).

Due to the clearly longer lifetime, the stratospheric aerosols have a larger potential to cool climate than the corresponding tropospheric aerosols. In

addition, the stratospheric aerosols do not a ect health related air quality. However, increasing the radiative impact of the stratospheric aerosols with the help of commercial air tra c would require lifting the ight altitude to the stratosphere as well as a major enhancement in the fuels sulphur concentration as well as repealing of current legal restrictions before one could obtain any signi cant cooling e ect. Furthermore, the cooling would be restricted to those areas where air tra c is concentrated, which currently is located mainly in the northern hemisphere (Papers III, IV). Based on this work, the largest cooling e ect by aerosols can be achieved by injecting aerosols into the stratosphere and tropics where solar radiation is on average at its largest.

This work shows the necessity of including aerosol microphysics into climate modelling i.e. most of the conclusions in this work could be obtained without aerosol microphysics or taking into account the interactions between clouds and aerosols. For example, Paper V showed that radiative and climate effects from volcanic eruption would be clearly di erent depending if the eruption took place in unperturbed stratospheric conditions or during stratospheric sulphur geoengineering. These di erent global climate impacts originate from aerosol microphysics on a micrometre scale. In Paper I, simulating aerosols and aerosol-cloud interactions resulted in a smaller cooling than would be expected if one based the estimations only by taking account of the geographical distribution of the aerosol emissions. Since aerosols can absorb the radiation or change the cloud properties, this might also lead to warming e ects in the end, even though the aerosol emissions are increased. In some circumstances, additional emissions can decrease the radiative e ect of already existing particles by changing clouds (Paper I) or leading to relatively larger particles (Paper V). Based on this study, aerosol microphysics should be included in simulations when aerosol radiative e ects are being studied and especially when solar radiation management by aerosols is modelled.

There are some limitations related to the solar radiation management which emerged in this work. Based on the simulations, the stratospheric sulphur geoengineering seems to be an e ective method to cool the climate but the limitations to this form of cooling start to emerge when the amount of injected sulphur is increased. Injecting more and more sulphur into the stratosphere would result in the formation of larger and larger particles and the aerosol eld would scatter radiation back to space less re ectively (Paper V). Thus even one of the most promising geoengineering method becomes ine ective if GHG emissions are still increasing and the warming is compensated exclusively by more and more stratospheric sulphur injections.

Papers III and IV showed that international sea and air tra c could be used for solar radiation management but a signi cant cooling e ect would require

changes in current legislation. Even then, the international tra c could compensate for only a small fraction of warming if GHG are still increasing. In addition, the cooling e ect would be concentrated to latitudes which are determined by tra c location and thus the radiative forcing will be concentrated on the northern hemisphere.

This work focussed mostly on the radiative e ects and the changes in temperature. However, changes in the precipitation might have even a larger impact on humankind than changes in the temperature. It would be very di cult to compensate for e ects on both temperature and precipitation due to the increased GHG by solar radiation management (Paper V). Furthermore, as was observed in Paper V, the changes in precipitation are highly sensitive to the sulphur aerosol eld in the stratosphere. Thus, the impact of geoengineering on precipitation should be studied more in the near future. This would require more detailed models and more accurate descriptions of clouds and dynamical processes in general. Furthermore, the conclusions emerging from this work are based on results from one model and robust conclusions would require wider investigations.

Overall, this work demonstrates that aerosols have the potential to cool the climate but slowing down the global warming would require large scale actions aimed at climate cooling. However, these actions include many uncertainties and risks which will need to be studied in detail. This requires simulations by global climate models and aerosol microphysics. If SRM methods are ever used, this would require a simultaneous reduction of GHG emissions and the methods cannot be viewed as a substitute for the mitigation policies.

References

Abdul-Razzak, H. and Ghan, S. J.: A parameterization of aerosol activation: 2. Multiple aerosol types, J. Geophys. Res., 105(D5), 6837-6844, doi:10.1029/1999JD901161, 2000.

Albrecht, B.: Aerosols, Cloud Microphysics and Fractional Cloudiness, Science, 245, 1227-1230, 1989.

Alterskj r, K. and Kristjansson, J. E.: The sign of the radiative forcing from marine cloud brightening depends on both particle size and injection amount, Geophys. Res. Lett., 40, 210-215, doi: 10.1029/2012GL054286, 2013a.

Alterskj r, K., Kristjansson, J. E., Boucher, O., Muri, H., Niemeier, U., Schmidt, H., Schulz, M and Timmreck, C.: Sea-salt injections into the low-latitude marine boundary layer: The transient response in three Earth system models, J. Geophys. Res. Atmos., 118, 12, 195-12, 206, doi:10.1002/2013JD020432, 2013b.

Aswathy, V. N., Boucher, O., Quaas, M., Niemeier, U., Muri, H., Mulmenstadt, J., and Quaas, J.: Climate extremes in multi-model simulations of stratospheric aerosol and marine cloud brightening climate engineering, Atmos. Chem. Phys., 15, 9593-9610, doi:10.5194/acp-15-9593-2015, 2015.

Bala G., Du y P. B., Taylor K. E.: Impact of geoengineering schemes on the global hydrological cycle. Proc Natl Acad Sci USA 105:7664-7669. doi: 10.1073/pnas.0711648105, 2008.

Barrett, S.: The Incredible Economics of Geoengineering, Environ. Resource Econ., 39, 45-54 doi: 10.1007/s10640-007-9174-8, 2008.

Barrett S. R. H., Britter R. E. and Waitz I. A.: Global mortality attributable to aircraft cruise emissions, Environ. Sci. Technol. 44, 7736-42, 2010.

Bergman, T., Kerminen, V.-M., Korhonen, H., Lehtinen, K. J., Makkonen, R., Arola, A., Mielonen, T., Romakkaniemi, S., Kulmala, M., and Kokkola, H.: Evaluation of the sectional aerosol microphysics module SALSA implementation in ECHAM5-HAM aerosol-climate model, Geosci. Model Dev., 5, 845-868, doi:10.5194/gmd-5-845-2012, 2012.

Bony, S., Bellon, G., Klocke, D., Sherwood, S., Fermepin, S., and Denvil, S.: Robust direct e ect of carbon dioxide on tropical circulation and regional precipitation, Nat. Geosci., 6, 447-451, 2013.

Boucher, O., Randall, D., Artaxo, P., Bretherton, C., Feingold, G., Forster, P., Kerminen, V.-M., Kondo, Y., Liao, H., Lohmann, U., Rasch, P., Satheesh, S. K., Sherwood, S., Stevens, B., Zhang, X., Y.: Clouds and aerosols. In: Climate Change 2013: The physical science basis. Contribution of working group I to the fth assessment report of the Intergovernmental Panel on Climate Change, chapter 7 [Stocker, T. F., Qin, D., Plattner, G.-K., Tignor, M., Allen, S. K., Boschung, J., Nauels, A., Xia, Y., Bex, V., Midgley, P. M., (eds.)]. Cambridge University Press, Cambridge, United Kingdom and New York, NY, USA, 2013.

Bruckner T., Bashmakov, I. A., Mulugetta, Y., Chum, H., de la Vega Navarro, A., Edmonds, J., Faaij, A., Fungtammasan, B., Garg, A, Hertwich, E., Honnery, D., In eld, D., Kainuma, M., Khennas, S., Kim, S., Nimir, H. B., Riahi, K., Strachan, N., Wiser, R. and Zhang X,: Energy Systems. In: Climate Change: Mitigation of Climate Change. Contribution of Working Group III to the Fifth Assessment Report of the Intergovernmental Panel on Climate Change [Edenhofer, O., R. Pichs-Madruga, Y. Sokona, E. Farahani, S. Kadner, K. Seyboth, A. Adler, I. Baum, S. Brunner, P. Eickemeier, B. Kriemann, J. Savolainen, S. Schlmer, C. von Stechow, T. Zwickel and J.C. Minx (eds.)]. Cambridge University Press, Cambridge, United Kingdom and New York, NY, USA, 2014.

Budyko, M. I.: Izmeniya Klimata. Gidrometeoizdat, also published as: Budyko, M. I., 1977 Climatic changes (transl. Izmeniia Klimata Leningrad: Gidrometeoizdat, 1974). Washington, DC: American Geophysical Union, 1974.

Caldeira, K. and Wood, L.: Global and Arctic climate engineering: numerical model studies, Phil. Trans. R. Soc. A, 366, 4039-4056, doi:10.1098/rsta.2008.0132, 2009.

Campmany, E., Grainger, R. G., Dean, S. M., and Sayer, A. M.: Automatic detection of ship tracks in ATSR-2 satellite imagery, Atmos. Chem. Phys., 9, 1899-1905, doi:10.5194/acp-9-1899-2009, 2009.

Cirisan, A., Spichtinger, P., Luo, B. P., Weisenstein, D. K., Wernli, H., Lohmann, U. and Peter T.: Microphysical and radiative changes in cirrus clouds by geoengineering the stratosphere, J. Geophys. Res. Atmos., 118, 4533-4548 doi:10.1002/jgrd.50388, 2013.

Corbett, J. J., Winebrake, J. J., Green, E. H., Kasibhatla, P., Eyring, V., and Lauer, A.: Mortality from ship emissions: a global assessment, Environ. Sci. Technol., 41, 8512-8518, 2007.

Croddy, E., Perez-Armendariz, C. and Hart, J.: Chemical and Biological Warfare: A Comprehensive Survey for the Concerned Citizen, 306 pp., Springer, New York, 2001.

Crutzen, P. J.: Albedo enhancement by stratospheric sulfur injections: A contribution to resolve a policy dilemma? Climatic Change, 77, 211 - 219, 2006.

Davis, M. B., Shaw, R. G.: Range Shifts and Adaptive Responses to Quaternary Climate Change, Science, 292, 673-679, doi: 10.1126/science.292.5517.673, 2001.

Dentener, F., Kinne, S., Bond, T., Boucher, O., Cofala, J., Generoso, S., Ginoux, P., Gong, S., Hoelzemann, J. J., Ito, A., Marelli, L., Penner, J. E., Putaud, J.-P., Textor, C., Schulz, M., van der Werf, G. R., and Wilson, J.: Emissions of primary aerosol and precursor gases in the years 2000 and 1750 prescribed data-sets for aerocom. Atmospheric Chemistry and Physics, 6(12):4321-4344, doi:10.5194/acp-6-4321-2006, 2006.

Edenhofer, O., Pichs-Madruga, R., Sokona, Y., Seyboth, K., Matschoss, P., Kadner, S., Zwickel, T., Eickemeier, P., Hansen, G., Schlmer, S., von Stechow, C.: IPCC : IPCC Special Report on Renewable Energy Sources and Climate Change Mitigation. Prepared by Working Group III of the Intergovernmental Panel on Climate Change . Cambridge University Press, Cambridge, United Kingdom and New York, NY, USA, 1075 pp, 2011.

E ong, U., and Neitzel, R. L.: Assessing the direct occupational and public health impacts of solar radiation management with stratospheric aerosols, Environmental Health, 15:7, doi 10.1186/s12940-016-0089-0, 2016.

Emmons, L. K., Walters, S., Hess, P. G., Lamarque, J.-F., P ster, G. G., Fillmore, D., Granier, C., Guenther, A., Kinnison, D., Laepple, T., Orlando, J., Tie, X., Tyndall, G., Wiedinmyer, C., Baughcum, S. L., and Kloster, S.: Description and evaluation of the Model for Ozone and Related chemical Tracers, version 4 (MOZART-4), Geosci. Model Dev., 3, 43-67, doi:10.5194/gmd-3-43-2010, 2010.

England, M. H., McGregor, S., Spence, P., Meehl, P. G., Timmermann, A., Cai, W., Gupta, A. S., McPhaden, M.,. Purich, A. and Santoso A.: Recent intensication of wind-driven circulation in the Pacic and the ongoing warming hiatus, Nat. Clim. Change, 4, 222-227, doi:10.1038/nclimate2106, 2014.

English, J. M., Toon, O. B., and Mills, M. J.: Microphysical simulations of sulfur burdens from stratospheric sulfur geoengineering, Atmos. Chem. Phys., 12, 4775-4793, doi:10.5194/acp-12-4775-2012, 2012.

Eyring, V., Isaksen, I. S. A., Berntsen, T., Collins, W. J., Corbett, J. J., Endresen, O., Grainger, R. G., Moldanova, J., Schlager, H., and Stevenson, D. S.: Transport impacts on atmosphere and climate: Shipping, Atmos. Environ., 44, 4735-4771, 2010.

Feichter, J., Kjellsttrom, E., Rodhe, H., Dentener, F., Lelieveldi, J., and Roelofs, G.-J.: Simulation of the tropospheric sulfur cycle in a global climate model. Atmospheric Environment, 30(10-11):1693 - 1707, doi:http://dx.doi.org/10.1016/1352-2310(95)00394-0. Joint 8th CAGCP and 2nd IGAC Conference on Global Atmospheric Chemistry, 1996.

Ferraro, A. J., Highwood, E. J. and Charlton-Perez, A. J.: Stratospheric heating by potential geoengineering aerosols, Geophys. Res. Lett., 38, L24706, doi:10.1029/2011GL049761, 2011.

Ferraro, A. J., Highwood, E. J., and Charlton-Perez, A. J.: Weakened tropical circulation and reduced precipitation in response to geoengineering, Environ. Res. Lett., 9, doi:10.1088/17489326/9/1/014001, 2014.

Forsyth, P. Y.: In the wake of Etna, 44 B.C., Classical Antiq., 7, 49 -57, 1988.

Fuglestvedt, J. S., Berntsen, T., Myhre, G., Rypdal, K., Bieltvedt Skeie, R.: Climate forcing from the transport sectors. Proceedings of the National Academy of Sciences USA 105, 454-458, 2007.

Fuglestvedt, J. S., Samset, B. H. and Shine K. P.: Counteracting the climate e ects of volcanic eruptions using short-lived greenhouse gases, Geophys. Res. Lett., 41, 8627-8635, doi:10.1002/2014GL0618, 2014.

Fujii, Y.: The role of atmospheric nuclear explosions on the stagnation of global warming in the mid 20th century, J. Atmos. Sol. Terr. Phys., 73, 643-652, doi:10.1016/j.jastp.2011.01.005, 2011

Giorgetta, M., Jungclaus, J., Reick, C. H., Legutke, S., Bader, J., Bttinger, M., Brovkin, V., Crueger, T., Esch, M., Fieg, K., Glushak, K., Gayler, V., Haak, H., Hollweg, H.-D., Ilyina, T., Kinne, S., Kornblueh, L., Matei, D., Mauritsen, T., Mikolajewicz, U., Mueller, W., Notz, D., Pi- than, F., Raddatz, T., Rast, S., Redler, R., Roeckner, E., Schmidt, H., Schnur, R., Segschneider, J., Six, K. D., Stockhause, M., Timmreck, C., Wegner, J., Widmann, H., Wieners, K.-H., Claussen, M., Marotzke, J., and Stevens,

B.: Climate and carbon cycle changes from 1850 to 2100 in MPI-ESM simulations for the coupled model intercomparison project phase 5, J. Adv. Model. Earth Syst., 5, 572-597, doi:10.1002/jame.20038, 2013.

GISTEMP Team: GISS Surface Temperature Analysis (GISTEMP). NASA Goddard Institute for Space Studies. Dataset accessed 2015-06-05 at http://data.giss.nasa.gov/gistemp/, 2015.

Glienke, S., Irvine, P. J. and Lawrence, M. G.: The impact of geoengineering on vegetation in experiment G1 of the GeoMIP, J. Geophys. Res. Atmos., 120, 10,196-10,213, doi:10.1002/ 2015JD024202, 2015.

Govindasamy, B. and Caldeira, K.: Geoengineering Earths radiative balance to mitigate CO_2-induced climate change, Geophys. Res. Lett., 27, 14, 2141-2144, doi: 10.1029/1999GL006086, 2000.

Govindasamy, B., Thompson, S., Du y, P. B., Caldeira, K., Delire, C.: Impact of geoengineering schemes on the terrestrial biosphere. Geophys Res Lett 29(22):2061. doi:10.1029/2002GL015911, 2002.

Govindasamy, B., Caldeira, K., and Du y, P.B.: Geoengineering Earths radiation balance to mitigate climate change from a quadrupling of CO_2, Global and Planet. Change, 37, 157-168, doi:10.1016/S0921- 8181(02)00195-9, 2003.

Guhrn, M., Bigler, C. and Renberg, I.: Liming placed in a long-term perspective: a paleolimnological study of 12 lakes in the Swedish liming program. Journal of Paleolimnology, 37, 247-258, 2007.

Guo, S., Rose, W. I., Bluth, G. J. S., and Watson, I. M.: Particles in the great Pinatubo volcanic cloud of June 1991: The role of ice, Geochemistry, Geophysics, Geosystems, 5, Q05003, doi:10.1029/2003GC000655, 2004a.

Guo, S., Bluth, G. J. S., Rose, W. I., Watson, I. M. and Prata, A. J.: Re-evaluation of SO_2 release of the 15 June 1991 Pinatubo eruption using ultraviolet and infrared satellite sensors, Geochem. Geophys. Geosyst., 5 , Q04001, doi:10.1029/ 2003GC000654, 2004b.

Hamill, P., Jensen, E. J., Russell, P. B. and Bauman, J. J.: The Life Cycle of Stratospheric Aerosol Particles. Bull. Amer. Meteor. Soc., 78, 1395-1410, doi: http://dx.doi.org/10.1175/1520-0477(1997)078 1395:TLCOSA 2.0.CO;2, 1997.

Hansen, J., Lacis, A., Ruedy, R., and Sato, M.: Potential climate impact of Mount-Pinatubo eruption, Geophys. Res. Lett., 19, 215-218, doi:10.1029/91GL02788, 1992.

Hansen, J., Ruedy, R., Sato, M. and Lo, K.: Global surface temperature change, Rev. Geophys., 48, RG4004, doi:10.1029/2010RG000345, 2010.

Hansen, J., Sato, M., Kharecha, P., and von Schuckmann, K.: Earths energy imbalance and implications, Atmos. Chem. Phys., 11, 13421-13449, doi:10.5194/acp-11-13421-2011, 2011.

Hartmann, D.L., Klein Tank, A. M. G.,. Rusticucci, M., Alexander, L. V., Brnnimann, S., Charabi, Y., Dentener, F. J., Dlugokencky, E. J., Easterling, D. R., Kaplan, A., Soden, B.J., Thorne, P. W., Wild M. and Zhai, P. M.: Observations: Atmosphere and Surface. In: Climate Change 2013: The Physical Science Basis. Contribution of Working Group I to the Fifth Assessment Report of the Intergovernmental Panel on Climate Change [Stocker, T.F., D. Qin, G.-K. Plattner, M. Tignor, S.K. Allen, J. Boschung, A. Nauels, Y. Xia, V. Bex and P.M. Midgley (eds.)]. Cambridge University Press, Cambridge, United Kingdom and New York, NY, USA, 2013.

Haywood, J. M., Jones, A., Bellouin, N., Stephenson, D.: Asymmetric forcing from stratospheric aerosols impacts Sahelian rainfall, Nature Clim. Change, 3, 660-665, doi:10.1038/nclimate1857, 2013.

Held, J. M. and Soden, B. J.: Robust Responses of the Hydrological Cycle to Global Warming. J. Climate, 19, 5686-5699, doi: http://dx.doi.org/10.1175/JCLI3990.1, 2006.

ICS: International Chamber of Shipping, Shipping, World Trade and the Reduction of CO_2 Emissions, 2014.

Ilyina, T., Six, K. D., Segschneider, J., Maier-Reimer, E., Li, H., and Nunez-Riboni, I.: Global ocean biogeochemistry model HAMOCC: Model architecture and performance as component of the MPI-Earth System Model in di erent CMIP5 experimental realizations. Journal of Advances in Modeling Earth Systems, 5, 287-315. doi:10.1029/2012MS000178, 2013.

Irvine, P. J., Ridgwell, A., and Lunt, D. J.: Assessing the regional disparities in geoengineering impacts, Geophys. Res. Lett., 37, L18702, doi:10.1029/2010GL044447, 2010.

Izrael, Y. A., Volodin, E. M., Kostrykin, S. V., Revokatova, A. P., and Ryaboshapko, A. G.: The ability of stratospheric climate engineering in stabilizing global mean temperatures and an assessment of possible side e ects, Atmos. Sci. Lett., doi: 10.1002/asl2.481, 2013.

Jacobson, M., Z.: Fundamentals of Atmospheric Modeling, Cambridge University Press, New York, 2nd Edition, 2005.

Jacobson, M. Z.: Energy modelling: Clean grids with current technology, Nature Climate Change, doi:10.1038/nclimate2926, 2016.

Jones, A., Haywood, J., and Boucher, O.: Climate impacts of geoengineering marine stratocumulus clouds, J. Geophys. Res., 114, D10106, 2009.

Jones, A., Haywood, J. M., Alterskj r, K., Boucher, O., Cole, J. N. S., Curry, C. L., Irvine, P. J., Ji, D., Kravitz, B., Kristjansson, J. E., Moore, J. C., Niemeier, U., Robock, A., Schmidt, H., Singh, B., Tilmes, S., Watanabe, S., and Yoon, J.-H.: The impact of abrupt suspension of solar radiation management (termination e ect) in experiment G2 of the Geoengineering Model Intercomparison Project (GeoMIP), J. Geophys. Res. Atmos., 118, 9743-9752, doi:10.1002/jgrd.50762, 2013.

Jones, A. C., Haywood, J. M., and Jones, A.: Climatic impacts of stratospheric geoengineering with sulfate, black carbon and titania injection, Atmos. Chem. Phys. Discuss., 15, 30043-30079, doi:10.5194/acpd-15-30043-2015, 2015.

Jungclaus, J. H., Fischer, N., Haak, H., Lohmann, K., Marotzke, J., Matei, D., Mikolajewicz, U., Notz, D., and von Storch, J.-S.: Characteristics of the ocean simulations in MPIOM, the ocean component of the MPI Earth System Model. J. Adv. Model. Earth Syst., 5, 422-446. doi:10.1002/jame.20023, 2013.

Ilyina, T., Six, K. D., Segschneider, J., Maier-Reimer, E., Li, H., and Nunez-Riboni, I.: Global ocean biogeochemistry model HAMOCC: Model architecture and performance as component of the MPI-Earth System Model in di erent CMIP5 experimental realizations.J. Adv. Model. Earth Syst., 5, 287-315, doi:10.1029/2012MS000178, 2013.

Karl, T. R., Arguez, A., Huang, B., Lawrimore, J. H., McMahon, J. R., Menne, M. J., Peterson, T. C., Vose, R. S., and Zhang, H.: Possible artifacts of data biases in the recent global surface warming hiatus, Science, 348, 1469-1472, doi:10.1126/science.aaa5632, 2015.

Kalidindi, S., Bala, G., Modak, A. and Caldeira, K.: Modeling of solar radiation management: a comparison of simulations using reduced solar constant and stratospheric sulphate aerosols, Climate Dynamics, 2015, 44, 9-10, 2909-2925, 2014.

Kasoar, M., Voulgarakis, A., Lamarque, J.-F., Shindell, D. T., Bellouin, N., Collins, W. J., Faluvegi, G., and Tsigaridis, K.: Regional and global climate response to anthropogenic SO_2 emissions from China in three climate models, Atmos. Chem. Phys. Discuss., doi:10.5194/acp-2015-1017, in review, 2016.

Keith, D. W.: Geoengineering the climate: History and prospect, Annual Review of Energy and the Environment, 25, 245 - 284, 2000.

Keith, D. W.: Photophoretic levitation of engineered aerosols for geoengineering, Proc. Natl. Acad. Sci., 107, 16428-16431, doi:10.1073/pnas.1009519107, 2010.

Khairoutdinov, M. and Kogan, Y.: A new cloud physics parameterization in a Large-Eddy Simulation model of marine stratocumulus, Mon. Weather Rev., 128, 229243, 2000.

Kilburn, K. H., and Warshaw, R. H.: Hydrogen sul de and reduced sulfur gases adversely a ect neurophysiological functions, Toxicol. Ind. Health, 11(2), 185 - 197, 1995.

Kinne, S., D. O Donnel, D., P. Stier, P., S. Kloster, S., K. Zhang, K., H. Schmidt, H., S. Rast, S., M. Giorgetta, M., T. F. Eck, T.F and B. Stevens, B.: MAC-v1: A new global aerosol climatology for climate studies, J. Adv. Model. Earth Syst., 5, 704-740, doi:10.1002/jame.20035, 2013.

Knutson, T. R. and Manabe S.: Time-mean response over the tropical paci c to increased CO_2 in a coupled ocean-atmosphere model, J. Clim., 8, 2181-99, 1995.

Koch, D. and Del Genio, A. D.: Black carbon semi-direct e ects on cloud cover: review and synthesis, Atmos. Chem. Phys., 10, 7685-7696, doi:10.5194/acp-10-7685-2010, 2010.

Kokkola, H., Korhonen, H., Lehtinen, K. E. J., Makkonen, R., Asmi, A., Jarvenoja, S., Anttila, T., Partanen, A.-I., Kulmala, M., Jarvinen, H., Laaksonen, A., and Kerminen, V.-M.: SALSA - a Sectional Aerosol module for Large Scale Applications, Atmos. Chem. Phys., 8, 2469-2483, doi: 10.5194/acp-8-2469-2008, 2008.

Kokkola, H., Hommel, R., Kazil, J., Niemeier, U., Partanen, A.-I., Feichter, J., and Timmreck, C.: Aerosol microphysics modules in the framework of the ECHAM5 climate model intercomparison under stratospheric conditions, Geosci. Model Dev., 2, 97-112, doi:10.5194/gmd-2-97-2009, 2009.

Korhola, T., Kokkola, H., Korhonen, H., Partanen, A.-I., Laaksonen, A., Lehtinen, K. E. J., and Romakkaniemi, S.: Reallocation in modal aerosol models: impacts on predicting aerosol radiative e ects, Geosci. Model Dev., 7, 161-174, doi:10.5194/gmd-7-161-2014, 2014.

Korhonen, H., Carslaw, K. S., and Romakkaniemi, S.: Enhancement of marine cloud albedo via controlled sea spray injections: a global model study of the in uence of emission rates, microphysics and transport, Atmos. Chem. Phys., 10, 4133-4143, doi:10.5194/acp-10-4133-2010, 2010.

Kosaka, Y., and S.-P. Xie, Recent global-warming hiatus tied to equatorial Pacic surface cooling, Nature, 501, 403-407, doi:10.1038/nature12534, 2013.

Kravitz, B., Robock, A., Oman, L., Stenchikov, G., and Marquardt, A. B.: Sulfuric acid deposition from stratospheric geoengineering with sulfate aerosols, J. Geophys. Res., 114, D14109, doi:10.1029/2009JD011918, 2009.

Kravitz, B., Robock, A., Shindell, D. T. and Miller M. A.: Sensitivity of stratospheric geoengineering with black carbon to aerosol size and altitude of injection. J. Geophys. Res., 117, D09203, doi:10.1029/2011JD017341, 2012.

Kravitz, B., Robock, A., Forster, P. M., Haywood, J. M., Lawrence M. G., and Schmidt, H.: An overview of the Geoengineering Model Intercomparison Project (GeoMIP), Journal of Geophysical Research, 118, 13103-13107, doi:10.1002/2013JD020569, 2013.

Kravitz, B., *et al.*, An energetic perspective on hydrological cycle changes in the Geoengineering Model Intercomparison Project, J. Geophys. Res. Atmos., 118, 13,087-13,102, doi:10.1002/2013JD020502, 2013a.

Kravitz, B., *et al.*,: Climate model response from the Geoengineering Model Intercomparison Project (GeoMIP), J. Geophys. Res. Atmos., 118, 8320-8332, doi:10.1002/jgrd.50646, 2013b.

Kravitz, B., MacMartin, D. G., Robock, A., Rasch, P. J., Ricke, K. L., Cole, J. N. S., Curry, C. L., Irvine, P. J., Ji, D., Keith, D.W., Kristjnsson, J. E., Moore, J.C. Muri, H., Singh, J., Tilmes, S., Watanabe, S., Yang,

S., and Yoon J.-H.: A multi-model assessment of regional climate disparities caused by solar geoengineering, Environ. Res. Lett., 9, 074013, doi:10.1088/1748-9326/9/7/074013, 2014.

Kuebbeler, M., Lohmann, U. and Feichter, J., E ects of stratospheric sulfate aerosol geoengineering on cirrus clouds, Geo. phys. Res. Lett., 39, L23803, DOI:10.1029/2012GL053797, 2012.

Laakso, A.-I. Partanen, H. Kokkola, K. E. J. Lehtinen, and H. Korhonen: Optimizing stratospheric sulfur geoengineering by seasonally changing sulfur injections, Geophysical Research Abstract Vol. 17, EGU2015-10223, EGU General Assembly 2015, 2015.

Latham, J.: Control of global warming?, Nature, 347, 339-340, doi:10.1038/347339b0, 1990.

Latham, J., Rasch, P., Chen, C.-C., Kettles, L., Gadian, A., Gettelman, A., Morrison, H., Bower, K., and Chourlaton, T.: Global temperature stabilization via controlled albedo enhancement of lowlevel maritime clouds, Phil. Trans. R. Soc. A, 366, 3969-3987, doi:10.1098/rsta.2008.0137, 2008.

Latham, J., Bower, K., Choularton, T., Coe, H., Connolly, P., Cooper, G., Craft, T., Foster, J., Gadian, A., Galbraith, L., Iacovides, H., Johnston, D., Launder, B., Leslie, B., Meyer, J., Neukermans, A., Ormond, B., Parkes, B., Rasch, P. J., Rush, J., Salter, S., Stevenson, T., Wang, H., Wang, Q., and Wood, R.: Marine cloud brightening, Phil. Trans. R. Soc. A, 370, 4217-4262, doi:10.1098/rsta.2012.00866, 2012.

Lauer, A., Eyring, V., Hendricks, J., Jockel, P., Lohmann, U.: E ects of oceangoing shipping on aerosols and clouds. Atmospheric Chemistry and Physics 7, 5061-5079, 2007.

Lauer, A., Eyring, V., Corbett, J. J., Wang, C., and Winebrake, J. J.: Assessment of near-future policy instruments for oceangoing shipping: impact on atmospheric aerosol burdens and the Earths radiation budget, Environ. Sci. Technol., 43, 5592-5598, 2009.

Lee, J., Yang, P., Dessler, A. E., Gao, B. C., Platnik, S.: Distribution and radiative forcing of tropical thin cirrus clouds, Journal of Atmospheric Science, 66, doi: 10.1175/2009JAS3183.1, 2009.

Lenton, T. M. and Vaughan, N. E.: The radiative forcing potential of di erent climate geoengineering options, Atmos. Chem. Phys., 9, 5539-5561, doi:10.5194/acp-9-5539-2009, 2009.

Lin, A. C.: Does Geoengineering Present a Moral Hazard?, Ecol. Law Q., 40, 3, 673-712, 2013.

Lin, H. and Leaitch, W.: Development of an in-cloud aerosol activation parameterization for climate modelling, in: Proceedings of the WMO Workshop on Measurement of Cloud Properties for Forecasts of Weather, Air Quality and Climate, Mexico City, 328-335, 1997.

Lohmann, U. and Feichter, J.: Global indirect aerosol e ects: a review, Atmos. Chem. Phys., 5, 715-737, doi:10.5194/acp-5-715-2005, 2005.

Makkonen, R., Asmi, A., Korhonen, H., Kokkola, H., Jarvenoja, S., Raisanen, P., Lehtinen, K. E. J., Laaksonen, A., Kerminen, V.-M., Jarvinen, H., Lohmann, U., Bennartz, R., Feichter, J., and Kulmala, M.: Sensitivity of aerosol concentrations and cloud properties to nucleation and secondary organic distribution in ECHAM5-HAM global circulation model, Atmos. Chem. Phys., 9, 1747-1766, doi:10.5194/acp-9-1747-2009, 2009.

Matthews H. D. and Caldeira K.: Transient climate-carbon simulations of planetary geoengineering, Proc. Natl. Acad. Sci., 104, 9949-9954, doi:10.1073/pnas.0700419104, 2007.

Mauritsen, T., et al.: Tuning the climate of a global model, J. Adv. Model. Earth Syst., 4, M00A01, doi:10.1029/2012MS000154, 2012.

McClellan, J., Keith, D. W., and Apt, J.: Cost analysis of stratospheric albedo modi cation delivery systems, Environ. Res. Lett., 7, doi:10.1088/1748-9326/7/3/034019, 2012.

McGu e, K. and Henderson-Sellers, A.: A Climate Modeling Primer, John Wiley & Sons, Inc, 2005.

Modak, A. and Bala, G.: Sensitivity of simulated climate to latitudinal distribution of solar insolation reduction in SRM geoengineering methods. In Atmos. Chem. Phys. Discuss. 13 (10), pp. 25387-25415, doi:10.5194/acpd-13-25387-2013, 2013.

Monahan, E., Spiel, D., and Davidson, K.: A model of marine aerosol generation via whitecaps and wave disruption, in Oceanic Whitecaps and Their Role in Air-Sea Exchange, 167-174, D. Reidel [ed.], Norwell, Mass, 1986.

Mitchell, D. L., Finnegan, W.: Modi cation of cirrus clouds to reduce global warming, Environmental Research Letters, 4, 45102, 2009.

Muri, H., J. E. Kristjansson, T. Storelvmo, and M. A. Pfe er, The climatic e ects of modifying cirrus clouds in a climate engineering framework, J. Geophys. Res. Atmos., 119, 4174-4191, doi:10.1002/2013JD021063, 2014.

Murphy, D. M., Solomon, S., Portmann, R. W., Rosenlof, K. H., Forster, P. M., and Wong, T.: An observationally based energy balance for the Earth since 1950, J. Geophys. Res., 114, D17107, doi:10.1029/2009JD012105, 2009.

Murphy, D. M., Little net clear-sky radiative forcing from recent regional redistribution of aerosols, Nat. Geosci., 6, 258-262, doi:10.1038/ngeo1740, 2013.

Myhre, G., Shindell, D., Breeon, F.-M., Collins, W., Fuglestvedt, J., Huang, J., Koch, D., Lamarque, J.-F., Lee, D., Mendoza, B., Nakajima, T., Robock, A., Stephens, G., Takemura, T., and Zhang, H.: Anthropogenic and Natural Radiative Forcing. In: Climate Change 2013: The Physical Science Basis. Contribution of Working Group I to the Fifth Assessment Report of the Intergovernmental Panel on Climate Change [Stocker, T.F., D. Qin, G.-K. Plattner, M. Tignor, S.K. Allen, J. Boschung, A. Nauels, Y. Xia, V. Bex and P.M. Midgley (eds.)]. Cambridge University Press, Cambridge, United Kingdom and New York, NY, USA, 2013a.

Myhre, G., Samset, B. H., Schulz, M., Balkanski, Y., Bauer, S., Berntsen, T. K., Bian, H., Bellouin, N., Chin, M., Diehl, T., Easter, R. C., Feichter, J., Ghan, S. J., Hauglustaine, D., Iversen, T., Kinne, S., Kirkevag, A., Lamarque, J.-F., Lin, G., Liu, X., Lund, M. T., Luo, G., Ma, X., van Noije, T., Penner, J. E., Rasch, P. J., Ruiz, A., Seland, ., Skeie, R. B., Stier, P., Takemura, T., Tsigaridis, K., Wang, P., Wang, Z., Xu, L., Yu, H., Yu, F., Yoon, J.-H., Zhang, K., Zhang, H., and Zhou, C.: Radiative forcing of the direct aerosol e ect from AeroCom Phase II simulations, Atmos. Chem. Phys., 13, 1853-1877, doi:10.5194/acp-13-1853-2013, 2013b.

Niemeier, U., Timmreck, C., Graf, H.-F., Kinne, S., Rast, S., and Self, S.: Initial fate of ne ash and sulfur from large volcanic eruptions, Atmos. Chem. Phys., 9, 9043-9057, doi:10.5194/acp-9-9043-2009, 2009.

Niemeier, U., Schmidt, H., and Timmreck, C.: The dependency of geoengineered sulfate aerosol on the emission strategy, Atmos. Sci. Lett., 12, 189-194, doi:10.1002/asl.304, 2011.

Niemeier, U. and Timmreck, C.: What is the limit of climate engineering by stratospheric injection of SO_2?, Atmos. Chem. Phys., 15, 9129-9141, doi:10.5194/acp-15-9129-2015, 2015.

Oldham P, Szerszynski B, Stilgoe J, Brown C, Eacott B, Yuille A.: Mapping the landscape of climate engineering: lessons for governance from scientometric research. Phil Trans R Soc A, 372:20140065, 2014.

Oman, L., Robock, A., Stenchikov, G. L. and Thordarson T.: High-latitude eruptions cast shadow over the African monsoon and the ow of the Nile, Geophys. Res. Lett., 33, L18711, doi:10.1029/2006GL027665, 2006.

Ostro, B.: Outdoor air pollution: assessing the environmental burden of disease at national and local levels, WHO Environmental Burden of Disease Series, 5, Geneva, World Health Organization, 2004.

Partanen, A.-I., Laakso, A, Kokkola, H. and Korhonen, H.: Climatic e ects of sea spray geoengineering simulated by ECHAM5 model. Geophysical Research Abstracts Vol. 14, EGU2012-7417-1, EGU General Assembly 2012, 2012a.

Partanen, A.-I., Kokkola, H., Romakkaniemi, S., Kerminen, V.-M., Lehtinen, K. E. J., Bergman, T., Arola, A., Korhonen, H.: Direct and indirect effects of sea spray geoengineering and the role of injected particle size, J. Geophys. Res., 117, D02203, doi:10.1029/2011JD016428, 2012b.

Partanen, A.-I., Dunne, E. M., Bergman, T., Laakso, A., Kokkola, H., Ovadnevaite, J., Sogacheva, L., Baisne, D., Sciare, J., Manders, A., O Dowd, C., de Leeuw, G., and Korhonen, H.: Global modelling of direct and indirect e ects of sea spray aerosol using a source function encapsulating wave state, Atmos. Chem. Phys., 14, 11731-11752, doi:10.5194/acp-14-11731-2014, 2014.

Penner, J. E., Lister, D. H., Griggs, D. J., Dokken D. J. and McFarland M.: IPCC (Intergovernmental Panel on Climate Change), Aviation and the Global Atmosphere, Cambridge University Press, 1990.

Penner, J. E., Zhou, C. and Liu, X.: Can cirrus cloud seeding be used for geoengineering?, Geophys. Res. Lett., 42, 8775-8782, doi:10.1002/2015GL065992, 2015.

Peters, K., Stier, P., Quaas, J., and Gral, H.: Aerosol indirect e ects from shipping emissions: sensitivity studies with the global aerosol-climate model ECHAM-HAM, Atmos. Chem. Phys., 12, 5985-6007, doi: 10.5194/acp-12-5985-2012, 2012.

Phillips, N. A., A.: Coordinate system having some special advantages for numerical forecasting. Journal of Meteorology, 14 , 184-185, 1957.

Pierce, J. R.; Weisenstein, D. K.; Heckendorn, P.; Peter, T.; Keith, D. W.: Efcient formation of stratospheric aerosol for climate engineering by emission of condensable vapor from aircraft, Geophysical Research Letters, 37, doi:10.1029/2010GL043975, 2010.

Pierrehumbert, R. T.: Principles of Planetary Climate, Cambridge University Press, United Kingdom, 2009.

Pietikainen, J.-P., Mikkonen, S., Hamed, A., Hienola, A. I., Birmili, W., Kulmala,M., and Laaksonen, A.: Analysis of nucleation events in the European boundary layer using the regional aerosol-climate model REMO-HAM with a solar radiation-driven OH-proxy. Atmos. Chem. Phys., 14, 11711-11729, doi:10.5194/acp-14-11711-2014, 2014.

Pincus, R. and Baker, M. B.: E ect of precipitation on the albedo susceptibility of clouds in the marine boundary layer. Nature, 372, 250-252. doi:10.1038/372250a0, 1994.

Pithan, F. and Mauritsen, T.: Arctic ampli cation dominated by temperature feedbacks in contemporary climate models, Nature Geoscience, 7, 181-184, doi:10.1038/ngeo2071, 2014.

Pope, F. D., Braesicke, P., Grainger, R. G., Kalberer, M., Watson, I. M., Davidson, P. J., and Cox, R. A.: Stratospheric aerosol particles and solar-radiation management, Nature Clim. Change, 2, 713-719, doi:10.1038/nclimate1528, 2012.

Ramanathan, V., Crutzen, P. J., Kiehl, J. T. and Rosenfeld, D.: Aerosols, climate, and the hydrological cycle, Science, 294(5549):2119-2124, doi:10.1126/science.1064034, 2001.

Rasch, P. J., Crutzen, P. J., and Coleman, D. B.: Exploring the geoengineering of climate using stratospheric sulfate aerosols: The role of particle size, Geophys. Res. Lett., 35, L02809, doi:10.1029/2007GL032179, 2008a.

Rasch, P. J., Tilmes, S., Turco, R. P., Robock, A., Oman, L., Chen, C.-C., Stenchikov, G. L., and Garcia, R. R.: An overview of geoengineering of climate using stratospheric sulphate aerosols, Phil. Trans. R. Soc. A, 366, 4007-4037, doi:10.1098/rsta.2008.0131, 2008b.

Reick, C., T. Raddatz, T.V., Brovkin, V. and V. Gayler, V.: The representation of natural and anthropogenic land cover change in MPI-ESM, J. Adv. Model. Earth Syst., 5, doi:10.1002/jame.20022, 2013.

Riahi, K., Rao, S., Krey, V., Cho, C., Chirkov, V., Fischer, G., Kindermann, G., Nakicenovic, N., and Rafaj, P.: RCP 8.5-A scenario of comparatively high greenhouse gas emissions, Clim. Change, 109, 33-57, doi:10.1007/s10584-011-0149-y, 2011.

Rickels, W., *et al.*: Large-scale intentional interventions into the climate system? Assessing the climate engineering debate, Scoping Report Conducted on Behalf of the German Federal Ministry of Education and Research (BMBF), Kiel Earth Institute, 2011.

Ricke, K. L., Morgan, M. G., and Allen, M.: Regional climate response to solar-radiation management, Nature Geo Sci., 3, 537-541, doi:10.1038/NGEO915, 2010.

Ricke, K. L., Moreno-Cruz, J. B., and Caldeira, K.: Strategic incentives for climate geoengineering coalitions to exclude broad participation, Environ. Res. Lett., 8, doi:10.1088/1748-9326/8/1/014021, 2013.

Ridley, D. A., *et al.* : Total volcanic stratospheric aerosol optical depths and implications for global climate change, Geophys. Res. Lett., 41, 7763-7769, doi:10.1002/2014GL061541, 2014.

Riipinen, I., Sihto, S.-L., Kulmala, M., Arnold, F., Dal Maso, M., Birmili, W., Saarnio, K., Teinila, K., Kerminen, V.-M., Laaksonen, A., and Lehtinen, K. E. J.: Connections between atmospheric sulphuric acid and new particle formation during QUEST III-IV campaigns in Heidelberg and Hyytiala, Atmos. Chem. Phys., 7, 1899-1914, doi:10.5194/acp-7-1899-2007, 2007.

Robock, A.: Volcanic eruptions and climate, Rev. of Geophys., 38, 191-219, 2000.

Robock, A., Oman, L., and Stenchikov G. L.: Regional climate responses to geoengineering with tropical and Arctic SO_2 injections, J. Geophys. Res., 113, D16101, doi:10.1029/2008JD010050, 2008.

Robock, A., Marquardt, A., Kravitz, B., and Stenchikov, G.: Bene ts, risks, and costs of stratospheric geoengineering, Geophys. Res. Lett., 36, L19703, doi:10.1029/2009GL039209, 2009.

Roeckner, E., Baeuml, G., Bonventura, L., Brokopf, R., Esch, M., Giorgetta, M., Hagemann, S., Kirchner, I., Kornblueh, L., Manzini, E., Rhodin, A., Schlese, U., Schulzweida, U., and Tompkins, A.: The atmospheric general circulation model ECHAM5. PART I: Model description, Report 349,

Max Planck Institute for Meteorology, Hamburg, Germany, available from http://www.mpimet.mpg.de, 2003.

Rogelj, J., D., McCollum, L., Reisinger, A., Meinshausen, M. and Riahi, K. Probabilistic cost estimates for climate change mitigation, Nature 493, 79-83, doi:10.1038/nature11787, 2013.

Royal Society: Geoengineering the climate - Science, governance and uncertainty, RS Policy document 10/09, ISBN: 978-0-85403-773-5, 2009.

Raisanen, P., Jarvenoja, S., and Jarvinen, H.: Noise due to Monte Carlo independent-column approximation: short-term and long-term impacts in ECHAM5, Q. J. Roy. Meteorol. Soc., 134, 481-495, doi:10.1002/qj.231, 2008.

Salter, S., Sortino, G., and Latham, J.: Sea-going hardware for the cloud albedo method of reversing global warming, Phil. Trans. Roy. Soc. A, 366, 3989-4006, doi:10.1098/rsta.2008.0136, 2008.

Santer, B. D., Bon ls, C., Painter, J. F., Zelinka, M. D., Mears, C., Solomon, S., Schmidt, G. A., Fyfe, J. C. Cole, J. N. S., Nazarenko, L., Taylor, K. E. and Wentz, F. J.: Volcanic contribution to decadal changes in tropospheric temperature, Nat. Geosci., 7, 185-189, doi:10.1038/ngeo2098, 2014.

Santer, B. D., Solomon, S., Bon ls, C., Zelinka, M. D., Painter, J. F., Beltran, F., Fyfe, J. C., Johannesson, G., Mears. C., Ridley, D. A., Vernier, J.-P. and Wentz F. J.: Observed multivariable signals of late 20th and early 21st century volcanic activity, Geophys. Res. Lett., 42, 500509, doi:10.1002/2014GL062366, 2015.

Schmidt, H., Alterskj r, K., Bou Karam, D., Boucher, O., Jones, A., Kristjansson, J. E., Niemeier, U., Schulz, M., Aaheim, A., Benduhn, F., Lawrence, M., and Timmreck, C.: Solar irradiance reduction to counteract radiative forcing from a quadrupling of CO_2 : climate responses simulated by four earth system models, Earth Syst. Dynam., 3, 63-78, doi:10.5194/esd-3-63-2012, 2012.

Schneider, S. H.: Introduction to climate modeling in Climate System Modeling, ed. K.E.Trenberth, Cambridge University Press, 1992.

Schulz, M., de Leeuw, G., and Balkanski, Y.: Sea-salt aerosol source functions and emissions, in Emission of Atmospheric Trace Compounds, 333-359, Kluwer Acad., Norwell, Mass, 2004.

SEDAC (NASA Socioeconomic Data and Applications Center): Gridded Population of the World, Version 3 (GPWv3): Population Count Grid, Future Estimates, Center for International Earth Science Information Network (CIESIN)/Columbia University, United Nations Food and Agriculture Programme (FAO), and Centro Internacional de Agricultura Tropical (CIAT), available at: http://sedac.ciesin.columbia.edu/data/set/gpw-v3-population-count-future-estimates, 2005.

Seinfeld, J. H. and Pandis, S. N.: Atmospheric Chemistry and Physics: From Air Pollution to Climate Change, 2nd edition, John Wiley and Sons, U.S., 2006.

Self, S.: The e ects and consequences of very large explosive volcanic eruptions, Philos. Trans. R. Soc. London, Ser. A, 364(1845), 2073-2097, doi:10.1098/rsta.2006.181, 2006.

Sihto, S.-L., Kulmala, M., Kerminen, V.-M., Dal Maso, M., Petaja, T., Riipinen, I., Korhonen, H., Arnold, F., Janson, R., Boy, M., Laaksonen, A., and Lehtinen, K. E. J.: Atmospheric sulphuric acid and aerosol formation: implications from atmospheric measurements for nucleation and early growth mechanisms, Atmos. Chem. Phys., 6, 4079-4091, doi:10.5194/acp-6-4079-2006, 2006.

Simmons, A. J. and Burridge, D. M.: An energy and angular-momentum conserving vertical nite di erence scheme and hybrid vertical coordinates. Mon. Wea. Rev., 109, 758-766, 1981.

Simmons, A. J. and Strung, R.: An energy and angular-momentum conserving nite di erence scheme, hybrid coordinates and medium-range weather prediction, Technical Report 28, ECMWF, Reading, UK, 1981.

Smith, M. and Harrison, N.: The sea spray generation function, J. Aerosol Sci., 29, S189-S190, doi:10.1016/S0021-8502(98)00280-8, 1998.

Smith, S. J., van Aardenne, J., Klimont, Z., Andres, R. J., Volke, A., and Delgado Arias, S.: Anthropogenic sulfur dioxide emissions: 1850-2005, Atmos. Chem. Phys., 11, 1101-1116, doi:10.5194/acp-11-1101-2011, 2011.

Sonnemann, G. R. and Grygalashvyly, M.: E ective CO_2 lifetime and future CO_2 levels based on t function, Ann. Geophys., 31, 1591-1596, doi:10.5194/angeo-31-1591-2013, 2013.

Stenchikov, G. L., Kirchner, I., Robock, A., Graf, H. F., Antuna, J. C., Grainger, R. G., Lambert, A, and Thomason L.: Radiative forcing from

the 1991 Mount Pinatubo volcanic eruption, J. Geophys. Res., 103(D12), 13837-13857, 1998.

Stevens, B., *et al.*,: The atmospheric component of the MPI-M Earth System Model: ECHAM6, J. Adv. Model. Earth Syst., 5, 1-27, doi:10.1002/jame.20015, 2013.

Stier, P., Feichter, J., Kinne, S., Kloster, S., Vignati, E., Wilson, J., Ganzeveld, L., Tegen, I., Werner, M., Balkanski, Y., Schulz, M., Boucher, O., Minikin, A., and Petzold, A.: The aerosol-climate model ECHAM5-HAM, Atmos. Chem. Phys., 5, 1125-1156, doi:10.5194/acp-5-1125-2005, 2005.

Stocker, T., Qin, D., Plattner, G.-K., Tignor, M., Allen, S., Boschung, J., Nauels, A., Xia, Y., Bex, V., and Midgley, P.: The Physical Science Basis. Working Group I Contribution to the Fifth Assessment Report of the Intergovernmental Panel on Climate Change. In IPCC, 2013: Climate Change 2013 . Cambridge University Press, Cambridge, United Kingdom and New York, NY, USA, 2013.

Sundqvist, H., Berge, E., and Kristjansson, J. E.: Condensation and Cloud Parameterization Studies with a Mesoscale Numerical Weather Prediction Model, Mon. Weather Rev., 117, 1641-1657, 1989.

Tegen, I., Harrison, S. P., Kohfeld, K., Prentice, I. C., Coe, M., and Heimann, M.: Impact of vegetation and preferential source areas on global dust aerosol: results from a model study, J. Geophys. Res., 107, 4576, doi: 10.1029/2001JD000963, 2002.

Textor, C., Schulz, M., Guibert, S., Kinne, S., Balkanski, Y., Bauer, S., Berntsen, T., Berglen, T., Boucher, O., Chin, M., Dentener, F., Diehl, T., Easter, R., Feichter, H., Fillmore, D., Ghan, S., Ginoux, P., Gong, S., Grini, A., Hendricks, J., Horowitz, L., Huang, P., Isaksen, I., Iversen, I., Kloster, S., Koch, D., Kirkevg, A., Kristjansson, J. E., Krol, M., Lauer, A., Lamarque, J. F., Liu, X., Montanaro, V., Myhre, G., Penner, J., Pitari, G., Reddy, S., Seland, ., Stier, P., Takemura, T., and Tie, X.: Analysis and quanti cation of the diversities of aerosol life cycles within AeroCom, Atmos. Chem. Phys., 6, 1777-1813, doi:10.5194/acp-6-1777-2006, 2006.

Tilmes, S., Muller, R., and Salawitch, R.: The Sensitivity of Polar Ozone Depletion to Proposed Geoengineering Schemes, Science, 320, 1201-1204, doi: 10.1126/science.1153966, 2008.

Tilmes, S., Garcia, R. R., Kinnison, D. E., Gettelman, A., and Rasch, P. J.: Impact of geoengineered aerosols on the troposphere and stratosphere, J. Geophys. Res., 114, D12305, doi:10.1029/2008JD011420, 2009.

Tilmes, S., Fasullo, J., Lamarque, J.-F., Marsch, D. R., Mills, M., Alterskjr, K., Boucher, O., Cole, J. N. S., Curry, C. L., Haywood, J. M., Irvine, P. I., Ji, D., Jones, A., Karam, D. B., Kravitz, B, Kristjnsson, J. E., Moore, J. C., Muri, H., Niemeier, N., Rasch, P.J., Robock, A., Schmidt, H., Schulz, M., Singh, B., Watanabe, S., Yang, S. and Yoon, J.-H.: The hydrological impact of geoengineering in the Geoengineering Model Intercomparison Project (GeoMIP), J. Geophys. Res., 118(19), 11036-11058, doi:10.1002/jgrd.50868, 2013.

Tjiputra, J. F., Grini, A. and Lee, H.: Impact of idealized future stratospheric aerosol injection on the large-scale ocean and land carbon cycles, J. Geophys. Res. Biogeosci., 121, 2-27, doi:10.1002/2015JG003045, 2016.

Tsay, S.-C., *et al.*,: From BASE-ASIA towards 7-SEAS: A satellite-surface perspective of boreal spring biomass-burning aerosols and clouds in Southeast Asia, Atmos. Environ., 78, 20-34, doi:10.1016/j.atmosenv.2012.12.013, 2013.

Twomey, S.: Pollution and the planetary albedo, Atmos. Environ., 8, 1251-1256, doi:10.1016/0004-6981(74)90004-3, 1974.

UNFCCC. Conference of the Parties (COP) 21, Adoption of the Paris Agreement. Proposal by the President., L.9, Rev.1, 2015.

Vecchi, G. A. and Soden, B. J.: Global warming and the weakening of the tropical circulation J. Clim. 20 4316-40, 2007.

Vehkamaki, H., Kulmala, M., Napari, I., Lehtinen, K. E. J., Timmreck, C., Noppel, M., and Laaksonen, A.: An improved parameterization for sulfuric acid water nucleation rates for tropospheric and stratospheric conditions, J. Geophys. Res., 107, D22, 4622, doi:10.1029/2002JD002184, 2002.

Vignati, E., Wilson, J., and Stier, P.: M7: An e cient size-resolved aerosol microphysics module for large-scale aerosol transport models, J. Geophys. Res., 109, D22202, 2004.

Volodin, E. M., Kostrykin, S V., Ryaboshapko, A. G.: Climate response to aerosol injection at di erent stratospheric locations, Atmos. Sci. Lett., 12, 381-385, doi: 10.1002/asl.351, 2011.

Weisenstein, D. K., Keith, D. W., and Dykema, J. A.: Solar geoengineering using solid aerosol in the stratosphere, Atmos. Chem. Phys., 15, 11835-11859, doi:10.5194/acp-15-11835-2015, 2015.

WHO (World Health Organization): The global burden of disease: 2004 update, Geneva, 2008.

Wild, M., Folini, D., Schar, C., Loeb, N., Dutton, E. G., and Konig-Langlo, G.: The global energy balance from a surface perspective, Clim. Dyn., 40, 3107-3134, doi:10.1007/s00382-012-1569-8, 2013.

Winebrake, J. J., Corbett, J. J., Green, E. H., Lauer, A., and Eyring, V.: Mitigating the health impacts of pollution from oceangoing shipping: an assessment of low-sulfur fuel mandates, Environ. Sci. Technol., 43, 4776-4782, 2009.

Wood, R.: Stratocumulus Clouds, Mon. Weather Rev., 140, 2012.

Young & Freedman: University Physics with Modern Physics, 11th edition. Pearson, 2004.

Xia, L., Robock, A., Cole, J., Curry, C. L., Ji, D., Jones, A., Kravitz, B., Moore, J. C., Muri, H., Niemeier, U., Singh, B., Tilmes, S., Watanabe, S., and Yoon, J.-H.: Solar radiation management impacts on agriculture in China: A case study in the Geoengineering Model Intercomparison Project (GeoMIP), J. Geophys. Res.-Atmos., 119, 8695-8711, doi:10.1002/2013JD020630, 2015.

Xia, L., Robock, A., Tilmes, S., and Neely III, R. R.: Stratospheric sulfate geoengineering could enhance the terrestrial photosynthesis rate, Atmos. Chem. Phys., 16, 1479-1489, doi:10.5194/acp-16-1479-2016, 2016.

Zhang, Y.; Macke, A.; Albers, F., E ect of crystal size spectrum and crystal shape on stratiform cirrus radiative forcing, Atmospheric Research, 52, 59-75, 1999.

Zhang, K., ODonnell, D., Kazil, J., Stier, P., Kinne, S., Lohmann, U., Ferrachat, S., Croft, B., Quaas, J., Wan, H., Rast, S., and Feichter, J.: The global aerosol-climate model ECHAM-HAM, version 2: sensitivity to improvements in process representations, Atmos. Chem. Phys., 12, 8911-8949, doi:10.5194/acp-12-8911-2012, 2012.

I

Paper I

T. Kuhn, A.-I. Partanen, A. Laakso, Z. Lu, T. Bergman, S. Mikkonen, H. Kokkola, H. Korhonen, P. Raisanen, D. G. Streets, S. Romakkaniemi, and A. Laaksonen,
Climate impacts of changing aerosol emissions since 1996.
Geophys. Res. Lett. 41, 13, 4711-4718, doi:10.1002/2014GL060349, 2014.

AGU PUBLICATIONS

Geophysical Research Letters

RESEARCH LETTER
10.1002/2014GL060349

Key Points:
- Asian aerosol emissions cannot explain the 16 year hiatus in global warming
- The warming effect of black carbon has offset sulfate cooling

Supporting Information:
- Readme
- Text S1

Correspondence to:
T. Kühn,
thomas.h.kuhn@uef.fi

Citation:
Kühn, T., et al. (2014), Climate impacts of changing aerosol emissions since 1996, *Geophys. Res. Lett.*, *41*, 4711–4718, doi:10.1002/2014GL060349.

Received 1 MAY 2014
Accepted 20 JUN 2014
Accepted article online 24 JUN 2014
Published online 14 JUL 2014

Climate impacts of changing aerosol emissions since 1996

T. Kühn[1,2], A.-I. Partanen[3], A. Laakso[3], Z. Lu[4], T. Bergman[3], S. Mikkonen[1], H. Kokkola[3], H. Korhonen[3], P. Räisänen[2], D. G. Streets[4], S. Romakkaniemi[1,3], and A. Laaksonen[1,2]

[1]Department of Applied Physics, University of Eastern Finland, Kuopio, Finland, [2]Finnish Meteorological Institute, Helsinki, Finland, [3]Finnish Meteorological Institute, Kuopio, Finland, [4]Decision and Information Sciences Division, Argonne National Laboratory, Argonne, Illinois, USA

Abstract Increases in Asian aerosol emissions have been suggested as one possible reason for the hiatus in global temperature increase during the past 15 years. We study the effect of sulphur and black carbon (BC) emission changes between 1996 and 2010 on the global energy balance. We find that the increased Asian emissions have had very little regional or global effects, while the emission reductions in Europe and the U.S. have caused a positive radiative forcing. In our simulations, the global-mean aerosol direct radiative effect changes by 0.06 W/m^2 during 1996 to 2010, while the effective radiative forcing (ERF) is 0.42 W/m^2. The rather large ERF arises mainly from changes in cloudiness, especially in Europe. In Asia, the BC warming due to sunlight absorption has largely offset the cooling caused by sulphate aerosols. Asian BC concentrations have increased by a nearly constant fraction at all altitudes, and thus, they warm the atmosphere also in cloudy conditions.

1. Introduction

Apart from greenhouse gases, anthropogenic aerosols make the largest contribution to human-induced radiative forcing to the atmosphere, with an estimated global average of −1.9 to −0.1 W/m^2 (90% confidence interval) [*Myhre et al.*, 2013]. Due to air quality legislations, anthropogenic aerosol emissions in Europe and North America have continuously decreased since the 1980s [*Smith et al.*, 2011; *Granier et al.*, 2011]. After the collapse of the Soviet Union a declining trend has also been observed in Russia [*Stern*, 2005]. At the same time the sulphate and carbonaceous aerosol emissions in China and India have increased at an almost equal rate, and while emissions in China have started to level off recently, emissions in India continue to increase [*Lu et al.*, 2011]. As solar radiation increases with decreasing latitude, it is expected that the contribution of Asian aerosols to the global radiation budget is larger than that of Europe and North America [*Murphy*, 2013]. Furthermore, there are indications that the oxidation of sulphur dioxide to sulphate aerosols before its removal from the atmosphere is more effective in Asia [*Manktelow et al.*, 2007]. The resulting spatial redistribution of aerosol emissions appears to have no notable effect on the global-mean net direct aerosol effect [*Murphy*, 2013]. However, there is little information about the total aerosol forcing (including indirect aerosol effects) from the past two decades.

Here we study both the radiative forcing and climate response caused by the effective redistribution of aerosol emissions toward the equator. To this end, we employed a state-of-the-art aerosol-climate model [*Roeckner et al.*, 2003, 2006; *Stier et al.*, 2005; *Zhang et al.*, 2012] to simulate Earth's climate with aerosol emissions from years 1996 through 2010. In order to analyze the effects of aerosols alone, we kept all other anthropogenic conditions (e.g., greenhouse gas concentrations and land use) fixed both between individual simulations and consecutive model years of the same simulation.

2. Data and Methods

2.1. Model

For our simulations, we used the atmospheric general circulation model ECHAM-HAMMOZ (ECHAM5.5-HAM-2.0) at a horizontal resolution of T42 (roughly 2.8° by 2.8°) and a vertical resolution of 19 hybrid sigma-pressure levels [*Roeckner et al.*, 2003, 2006]. Aerosol processes are modeled within the HAM module which describes the aerosol size distribution using seven log-normal modes [*Stier et al.*, 2005; *Zhang et al.*, 2012]. It has been shown that the model simulates anthropogenic aerosol concentrations and aerosol optical depths (AOD) reasonably well [*Folini and Wild*, 2011; *Henriksson et al.*, 2011]. Cloud condensation nuclei (CCN) activation is described explicitly in the model using the Abdul-Razzak-Ghan parameterization

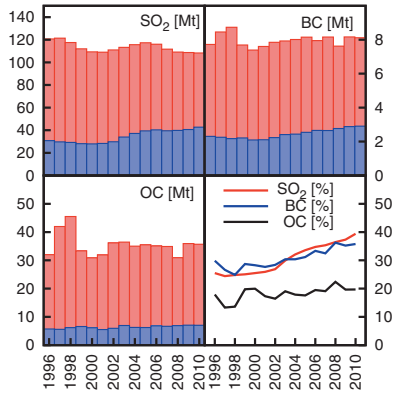

Figure 1. Yearly totals of anthropogenic aerosol emissions computed from the input data used for the simulations. Blue bars: combined emissions of China and India, red + blue bars: global total. Percentual contribution of China and India to the global total is shown in the bottom right panel.

[*Abdul-Razzak et al.*, 1998], thus accounting for aerosol microphysical effects on clouds (e.g., first indirect effect and lifetime effect). Semidirect effects via black carbon (BC) heating are also included. The oceans were either represented using prescribed sea surface temperatures or using a 50 m slab ocean model [*Roeckner et al.*, 2003; *Räisänen et al.*, 2008]. The version of ECHAM5 used for Intergovernmental Panel on Climate Change (IPCC) AR4 had an equilibrium climate sensitivity of 3.4 K due to doubling of atmospheric CO_2, with the average over all evaluated models being 3.2 K [*Randall et al.*, 2007]. However, that version did not include an interactive aerosol module and had somewhat higher resolution (T63L31).

2.2. Emission Data

A global inventory of SO_2, BC, and organic carbon (OC) emissions from all anthropogenic sectors including wildfires was built for the period 1996–2010 to support the model simulation. For China and India, the world's two largest anthropogenic aerosol generating countries, the comprehensive inventory developed by *Lu et al.* [2011] was used. Although there are some previous studies reporting aerosol emissions from China and India, none of them have presented year-by-year trends with up-to-date information, especially for the period after 2005 (see *Lu et al.* [2011] for details). Using a consistent technology-based methodology, *Lu et al.*'s [2011] inventory was based on time-dependent activity rates, technology penetration, emission factors, spatial proxies, etc., and was developed specifically for China and India during 1996–2010. Additionally, their emission trends have been shown to be in good agreement with the trends of aerosol optical depth (AOD) and SO_2 satellite observations [*Lu et al.*, 2011]. For all other regions, emissions were taken directly from the AeroCom-II-ACCMIP data set [*Lamarque et al.*, 2010; *Riahi et al.*, 2011] (Figure 1).

2.3. Experiments

Changes in the radiation budget were assessed by performing two simulations with the same prescribed sea surface temperature (SST) values (of year 1996) [*Uppala et al.*, 2005], but different, fixed aerosol emissions, corresponding to the years 1996 and 2010 (hereafter referred to as EMI-1996 and EMI-2010, respectively), thereby only allowing for rapid adjustments (including aerosol-radiation and aerosol-cloud interactions) of the climate. All other anthropogenic influences were fixed. Integration time was 20 years plus spin-up, and all results are given as averages over the whole modeling period.

To assess the long-term climate response, ECHAM-HAMMOZ was coupled to a 50 m thick slab ocean model [*Roeckner et al.*, 2003; *Räisänen et al.*, 2008]; otherwise, the simulation conditions were the same as for EMI-1996 and EMI-2010. Slab ocean models are commonly used for simulating equilibrium climate configurations as they greatly shorten integration times while introducing acceptable errors [*Danabasoglu and Gent*, 2009; *Li et al.*, 2013]. The first simulation, EQ-1996, was used as a baseline equilibrium configuration corresponding to the aerosol emissions of year 1996. The equilibrium climate response was then computed performing a second simulation, EQ-2010, with aerosol emissions for 2010. The equilibration time was 35 years whereafter the model was integrated for another 70 years, the latter of which were used for analysis.

To ascertain that the results of the above simulations are robust, we performed another set of 12 slab ocean simulations which were forced by yearly changing aerosol emissions. Each simulation was integrated over 15 years with aerosol emissions for the period from 1996 through 2010 (see Figure 1), with all other forcings constant. Each simulation was branched from a different model year of the EQ-1996 simulation. Note that these simulations are not meant to produce a realistic scenario for transient climate change, as for such simulations a full ocean model would be required. Instead, their sole purpose is to verify that the trends reported below are not the outcome of possible outliers in emission location and intensity of, e.g., wildfires of a certain year.

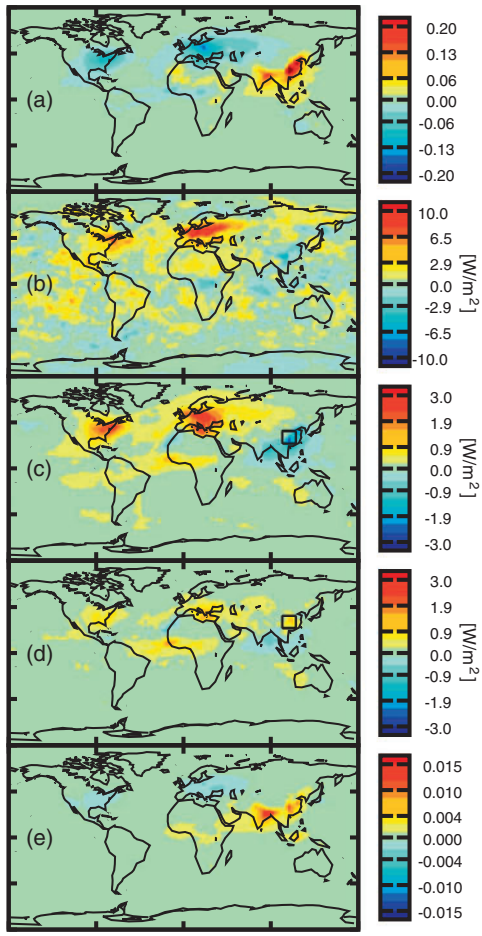

Figure 2. Results of the fixed SST simulations. (a) Change in AOD. (b) ERF. (c) Clear-sky and (d) all-sky direct aerosol forcings (with region of interest marked). (e) Change in BC absorption optical depth.

2.4. Statistical Tools

The statistical significance in the difference between simulations was tested using a multivariate dynamic linear model in which the autocorrelated structure of the data and the seasonal variation of the observations were taken into account. The Tukey HSD (honestly significant difference) test was used to perform multiple comparisons and thus define the significance (p value) for the change in the global-mean radiation balance (effective radiative forcing).

3. Results

3.1. Radiation Budget

The radiation budget results were obtained as the difference between the simulations EMI-1996 and EMI-2010 (see section 2.3), both of which used prescribed sea surface temperatures for year 1996. The difference in AOD agrees well with the change in aerosol emissions (Figure 2a). The absolute increase in AOD over China is larger in magnitude than the decrease over Europe and North America, with the relative change at peak points being roughly 50% over all affected areas. The regional trends in AOD change found here agree with the trends reported elsewhere [*Hsu et al.*, 2012; *Streets et al.*, 2009]. On the global scale the change in AOD is very small, totaling a decrease of 0.002 (1.3%).

The resulting change in total radiative forcing is quantified by means of the effective radiative forcing (ERF), which includes both direct and indirect aerosol effects [*Hansen et al.*, 2005; *Lohmann et al.*, 2010; *Myhre et al.*, 2013]. Here the ERF is calculated as the change in the total radiation balance at the top of the atmosphere between EMI-1996 and EMI-2010 (Figure 2b). We found a statistically highly significant global-mean ERF of 0.42 W/m^2 ($p = 2 \times 10^{-7}$). The strongest contribution to this value is a large positive ERF over Europe. In comparison, the magnitude of ERF over China and India is relatively small.

The global clear-sky direct aerosol radiative forcing (RF_c) amounts to 0.09 W/m^2 (Figure 2c), agreeing very well with recent findings [*Murphy*, 2013]. Due to masking by clouds, the all-sky global-mean direct aerosol radiative forcing (RF_a) is, in general, smaller in amplitude than RF_c, with a global average of 0.06 W/m^2 (Figure 2d). However, over East China where RF_c is negative, RF_a becomes positive (see the region of interest (ROI) marked in Figures 2c and 2d), thereby contributing to heating instead of cooling. For comparison, *Shindell et al.* [2013] find a weakening (i.e., a positive change) of global RF_a between 1980 and 2000 in six of nine models, with a spatial distribution that agrees qualitatively with Figure 2d. There, however, RF_a is slightly negative over East Asia.

These findings give rise to at least two questions. First, why is there such a large positive ERF over Europe? and second, why is the ERF small (and RF_a even slightly positive) over East China, in spite of a substantial increase in aerosol emissions and AOD there?

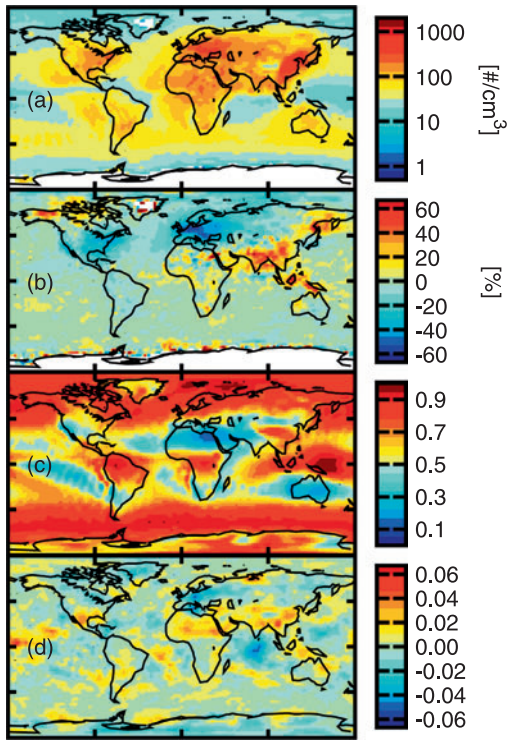

Figure 3. Change in cloud properties due to aerosol emission changes. (a) CDNC at cloud top for 1996 emissions. (b) CDNC relative change between 1996 and 2010. (c) Total cloud fraction for 1996 emissions. (d) Absolute change in total cloud fraction between 1996 and 2010.

Since the RF_a over Europe is much smaller than the ERF, the large and positive ERF has to be associated with changes in clouds. Figure 3a shows the average cloud droplet number concentration (CDNC) at cloud top for the 1996 emission inventory, and Figure 3b shows the corresponding relative change between 1996 and 2010. Over Europe, the relative decrease in CDNC is at maximum ≈60%. Furthermore, the total cloud fraction is decreased over Europe, with the decrease locally exceeding 0.04. The substantial decrease in CDNC and the reduction in total cloud fraction both reduce the reflection of solar radiation, thus explaining the large positive ERF over Europe.

Over China, total cloud fraction is increased by an amount comparable to the decrease over Europe (Figure 3d), and the CDNC is increased. In fact, the increase in CDNC between 1996 and 2010 is, in absolute terms, comparable to the decrease in Europe (not shown). However, the CDNC over China is very high already for the year 1996 emissions (Figure 3a), especially over the ROI marked in Figure 2c, the maximum over China being approximately twice as high as that over Europe. Consequently, the relative increase in CDNC in China (at maximum ≈40%) is smaller than the corresponding relative decrease over Europe (at maximum ≈60%). When other cloud properties are unchanged, cloud optical depth (COD) scales as $CDNC^{1/3}$ [see, e.g., *Platnick and Twomey*, 1994], which suggests that the increase in COD over China (up to 12%) would be less than the corresponding decrease over Europe (up to 26%). Thus, aerosol indirect effects are closer to saturation over China, which is consistent with the relatively small negative ERF there (see Figure 2b). It can also be seen from Figure 3b that over India, relative changes in CDNC are locally larger than over China, but there the local cloud fraction is much lower (Figure 3c), thus limiting the effect of the increase.

Furthermore, to explain why the RF_a over China is slightly positive in spite of a substantial increase in AOD, aerosol absorption optical depth (AAOD) needs to be considered. Looking at the change in BC AAOD between EMI-1996 and EMI-2010 (Figure 2e), we find that the increase over China and India is much stronger than the decrease over Europe and North America. Figure 4 shows vertical profiles of total AAOD, cloud optical depth (COD), and BC mass mixing ratio (Figure 4, left) and their change (Figure 4, middle and right) over the ROI marked in Figure 2d, visualizing both the strong increase of BC concentrations, which extends above the typical cloud level, and the relatively stronger increase in AAOD compared to COD. In our model the main contributors to AAOD are BC, OC, and dust. While the relative increase in BC mixing ratio is nearly constant above the ROI, relative changes in OC and dust mixing ratios (not shown) decline with height. We therefore attribute the increase in AAOD mainly to the increase in BC concentrations. This increase of BC, especially at high altitudes strongly counteracts the cooling effects of sulphate aerosols. Above Europe the overall BC concentration is much lower, thus making the effect of decreasing BC concentrations on AAOD much less pronounced. *Tsay et al.* [2013] find a frequent occurrence of absorbing aerosols (smoke plumes)

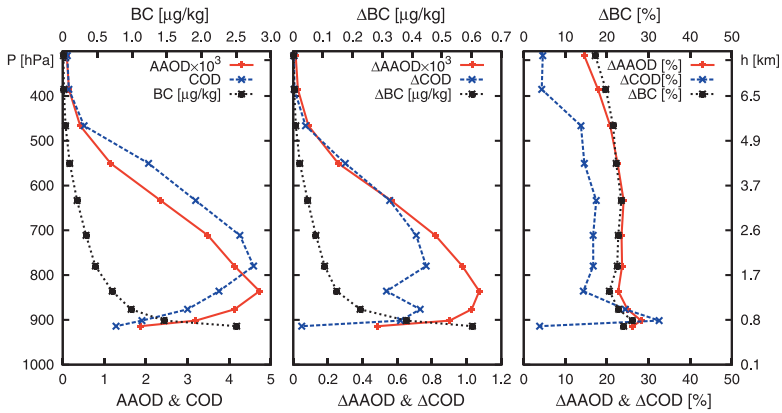

Figure 4. BC and clouds over East China over the region of interest as marked in Figures 2c and 2d. (left) AAOD (red), COD (blue), and BC mass mixing ratio (black) for EMI-1996. (middle) Absolute change and (right) relative change of the same quantities between EMI-1996 and EMI-2010. Note that AAOD and COD depend linearly on the (varying) model layer thickness.

above cloud over East Asia, and *Shindell et al.* [2013] report a strong positive RF_a over East Asia due to BC emissions from fossil and biofuel between 1980 and 2000. The relative increase in efficiency of BC light absorption in South and East Asia has also been noted in other studies [*Ramanathan et al.*, 2007; *Chand et al.*, 2009; *Ramana et al.*, 2010].

In summary, the large ERF over Europe in Figure 2b is explained by the decrease in CDNC and cloud fraction. However, over China and India, the ERF is small, in spite of increased CDNC and cloud fraction. We hypothesize that this occurs in part due to the increase of absorbing BC aerosols above clouds, and in part because the aerosol indirect effects are already nearly saturated for the 1996 emission values over China and India.

3.2. Climate Response

The climate response to changes in aerosol emissions was evaluated as the difference between the two equilibrium slab ocean simulations EQ-1996 and EQ-2010 (see section 2.3). A global annual-mean 2 m temperature increase of 0.25°C was found, with a larger warming over the Northern Hemisphere. Note that this kind of equilibrium experiment overestimates the contribution of aerosol changes to the transient temperature change between years 1996 and 2010, as in reality, part of the heat flux associated with the positive ERF would be stored deeper in the ocean (see the supporting information and Figure S1 for more discussion of this experiment).

The ensemble global-mean temperature of the additionally performed slab ocean simulations forced with yearly changing emissions increased fairly linearly with time, with a total increase of 0.014°C/yr between 1996 and 2010. Qualitatively, this result strengthens our conclusion that the warming due to changes in aerosol emissions is a robust feature and not only occurs due to possible outliers in emissions strengths of a particularly chosen year. Quantitatively, since the slab ocean model lacks the heat capacity of the deeper ocean layers, the transient temperature trend is overestimated and thus only the direction of the change is meaningful here.

4. Discussion and Conclusions

In general, climate projections of single models are problematic as the uncertainties in both emission strengths and model outcomes are large. *Granier et al.* [2011] find differences of up to a factor of 3 in the emission strengths between inventories for some regions and species. Model intercomparison projects like Coupled Model Intercomparison Project (CMIP), Atmospheric Chemistry and Climate Model Intercomparision Project (ACCMIP), and AeroCom address the discrepancies between the results of different climate models [*Shindell et al.*, 2013; *Stier et al.*, 2013; *Samset et al.*, 2013]. Vertical profiles of aerosol distributions

(especially BC) agree poorly between models, with the model used here agreeing well with average modeling results [*Samset et al.*, 2013]. A comparison has been made in the IPCC AR5 report (Figure 7.15) between BC vertical profiles measured in the Asian outflow over the East China Sea and the Yellow Sea and those from several climate models. The figure shows that ECHAM5-HAM is in excellent agreement with the measurements up to 600 mbar and underestimates the concentrations at higher altitudes [*Oshima et al.*, 2012; *Boucher et al.*, 2013]. Furthermore, the total increase in BC AAOD found by our model for the industrial era (1850–1996) of 0.00142 compares reasonably well to the recently reported model average of 0.00171 (1750 to the present) in *Bond et al.* [2013].

The AOD, RF_c, and RF_a trends found here agree reasonably well with results reported elsewhere [*Hsu et al.*, 2012; *Streets et al.*, 2009; *Murphy*, 2013; *Shindell et al.*, 2013]. Values for the aerosol ERF, on the other hand, vary a lot between models. *Shindell et al.* [2013] compared industrial era ERF values from eight models and found that the global-mean value of the local intermodel standard deviation of ERF was 1.27 W/m^2, with substantially larger values over much of South and East Asia.

Since the simulated aerosol forcing between 1996 and 2010, 0.42 W/m^2, appears quite large, it is pertinent to verify whether our model results are consistent with other aerosol-climate models. While we are not aware of other model estimates for the ERF for the time period 1996–2010, *Shindell et al.* [2013] report an aerosol ERF of -1.17 ± 0.29 W/m^2 between preindustrial (1850) and present day (2000) conditions, based on results of eight models. We performed an additional 20 year simulation for year 1850 emissions and found an ERF of -1.34 W/m^2 for the period 1850–1996, which lies well within the range of *Shindell et al.* [2013]. The ERF of -1.34 W/m^2 is mainly caused by the global SO_2 emission increase of 116.5 Mt/yr. The simultaneous BC emission increase of 4.6 Mt/yr has to some degree counteracted the negative aerosol forcing due to SO_2. On the other hand, as the aerosol radiative forcing between 1996 and 2010 caused by emission changes in China and India is relatively small, the ERF of 0.42 W/m^2 is mainly caused by the 25 Mt/yr SO_2 emission decrease and 0.6 Mt/yr BC emission decrease in other parts of the world. Taking into account these changes in the emissions, the ERF values for 1850–1996 and 1996–2010 are in fact in reasonable agreement.

Considering the large variation in ERF between different models [*Shindell et al.*, 2013], other models may not obtain the same quantitative results presented here. Indeed, it would be worth repeating the simulations with other state-of-the-art aerosol-climate models. Note also that in our simulations we do not address the dramatic increases of nitrogen oxide emissions (NO_x) in China and India [*Wang et al.*, 2012; *Lu and Streets*, 2012], which affect aerosols through changes in tropospheric ozone (thereby altering secondary organic aerosol formation) and by changing the competition between nitrate and sulphate for ammonia. This may very well "tip the scales" in areas where sulphate cooling and BC warming cancel each other.

In summary, our results suggest that the recent redistribution of anthropogenic aerosols from Europe and North America to South and East Asia has had a net warming effect. The positive ERF arises mainly from changes in clouds in Northern Hemisphere midlatitudes, especially Europe, and is related to reduced sulphate aerosols. Other studies have suggested that the recent hiatus in global warming may be caused by the internal dynamics of the climate system, like, for instance, large amounts of heat being stored in deeper ocean levels [*Meehl et al.*, 2011]. We find that the results obtained here support this notion. At a more general level, our results demonstrate that estimating aerosol radiative forcing based on global-mean AOD or emission inventories alone [*Kaufmann et al.*, 2011] may not be reliable, when aerosols are spatially redistributed. In particular, indirect aerosol effects can play a major role and they depend strongly on local conditions and meteorology. Finally, with Asian BC concentrations strongly increasing at all altitudes, thereby enhancing the warming effect of BC absorption also in cloudy conditions, BC mitigation measures become increasingly important.

Acknowledgments

The research has been supported by the strategic funding of the University of Eastern Finland, the Academy of Finland Centre of Excellence Program (project 1118615), and by the European Integrated Project Pegasos (FP7-ENV-2010-265148). Computational resources have been provided by CSC-IT Center for Science, Finland (project uef1593). H.K. and S.R. acknowledge Academy of Finland for the Academy Research Fellow positions (decisions 250348 and 267514). The ECHAM-HAMMOZ model is developed by a consortium composed of ETH Zürich, Max Planck Institut für Meteorologie, Forschungszentrum Jülich, University of Oxford, and the Finnish Meteorological Institute, and managed by the Center for Climate Systems Modeling (C2SM) at ETH Zürich. The data for this paper are available on request.

The Editor thanks two anonymous reviewers for their assistance in evaluating this paper.

References

Abdul-Razzak, H., S. J. Ghan, and C. Rivera-Carpio (1998), A parameterization of aerosol activation: 1. Single aerosol type, *J. Geophys. Res.*, *103*(D6), 6123–6131, doi:10.1029/97JD03735.

Bond, T. C., et al. (2013), Bounding the role of black carbon in the climate system: A scientific assessment, *J. Geophys. Res. Atmos.*, *118*, 5380–5552, doi:10.1002/jgrd.50171.

Boucher, O., et al. (2013), Clouds and aerosols, in *Climate Change 2013: The Physical Science Basis. Contribution of Working Group I to the Fifth Assessment Report of the Intergovernmental Panel on Climate Change*, pp. 571–657, Cambridge Univ. Press, Cambridge, U. K., and New York.

Chand, D., R. Wood, T. L. Anderson, S. K. Satheesh, and R. J. Charlson (2009), Satellite-derived direct radiative effect of aerosols dependent on cloud cover, *Nat. Geosci.*, *2*(3), 181–184, doi:10.1038/NGEO437.

Danabasoglu, G., and P. R. Gent (2009), Equilibrium climate sensitivity: Is it accurate to use a slab ocean model? *J. Clim.*, *22*, 2494–2499, doi:10.1175/2008JCLI2596.1.

Folini, D., and M. Wild (2011), Aerosol emissions and dimming/brightening in Europe: Sensitivity studies with ECHAM5-HAM, *J. Geophys. Res.*, *116*, D21104, doi:10.1029/2011JD016227.

Granier, C., et al. (2011), Evolution of anthropogenic and biomass burning emissions of air pollutants at global and regional scales during the 1980–2010 period, *Clim. Change*, *109*(1-2), 163–190, doi:10.1007/s10584-011-0154-1.

Hansen, J., et al. (2005), Efficacy of climate forcings, *J. Geophys. Res.*, *110*, D18104, doi:10.1029/2005JD005776.

Henriksson, S. V., A. Laaksonen, V.-M. Kerminen, P. Räisänen, H. Järvinen, A.-M. Sundström, and G. de Leeuw (2011), Spatial distributions and seasonal cycles of aerosols in India and China seen in global climate-aerosol model, *Atmos. Chem. Phys.*, *11*(15), 7975–7990, doi:10.5194/acp-11-7975-2011.

Hsu, N. C., R. Gautam, A. M. Sayer, C. Bettenhausen, C. Li, M. J. Jeong, S.-C. Tsay, and B. N. Holben (2012), Global and regional trends of aerosol optical depth over land and ocean using SeaWiFS measurements from 1997 to 2010, *Atmos. Chem. Phys.*, *12*(17), 8037–8053, doi:10.5194/acp-12-8037-2012.

Kaufmann, R. K., H. Kauppi, M. L. Mann, and J. H. Stock (2011), Reconciling anthropogenic climate change with observed temperature 1998–2008, *Proc. Natl. Acad. Sci.*, *108*, 11,790–11,793, doi:10.1073/pnas.1102467108.

Lamarque, J.-F., et al. (2010), Historical (1850–2000) gridded anthropogenic and biomass burning emissions of reactive gases and aerosols: Methodology and application, *Atmos. Chem. Phys.*, *10*(15), 7017–7039, doi:10.5194/acp-10-7017-2010.

Li, C., J.-S. von Storch, and J. Marotzke (2013), Deep-ocean heat uptake and equilibrium climate response, *Clim. Dyn.*, *40*, 1071–1086, doi:10.1007/s00382-012-1350-z.

Lohmann, U., L. Rotstayn, T. Storelvmo, A. Jones, S. Menon, J. Quaas, A. M. L. Ekman, D. Koch, and R. Ruedy (2010), Total aerosol effect: Radiative forcing or radiative flux perturbation? *Atmos. Chem. Phys.*, *10*(7), 3235–3246, doi:10.5194/acp-10-3235-2010.

Lu, Z., and D. G. Streets (2012), Increase in NO_x emissions from Indian thermal power plants during 1996–2010: Unit-based inventories and multisattelite observations, *Environ. Sci. Technol.*, *46*, 7463–7470, doi:10.1021/es300831w.

Lu, Z., Q. Zhang, and D. G. Streets (2011), Sulfur dioxide and primary carbonaceous aerosol emissions in China and India, 1996–2010, *Atmos. Chem. Phys.*, *11*(18), 9839–9864, doi:10.5194/acp-11-9839-2011.

Manktelow, P. T., G. W. Mann, K. S. Carslaw, D. V. Spracklen, and M. P. Chipperfield (2007), Regional and global trends in sulfate aerosol since the 1980s, *Geophys. Res. Lett.*, *34*, L14803, doi:10.1029/2006GL028668.

Meehl, G. A., J. M. Arblaster, J. T. Fasullo, A. Hu, and K. E. Trenberth (2011), Model-based evidence of deep-ocean heat uptake during surface-temperature hiatus periods, *Nat. Clim. Change*, *1*, 360–364, doi:10.1038/nclimate1229.

Murphy, D. M. (2013), Little net clear-sky radiative forcing from recent regional redistribution of aerosols, *Nat. Geosci.*, *4*, 258–262, doi:10.1038/ngeo1740.

Myhre, G., et al. (2013), Anthropogenic and natural radiative forcing, in *Climate Change 2013: The Physical Science Basis. Contribution Of Working Group I To The Fifth Assessment Report of the Intergovernmental Panel On Climate Change*, pp. 659–740, Cambridge Univ. Press, Cambridge, U. K., and New York.

Oshima, N., et al. (2012), Wet removal of black carbon in Asian outflow: Aerosol radiative forcing in East Asia (A-FORCE) aircraft campaign, *J. Geophys. Res.*, *117*, D03204, doi:10.1029/2011JD016552.

Platnick, S., and S. Twomey (1994), Determining the susceptibility of cloud albedo to changes in droplet concentration with the Advanced Very High Resolution Radiometer, *J. Appl. Meteorol.*, *33*, 334–347, doi:10.1175/1520-0450(1994)0332.0.CO.

Räisänen, P., S. Järvenoja, and H. Järvinen (2008), Noise due to the Monte Carlo independent-column approximation: Short-term and long-term impacts in ECHAM5, *Q. J. R. Meteorol. Soc.*, *134*, 481–495, doi:10.1002/qj.231.

Ramana, M. V., V. Ramanathan, Y. Feng, S.-C. Yoon, S.-W. Kim, G. R. Carmichael, and J. J. Schauer (2010), Warming influenced by the ratio of black carbon to sulphate and the black-carbon source, *Nat. Geosci.*, *3*, 542–545, doi:10.1038/ngeo918.

Ramanathan, V., M. V. Ramana, G. Roberts, D. Kim, C. Corrigan, C. Chung, and D. Winker (2007), Warming trends in Asia amplified by brown cloud solar absorption, *Nature*, *448*, 575–578, doi:10.1038/nature06019.

Randall, D., et al. (2007), Climate models and their evaluation, in *Climate Change 2007: The Physical Science Basis. Contribution of Working Group I to the Fourth Assessment Report of the Intergovernmental Panel on Climate Change*, pp. 589–662, Cambridge Univ. Press, Cambridge, U. K., and New York.

Riahi, K., S. Rao, V. Krey, C. Cho, V. Chirkov, G. Fischer, G. Kindermann, N. Nakicenovic, and P. Rafaj (2011), Rcp 8.5—A scenario of comparatively high greenhouse gas emissions, *Clim. Change*, *109*, 33–57, doi:10.1007/s10584-011-0149-y.

Roeckner, E., et al. (2003), The atmospheric general circulation model ECHAM5, Part I: Model description, *Report 349*, Max Planck Institute for Meteorology, Hamburg, Germany.

Roeckner, E., R. Brokopf, M. Esch, M. Giorgetta, S. Hagemann, L. Koernblueh, E. Manzini, U. Schlese, and U. Schulzweida (2006), Sensitivity of simulated climate to horizontal and vertical resolution in the ECHAM5 atmosphere model, *J. Clim.*, *19*, 3771–3791, doi:10.1175/JCLI3824.1.

Samset, B. H., et al. (2013), Black carbon vertical profiles strongly affect its radiative forcing uncertainty, *Atmos. Chem. Phys.*, *13*(5), 2423–2434, doi:10.5194/acp-13-2423-2013.

Shindell, D. T., et al. (2013), Radiative forcing in the ACCMIP historical and future climate simulations, *Atmos. Chem. Phys.*, *13*(6), 2939–2974, doi:10.5194/acp-13-2939-2013.

Smith, S. J., J. van Aardenne, Z. Klimont, R. J. Andres, A. Volke, and S. Delgado Arias (2011), Anthropogenic sulfur dioxide emissions: 1850–2005, *Atmos. Chem. Phys.*, *11*(3), 1101–1116, doi:10.5194/acp-11-1101-2011.

Stern, D. I. (2005), Global sulfur emissions from 1850 to 2000, *Chemosphere*, *58*(2), 163–175, doi:10.1016/j.chemosphere.2004.08.022.

Stier, P., et al. (2005), The aerosol-climate model ECHAM5-HAM, *Atmos. Chem. Phys.*, *5*, 1125–1156, doi:10.5194/acp-5-1125-2005.

Stier, P., et al. (2013), Host model uncertainties in aerosol radiative forcing estimates: Results from the AeroCom prescribed intercomparison study, *Atmos. Chem. Phys.*, *13*(6), 3245–3270, doi:10.5194/acp-13-3245-2013.

Streets, D. G., F. Yan, M. Chin, T. Diehl, N. Mahowald, M. Schultz, M. Wild, Y. Wu, and C. Yu (2009), Anthropogenic and natural contributions to regional trends in aerosol optical depth, 1980–2006, *J. Geophys. Res.*, *114*, D00D18, doi:10.1029/2008JD011624.

Tsay, S.-C., et al. (2013), From BASE-ASIA towards 7-SEAS: A satellite-surface perspective of boreal spring biomass-burning aerosols and clouds in Southeast Asia, *Atmos. Environ.*, *78*, 20–34, doi:10.1016/j.atmosenv.2012.12.013.

Uppala, S. M., et al. (2005), The ERA-40 re-analysis, *Q. J. R. Meteorol. Soc.*, *131*, 2961–3012, doi:10.1256/qj.04.176.
Wang, S. W., Q. Zhang, D. G. Streets, K. B. He, R. V. Martin, L. N. Lamsal, D. Chen, Y. Lei, and Z. Lu (2012), Growth in NO_x emissions from power plants in China: Bottom-up estimates and satellite observations, *Atmos. Chem. Phys.*, *12*(10), 4429–4447, doi:10.5194/acp-12-4429-2012.
Zhang, K., et al. (2012), The global aerosol-climate model ECHAM-HAM, version 2: Sensitivity to improvements in process representations, *Atmos. Chem. Phys.*, *12*, 8911–8949, doi:10.5194/acp-12-8911-2012.

II

Paper II

T. Mielonen, A. Laakso, A. Karhunen, H. Kokkola, A.-I. Partanen, H. Korhonen, S. Romakkaniemi and K. E.J. Lehtinen,
From nuclear power to coal power: Aerosol-induced health and radiative effects
J. Geophys. Res. Atmos., 120, 12,631-12,643, 2015.

AGU PUBLICATIONS

JGR

Journal of Geophysical Research: Atmospheres

RESEARCH ARTICLE

10.1002/2015JD024183

Key Points:
- Replacement of nuclear power with coal power would cause 150,000 deaths per year
- Two thirds of the premature deaths would occur in Europe
- CO_2 emissions from coal power would accelerate climate warming after 37 years

Correspondence to:
T. Mielonen,
tero.mielonen@fmi.fi

Citation:
Mielonen, T., A. Laakso, A. Karhunen, H. Kokkola, A.-I. Partanen, H. Korhonen, S. Romakkaniemi, and K. E. J. Lehtinen (2015), From nuclear power to coal power: Aerosol-induced health and radiative effects, *J. Geophys. Res. Atmos.*, *120*, 12,631–12,643, doi:10.1002/2015JD024183.

Received 4 SEP 2015
Accepted 24 NOV 2015
Accepted article online 27 NOV 2015
Published online 22 DEC 2015

From nuclear power to coal power: Aerosol-induced health and radiative effects

Tero Mielonen[1], Anton Laakso[1], Anni Karhunen[1], Harri Kokkola[1], Antti-Ilari Partanen[2,3], Hannele Korhonen[2], Sami Romakkaniemi[1], and Kari E. J. Lehtinen[1,4]

[1]Finnish Meteorological Institute, Kuopio, Finland, [2]Finnish Meteorological Institute, Helsinki, Finland, [3]Department of Geography, Planning and Environment, Concordia University, Montreal, Quebec, Canada, [4]Department of Applied Physics, University of Eastern Finland, Kuopio, Finland

Abstract We have investigated what would be the climate and PM-induced air quality consequences if all nuclear reactors worldwide were closed down and replaced by coal combustion. In a way, this presents a "worst-case scenario" since less polluting energy sources are available. We studied simultaneously the radiative and health effects of coal power emissions using a global 3-D aerosol-climate model (ECHAM-HAMMOZ). This approach allowed us to estimate the effects of a major global energy production change from low carbon source to a high carbon one using detailed spatially resolved population density information. We included the radiative effects of both CO_2 and $PM_{2.5}$ but limited the study of health effects to $PM_{2.5}$ only. Our results show that the replacement of nuclear power with coal power would have globally caused an average of 150,000 premature deaths per year during the period 2005–2009 with two thirds of them in Europe. For 37 years the aerosol emissions from the additional coal power plants would cool the climate but after that the accumulating CO_2 emissions would accelerate the warming of the climate.

1. Introduction

Energy supply sector accounts for ~35% of global greenhouse gas (GHG) emissions [*Intergovernmental Panel on Climate Change* (*IPCC*), 2014], with electricity and heat production accounting for ~42% of carbon dioxide (CO_2) emissions [*International Energy Agency*, 2014]. In addition, it is a major source of other air pollutants [*European Environment Agency*, 1999]. It is therefore evident that the energy strategies we choose during the coming decades have a crucial role in determining our success in solving two major global challenges: mitigation of climate change and improvement of air quality. To ensure sustainable development and significant greenhouse gas and air pollution emission reductions, very likely, all technological options—nuclear, many types of renewables, carbon capture and storage, and smart grids and new transport technologies—are needed in the near future [*IPCC*, 2014].

Nuclear power (fission) can be considered a clean energy source with respect to climate and air quality, as it produces significantly less greenhouse gases and traditional air pollutants than, e.g., energy production from fossil fuels [*Lenzen*, 2008]. It has been calculated that GHG emissions from the full life cycle of hard coal and natural gas technologies are 410–950 g CO_2-e/kWh_{el} (CO_2-equivalent GHG emissions for every kWh of electricity generated) [*IPCC*, 2014]. On the other hand, the actual energy production with fission does not produce greenhouse gas emissions but there are indirect emissions originating from the nuclear fuel cycle. The sources for these emissions are uranium mining, milling, enrichment, fuel fabrication, reactor construction and operation, decommissioning, fuel reprocessing, nuclear waste storage and disposal, and transport. Thus, for the whole cycle, greenhouse gas emissions from nuclear power are 4–110 g CO_2-e/kWh_{el}, i.e., roughly 1 to 2 orders magnitude lower than for combustion of coal. As a comparison, the corresponding emissions from wind turbines and hydroelectricity are 7–56 g CO_2-e/kWh_{el} and 10–30 g CO_2-e/kWh_{el}, respectively. From solar photovoltaic and concentrated solar power the emissions are 18–180 g CO_2-e/kWh_{el} and 9–63 g CO_2-e/kWh_{el}, respectively [*IPCC*, 2014].

However, a major concern with nuclear power is the (however small) possibility of release of radioactive material into the atmosphere, hydrosphere, or soil. In 2011, this risk was demonstrated in the nuclear accident in Fukushima, Japan. Several countries are thus facing the question whether the economic and environmental benefits of nuclear energy outweigh the risks related to radioactive contamination [*Wolf*, 2015]. In Japan the nuclear power plants were progressively shut down following the Fukushima accident but the government has recommenced nuclear power generation even though the majority of public opinion is opposing [*Ipsos*, 2011]. The first nuclear reactor was restarted in August 2015 (World Nuclear Association (WNA), world-nuclear.org/info/Country-Profiles/Countries-G-N/Japan/). On the other hand, in Germany the

government is planning a complete phase out of nuclear energy by the year 2022, and the fraction of electricity from nuclear energy has already dropped from 18% in 2011 to the current 16% [*AG Energiebilanzen*, 2015]. Although the reduction in nuclear power has been replaced with renewable energy to some extent (mainly wind power, biomass burning, and solar power), the fraction of coal combustion also increased up to 2013 [*AG Energiebilanzen*, 2015]. Furthermore, when the overall energy demand recovers, the use of coal might increase again. As global GHG emissions are rising at an alarming rate, it is important to investigate the effects of these significant shifts with state-of-the-art modeling tools.

In this study, we investigate what would be the climate and PM-induced air quality consequences if all nuclear reactors worldwide were closed down and replaced by coal combustion. In a way, this presents a "worst-case scenario" since less polluting energy sources are available. However, coal combustion is one of the cheapest sources of energy [*U.S. Energy Information Administration*, 2015] and its usage can increase the national energy supply security in countries with abundant national supplies [*Sims et al.*, 2007]. Currently, approximately 25% of the energy consumption worldwide is produced by burning coal, constituting of over 40% share of anthropogenic CO_2 emissions [*Smith et al.*, 2013]. In addition, burning of coal produces a significant amount of pollutants; thus, the largest air quality hazard from coal power arises from inhalation of the combustion products emitted to the atmosphere [*Krewitt et al.*, 1998; *Rashad and Hammad*, 2000]. Of the emitted and inhaled combustion products, the most hazardous are fine particles ($PM_{2.5}$, aerosol particles smaller than 2.5 μm in diameter) that may have several adverse effects on human health, such as lung cancer and cardiopulmonary diseases [*Markandya and Wilkinson*, 2007]. In a very recent study, *Apte et al.* [2015] found that of the 3.2 million annual deaths globally attributed to ambient $PM_{2.5}$ from all emission sources, several hundred thousands could be avoided with pollution prevention according to the World Health Organization (WHO) guidelines. However, the same aerosol particles emitted from coal combustion, which are responsible for the adverse negative health effects, mask a part of the positive radiative forcing caused by greenhouse gases [*IPCC*, 2014]. Therefore, PM-targeted air pollution controls can be expected to lead to regional warming in many parts of the world [*Pietikäinen et al.*, 2015]. All these challenges are especially important in Asia, where both the population and the average standard of living are increasing fast, and significant investments to the energy system are needed in order to meet the climate and the air quality goals [*van Vliet et al.*, 2012].

Our work was very much motivated by the study by *Kharecha and Hansen* [2013], who investigated the contribution of nuclear power generation on preventing air pollution-related deaths and greenhouse gas emissions during the years 1971–2009, when compared to a world in which the equivalent amount of energy would have been produced with coal and natural gas. They concluded that during this time nuclear power has been responsible for preventing an average of 1.84 million deaths and 64 Gt of CO_2-e emissions cumulatively. Their estimates were based on simple mortality and GHG emission factors, in deaths/TWh and CO_2-e/TWh, respectively. While these factors took into account all stages of the fuel cycle, from fuel extraction to electricity transport, the climate impacts of particulate matter were not considered. The climate (but not health) impacts of PM were investigated by *Shindell and Faluvegi* [2010] who used the Goddard Institute for Space Studies general circulation model which incorporates aerosol chemistry to study the radiative forcing from global coal-fired power plant emissions. They found that the combined forcing of coal combustion emitted CO_2, ozone, and aerosol precursors from 1970 to 2000 was strongly positive and that imposing air quality pollution controls will likely accelerate warming rates in the future.

In our work, we simultaneously focus on the climate and air quality effects from coal power emissions using a state-of-the-science global 3-D climate model. This approach allows us, to our knowledge for the first time, to estimate the radiative and health effects of a major global energy production change using detailed spatially resolved population density information. We include the climate effects of both CO_2 and $PM_{2.5}$ but limit the study of health effects to $PM_{2.5}$ only. Health effects of ozone were not considered because they are insignificant when compared with effects from $PM_{2.5}$ [*Friedrich*, 2005]. Since the dominant effects of the coal fuel cycle on public health arise from exposure to air pollution emitted during power plant operation, our investigation is limited to these emissions only [*European Commission*, 1995].

2. Methods

In order to investigate the climate and PM-based air quality impacts of replacing nuclear energy with coal power plants, we assumed that all operational nuclear reactors in year 2012 (shown in Figure 1) would be

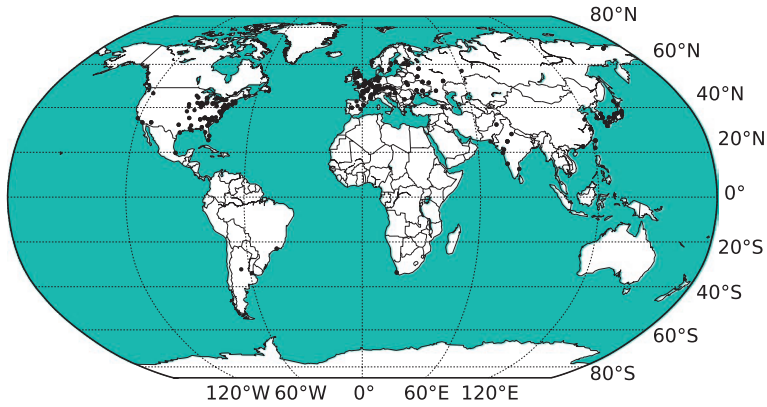

Figure 1. Locations of nuclear power plants which were operational in 2012 (WNA, world-nuclear.org/NuclearDatabase/Default.aspx?id=27232). Note that the Japanese nuclear power plants shown in the figure were stopped by May 2012 following the Fukushima accident.

replaced by coal power plants producing the same amount of energy at the location of the original nuclear plant. To calculate the climate and air quality impacts of particulate emissions (organic carbon, black carbon, and sulfate) from the coal power plants, we applied the 3-D global climate model ECHAM-HAMMOZ (section 2.1.1). On the other hand, the climate impacts from the additional CO_2 emissions from the coal plants were calculated offline (section 2.2). The PM-induced health effects were estimated by calculating annual excess mortality rates (section 2.1.3).

2.1. Radiative and Health Effects of Particulate Matter

2.1.1. ECHAM-HAMMOZ

In this study, we have used the development version of the global aerosol-climate model ECHAM-HAMMOZ (ECHAM6.1-HAM2.2-SALSA) [*Stier et al*., 2005; *Zhang et al*., 2012; *Bergman et al*., 2012]. The model consists of an atmospheric core model ECHAM, which solves the fundamental equations for the atmospheric flow and physics and tracer transport, and of an aerosol model HAM. The aerosol microphysics was calculated using Sectional Aerosol module for Large Scale Applications (SALSA) [*Bergman et al*., 2012; *Kokkola et al*., 2008] which describes the aerosol population consisting of sulfate (SO_4), sea salt, organic carbon (OC), black carbon (BC), and dust using 10 size sections to cover the size range from 3 nm to 10 μm. AeroCom-II Atmospheric Chemistry and Climate Model Intercomparison Project (ACCMIP) data [*Riahi et al*., 2007, 2011] were used for the anthropogenic and biomass burning aerosol emissions in the model. Natural emissions were simulated as described in *Zhang et al*. [2012]. The formation of secondary organic aerosol (SOA) from biogenic emissions was taken into account according to *Tunved et al*. [2006]. Significant amounts of SOA are also produced from burning of biomass, biofuel, and fossil fuels [*Shrivastava et al*., 2015], but they are not considered in the model. This may cause an underestimation of $PM_{2.5}$ values over areas where SOA from other than biogenic sources compose a large fraction of aerosol mass. Interactions between the aerosols and radiation were calculated online [*Zhang et al*., 2012], and the first and the second indirect effects were calculated following *Lohmann and Hoose* [2009]. The activation of aerosol particles into cloud droplets was calculated with the semiempirical parameterization of *Lin and Leaitch* [1997]. The simulations were done using T63 horizontal resolution (roughly $1.9 \times 1.9°$) and 31 pressure levels that reached up to 10 hPa.

2.1.2. Experiment Design

Figure 1 presents the locations of the operational nuclear reactors in 2012 (WNA, world-nuclear.org/NuclearDatabase/Default.aspx?id=27232) which were used in this study. To get the amount of energy produced by these plants, we multiplied the maximum powers of the plants with the energy availability factor (EAF) (International Atomic Energy Agency (IAEA), www.iaea.org/PRIS/home.aspx). We used an average EAF of 78% based on the active reactors for all the plants. Typically, the EAFs for nuclear reactors range from around 60% to about 90% and during the last 20 years the globally averaged EAF has varied between 73% and 84% (IAEA, www.iaea.org/PRIS/home.aspx). Therefore, we feel that the selected EAF value is a reasonable estimate for this study.

The average emissions from coal power plants in the U.S. from the year 2009 were used as emission estimates for the coal power plants that are used to replace nuclear power. Most of the nuclear reactors are located in western countries; thus, this can be considered a reasonable simplification. However, we acknowledge that if building of new coal plants with the best available technology were required, their emission factors could be even 90% lower than those of the current plants used in our calculations [*Global Energy Assessment*, 2012]. The emissions consist of 2.97 kg/MWh of sulfur dioxide (SO_2) and 0.196 kg/MWh of $PM_{2.5}$ [*Global Energy Assessment*, 2012]. Black carbon (BC) and organic carbon (OC) emissions were calculated from the $PM_{2.5}$ emissions. *Chow et al.* [2011] estimated that elemental carbon (EC) and OC fractions from $PM_{2.5}$ emissions are 1.38–4.1% and 5.2–27%, respectively. Although BC and EC are fundamentally different quantities [*Jeong et al.*, 2004], they are typically used interchangeably when discussing light-absorbing carbon emissions from coal power plants [*Chow et al.*, 2011]. Therefore, we did not find a usable ratio for BC and EC emissions and assumed that BC emissions are equal to EC emissions. Furthermore, we chose the upper limits of these ranges in order to see the maximum effect of the emissions on radiative transfer (although other studies such as *Bond et al.* [2013] have used lower fractions for this source). The remaining particulate mass in the emissions was assumed to consist of sulfates.

We made two simulations with the ECHAM-HAMMOZ climate model for the years 2005–2009. In the simulations, the model meteorology was nudged toward European Centre for Medium-Range Weather Forecasts ERA-Interim reanalysis data [*Dee et al.*, 2011] and the simulations were started with 4 month spin-ups. The control run was made using the Aerocom-II ACCMIP emissions for the year 2006, while the coal power simulation was made using additional OC, BC, and SO_2 emissions that were placed to the sites of the nuclear power plants. The CO_2 emissions were not increased in the modified model run because CO_2 is a long-lived species in the atmosphere; thus, its effect could be calculated offline. We assumed that the coal power plants produced energy as much as the nuclear power plants they replaced.

Based on these two model runs, we were able to calculate the PM-induced health and radiative effects of the aerosol emissions. As an estimate of health effects, we used premature deaths (see section 2.1.3 for more details). The climate effects of aerosols were estimated as the effective radiative forcing (ERF, also known as radiative flux perturbation) [*Haywood et al.*, 2007]. In practice, we calculated the difference between all-sky top-of-the atmosphere net total radiation from the two simulations. Aerosol direct and indirect effects are included in ERF; thus, the total aerosol forcing can be directly compared with the forcing from well-mixed greenhouse gases [*Lohmann et al.*, 2010]. The nudging of the model meteorology reduces the noise of the spatial distribution of the aerosol forcing and may result in somewhat different patterns than simulations with free meteorology. However, the global mean radiative forcing values are similar in both nudged and free model runs [*Lohmann and Hoose*, 2009]. We also analyzed the aerosol direct radiative effect (ADRE) to see how the increased aerosol emissions affect scattering and absorption of incoming solar radiation.

2.1.3. Premature Mortality Due To Increased PM Emissions From Coal Power Plants

The aerosol-climate model produced the mass concentrations of particulate matter with dry diameters less than 2.5 μm ($PM_{2.5}$). The long-term health effects for the scenario with increased coal power were estimated using the 5 year mean (2005–2009) values of surface level $PM_{2.5}$ concentration. The control simulation was used as the reference. Similarly to the study by *Partanen et al.* [2013], we used the methods by *Ostro* [2004] to calculate the premature mortality from cardiopulmonary diseases (cardiovascular diseases and chronic obstructive pulmonary disease) and lung cancer (trachea, bronchus, and lung cancers) due to long-term exposure to emissions from coal power plants. The changes in $PM_{2.5}$ concentrations can be related to annual excess mortality rates (E, deaths per year) with the following concentration-response function

$$E = \left[1 - \left(\frac{PM_{2.5,c} + 1}{PM_{2.5} + 1}\right)^{\beta}\right] \times B_y \times P_{30+}, \quad (1)$$

where $PM_{2.5,c}$ is the reference concentration (μg m^{-3}) from the control run and $PM_{2.5}$ the concentration in the scenario with additional coal power emissions; β is a cause-specific coefficient with a value of 0.15515 (95% confidence interval: 0.0562–0.2541) for cardiopulmonary diseases and 0.23218 (95% confidence interval: 0.08563–0.37873) for lung cancer [*Ostro*, 2004]; B_y is the baseline mortality rate (e.g., deaths per year

per 1000 people) for cardiopulmonary diseases or lung cancer in the exposed population with age over 30 years (P_{30+}) (the analysis by *Ostro* [2004] considered only this age group). The uncertainties related to equation (1) are discussed in section 3.5, and they are taken into account to some degree by using the 95% confidence intervals for β. More refined concentration-response functions have been published [e.g., *Burnett et al.*, 2014], but they are also limited by the lack of long-term cohort studies from East and South Asia and Middle East where the ambient exposures to particulate matter are much higher than in Europe and North America. Furthermore, the toxicity of $PM_{2.5}$ is assumed to depend solely on the mass and not on the composition or size also in the newer concentration-response functions. Therefore, we feel that the selected function is sufficient for an order of magnitude study. In the future, this approach should be revised as more information on the relationships between mortality, aerosol composition, and size distribution become available.

Baseline mortality rates and the fraction of people in the exposed age group were calculated using data provided by the *World Health Organization* [2008] based on six WHO regions (WHO, www.who.int/about/regions/en/index.html) [see *Partanen et al.*, 2013, Figure 2] gridded onto the model grid resolution. We used the population density data for the year 2010 from the Socioeconomic Data and Applications Center at Columbia University [*NASA Socioeconomic Data and Applications Center*, 2005]. Population density data (with 2.5 arc min grid cells originally) were also interpolated onto the model grid resolution.

2.2. CO_2 Emissions and Their Radiative Effects

To estimate the radiative effects of CO_2 originating from power production, we assumed that it is well mixed in the atmosphere and thus we calculated only the global radiative effects of CO_2 offline. We assumed that CO_2 has no health effects because the atmospheric concentrations do not rise to detrimental levels [*Robertson*, 2006]. Furthermore, increased CO_2 levels will increase the temperature which in turn will cause adverse health effects. However, they are also ignored in this study due to the large variety and uncertainties of the effects [*Watts et al.*, 2015].

The mass of the CO_2 emissions, m_{CO2}, from the coal power plants was calculated as follows:

$$m_{CO2} = P \cdot e, \tag{2}$$

where P is the total amount of electricity produced by all nuclear power plants in 2012, namely, $2346.2° \times 10^6$ MWh [*International Atomic Energy Agency*, 2013], and e is the average CO_2 emission from coal and peat power plants in 2009, namely, 977 kg/MWh [*International Energy Agency*, 2012]. Consequently, the total mass of the CO_2 emissions from the coal power plants assumed in this study to replace nuclear plants is 2.29 Gt CO_2 annually.

Not all of the CO_2 emissions stay in the atmosphere, and thus, we calculated the increase in the atmospheric CO_2 concentration as follows:

$$\Delta X_{CO_2} = \frac{m_{CO2} \cdot M_C}{M_{CO2}} \cdot \frac{a}{2.13}, \tag{3}$$

where M_C is the molar mass of carbon (12.011 g/mol) and M_{CO2} is the molar mass of CO_2 (44.011 g/mol); a is the fraction of CO_2 that remains in the atmosphere, which was chosen to be 0.43 [*Raupach et al.*, 2008]. The factor 2.13 (Gt C/ppm CO_2) is used to convert the carbon mass to atmospheric concentration of CO_2 (Carbon Dioxide Information Analysis Center, http://cdiac.ornl.gov/pns/convert.html). Finally, the change in the radiative forcing, ΔF, was calculated using the following equation [*Myhre et al.*, 1998]:

$$\Delta F = 5.35 \cdot \ln\left(\frac{X_{CO2} + \Delta X_{CO2}}{X_{CO2}}\right) \left[\mathrm{W/m^2}\right], \tag{4}$$

where X_{CO2} is the average CO_2 concentration in the year 2013, i.e., 395 ppm (NOAA, www.esrl.noaa.gov/gmd/ccgg/trends/global.html).

3. Results and Discussion

3.1. Effects of Increased Coal Power Emissions on CO_2 Concentrations

The annual increase in CO_2 emissions was calculated with equation (2). The result of 2.29 Gt CO_2 is in a good agreement with previous studies. *International Energy Agency* [2011] calculated that if electricity produced with nuclear power in 2010 had been produced in equal parts with natural gas and coal instead, the CO_2

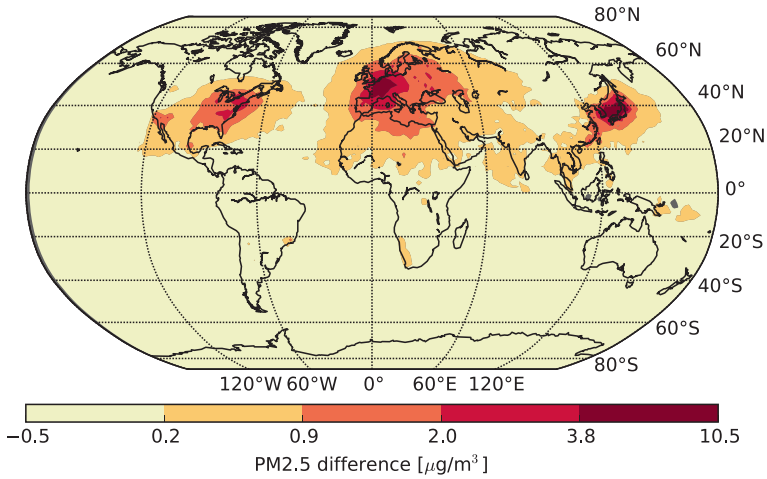

Figure 2. Change in simulated surface $PM_{2.5}$ concentration when nuclear power plants were replaced with coal power plants. The average difference is calculated from a 5 year simulation (2005–2009).

emissions would have increased by 2.1 Gt CO_2. The estimate by *Kharecha and Hansen* [2013] of 2.6 Gt CO_2 is also in the same range. In both studies nuclear power was partly replaced by natural gas which would explain why our estimate is larger than the estimate by IEA. On the other hand, our estimate is smaller than the estimate by Kharecha and Hansen because they used slightly different emission factors and nuclear energy production values.

In 2012, nonindustrial energy production with coal and peat produced the largest share of CO_2 emissions from fuel combustion, 9.0 Gt CO_2 [*International Energy Agency*, 2014]. If the nuclear power plants would have been replaced by coal power, the CO_2 emissions from this source would have increased by 25% according to our calculations.

The emissions from the additional coal power would have increased the atmospheric CO_2 concentration by 0.126 ppm/yr (equation (3)). In 2013 anthropogenic emissions increased the atmospheric CO_2 concentration by 2.53 ppm which means that the increase due to the additional coal power would be roughly 5% of the current increase (NOAA, www.esrl.noaa.gov/gmd/ccgg/trends/global.html).

3.2. Effects of Increased Coal Power Emissions on $PM_{2.5}$ Concentrations

Figure 2 shows the difference in the $PM_{2.5}$ concentrations at ground level between the control and the coal power model runs. This average difference is calculated from the 5 year model runs (2005–2009). Due to the short lifetime of aerosols (a few days), $PM_{2.5}$ concentrations are increased mostly near the source regions. Consequently, the largest changes are in Japan (+2.8 $\mu g/m^3$), western Europe (EU25 countries, +2.3 $\mu g/m^3$), and eastern U.S. (east from 90°W, +1.8 $\mu g/m^3$). In Japan, the increased $PM_{2.5}$ level is 19.9 $\mu g/m^3$. In western Europe (see Figure 3), the largest increase occurs in the Benelux countries (+5.0 $\mu g/m^3$) and the 5 year average $PM_{2.5}$ level rises to 19.0 $\mu g/m^3$. The EU has set a goal that the 3 year average of $PM_{2.5}$ exposure concentration should be less than 20 $\mu g/m^3$ [*European Environment Agency*, 2014], which means that this limit would have most likely been exceeded in the Benelux countries in our coal power scenario. In Japan, the legislative limit for an annual average is 15 $\mu g/m^3$ (Ministry of the Environment, Government of Japan, www.env.go.jp/en/air/aq/aq.html), while in the U.S. it is 12 $\mu g/m^3$ (U.S. Environmental Protection Agency, www.epa.gov/ttn/naaqs/standards/pm/s_pm_history.html). The annual limits in Japan and eastern U.S. were already exceeded in our control run (17.1 $\mu g/m^3$ and 13.2 $\mu g/m^3$, respectively); thus, with the additional coal power emissions a significant decrease in air quality in the proximity of the power plants would have occurred.

Figure 3 shows the simulated average $PM_{2.5}$ levels in Europe (the continent with the highest number of nuclear reactors) from both model runs. It is evident from Figure 3 that the coal power plants would have increased

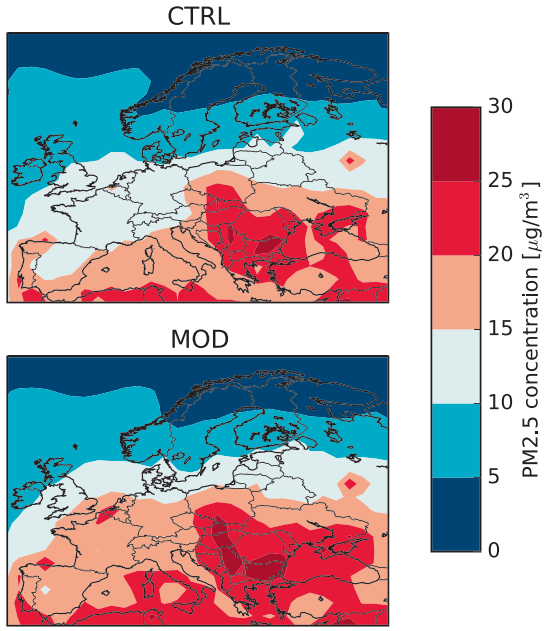

Figure 3. Simulated mean 2005–2009 surface $PM_{2.5}$ concentrations over Europe in the control run (CTRL) and in the run with additional coal power plants (MOD). Red represents regions where the limit set by the EU for 3 year averaged $PM_{2.5}$ exposure (20 $\mu g/m^3$) is exceeded.

$PM_{2.5}$ values in southern and middle Europe. In Romania and Bulgaria, the 5 year $PM_{2.5}$ averages would have exceeded 25 $\mu g/m^3$, which is the upper limit for daily exposure according to WHO. This implies that the deterioration in air quality due to the additional coal power would have been drastic and continuous in these countries.

3.3. Premature Mortality Due To Increased Coal Power Emissions

Lim et al. [2012], *Apte et al.* [2015], and *Lelieveld et al.* [2015] estimated that approximately 3.1–3.2 million premature deaths annually can be attributed to ambient $PM_{2.5}$. We did a similar calculation using equation (1) with our control run and a theoretical minimum-risk concentration of 5.8 $\mu g/m^3$ (following *Apte et al.* [2015]). We found a slightly larger estimate for the premature mortality (4.04 million) than the other studies. However, our 95% confidence interval (CI 95%, 1.60–6.09 million) overlaps with the 95% confidence interval given by Lelieveld et al. (CI 95%, 1.52–4.60 million). Even though our $PM_{2.5}$ values are somewhat higher than the observed particulate masses in North America and Europe (as discussed in section 3.5), the slightly higher mortality value is most likely due to the selected concentration-response function which is expected to overestimate mortality at the most polluted regions (annual $PM_{2.5}$ averages greater than 30 $\mu g/m^3$, e.g., South and East Asia) [*Burnett et al.*, 2014].

Based on the average of our 5 year simulations, the global replacement of nuclear power with coal power would have caused globally 149,800 premature deaths per year for 2005–2009 on average. We predict that cardiopulmonary diseases would have caused 133,800 deaths and lung cancer 16,000 deaths. Approximately two thirds of the deaths would have occurred in Europe. The global distribution of premature deaths is presented in Table 1, whereas Figure 4 shows in more detail the mortality in the Northern Hemisphere, where most of the deaths would have occurred. From these results it is evident that Europe and Japan would have been the most affected regions. In Europe, the largest effect would have been in Germany (13,500 premature deaths per year) and the Benelux countries (3600 premature deaths per year) due to the high population density. Table 1 shows that cardiopulmonary diseases are a much more significant cause for excess mortality than lung cancer in all the studied regions. This stems from the substantially higher baseline deaths due to the former—i.e., a higher value of B_y for cardiopulmonary diseases in equation (1) [*Ostro*, 2004]. In Africa, eastern Mediterranean, and Southeast Asia almost all premature deaths are caused by cardiopulmonary diseases. In Europe the fraction is 90%, whereas in Americas and western Pacific it is slightly lower, about 85%.

The Clean Air for Europe (CAFE, ec.europa.eu/environment/archives/cafe) program estimated that atmospheric aerosols caused 347,900 premature deaths per year resulting from cardiopulmonary diseases in the western Europe (EU25 countries). Our estimate for the EU25 countries during the years 2005–2009 is slightly smaller: 277,600 premature deaths per year on average. However, the CAFE estimate fits well within our 95% confidence interval (CI 95% 105,300–435,200). Based on these results, the increased coal power emissions in the EU25 countries would have increased the number of premature deaths resulting from cardiopulmonary diseases by 26%.

Table 1. Excess Mortality for the WHO Regions in Total and Separately Due To Cardiopulmonary Diseases and Due To Lung Cancer (Deaths per Year)[a]

	Excess Mortality	CI 95%	Excess Mortality Due To Cardiopulmonary Diseases	CI 95%	Excess Mortality Due To Lung Cancer	CI 95%
Africa	1,290 (470–2,100)	310–2,260	1,260 (460–2,070)	300–2,220	20 (10–40)	10–40
Americas	15,990 (5,840–26,030)	15,170–16,760	13,660 (4,980–22,260)	12,960–14,330	2,330 (860–3,770)	2,200–2,440
Southeast Asia	5,510 (2,000–9,010)	2,390–8,600	5,280 (1,920–8,640)	2,290–8,250	230 (80–370)	100–350
Europe	99,910 (36,640–161,850)	97,020–102,700	89,500 (32,750–145,130)	86,920–92,010	10,400 (3,890–16,720)	10,100–10,690
Eastern Mediterranean	3,340 (1,210–5,460)	2,600–4,090	3,240 (1,180–5,300)	2,530–3,980	90 (40–150)	70–120
Western Pacific	23,800 (8,680–38,760)	16,880–30,620	20,800 (7,570–33,910)	14,750–26,760	3,000 (1,110–4,850)	2,120–3,860
Global	149,830 (54,840–243,210)	139,290–160,100	133,760 (48,850–217,310)	124,310–142,980	16,070 (6,000–25,900)	14,960–17,140

[a]The first number is the best estimate for the mortality, and the numbers in the parentheses represent the 95% uncertainty interval from the concentration-response function coefficients (equation (1)). The 95% confidence interval (CI) column presents the variability caused by the differences in the meteorology between the modeled years. The mortality values are rounded to the nearest 10.

Kharecha and Hansen [2013] estimated that the replacement of nuclear power with coal (95%) and natural gas (5%) would cause 19,000–300,000 premature deaths globally per year (CI 95%); thus, our estimate fits well in this range even though they had included health effects from the whole process cycle. Our estimate has a narrower range (55,000–243,000) which can be expected because we only considered the health effects of particulate emissions from the actual energy generation. However, our lower limit is clearly higher than in Kharecha and Hansen's estimate. Furthermore, the average of their estimate was 76,000 which is only half of our average estimate. Most likely, the difference stems from the differences in the modeled dispersion of the emissions and estimation of health effects in the source study of Kharecha and Hansen's mortality factors [*Markandya and Wilkinson*, 2007]. Despite the very different methods used in our analysis and theirs, the large overlap between the results suggests at least order-of-magnitude robustness of the numbers.

3.4. Radiative Effects of the Increased Coal Power Emissions

The climate effects of the increased coal power emissions consist of a net cooling effect caused by the particulate emissions and a warming effect caused by the CO_2 emissions. Due to the short lifetime of the aerosols in the atmosphere, their radiative effect does not change over time, whereas the CO_2 emissions accumulate

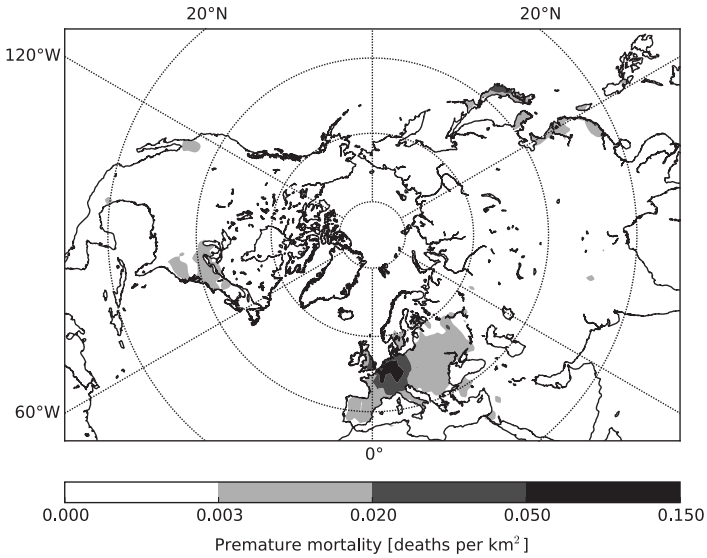

Figure 4. Premature mortality per year in Northern Hemisphere due to increase in coal power $PM_{2.5}$ emissions. Average from a 5 year simulation (2005–2009).

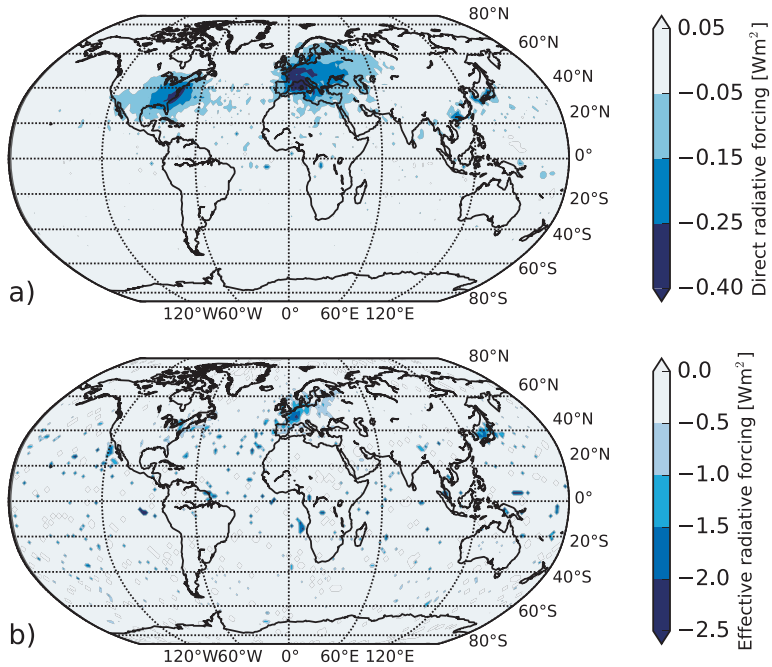

Figure 5. Aerosol (a) direct and (b) effective radiative forcing caused by the increase in coal power emissions between the control and the modified runs. Averages from a 5 year simulation (2005–2009). Only statistically significant changes (based on a paired *t* test) and negative forcings are shown in order to clarify the figures.

into the atmosphere and stay there for centuries. Based on our simulations, the global mean aerosol effective radiative forcing (ERF) is −0.062 W/m^2, whereas the CO_2 radiative effect is 0.0017 W/m^2 after the first year of increased coal power emissions. The global mean aerosol direct radiative effect (ADRE) is −0.016 W/m^2. As Figure 5 shows, cooling is strongest close to the emission sources in the eastern U.S. (ERF: −0.46 W/m^2, ADRE: −0.20 W/m^2), Europe (ERF: −0.64 W/m^2, ADRE: −0.17 W/m^2), and Japan (ERF: −0.94 W/m^2, ADRE: −0.14 W/m^2). Thus, the aerosol radiative effects are about 10 times higher than the global averages near the emission sources. CO_2 emissions, on the other hand, accumulate into the atmosphere; thus, their warming effect would surpass the cooling by the aerosols after 37 years of continuous emissions from the coal power plants (based on the global mean ERF value given above). This was calculated by assuming that the radiative effect increases linearly as CO_2 concentration increases. This is a valid assumption because the addition of CO_2 in our scenario is small when compared to the total amount of atmospheric CO_2 (only 0.126 ppm/395 ppm = 0.03%). According to *Myhre et al*. [2013], the total aerosol ERF (excluding BC on snow and ice) is −0.9 (−1.9 to −0.1) W/m^2. Thus, the additional aerosol effect from increased coal power emissions would be only marginal (approximately 7%).

3.5. Uncertainties and Limitations of the Study

Evidently, uncertainties are large in a study like this. However, with an aerosol-climate model, we are able to give an order of magnitude estimate on the PM-induced air quality and climate effects arising from dramatic changes in energy production. Furthermore, we can estimate which regions would be the most affected.

To evaluate the model's ability to simulate $PM_{2.5}$ concentrations, we compared the annual averages of surface $PM_{2.5}$ from the control simulation to observed annual mean values (2005–2009) from measurement stations of the European Monitoring and Evaluation Programme (EMEP, www.emep.int/) and United States Interagency Monitoring of Protected Visual Environment (IMPROVE, vista.cira.colostate.edu/improve/) networks. EMEP includes 90 measurement stations, but the availability of data from different stations depends

on the year. In our comparison the maximum number of stations was 26 for a single year. The situation is the same with IMPROVE's 212 measurement stations. In our comparison the maximum number of stations was 177 for a single year.

Based on these comparisons, our model seems to slightly overestimate $PM_{2.5}$ concentrations in Europe and United States. The normalized mean biases (and correlation coefficients) are 0.20 (0.25) and 0.71 (0.75) for EMEP and IMPROVE, respectively. These values indicate that the model agrees reasonably well with the measurements. However, it is worth noting that the comparison of a model grid (in the order of 10,000 km^2) to a point measurement is not straightforward and the model is not able to capture the subgrid-scale variability, especially close to the emission sources.

In this work, we assumed that the emissions per produced energy unit were the same in all of the coal power plants globally. This is a crude simplification because different countries have different emission limits and there are large differences in the technologies used. However, most of the nuclear reactors are located in western countries which have similar emission limits and technologies; thus, this simplification should not have a significant effect on our results.

Table 1 presents the 95% confidence intervals for the concentration-response function (in the parentheses in the columns labeled "excess mortality") and for the meteorology (CI 95% column, calculated from the annual averages of the modeled 5 years). Based on these values, it is evident that the changes in the meteorology over the simulation period are not a significant source of variability. The concentration-response function, on the other hand, has a much greater impact on the results. The main sources of uncertainty in the concentration-response function originate from the assumed shape of the function, the assumed background concentration, the assumed highest concentration and the relative risk that are used in the extrapolation, and the exposure data used in the original estimates [*Ostro*, 2004]. *Ostro* [2004] presented a sensitivity study regarding the assumptions in the concentration-response function and showed that the mortality estimates could vary up to 50% depending on these assumptions. In our study, a high bias in the estimation of mortality caused by ambient aerosols can be expected because the concentration-response function is based on relatively low $PM_{2.5}$ concentrations (below 30 $\mu g/m^3$). Thus, in regions with high $PM_{2.5}$ levels (such as East and South Asia) extrapolation is required which typically leads to overestimation of mortality [*Apte et al*., 2015]. However, this limitation does not have a significant effect in the estimation of health effects from the addition of coal power because the increase in $PM_{2.5}$ levels is relatively small (10 $\mu g/m^3$ at maximum) and the majority of the power plants are located in North America and Europe where ambient aerosol concentrations are in a suitable range for the concentration-response function.

The complete replacement of nuclear power with coal power is not likely. However, we selected this scenario to see the maximum effect of a dramatic change in global energy production. Other scenarios would produce lower emissions and smaller effects. For example, instead of coal, nuclear power could be replaced with biomass burning (since bioenergy can also serve as a base load power source). This would change the emissions to some degree. The SO_2 emissions from a biomass burning power plant are estimated to be around 0.026–0.16 kg/MWh [*International Energy Agency*, 2000], whereas the $PM_{2.5}$ emissions range around 0.072–0.216 kg/MWh [*Abbot et al*., 2008]. Moreover, the fractions of EC and OC from the $PM_{2.5}$ emissions are between 6.15–13.8% and 32.6–62.63%, respectively [*Jeong et al*., 2004]. When compared to the emissions from coal power plants, it is clear that biomass power plants produce ~30–100 times less SO_2 while the primary $PM_{2.5}$ emissions are slightly smaller or in the same range. However, the composition (EC and OC fractions) of the $PM_{2.5}$ emissions is clearly different. Furthermore, the photochemical aging of organics and resulting SOA production are expected to be larger for biomass burning emissions than for coal burning emissions [*Shrivastava et al*., 2015]. Consequently, the compositions of the particulate emissions from these sources are different which could impact the health effects. Recent studies have shown that especially BC (or elemental carbon, EC) and also sulfates are associated with adverse health effects [*Atkinson et al*., 2015; *Dai et al*., 2014; *Grahame et al*., 2014; *Janssen et al*., 2011]. The carbonaceous emissions are larger for biomass burning, whereas the SO_2 emissions are larger for coal power. Due to the limitations of the tools in our disposal, we cannot take into account the differences in the production of SOA or the toxicity of different $PM_{2.5}$ components. Therefore, our tools would produce similar health and climate effects for both fuels, although in reality there could be some differences.

Even though fossil fuel combustion and coal mining have the largest adverse health impacts in energy production [*Treyer et al*., 2014], it is good to note that also cultivation of biofuels can affect human mortality. For example, *Ashworth et al*. [2013] estimated that maximizing biofuel cultivation in Europe would cause 1365 premature deaths annually in Europe due to increasing ground level ozone concentration. Based on GHG emissions and health impacts throughout the life cycles of individual power generation chains, sustainable energy not based on combustion (wind, solar, geothermal, hydro, and nuclear) appears to be the best option [*Treyer et al*., 2014].

4. Discussion and Conclusions

We have studied how a global shift from nuclear power to coal power would affect air quality and climate. In a way, this study presents a worst-case scenario since less polluting energy sources are available. Our results showed that the replacement of nuclear power with coal power would have globally caused approximately 150,000 premature deaths per year during the period 2005–2009, with two thirds of them in Europe. For 37 years, the aerosol emissions from the additional coal power plants would cool the climate but after that the accumulating CO_2 emissions would accelerate the warming of the climate. Assuming that the coal-fired power plants would be eventually closed down, the small cooling effect of aerosols would disappear and have negligible effect on the climate change, but the warming impact of CO_2 would remain for centuries [*Bowerman et al*., 2013]. If biomass would be used instead of coal, the health and climate effects could be similar because the primary $PM_{2.5}$ emissions are in the same range. However, we are not able to assess the effects quantitatively with our tools because the differences in the production of SOA or the toxicity of different $PM_{2.5}$ components cannot be taken into account.

The paper should not be taken as a statement for or against either coal or nuclear energy but rather as an examination of an extreme strategic choice regarding energy production options, using state-of-the-science climate and exposure modeling tools. Our analysis mainly emphasizes the significant negative health and climate effects of fossil fuel combustion. We have, however, neglected many important details and effects in our analysis, especially related to fuel harvesting and transportation. In the case of nuclear energy, we have completely left out the possible risks related with accidents and storage of radioactive waste as well as connections between nuclear energy and capability to enrich uranium for nuclear weapons [*Jacobson*, 2009]. As the global energy demand is steadily rising and a shift to a completely renewable energy portfolio is years away, both of these analyzed energy sources will still be used in the near future. Furthermore, as there are clear shifts in the energy policies of some large countries with energy-intensive industry, it is important to study the effects of these shifts with care and with best available methods.

Acknowledgments

This work was funded by the Academy of Finland Centre of Excellence in Atmospheric Science (272041) and Academy of Finland Research Fellowships (250348 and 283031). The first version of this study has been published as a part of Anni Karhunen's master's thesis at Aalto University. The ECHAM-HAMMOZ model is developed by a consortium composed of ETH Zurich, Max Planck Institut für Meteorologie, Forschungszentrum Jülich, University of Oxford, the Finnish Meteorological Institute, and the Leibniz Institute for Tropospheric Research and managed by the Center for Climate Systems Modeling (C2SM) at ETH Zurich. All global model results are available from the author upon request. Please contact via e-mail using tero.mielonen@fmi.fi.

References

Abbot, J., R. Stewart, S. Fleming, K. Stevenson, J. Green, and P. Coleman (2008), Measurement and modelling of fine particulate emissions (PM10 & PM2.5) from wood-burning biomass boilers Report to The Scottish Government; Scottish Government. [Available at www.gov.scot/resource/doc/243574/0067768.pdf.]

AG Energiebilanzen (2015), Stromerzeugung nach Energieträgern (Strommix) von 1990 bis 2014 (in TWh) Deutschland insgesamt. [Available at www.ag-energiebilanzen.de/28-0-Zusatzinformationen.html.]

Apte, J. S., J. D. Marshall, A. J. Cohen, and M. Brauer (2015), Addressing global mortality from ambient $PM_{2.5}$, *Environ. Sci. Technol.*, *49*(13), 8057–8066, doi:10.1021/acs.est.5b01236.3.

Ashworth, K., O. Wild, and C. N. Hewitt (2013), Impacts of biofuel cultivation on mortality and crop yields, *Nat. Clim Change*, *3*, 429–496, doi:10.1038/nclimate1788.

Atkinson, R. W., I. C. Mills, H. A. Walton, and H. S. Anderson (2015), Fine particle components and health—A systematic review and meta-analysis of epidemiological time series studies of daily mortality and hospital admissions, *J. Exposure Sci. Environ. Epidemiol.*, *25*, 208–214, doi:10.1038/jes.2014.63.

Bergman, T., V.-M. Kerminen, H. Korhonen, K. E. J. Lehtinen, R. Makkonen, A. Arola, T. Mielonen, S. Romakkaniemi, M. Kulmala, and H. Kokkola (2012), Evaluation of the sectional aerosol microphysics module SALSA implementation in ECHAM5-HAM aerosol-climate model, *Geosci. Model. Dev.*, *5*, 845–868, doi:10.5194/gmd-5-845-2012.

Bond, T. C., et al. (2013), Bounding the role of black carbon in the climate system: A scientific assessment, *J. Geophys. Res. Atmos.*, *118*, 5380–5552, doi:10.1002/jgrd.50171.

Bowerman, N. H. A., D. J. Frame, C. Huntingford, J. A. Lowe, S. M. Smith, and M. R. Allen (2013), The role of short-lived climate pollutants in meeting temperature goals, *Nat. Clim. Change*, *3*, 1021–1024.

Burnett, R. T., et al. (2014), An integrated risk function for estimating the global burden of disease attributable to ambient fine particulate matter exposure, *Environ. Health Perspect.*, *122*(4), 397–403, doi:10.1289/ehp.1307049.

Chow, J. C., J. G. Watson, D. H. Lowenthal, L.-W. Antony Chen, and N. Motallebi (2011), $PM_{2.5}$ source profiles for black and organic carbon emission inventories, *Atmos. Environ.*, *45*(31), 5407–5414.

Dai, L., A. Zanobetti, P. Koutrakis, and J. D. Schwartz (2014), Associations of fine particulate matter species with mortality in the United States: A multicity time-series analysis, *Environ. Health Perspect*, *122*(8), 837–842, doi:10.1289/ehp.1307568.

Dee, D. P., et al. (2011), The ERA-Interim reanalysis: Configuration and performance of the data assimilation system, *Q. J. R. Meteorol. Soc.*, *137*, 553–597.
European Commission (1995), ExternE studies Vol. 3—Coal & Lignite; ETSU, UK, and IER, D. [Available at www.externe.info/externe_d7/sites/default/files/vol31c23.pdf.]
European Environment Agency (1999), Air and health—Local authorities, health and environment Brochure No 1/1999; Copenhagen, Denmark. [Available at www.eea.europa.eu/publications/2599XXX.]
European Environment Agency (2014), Air quality in Europe: 2014 report EEA Report No 5/2014; Luxembourg. [Available at www.eea.europa.eu/publications/air-quality-in-europe-2014/at_download/file.]
Friedrich, R. (2005), ExternE: Methodology and results. External costs of energy and their internalisation in Europe Dialogue with industry, NGO, and policy-makers, European Commission, December 9, 2005. [Available at www.externe.info/externe_d7/sites/default/files/br0900.pdf.]
Global Energy Assessment (2012), *Toward A Sustainable Future*, Cambridge Univ. Press: And the International Institute for Applied Systems Analysis, Cambridge, U. K., and New York, Laxenburg, Austria.
Grahame, T. J., R. Klemm, and R. B. Schlesinger (2014), Public health and components of particulate matter: The changing assessment of black carbon, *J. Air Waste Manage.*, *64*(6), doi:10.1080/10962247.2014.912692.
Haywood, J. M., L. J. Donner, A. Jones, and J.-C. Golaz (2007), Global indirect radiative forcing caused by aerosols: IPCC, and beyond, in *Clouds in the Perturbed Climate System*, edited by J. Heintzenberg and R. J. Charlson, pp. 451–467, MIT Press, Cambridge 2009.
International Atomic Energy Agency (2013), Nuclear power reactors in the world, 2013 edition Vienna, Austria. [Available at www-pub.iaea.org/MTCD/Publications/PDF/rds2-33_web.pdf.]
International Energy Agency (2000), Hydropower and the environment: Present context and guidelines for future action. [Available at ieahydro.org/reports/HyA3S5V2.pdf.]
International Energy Agency (2011), World energy outlook 2011. [Available at www.iea.org/publications/freepublications/publication/WEO2011_WEB.pdf.]
International Energy Agency (2012), CO_2 emissions from fuel combustion—Highlights 2012 Edition; Paris, France.
International Energy Agency (2014), CO_2 emissions from fuel combustion Highlights 2014; Paris, France. [Available at www.iea.org/publications/freepublications/publication/CO2EmissionsFromFuelCombustionHighlights2014.pdf.]
Intergovernmental Panel on Climate Change (IPCC) (2014), Summary for policymakers, in *Climate Change 2014: Mitigation of Climate Change. Contribution of Working Group III to the Fifth Assessment Report of the Intergovernmental Panel on Climate Change*, edited by O. Edenhofer et al., pp. 1–30, Cambridge Univ. Press, Cambridge, U. K., and New York.
Ipsos (2011), Global citizen reaction to the Fukushima nuclear plant disaster. [Available at www.ipsos-mori.com/Assets/Docs/Polls/ipsos-global-advisor-nuclear-power-june-2011.pdf.]
Jacobson, M. Z. (2009), Review of solutions to global warming, air pollution, and energy security, *Energy Environ. Sci.*, *2*, 148–173.
Janssen, N. A., et al. (2011), Black carbon as an additional indicator of the adverse health effects of airborne particles compared with PM10 and PM2.5, *Environ. Health Perspect.*, *119*(12), 1691–1699, doi:10.1289/ehp.1003369.
Jeong, C.-H., P. K. Hopke, R. Kim, and D.-W. Lee (2004), The comparison between thermal-optical transmittance elemental carbon and Aethalometer black carbon measured at multiple monitoring sites, *Atmos. Environ.*, *38*, 5193–5204.
Kharecha, P. A., and J. E. Hansen (2013), Prevented mortality and greenhouse gas emissions from historical and projected nuclear power, *Environ. Sci. Technol.*, *47*(9), 4889–4895.
Kokkola, H., et al. (2008), SALSA—A Sectional Aerosol module for Large Scale Applications, *Atmos. Chem. Phys.*, *8*(9), 2469–2483.
Krewitt, W., F. Hurley, A. Trukenmuller, and R. Friedrich (1998), Health risks of energy systems, *Risk Anal.*, *18*, 377–383.3.
Lelieveld, J., J. S. Evans, M. Fnais, D. Giannadaki, and A. Pozzer (2015), The contribution of outdoor air pollution sources to premature mortality on a global scale, *Nature*, *525*, 367–371.
Lenzen, M. (2008), Life cycle energy and greenhouse gas emissions of nuclear energy: A review, *Energy Convers. Manage.t*, *49*, 2178–2199.
Lim, S. S., et al. (2012), A comparative risk assessment of burden of disease and injury attributable to risk factors and risk factor clusters in 21 regions, 1990–2010: A systematic analysis for the Global Burden of Disease Study 2010, *Lancet*, *380*, 2224–2260.
Lin, H., and W. R. Leaitch (1997), Development of an in-cloud aerosol activation parameterization for climate modeling, in *Proceedings of the WMO Workshop on Measurement of Cloud Properties for Forecasts of Weather, Air Quality and Climate*, edited by D. Baumgardner and G. Raga, pp. 328–335, World Meteorol. Organ., Geneva.
Lohmann, U., and C. Hoose (2009), Sensitivity studies of different aerosol indirect effects in mixed-phase clouds, *Atmos. Chem. Phys.*, *9*, 8917–8934, doi:10.5194/acp-9-8917-2009.
Lohmann, U., L. Rotstayn, T. Storelvmo, A. Jones, S. Menon, J. Quaas, A. M. L. Ekman, D. Koch, and R. Ruedy (2010), Total aerosol effect: Radiative forcing or radiative flux perturbation?, *Atmos. Chem. Phys.*, *10*, 3235–3246, doi:10.5194/acp-10-3235-2010.
Markandya, A., and P. Wilkinson (2007), Electricity generation and health, *Lancet*, *370*, 979–990.
Myhre, G., E. J. Highwood, K. P. Shine, and F. Stordal (1998), New estimates of radiative forcing due to well mixed greenhouse gases, *Geophys. Res. Lett.*, *25*(14), 2715–2718, doi:10.1029/98GL01908.
Myhre, G., et al. (2013), Anthropogenic and natural radiative forcing, in *Climate Change 2013: The Physical Science Basis. Contribution of Working Group I to the Fifth Assessment Report of the Intergovernmental Panel on Climate Change*, edited by T. F. Stocker et al., pp. 659–740, Cambridge Univ. Press, Cambridge, U. K., and New York.
Ostro, B. (2004), *Outdoor Air Pollution: Assessing the Environmental Burden of Disease at National and Local Levels*, *WHO Environ. Burden of Disease Ser.*, vol. 5, World Health Organization, Geneva.
Partanen, A.-I., A. Laakso, A. Schmidt, H. Kokkola, T. Kuokkanen, J.-P. Pietikäinen, V.-M. Kerminen, K. E. J. Lehtinen, L. Laakso, and H. Korhonen (2013), Climate and air quality trade-offs in altering ship fuel sulfur content, *Atmos. Chem. Phys.*, *13*, 12,059–12,071, doi:10.5194/acp-13-12059-2013.
Pietikäinen, J.-P., et al. (2015), Impacts of emission reductions on aerosol radiative effects, *Atmos. Chem. Phys.*, *15*, 5501–5519.
Rashad, S. M., and F. H. Hammad (2000), Nuclear power and the environment: Comparative assessment of environmental and health impacts of electricity generating systems, *Appl. Energy*, *65*, 211–229.
Raupach, M. R., J. G. Canadell, and C. Le Quéré (2008), Anthropogenic and biophysical contributions to increasing atmospheric CO_2 growth rate and airborne fraction, *Biogeosciences*, *5*(6), 1601–1613.
Riahi, K., A. Grübler, and N. Nakicenovic (2007), Scenarios of long-term socio-economic and environmental development under climate stabilization, *Technol. Forecasting Soc.*, *74*, 887–935.
Riahi, K., S. Rao, V. Krey, C. Cho, V. Chirkov, G. Fischer, G. Kindermann, N. Nakicenovic, and P. Rafaj (2011), RCP 8.5—A scenario of comparatively high greenhouse gas emissions, *Clim. Change*, *109*, 33–57.
Robertson, D. S. (2006), Health effects of increase in concentration of carbon dioxide in the atmosphere, *Curr. Sci.*, *90*, 1607–1609.

NASA Socioeconomic Data and Applications Center (2005), Gridded Population of the World Version 3 (GPWv3): Population Count Grid, Future Estimates, Center for International Earth Science Information Network (CIESIN)/Columbia University United Nations Food and Agriculture Programme (FAO), and Centro Internacional de Agricultura Tropical (CIAT). [Available at sedac.ciesin.columbia.edu/data/set/gpw-v3-population-count-future-estimates.]

Shindell, D., and G. Faluvegi (2010), The net climate impact of coal-fired power plant emissions, *Atmos. Chem. Phys.*, *10*(7), 3247–3260.

Shrivastava, M., et al. (2015), Global transformation and fate of SOA: Implications of low volatility SOA and gas-phase fragmentation reactions, *J. Geophys. Res. Atmos.*, *120*, 4169–4195, doi:10.1002/2014JD022563.

Sims, R. E. H., et al. (2007), Energy supply, in *Climate Change 2007: Mitigation. Contribution of Working Group III to the Fourth Assessment Report of the Intergovernmental Panel on Climate Change*, edited by B. Metz et al., pp. 252–322, Cambridge Univ. Press, Cambridge, U. K., and New York.

Smith, K. R., et al. (2013), Energy and human health, *Annu Rev. Public Health*, *34*, 159–188.

Stier, P., et al. (2005), The aerosol-climate model ECHAM5-HAM, *Atmos. Chem. Phys.*, *5*, 1125–1156, doi:10.5194/acp-5-1125-2005.

Treyer, K., C. Bauer, and A. Simons (2014), Human health impacts in the life cycle of future European electricity generation, *Energy Policy*, *74*, 31–44.

Tunved, P., H. C. Hansson, V. M. Kerminen, J. Ström, M. D. Maso, H. Lihavainen, Y. Viisanen, P. P. Aalto, M. Komppula, and M. Kulmala (2006), High natural aerosol loading over boreal forests, *Science*, *312*, 261–263.

U.S. Energy Information Administration (2015), Levelized cost and levelized avoided cost of new generation resources The Annual Energy Outlook 2015: Washington, D. C. [Available at www.eia.gov/forecasts/aeo/electricity_generation.cfm.]

van Vliet, O., V. Krey, D. McCollum, S. Pachauri, Y. Nagai, S. Rao, and K. Riahi (2012), Synergies in the Asian energy system: Climate change, energy security, energy access and air pollution, *Energy Econ.*, *34*, S470–S480.

Watts, N., et al. (2015), Health and climate change: Policy responses to protect public health, *Lancet*, doi:10.1016/S0140-6736(15)60854-6.

Wolf, R. (2015), Why wealthy countries must not drop nuclear energy: Coal power, climate change and the fate of the global poor, *Int. Aff.*, *92*, 287–301.

World Health Organization (2008), The global burden of disease: 2004 update Geneva, Switzerland. [Available at http://www.who.int/healthinfo/global_burden_disease/GBD_report_2004update_full.pdf?ua=1.]

Zhang, K., et al. (2012), The global aerosol-climate model ECHAM-HAM, version 2: Sensitivity to improvements in process representations, *Atmos. Chem. Phys.*, *12*, 8911–8949, doi:10.5194/acp-12-8911-2012.

III

Paper III

A.-I. Partanen, A. Laakso, A. Schmidt, H. Kokkola, T. Kuokkanen, J.-P. Pietikäinen, V.-M. Kerminen, K. E. J. Lehtinen, L. Laakso, and H. Korhonen, Climate and air quality trade-offs in altering ship fuel sulfur content. *Atmospheric Chemistry and Physics 13*,12059-12071, doi:10.5194/acp-13-12059-2013, 2013.

Atmos. Chem. Phys., 13, 12059–12071, 2013
www.atmos-chem-phys.net/13/12059/2013/
doi:10.5194/acp-13-12059-2013

Atmospheric Chemistry and Physics Open Access

Climate and air quality trade-offs in altering ship fuel sulfur content

A. I. Partanen[1], A. Laakso[1], A. Schmidt[2], H. Kokkola[1], T. Kuokkanen[3], J.-P. Pietikäinen[4], V.-M. Kerminen[5], K. E. J. Lehtinen[1,6], L. Laakso[4,7], and H. Korhonen[1]

[1]Kuopio Unit, Finnish Meteorological Institute, Kuopio, Finland
[2]School of Earth and Environment, University of Leeds, Leeds, UK
[3]Department of Law, University of Eastern Finland, Joensuu Campus, Joensuu, Finland
[4]Climate change, Finnish Meteorological Institute, Helsinki, Finland
[5]Department of Physics, University of Helsinki, Helsinki, Finland
[6]Department of Applied Physics, University of Eastern Finland, Kuopio campus, Kuopio, Finland
[7]School of Physical and Chemical Sciences, North-West University, Potchefstroom Campus, Potchefstroom, South Africa

Correspondence to: A.-I. Partanen (antti-ilari.partanen@fmi.fi)

Received: 20 June 2013 – Published in Atmos. Chem. Phys. Discuss.: 23 August 2013
Revised: 8 November 2013 – Accepted: 12 November 2013 – Published: 12 December 2013

Abstract. Aerosol particles from shipping emissions both cool the climate and cause adverse health effects. The cooling effect is, however, declining because of shipping emission controls aiming to improve air quality. We used an aerosol-climate model ECHAM-HAMMOZ to test whether by altering ship fuel sulfur content, the present-day aerosol-induced cooling effect from shipping could be preserved, while at the same time reducing premature mortality rates related to shipping emissions. We compared the climate and health effects of a present-day shipping emission scenario (ship fuel sulfur content of 2.7 %) with (1) a simulation with strict emission controls in the coastal waters (ship fuel sulfur content of 0.1 %) and twofold the present-day fuel sulfur content (i.e. 5.4 %) elsewhere; and (2) a scenario with global strict shipping emission controls (ship fuel sulfur content of 0.1 % in coastal waters and 0.5 % elsewhere) roughly corresponding to international agreements to be enforced by the year 2020. Scenario 1 had a slightly stronger aerosol-induced effective radiative forcing (ERF) from shipping than the present-day scenario ($-0.43\,\mathrm{W\,m^{-2}}$ vs. $-0.39\,\mathrm{W\,m^{-2}}$) while reducing premature mortality from shipping by 69 % (globally 34 900 deaths avoided per year). Scenario 2 decreased the ERF to $-0.06\,\mathrm{W\,m^{-2}}$ and annual deaths by 96 % (globally 48 200 deaths avoided per year) compared to present-day. Our results show that the cooling effect of present-day emissions could be retained with simultaneous notable improvements in air quality, even though the shipping emissions from the open ocean clearly have a significant effect on continental air quality. However, increasing ship fuel sulfur content in the open ocean would violate existing international treaties, could cause detrimental side-effects, and could be classified as geoengineering.

1 Introduction

Aerosol emissions from shipping have a net cooling effect on the Earth's climate, mainly through altering cloud properties, and cause detrimental health effects by degrading air quality (Eyring et al., 2010). Aerosol particles affect the climate in two ways. First, they scatter and absorb solar and terrestrial radiation (the aerosol direct effect, e.g. Myhre et al., 2013). Second, changes in the aerosol loading induce changes in cloud microphysical properties and cloud lifetime (the aerosol indirect and semidirect effects, e.g. Koch and Del Genio, 2010; Lohmann and Feichter, 2005). One well-known example of the aerosol indirect effects are the so-called ship tracks that sometimes manifest along the shipping routes (Christensen and Stephens, 2011; Coakley et al., 1987). They are clouds with enhanced reflectivity due to increased droplet number concentration (accompanied by decreased droplet size) caused by aerosol emissions from shipping. Eyring et al. (2010) reported a range between $-0.038\,\mathrm{W\,m^{-2}}$ and $-0.6\,\mathrm{W\,m^{-2}}$ for the aerosol indirect effects from shipping for the year 2000 from several independent modelling studies.

In terms of health effects, aerosol particles increase premature mortality due to lung cancer and cardiopulmonary diseases (Pope and Dockery, 2006). Globally, air pollution is estimated to cause about 0.8 million premature deaths per year (Cohen et al., 2005). Particulate emissions from international shipping have been considered responsible for 18 900–90 600 deaths per year (Corbett et al., 2007; Winebrake et al., 2009).

As the knowledge of the adverse health and environmental effects of shipping emissions has increased, governments have negotiated treaties to reduce air pollution, especially sulfur emissions from ship traffic. The International Maritime Organization (IMO) has been responsible for the detailed regulation of pollution from ships. The leading IMO agreement on the pollution from ships is the MARPOL 73/78 Convention (IMO, 1978). In 1997, Annex VI was added to the convention to minimize airborne emissions from ships. In 2008, emissions limits of the annex, including sulfur oxides in Regulation 14, were further tightened (IMO, 2008). According to the amendment, a global cap of 3.5 % has been applied for ship fuel sulfur content from 1 January 2012 onwards. In certain emission control areas, such as in the North Sea, Baltic Sea and the coastal areas of the USA and Canada, a stricter restriction of 0.1 % will be in effect by 2015. The global sulfur cap will be progressively reduced to 0.5 % by the year 2020, although the IMO is required to complete a review by 2018 of the availability of fuel with sulfur content no greater than 0.5 %.

The health benefits of shipping emission cuts have been estimated by model studies. Winebrake et al. (2009) calculated that setting a ship fuel sulfur limit of 0.1 % in the coastal regions within 200 nautical miles (370 km) from the coastlines could save 15 400–73 500 lives annually. However, there are trade-offs involved in decreasing sulfur and organic carbon emissions from shipping by reducing sulfur content in the ship fuel. The net cooling effect from ship-emitted aerosols will decrease simultaneously with the adverse health effects. Lauer et al. (2009) estimated that applying a ship fuel sulfur content limit of 0.5 % globally would decrease the radiative forcing of shipping emissions from $-0.6\,\mathrm{W\,m^{-2}}$ to $-0.3\,\mathrm{W\,m^{-2}}$ and hence accelerate global warming.

Fuglestvedt et al. (2009) discussed the idea of refraining from shipping emission reductions to cool the climate, and rejected it based on the many uncertainties and risks involved. However, several technologies using controlled aerosol emissions to cool the climate have been proposed in recent years (e.g. marine cloud whitening, Latham, 1990, and stratospheric sulfur injections, Crutzen, 2006). In a broader context, these technologies are known as solar radiation management (SRM) or geoengineering (Fox and Chapman, 2011). Despite the uncertainties and risks involved (Robock, 2008) it may be worth studying these technologies as they may be considered in the future if greenhouse gas emission reductions are not successful or climate sensitivity is underestimated.

The aim of our study is to test whether the present-day radiative aerosol-induced cooling (excluding greenhouse gases) from shipping could be preserved while at the same time reducing the mortality related to shipping emissions. Using a global model, we explore a scenario in which the ship fuel sulfur content is increased in the open oceans (entire sea area excluding coastal zones) but reduced in the coastal zones. This scenario can be considered a form of geoengineering because of the deliberate attempt to assert a cooling effect on the climate. The geoengineering scenario is compared to shipping emission scenarios for the years 2010 and 2020. To make the climate and air quality trade-offs evident, different scenarios are compared with respect to the global mean effective radiative forcing (ERF) resulting from aerosol effects and global premature mortality due to shipping emissions. We do not attempt to compare these metrics with each other (i.e. try to evaluate how many deaths caused by climate change could be avoided with a certain amount of ERF), because that would require several arbitrary simplifications (Löndahl et al., 2010), and would be outside the scope of this paper. Our study is not intended as a policy recommendation, but it provides valuable information about the climate and air quality trade-offs related to aerosol emissions from international shipping.

2 Methods

2.1 Model description

We used the global aerosol-climate model ECHAM-HAMMOZ (ECHAM5.5-HAM2.0) (Stier et al., 2005; Zhang et al., 2012) to quantify the effects of shipping emissions on climate and air quality. The model uses the M7 aerosol microphysics scheme (Vignati et al., 2004) to describe the externally and internally mixed aerosol population and its size distribution with seven log-normal modes containing the aerosol species of sulfate (SO_4), sea salt, organic carbon, black carbon and mineral dust. The aerosol model resolves nucleation of new particles from sulfuric acid (Kazil and Lovejoy, 2007), condensation of sulfuric acid vapor, coagulation, hydration and removal of aerosol particles by dry deposition, sedimentation and wet deposition. We used AEROCOM-II ACCMIP data for anthropogenic aerosol emissions and biomass burning emissions for the year 2010 (Riahi et al., 2007, 2011) and natural aerosol emissions as described by Zhang et al. (2012). The model simulates the aerosol–cloud interactions, including both first and second aerosol indirect effects as described by Lohmann and Hoose (2009). The cloud droplet activation was calculated with a physically based parameterization (Abdul-Razzak and Ghan, 2000). We implemented the model modifications done by Peters et al. (2012) to set all shipping emissions consistently in the first model layer, assigning primary sulfate, organic carbon and black carbon emissions from shipping to the soluble Aitken

mode with a geometric mean radius of 44 nm for sulfate and 30 nm for carbonaceous species. The chosen mode diameters are smaller than the default sizes in ECHAM-HAM (Stier et al., 2005; Zhang et al., 2012) reflecting recent measurements of ship emissions (e.g., Petzold et al., 2008; Jonsson et al., 2011). Our choice of diameter for carbonaceous aerosols is close to the value reported by Petzold et al. (2008), who measured the number density of the non-volatile combustion mode to be dominated by particles with radius of 40 nm. However, the diameter for primary sulfate emissions in our study is somewhat larger than found in the Petzold et al. (2008) study. Since smaller particles mean more cloud condensation nuclei (provided that the particles are still large enough to activate as cloud droplets), the sulfate diameter used in our model version can potentially lead to an underestimation of the aerosol indirect effect (Peters et al., 2013). However, different measurements campaigns have yielded highly varying results for the primary sulfate particle size (Petzold et al., 2008; Jonsson et al., 2011) reflecting the fact that it is difficult to extract the diameter of particles from shipping emissions based on measurements due to, e.g. several chemical components involved, plume aging, and variability of engines.

2.2 Experiment design

Our simulations differed from each other only with respect to shipping emissions. A list of all simulations is provided in Table 1. The reference simulation called no-ships was run without any shipping emissions at all. To assess the effects of present-day aerosol emissions from shipping, we used the shipping emissions from ACCMIP database (Riahi et al., 2007, 2011) for the year 2010 (Fig. 1a) in the simulation ships-2010.

For the rest of the simulations, we defined the coastal zones within one or two (depending on the simulation) model grid cells away from the continent as emission control areas where fuel sulfur content was assumed to be 0.1 %, corresponding to the limit in existing emission reduction areas from the year 2015. The width of the emission reduction zones corresponds roughly to the 200 nautical miles (370 km) equivalent to the width of the current emission control area surrounding North America (IMO, 2010). In the geoengineering simulations geo-wide and geo-narrow we set the fuel sulfur content to 5.4 % (double the current global mean value) outside the coastal waters (i.e., in the area at least two grid cells (400–600 km) or one grid cell (200–300 km) away from the coastline, respectively).

To compare the geoengineering simulations against a strict emission control scenario, we set up a simulation ships-2020 that roughly corresponds to the shipping emission regulation planned for the year 2020. In ships-2020, we assumed that the coastal zones, within 2 grid cells from the continent, correspond to the emission control areas with a limit of 0.1 % on the ship fuel sulfur content, and applied the global cap of 0.5 % elsewhere. The assumption that emission control areas cover all the coastal waters is overestimating the extent of the emission reduction areas, but it gives an idea of the effects of the planned future emission control legislation. We did not take into account any possible changes in the shipping routes or shipping activity in the future because we wanted to compare different idealized emission control scenarios, and not make future projections.

To calculate the actual sulfur dioxide (SO_2) emissions in different scenarios, the ACCMIP shipping emissions for the year 2010 were used as a baseline. We assumed that the fuel sulfur content in each grid cell of the ACCMIP emissions was equal to the current global mean value of 2.7 % (Lauer et al., 2009) and that SO_2 emissions were linearly dependent on the fuel sulfur content. Thus, in emission control areas with a sulfur content limit of 0.1 %, the baseline shipping emissions were multiplied by 0.037 (= 0.1 %/2.7 %) and doubled in the geoengineered regions to a ship fuel sulfur content of 5.4 %. Organic carbon emissions were scaled similarly using the relationship reported by Lack et al. (2009) for fuel sulfur content (S %) and organic carbon emissions (OC) (OC ($g\,kg^{-1}$) = 0.65× S% +0.5). There is no such simple dependence of black carbon emissions on fuel sulfur content as one major determining factor is engine load, although fuel quality also plays a role (Lack and Corbett, 2012). Lacking a precise formulation, we used the unmodified black carbon emissions from the ACCMIP database for all simulations. Not accounting for any changes in black carbon emissions is unlikely to affect our results significantly. First, Peters et al. (2012) showed that omitting black carbon emissions from shipping had little effect on the net aerosol radiative forcing from shipping as increased nucleation of new particles compensated for the missing black carbon. Second, emitted black carbon mass from shipping is low compared to sulfur dioxide mass (Table 1), and changes in aerosol mass (instead of in composition) determines the calculated health effects in our study (see Sect. 2.3).

The fraction of sulfur emissions that should be treated as primary sulfate due to subgrid scale nucleation in models is uncertain (Luo and Yu, 2011; Stevens et al., 2012) and affects the impacts of shipping emissions as the burden of sulfate increases with increasing primary sulfate fraction (Peters et al., 2012). To test the sensitivity of our results to this factor, we did sensitivity simulations ships-2010_45 and geo-wide_45 in which 4.5 % (instead of 2.5 %) of sulfur mass emissions from ships was emitted as primary sulfate. In all other respects, the simulations were identical to ships-2010 and geo-wide, respectively. For other anthropogenic sources besides shipping, a fraction of 2.5 % (Dentener et al., 2006; Zhang et al., 2012) was used in all the simulations.

Different shipping emission inventories differ greatly from each other with respect to both the spatial distribution and the global sum of the emissions (Eyring et al., 2010). To assess the sensitivity of our results to the spatial distribution of the shipping emissions, we carried out two additional sensitivity

Table 1. List of simulations*.

Simulation	S % coast	S % ocean	Coast width	SO_2 ($Tg\,yr^{-1}$)	OC ($Tg\,yr^{-1}$)	BC ($Tg\,yr^{-1}$)	f_{SO_4}
Main simulations	–	–	–	–	–	–	–
no-ships	–	–	–	0	0	0	–
ships-2010	2.7 %	2.7 %	–	12.50	0.16	0.15	2.5 %
geo-narrow	0.1 %	5.4 %	1	17.37	0.21	0.15	2.5 %
geo-wide	0.1 %	5.4 %	2	13.12	0.17	0.15	2.5 %
ships-2020	0.1 %	0.5 %	2	1.42	0.05	0.15	2.5 %
Sensitivity simulations							
ships-2010_45	2.7 %	2.7 %	–	12.50	0.16	0.15	4.5 %
geo-wide_45	0.1 %	5.4 %	2	13.12	0.17	0.15	4.5 %
ships-2010_corbett	2.7 %	2.7 %	–	12.52	0.16	0.15	2.5 %
geo-wide_corbett	0.1 %	5.4 %	2	11.81	0.15	0.15	2.5 %

* The second and third columns give the ship fuel sulfur content (S %) for coastal zones and open ocean, respectively. Sulfur content is used to scale SO_2 and OC emissions. Coast width is the number of grid cells from the coastline that determine the coastal zone for emission reductions. The next three columns give the total global annual emissions of sulfur dioxide (SO_2, including the fraction emitted as primary sulfate), organic carbon (OC) and black carbon (BC) from shipping. The last column gives the fraction of sulfur mass emissions from shipping which is actually emitted as primary sulfate particles in the model to emulate subgrid scale sulfate formation.

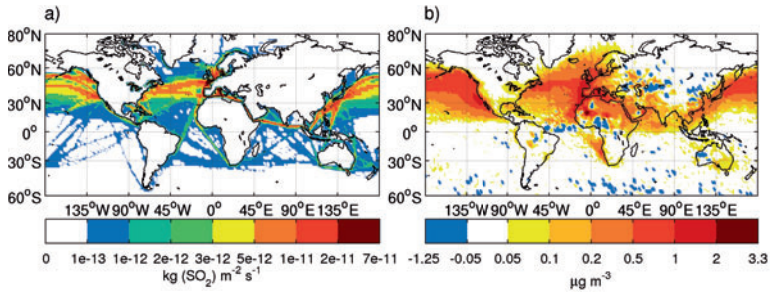

Fig. 1. (a) SO_2 emissions from ship traffic in the simulation ships-2010. The emissions are from the ACCMIP database for the year 2010. **(b)** The contribution of shipping emissions to $PM_{2.5}$ mass concentrations in the simulation ships-2010.

simulations that used the combined shipping emission data compiled by Corbett et al. (2010) for the Arctic and by Wang et al. (2008) for the rest of the world. Simulation ships-2010_corbett used these combined emissions for the year 2010. As the global sum of the shipping emissions by Wang et al. (2008) was also taken from the RCP8.5 scenario (Riahi et al., 2007, 2011), the total global shipping emissions were almost the same in both ships-2010 and ships-2010_corbett (Table 1). Shipping emissions for the simulation geo-wide_corbett were calculated in the same way as for geo-wide, but emissions from Wang et al. (2008) and Corbett et al. (2010) were used as the baseline instead of the ACCMIP emissions.

Due to the model version used, our analysis includes only sulfur, organic carbon, and black carbon aerosol emissions from shipping. Other main aerosol and aerosol precursor compounds in shipping emissions include nitrogen oxides and volatile organic compounds (Eyring et al., 2010). Lieke et al. (2013) measured also crystalline salts in the ship exhausts. Not including these other compounds may lead to an underestimation of aerosol-related climate and health effects of shipping.

All the simulations were run in the horizontal resolution of T63 corresponding roughly to a $1.9° \times 1.9°$ grid. The model had 31 vertical levels and extended to a pressure level of 10 hPa. The simulation time was five model years from 2001 to 2005 for each simulation. The model meteorology (vorticity, divergence, temperature and surface pressure) was nudged towards the reference state by ERA-interim reanalysis data (Dee et al., 2011). The runs were preceded by a three-month spinup period of which the first two months were common in all simulations and had no shipping emissions. The model was run with climatological sea surface temperatures.

2.3 Calculation of premature mortality due to shipping emissions

The model diagnosed the mass concentrations of particulate matter with dry diameters less than 2.5 μm ($PM_{2.5}$) by integrating the contribution of each of the seven modes separately. We used five-year-mean values of surface level $PM_{2.5}$ concentration to estimate the long-term health effects for each shipping emission scenario. The simulation no-ships was used as the reference. We followed the recommendations by Ostro (2004) to calculate the premature mortality from lung cancer (Trachea, bronchus and lung cancers) and cardiopulmonary diseases (cardiovascular diseases and chronic obstructive pulmonary disease) due to long-term exposure to shipping emissions. The concentration-response function that relates changes in $PM_{2.5}$ concentrations to annual excess mortality rates (E, deaths per year) can be expressed as

$$E = \left[1 - \left(\frac{PM_{2.5,0}+1}{PM_{2.5,1}+1}\right)^{\beta}\right] \times B_y \times P_{30+}, \quad (1)$$

where $PM_{2.5,0}$ is the reference concentration ($\mu g\,m^{-3}$) in no-ships and $PM_{2.5,1}$ the concentration in the simulation under investigation; β is a cause-specific coefficient with a value of 0.23218 (95 % confidence interval: 0.08563–0.37873) for lung cancer and 0.15515 (95 % confidence interval: 0.0562–0.2541) for cardiopulmonary diseases (Ostro, 2004); B_y is the baseline mortality rate (e.g., deaths per year per 1000 people) for lung cancer or cardiopulmonary diseases in the exposed population with age over 30 yr (P_{30+}).

Baseline mortality rates and the fraction of people in the exposed age-group were calculated using data provided by the World Health Organisation (WHO, 2008) based on six WHO regions (Fig. 2) gridded onto the model grid resolution. We used the population density data for the year 2010 from the Sosioeconomic Data and Applications Center at Columbia University (SEDAC, 2005). Population density was also interpolated onto the model grid resolution.

3 Results

3.1 Effects of shipping emissions on $PM_{2.5}$ concentrations

We estimated the contribution of shipping emissions to $PM_{2.5}$ by calculating the difference between the $PM_{2.5}$ values of the simulation no-ships and those of the other simulations. The comparison of the modelled $PM_{2.5}$ concentrations against measurements is discussed in Sect. 3.4.1.

Contribution of shipping emissions to $PM_{2.5}$ in the simulation ships-2010 is shown in Fig. 1b. The effect of ship traffic was most prominent in the coastal areas of western Europe, where $PM_{2.5}$ is about 0.5–2 $\mu g\,m^{-3}$ higher due to shipping emissions. In the coastal regions of Europe this corresponds to a relative increase of up to about 20 % due to the major shipping routes passing through the English Channel and Mediterranean Sea (Fig. 1a). Corbett et al. (2007) and Winebrake et al. (2009) estimated a contribution of ship traffic to $PM_{2.5}$ of up to about 2 $\mu g\,m^{-3}$ and about 3 $\mu g\,m^{-3}$, respectively. These numbers agree quite well with the maximum $PM_{2.5}$ contribution of 3.3 $\mu g\,m^{-3}$ from shipping in our simulation ships-2010.

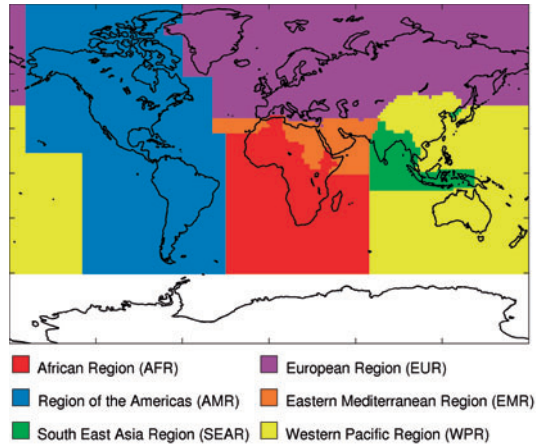

Fig. 2. Definition of the WHO regions based on a list of countries in each region (WHO, 2012) and gridded data set of the world's countries (Lerner et al., 1988).

Continental air quality was notably improved in the simulations with emission reductions near the coasts. For example, in the geoengineering simulation with the wide emission reduction zone (geo-wide), the contribution of shipping emissions to $PM_{2.5}$ concentration was less than 0.5 $\mu g\,m^{-3}$ almost everywhere in Europe. That is a reduction of roughly between −1 % and −15 % in total $PM_{2.5}$ mass concentration in Europe compared to the simulation ships-2010. In the simulation corresponding to future emission controls ships-2020), the contribution of shipping emissions to $PM_{2.5}$ was less than 0.1 $\mu g\,m^{-3}$ almost everywhere in Europe. The effect of shipping emissions in ships-2020 on $PM_{2.5}$ was so low that the natural variability of aerosol concentrations is greater than the contribution of shipping emissions to $PM_{2.5}$ in most parts of the world. The difference in continental $PM_{2.5}$ concentration between geo-wide and ships-2020, which have the same coastal emissions, shows that emissions from the open ocean contributed significantly to continental $PM_{2.5}$ concentration in geo-wide.

3.2 Premature mortality due to shipping emissions

We calculated premature mortality from lung cancer and cardiopulmonary diseases due to long-term exposure to shipping emissions using the $PM_{2.5}$ concentration in the simulation no-ships as the reference concentration. Of the studied

main cases (i.e. excluding sensitivity simulations which are discussed in Sect. 3.4), current shipping emissions caused the most deaths (50 200 deaths per year in ships-2010, Table 2). Both geoengineering scenarios resulted in significant drops in mortality rates due to ship-$PM_{2.5}$ compared to the simulation ships-2010. The global excess mortality due to shipping decreased by 15 400 (31 %) and by 34 900 (69 %) in the simulations geo-narrow and geo-wide, respectively. The large difference between the geoengineering scenarios shows that the width of the emission reduction zone had a significant impact. As expected, the simulation ships-2020 offered the most health benefits, reducing ship-$PM_{2.5}$-induced mortality by 48 200 (96 %) compared to ships-2010. The relative decrease of ship-$PM_{2.5}$-induced mortality was much higher than estimates by Winebrake et al. (2009) for different emission control scenarios. They calculated that a cap of 0.1 % for ship fuel sulfur content in the coastal areas would decrease the mortality from shipping emissions by about 50 % and a global cap of 0.5 % by about 40 % or 50 % depending on the emission inventory used. Simulations by Winebrake et al. (2009) are not directly comparable to our simulation ships-2020, because ships-2020 had both coastal and global caps for fuel sulfur content in use.

Figure 3 shows the excess mortality due to ship-$PM_{2.5}$ for ships-2010, geo-wide and ships-2020. As expected from the results on $PM_{2.5}$ concentration (Fig. 1b), Europe was estimated to suffer most from current shipping emissions and could greatly benefit from emission reductions. We estimated the total excess mortality from shipping emissions in the European Region (includes Northern Asia in the WHO definition, see Fig. 2) to be about 27 300, 7500 and 1300 in ships-2010, geo-wide and ships-2020, respectively (Table 3). Summing the total mortality rates for South East Asia Region and Western Pacific Region (as defined by WHO (2012), see Fig. 2), the respective figures are only about 13 100, 4800 and 100, although the total exposed population (age > 30 yr) is 1.7 billion in those regions compared to 0.5 billion in the European Region. The area displayed in Fig. 3 (between latitudes of 15° S and 65° N) encompasses 98 % of the global excess mortality due to shipping emissions in ships-2010. Therefore, countries in the Southern Hemisphere suffered relatively little from shipping emissions and use of low-sulfur fuel would thus bring few health benefits there.

The simulation ships-2020 predicted at least 91 % decrease in total mortality resulting from shipping for all the WHO regions (compared to ships-2010). Of the two main geoengineering runs, geo-wide decreased regional mortality rates caused by shipping by between 55 % and 81 %. In general, the relative decrease of regional excess mortality was very similar in each region for a given simulation. The main exception was the simulation geo-narrow. For example, the total mortality from shipping emissions in geo-narrow in the eastern Mediterranean Region dropped by 58 % (about 1600 less than in ships-2010), but increased by 1 % (about 100 deaths more than in ships-2010) in the Western Pacific Region. This was most likely caused by the fact that shipping routes in the Mediterranean Sea and North Sea are located very close the coasts, but the shipping routes near China are further away from the continent (Fig. 1a) and beyond the one-grid-cell emission reduction zone.

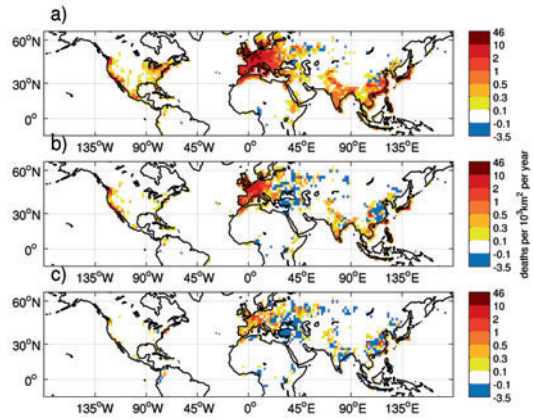

Fig. 3. Sum of excess annual mortality from cardiopulmonary diseases and lung cancer due to shipping emissions in simulations **(a)** ships-2010, **(b)** geo-wide and **(c)** ships-2020.

3.3 Comparison of the radiative effects

We estimated the radiative effect of shipping emissions as effective radiative forcing (ERF, also known as radiative flux perturbation, RFP) (Haywood et al., 2009) (i.e. the difference of all-sky top-of-the-atmosphere net (down minus up) total (short- and longwave) radiation between two simulations with fixed sea surface temperatures). ERF includes both aerosol direct and indirect effects, and makes it possible to compare total aerosol forcing with forcing from well-mixed greenhouse gases (Lohmann et al., 2010). In the simulation ships-2010, the global mean ERF (compared to no-ships) was $-0.39\,W\,m^{-2}$ (Table 2). This is close to the mean value of $-0.44\,W\,m^{-2}$ for the shipping-induced aerosol forcing (for the year 2005) estimated by Eyring et al. (2010) by combining several independent modelling studies. Peters et al. (2012) estimated a similar ERF of $-0.36\,W\,m^{-2}$ for the total aerosol radiative effect with the same model, a similar treatment of shipping emissions, and similar amount of SO_2 emissions ($12.95\,Tg\,(SO_2)\,yr^{-1}$ compared to $12.50\,Tg\,(SO_2)\,yr^{-1}$ in our simulation) as used in our study. There are two major differences between our study and the simulations by Peters et al. (2012). First, they used an empirical parameterization (Lin and Leaitch, 1997) for cloud droplet activation as opposed to the physically based parameterization (Abdul-Razzak and Ghan, 2000) in our study. Second, Peters et al. (2012) assumed that 4.5 % of the sulfur mass emissions from shipping are emitted as primary SO_4

Table 2. Global mean effective radiative forcing (ERF) ($W m^{-2}$) and global excess mortality due to shipping emissions (deaths per year)*.

Simulation	ERF	Lung cancer	Cardiopulmonary diseases
ships-2010	-0.39 ± 0.03	5100 (1900–8300)	45 100 (16 400–73 700)
geo-narrow	-0.53 ± 0.02	3600 (1300–5900)	31 200 (11 300–51 100)
geo-wide	-0.43 ± 0.02	1600 (600–2600)	13 800 (5000–22 600)
ships-2020	-0.06 ± 0.02	200 (100–400)	1800 (600–2900)
ships-2010_45	-0.50 ± 0.02	5500 (2000–9000)	48 800 (17 700–79 700)
geo-wide_45	-0.54 ± 0.02	2100 (800–3400)	17 900 (6500–29 300)
ships-2010_corbett	-0.37 ± 0.01	4800 (1800–7800)	42 500 (15 400–69 500)
geo-wide_corbett	-0.40 ± 0.01	1800 (700–3000)	16 400(6000–26 900)

* The uncertainty of global mean ERF is given as a standard deviation of annual global mean of ERF. The first number for mortality rates is the best estimate for the mortality, and the numbers in the parentheses represent the uncertainty range (95 % confidence interval) from the concentration–response function coefficients. The mortality values are rounded to the nearest 100.

Table 3. Regional annual premature mortality due to shipping emissions in different scenarios (deaths per year)*.

Simulation	AFR	AMR	SEAR	EUR	EMR	WPR
			Lung cancer			
ships-2010	20 (10–30)	880 (330–1430)	170 (60–270)	2850 (1060–4630)	80 (30–120)	1140 (420–1850)
geo-narrow	20 (10–30)	680 (250–1100)	140 (50–230)	1630 (600–2650)	30 (10–50)	1150 (420–1870)
geo-wide	10 (0–10)	320 (120–520)	80 (30–120)	790 (290–1280)	10 (10–20)	370 (140–2570)
ships-2020	0 (0–0)	80 (30–130)	−10 (0–10)	140 (50–220)	0 (0–0)	30 (10–400)
ships-2010_45	30 (10–40)	960 (360–1560)	180 (70–290)	3160 (1170–5130)	80 (30–130)	1120 (410–8980)
geo-wide_45	10 (0–20)	410 (150–670)	80 (30–140)	970 (360–1580)	20 (10–40)	570 (210–3360)
ships-2010_corbett	30 (10–40)	1060 (390–1730)	200 (80–330)	2320 (860–3760)	80 (30–120)	1100 (410–7790)
geo-wide_corbett	10 (0–20)	350 (130–570)	110 (40–180)	810 (300–1330)	20 (10–30)	510 (190–2960)
			Cardiopulmonary diseases			
ships-2010	1150 (420–1880)	5150 (1870–8420)	3890 (1410–6370)	24 420 (8880–39 860)	2620 (950–4280)	7870 (2850–12 880)
geo-narrow	950 (340–1560)	3970 (1440–6500)	3310 (1200–5420)	13 940 (5060–22 780)	1110 (400–1810)	7950 (2880–13 010)
geo-wide	340 (120–550)	1890 (680–3090)	1760 (640–2890)	6720 (2440–11 000)	500 (180–820)	2580 (930–4220)
ships-2020	−60 (−20–100)	470 (170–770)	−130 (−50–210)	1180 (430–1920)	80 (30–120)	230 (80–370)
ships-2010_45	1410 (510–2300)	5640 (2050–9220)	4110 (1490–6730)	27 060 (9840–44 150)	2810 (1020–4590)	7760 (2810–12 690)
geo-wide_45	550 (200–890)	2410 (870–3940)	1960 (710–3200)	8310 (3010–13 590)	750 (270–1230)	3920 (1420–6420)
ships-2010_corbett	1440 (520–2360)	6240 (2260–10 200)	4740 (1720–7770)	19 820 (7200–32 380)	2620 (950–4280)	7630 (2760–12 480)
geo-wide_corbett	720 (260–1180)	2060 (750–3370)	2520 (910–4120)	6960 (2520–11 390)	650 (240–1070)	3510 (1270–5750)

* The regions are African Region (AFR), Region of the Americas (AMR), South East Asia Region (SEAR), European Region (EUR), Eastern Mediterranean Region (EMR), and Western Pacific Region (WPR) (see Fig. 2). The values are rounded to the nearest 10.

particles, compared to 2.5 % used in our ships-2010 simulation. The sensitivity of our results to this parameter is discussed in Sect. 3.4.2.

The ERF in ships-2010 had a strong spatial variation (Fig. 4a). The effect of shipping emissions was largely confined to the Northern Hemisphere. The strongest cooling effect was in the stratocumulus region of the North Pacific where the regional ERF attained values in the order of $-10\,W m^{-2}$. In this region, there are both frequent low-level clouds that are susceptible to additional aerosol emissions (e.g. Partanen et al., 2012) and high shipping emissions from major trade routes (Fig. 1a).

In the simulation geo-wide, the largest (most negative) ERF was in the open sea due to emission reductions near the coasts (Fig. 4b). The ERF in the stratocumulus region of South Atlantic was diminished compared to ships-2010 as the cloud region and the nearby major shipping route (Fig. 1a) lie partly in the emission reduction zone. In North Pacific, the stratocumulus region and shipping routes extend further away to the sea and the total radiative effect was stronger in the geoengineering simulations than in ships-2010. Despite the large emission reduction near the continents, the global mean ERFs in the geoengineering simulations ($-0.43\,W m^{-2}$ in geo-wide and $-0.53\,W m^{-2}$ in geo-narrow) were stronger compared to that in ships-2010. In the simulation ships-2020, the radiative effect of shipping emissions almost disappears (Fig. 4c) as the global mean ERF is only $-0.06\,W m^{-2}$. The absolute difference in ERFs between ships-2020 and ships-2010 was very similar to the estimates by Lauer et al. (2009) for a scenario with a global fuel sulfur content cap of 0.5 % and a non-controlled emission scenario for the year 2012. However, the relative difference in the radiative effects between their scenarios was only 53 % whereas in our case it was 85 %.

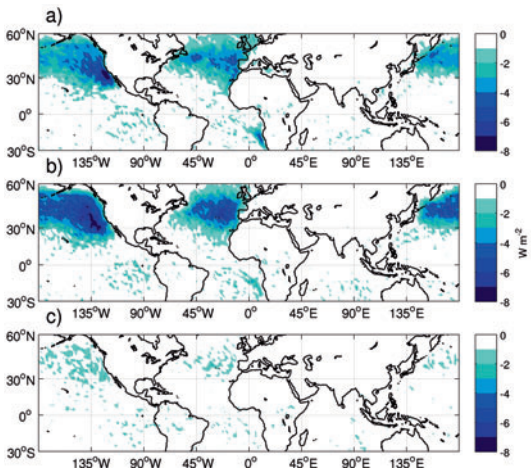

Fig. 4. 5 yr mean of effective radiative forcing compared to no-ships in simulations **(a)** ships-2010, **(b)** geo-wide and **(c)** ships-2020.

3.4 Uncertainties and sensitivity tests

3.4.1 Uncertainty in modelling $PM_{2.5}$ mass concentrations

To evaluate the model's ability to simulate $PM_{2.5}$ mass concentrations, we compared five-year-mean values of $PM_{2.5}$ concentration from the simulation ships-2010 to observed annual mean values from remote measurement stations of the European Monitoring and Evaluation Programme (EMEP, 2013) and United States Interagency Monitoring of Protected Visual Environment (IMPROVE, 2013) networks. We used the last five available years for both data sets. Thus, EMEP data from 2006 to 2010 and IMPROVE data for the years 2007–2011 have been compared to the model values. In cases where more than one station corresponded to a single model grid box, we averaged the stations' data.

Figure 5 shows that the model tended to underestimate the $PM_{2.5}$ concentrations both in US and Europe. The normalized mean biases were −0.74 and −0.34 for the EMEP and IMPROVE data, respectively. However, a more detailed analysis showed that there was a better agreement between the model and the observations in coastal areas and the differences were largest at inland stations. The global model grid size is of the order of 10 000 km^2, so it is difficult to compare a model value to a point-measurement value as the model cannot capture the subgrid-scale variability in aerosol concentrations especially near the emissions sources. It should be noted that in our scenarios, the ship-induced $PM_{2.5}$ concentrations over the continents depend largely on aerosol transport over just one or two grid cells. This means that the simulated $PM_{2.5}$ concentrations are sensitive to the accuracy of the advection scheme.

We analyzed the sensitivity of the excess mortality to the bias in the modelled $PM_{2.5}$ using two different methods. In the first method, we assumed that the model underestimates $PM_{2.5}$ concentrations in all simulations so that the ratio of the real (or corrected) and modeled $PM_{2.5}$ concentrations equal the slope of the linear fit between measured and modeled $PM_{2.5}$ concentrations (Fig. 5, red lines). Using this assumed dependency, we re-calculated the premature mortality due to shipping emissions with total $PM_{2.5}$ concentrations multiplied with 1.61 (fit to EMEP data) or 1.18 (fit to IMPROVE data). Based on these calculations, the underestimation of $PM_{2.5}$ concentrations lead to a relative error of between −4 % and −6 % for global total mortality in different scenarios. In the second method, we assumed that the model underestimates $PM_{2.5}$ concentrations only in the simulation no-ships, and that the contribution from shipping emissions to $PM_{2.5}$ is correct in the other simulations. The $PM_{2.5}$ for the simulation no-ships was scaled following the same procedure as outlined above for the first method. For the other simulations we added the $PM_{2.5}$ contribution from shipping in each simulation to the re-calculated $PM_{2.5}$ of no-ships. With these re-calculated $PM_{2.5}$ values we calculated the excess mortality in each scenario. The estimates for the relative errors in the mortality rate varied in different simulations from an overestimation of 50–54 % (fit to EMEP data) and of 15–16 % (fit to IMPROVE data).

Based on these calculations, the uncertainty in the mortality estimates due to uncertainty in the $PM_{2.5}$ concentrations can be significant. However, both methods probably overestimate the error as the modelled $PM_{2.5}$ concentration compared better with measurements near the coasts where shipping emissions had the largest effect. Furthermore, the relative difference in excess mortality between different scenarios is not sensitive to a systematic bias in the model estimate for $PM_{2.5}$. Thus, we expect that the main conclusions of this study are not significantly affected by the bias in the simulated $PM_{2.5}$ concentrations.

3.4.2 Sensitivity to strength of the subgrid-scale sulfate formation

Changing the fraction of sulfur emissions emitted as primary sulfate particles in the model from 2.5 % to 4.5 % in ships-2010_45 and in geo-wide_45 intensified the impacts on both radiative balance and mortality rates (Table 2). In ships-2010_45, the global mean ERF was −0.50 W m^{-2} (−0.39 W m^{-2} in ships-2010) and the total excess mortality due to shipping was 54 300 (50 200 in ships-2010) (Table 2). Despite these differences caused by varying the SO_4 fraction, the difference in ERF between the simulations with standard emissions and the geoengineering runs (i.e. geo-wide minus ships-2010, and geo-wide_45 minus ships-2010_45) was the same (−0.04 W m^{-2}) with both SO_4 fractions (Table 2). This implies that the conclusions of this study do not depend on the chosen SO_4 fraction.

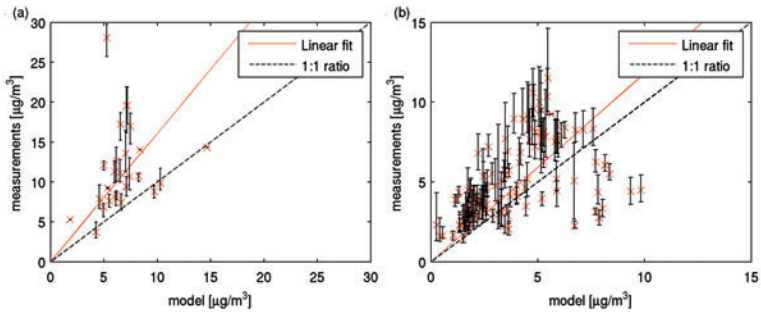

Fig. 5. Scatter plot of the observed annual mean $PM_{2.5}$ concentrations at various sites and the simulated five-year mean surface $PM_{2.5}$ in model grid boxes corresponding to these sites. The measurement data have been taken from **(a)** EMEP and **(b)** IMPROVE. The error bars represent the year-to-year variation and the red dots the five-year mean value of the observations. The dashed lines indicate the 1 : 1 ratio between the simulated values and observations, and the red lines indicate a linear fit to the data.

3.4.3 Sensitivity to shipping emission data

The total global shipping emissions are almost equal in the ACCMIP data set and in the combined data set from Wang et al. (2008) and Corbett et al. (2010) (Table 1). Yet, there are large spatial differences between the data sets. Most notably, the emissions in the simulation ships-2010_corbett are slightly more concentrated on the coasts than in the simulation ships-2010. In ships-2010, 48 % of the shipping emissions are within the two-grid-cell emission reduction zone near the coasts and 31 % in the one-grid-cell emission reduction zone. The respective fractions for ships-2010_corbett are 54 % and 35 %. An exception to this pattern is that ships-2010_corbett has lower emissions near the densely populated European coasts.

In general, the choice of the emission data set had little effect on our results (Table 2). The global total of premature mortality due to shipping was 6 % lower in ships-2010_corbett than in ships-2010 (Table 2) and 19 % higher in geo-wide_corbett than in geo-wide. The ERF was 0.02 W m^{-2} less negative in ships-2010_corbett than in ships-2010 and 0.03 W m^{-2} less negative in geo-wide_corbett than in geo-wide. The mortality difference between ships-2010 and geo-wide is larger than the difference between ships-2010_corbett and geo-wide_corbett. This is probably caused by the fact that shipping emissions near Europe are higher in the ACCMIP data set and emission reductions in the coastal zones have consequently stronger effect. Overall, however, the choice of emission data does not affect our conclusions.

4 Discussion

4.1 Weighting the different emission scenarios

The previous sections addressed how different scenarios of aerosol emissions from shipping would affect the global radiative balance and the number of premature deaths caused by shipping-induced particulate matter air pollution. To draw conclusions on the relative benefits of the different emission scenarios, we simplified the effects in two metrics: global mean ERF and global total premature mortality due to shipping emissions. We acknowledge that the former is an inadequate metric to fully express the climatic impacts of shipping emissions (Lauer et al., 2009), but these two metrics offer a tool to rate different scenarios with respect to climate and health effects. Figure 6 depicts both of these metrics for all our simulations using the simulation no-ships as a reference. Assuming that a large negative ERF is desirable, the optimal scenario would lie in the lower-left corner where shipping emissions have no adverse health effects but a large cooling effect. Optimal level of ERF is of course a subjective definition, because some regions might benefit from stronger cooling and others from less cooling (MacMartin et al., 2012). Note that, because ERF and total premature mortality rate are not comparable, the distance from the lower-left corner cannot be used as measure of optimality. For example, the geoengineering simulations are near the "optimal" corner, but have clearly larger mortality rates than ships-2020, which would be the most favorable in terms of health benefits, but offer little cooling compared to the other scenarios.

Most importantly, we find that the cooling effect and the total mortality rate combination of the simulation ships-2010 is not Pareto optimal (i.e. there are potential scenarios in which the mortality rate can be reduced without a reduction in the climate-cooling effect). Both geoengineering simulations geo-wide and geo-narrow have at least the same cooling effect but lower mortality rates than ships-2010. One cannot put simulations geo-wide, geo-narrow, and ships-2020 into a preferred order without deciding some conversion method between ERF and mortality rate. For example, geo-narrow offered a stronger cooling (-0.53 W m^{-2} vs. -0.43 W m^{-2}) than geo-wide but also had a greater annual mortality rate (34 900 yr^{-1} vs. 15 400 yr^{-1}).

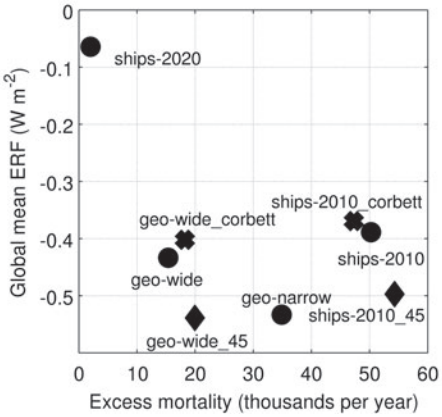

Fig. 6. Global premature mortality due to shipping (x axis) and global mean effective radiative forcing (y axis) with respect to no-ships for different simulations. The upper-left corner represents a zero effect of shipping emissions and the lower-left corner the "optimal" combination of mortality avoided and radiative effects where shipping emissions do not cause premature deaths, but have a large cooling effect. Circles represent the main simulations where AC-CMIP shipping emissions were used as a baseline. Simulations marked with diamonds (ships-2010_45 and geo-wide_45) were run with 4.5 % (instead of 2.5 %) of sulfur mass emissions from ships emitted as primary sulfate. The crosses denote simulations in which shipping emissions inventories compiled by Wang et al. (2008) and Corbett et al. (2010) were used to construct the actual shipping emissions.

4.2 Limitations of the study

In our simulations, aerosols from shipping emissions caused a strongly localized radiative effect (Fig. 4b). Previous studies have shown that regional forcing over the oceans creates a global cooling effect, although the regions with strong local radiative forcing cool the most (Hill and Ming, 2012; Jones et al., 2009; Rasch et al., 2009). This would probably be true also for the cooling effect from shipping emissions. Still, precipitation response depends much more strongly on the location of the forcing and cannot be predicted by using global mean values (Shindell et al., 2012). Jones et al. (2009) found that modifying marine clouds could cause a dramatic decrease of precipitation over the Amazon rain forest. The local forcings in our study are smaller (especially if geoengineering simulations are compared against ships-2010) which would probably limit the extent of side effects. However, the possibility of such detrimental side-effects cannot be entirely excluded. It cannot even be ruled out, that removing aerosol forcing from shipping could cause detrimental precipitation changes in addition to the warming effect. Thus, further climate model studies with dynamic ocean model are needed to fully assess the climate effects of different shipping scenarios.

Our study has been restricted to the effects of sulfur and organic carbon emissions, which are the main emission components expected to change when the fuel sulfur content is manipulated (Lack et al., 2009). While it is important to remember that carbon dioxide emissions from shipping will in the long term dominate over the aerosol emissions when the total radiative impact of shipping emissions is assessed (Fuglestvedt et al., 2009), the change in the fuel sulfur content, which is the focus of this study, is unlikely to have a significant effect on the carbon dioxide emissions. This is because carbon dioxide emissions from shipping are mostly determined by the efficiency of ship motors or ship design (ICCT, 2007), not the fuel composition. Therefore, an increase of ship fuel sulfur content in certain regions would not directly change the total carbon dioxide emissions from shipping or hinder efforts to reduce these emissions by other means. One point to remember, however, is that if the aerosol cooling from shipping was to be maintained to slow down global warming, sulfur emissions from shipping would need to be continued on timescales comparable to lifetimes of long-lived greenhouse gases (i.e. centuries or millennia) due to the short lifetime of aerosol particles (Fuglestvedt et al., 2009; Brovkin et al., 2007).

The increased sulfur emissions over the open oceans in the geoengineering simulations could potentially increase ocean acidification. Hassellöv et al. (2013) concludes that ocean acidification due to SO_x and NO_x from shipping emissions could be in the same order of magnitude as the effect of increased CO_2 concentration near the major shipping routes. However, the coastal areas, which are most vulnerable to acidification (Doney et al., 2007), had either present-day or decreased sulfur emissions in our simulations, although the coastal impact of acidifying compounds transported from the open oceans cannot be totally excluded based on our simulations.

4.3 International law and manipulation of ship fuel sulfur content

Increasing aerosol emissions deliberately to create a global cooling effect would raise complex and controversial legal issues (Redgwel, 2011). Such geoengineering could violate several existing international agreements and international customary rules. In addition, the fuel sulfur content that we have assumed in the geoengineering scenarios would exceed the sulfur limits imposed by the MARPOL Annex VI (IMO, 2008). So far, IMO has focused on the prevention of air pollution from ships. In addition, IMO has done extensive climate-related work to further improve energy efficiency and reduce greenhouse gases from international shipping. In these circumstances, a proposal to increase sulfur content would be controversial and might be regarded as an attempt to undermine the ongoing work and the important achievements

already made. With regard to other geoengineering techniques, similar radiative effects without the adverse health and environmental effects could possibly be achieved with sea spray injections (Latham, 1990). However, there are several risks and legal issues related also to sea spray injections.

5 Conclusions

We have simulated the effects of aerosol emissions from shipping on premature mortality and Earth's radiative balance with an aerosol-climate model ECHAM-HAMMOZ. We compared a present-day shipping emission scenario with two geoengineering scenarios with doubled sulfur dioxide emissions over the open oceans and reduced sulfur emissions near the continents, and a scenario corresponding roughly to emission regulation as currently considered for the year 2020 by the International Maritime Organization in MARPOL Annex VI (IMO, 2008).

According to our results, notable improvements in air quality are possible without losing the current cooling effect from ship-emitted aerosol. In the two geoengineering scenarios, the present-day radiative cooling was increased (by 10 % and 36 %) with simultaneous significant reductions in premature mortality from aerosol emissions from shipping (reductions of 69 % and 31 %). Furthermore, our model indicates that the shipping emission regulation planned for the year 2020 would substantially reduce both the cooling effect (83 %) and global premature mortality (96 %) caused by aerosol emissions from shipping, confirming the findings of previous studies (Lauer et al., 2009; Winebrake et al., 2009).

One important aspect of our results is that regulation of aerosol emissions from shipping near the continents is vital for reducing adverse health effects. Not implementing the ship fuel sulfur content regulation in coastal waters would cause tens of thousands premature deaths annually. Thus, our results should not be interpreted to support removing the regulation of shipping emissions in the existing emission control areas.

Although the emissions from coastal water dominate the health impacts of shipping emissions, emissions originating from the open oceans (several hundreds of kilometers from the coasts) can have significant adverse health effects over the continents due to long-range transport of the pollutants. This can been seen in the large difference in premature mortality (about 13 000 deaths per year) between the geoengineering simulation (geo-wide) and the simulation corresponding to the year 2020 emission controls with equal emission reductions near the coasts.

The cooling effect of aerosol emissions from shipping could be preserved by manipulating aerosol emissions from shipping over the open oceans. However, such manipulation is not without risks, would be in conflict with current international agreements, and is always a trade-off between climate cooling and adverse health effects. Therefore, it should be considered only if radical measures to tackle climate change are needed.

Acknowledgements. We thank K. Peters for kindly providing us with the model modifications to improve the treatment of aerosol emissions from shipping and for giving detailed instruction how to implement them. We also thank T. Kühn for interpolating the ACCMIP emissions for ECHAM, and T. Ekholm and NASA for providing the gridded data set of the world's countries. We are grateful to W. J. Collins and two anonymous referees, whose comments and suggestions helped to improve the paper. The ECHAM-HAMMOZ model is developed by a consortium composed of ETH Zurich, Max Planck Institut für Meteorologie, Forschungszentrum Jülich, University of Oxford, and the Finnish Meteorological Institute and managed by the Center for Climate Systems Modeling (C2SM) at ETH Zurich. This work was funded by the Maj and Tor Nessling foundation (grant 2012116) and the Academy of Finland via the Research Program on Climate Change (FICCA) (project 140867) and an Academy Research Fellow position (decision 250348). A. Schmidt was funded by an Academic Research Fellowship from the School of Earth and Environment, University of Leeds.

Edited by: I. Riipinen

References

Abdul-Razzak, H. and Ghan, S. J.: A parameterization of aerosol activation: 2. multiple aerosol types, J. Geophys. Res., 105, 6837–6844, 2000.

Brovkin, V., Petoukhov, V., Claussen, M., Bauer, E., Archer, D., and Jaeger, C.: Geoengineering climate by stratospheric sulfur injections: Earth system vulnerability to technological failure, Climatic Change, 92, 243–259, doi:10.1007/s10584-008-9490-1, 2009.

Christensen, M. W. and Stephens, G. L.: Microphysical and macrophysical responses of marine stratocumulus polluted by underlying ships: evidence of cloud deepening, J. Geophys. Res., 116, D03201, doi:10.1029/2010JD014638, 2011.

Coakley, J. A., Bernstein, R. T. L., and Durkee, P. A.: Effect of shipstack effluents on cloud reflectivity, Science, 237, 1020–1022, 1987.

Cohen, A. J., Ross Anderson, H., Ostro, B., Pandey, K. D., Krzyzanowski, M., Kunzli, N., Gutschmidt, K., Pope, A., Romieu, I., Samet, J. M., and Smith, K.: The global burden of disease due to outdoor air pollution, J. Toxicol. Environ. Health A, 68, 1301–1307, 2005.

Corbett, J. J., Winebrake, J. J., Green, E. H., Kasibhatla, P., Eyring, V., and Lauer, A.: Mortality from ship emissions: a global assessment, Environ. Sci. Technol., 41, 8512–8518, 2007.

Corbett, J. J., Lack, D. A., Winebrake, J. J., Harder, S., Silberman, J. A., and Gold, M.: Arctic shipping emissions inventories and future scenarios, Atmos. Chem. Phys., 10, 9689–9704, doi:10.5194/acp-10-9689-2010, 2010.

Crutzen, P.: Albedo enhancement by stratospheric sulfur injections: a contribution to resolve a policy dilemma?, Clim. Change, 77, 211–220, 2006.

Dee, D. P., Uppala, S. M., Simmons, A. J., Berrisford, P., Poli, P., Kobayashi, S., Andrae, U., Balmaseda, M. A., Balsamo, G.,

Bauer, P., Bechtold, P., Beljaars, A. C. M., van de Berg, L., Bidlot, J., Bormann, N., Delsol, C., Dragani, R., Fuentes, M., Geer, A. J., Haimberger, L., Healy, S. B., Hersbach, H., Hólm, E. V., Isaksen, L., Kållberg, P., Köhler, M., Matricardi, M., McNally, A. P., Monge-Sanz, B. M., Morcrette, J.-J., Park, B.-K., Peubey, C., de Rosnay, P., Tavolato, C., Thépaut, J.-N., and Vitart, F.: The ERA-Interim reanalysis: configuration and performance of the data assimilation system, Q. J. Roy. Meteor. Soc., 137, 553–597, 2011.

Dentener, F., Kinne, S., Bond, T., Boucher, O., Cofala, J., Generoso, S., Ginoux, P., Gong, S., Hoelzemann, J. J., Ito, A., Marelli, L., Penner, J. E., Putaud, J.-P., Textor, C., Schulz, M., van der Werf, G. R., and Wilson, J.: Emissions of primary aerosol and precursor gases in the years 2000 and 1750 prescribed data-sets for AeroCom, Atmos. Chem. Phys., 6, 4321–4344, doi:10.5194/acp-6-4321-2006, 2006.

Doney, S. C., Mahowald, N., Lima, I., Feely, R. A., Mackenzie, F. T., Lamarque, J., and Rasch, P. J.: Impact of anthropogenic atmospheric nitrogen and sulfur deposition on ocean acidification and the inorganic carbon system, P. Natl. Acad. Sci. USA, 104, 14580–14585, 2007.

EMEP (European Monitoring and Evaluation Programme): available at: http://www.emep.int/, last access: 24 January 2013, 2013.

Eyring, V., Isaksen, I. S. A., Berntsen, T., Collins, W. J., Corbett, J. J., Endresen, O., Grainger, R. G., Moldanova, J., Schlager, H., and Stevenson, D. S.: Transport impacts on atmosphere and climate: shipping, Atmos. Environ., 44, 4735–4771, 2010.

Fox, T. A. and Chapman, L.: Engineering geo-engineering, Meteorol. Appl., 18, 1–8, 2011.

Fuglestvedt, J., Berntsen, T., Eyring, V., Isaksen, I., Lee, D. S., and Sausen, R.: Shipping emissions: from cooling to warming of climate and reducing impacts on health, Environ. Sci. Technol., 43, 9057–9062, 2009.

Hassellöv, I.-M., Turner, D., Lauer, A., and Corbett, J. J.: Shipping contributes to ocean acidification, Geophys. Res. Lett., 40, 2731–2736, doi:10.1002/grl.50521, 2013.

Haywood, J., Donner, L., Jones, A., and Golaz, J.-C.: Global indirect radiative forcing caused by aerosols: IPCC (2007) and beyond, in: Clouds in the Perturbed Climate System: Their Relationship to Energy Balance, Atmospheric Dynamics, and Precipitation, edited by: Heintzenberg, J. and Charlson, R. J., Strüngmann Forum Report, MIT Press, Cambridge, USA, 451–467, 2009.

Hill, S. and Ming, Y.: Nonlinear climate response to regional brightening of tropical marine stratocumulus, Geophys. Res. Lett., 39, L15707, doi:10.1029/2012GL052064, 2012.

ICCT (The International Council on Clean Transportation): Air pollution and Greenhouse Gas Emissions from Ocean-going Ships: Impacts, Mitigation Options and Opportunities for Managing Growth, The International Council on Clean Transportation, 2007.

IMO: International Convention for the Prevention of Pollution from Ships, London, 2 November 1973 and the Protocol, London, relating thereto (MARPOL 73/78), available at: http://www.imo.org/last access: 17 February 1978, 1978.

IMO: Amendments to the Annex of the Protocol of 1997 to amend the International Convention for the Prevention of Pollution from Ships, 1973, as modified by the Protocol of 1978 relating thereto (Revised MARPOL Annex VI), IMO MEPC.176(58), available at: http://www.imo.org/ (last access: March 2013), 2008.

IMO: Amendments to the Annex of the Protocol of 1997 to amend the International Convention for the Prevention of Pollution from Ships, 1973, as modified by the Protocol of 1978 relating thereto (North American Emission Control Area), IMO MEPC.190(60), available at: http://www.imo.org/ (last access: March 2013), 2010.

IMPROVE (United States Interagency Monitoring of Protected Visual Environment), available at: http://vista.cira.colostate.edu/improve/last access: 29 January 2013, 2013.

Jones, A., Haywood, J., and Boucher, O.: Climate impacts of geoengineering marine stratocumulus clouds, J. Geophys. Res., 114, D10106, doi:10.1029/2008JD011450, 2009.

Jonsson, Å. M., Westerlund, J., and Hallquist, M.: Size-resolved particle emission factors for individual ships, Geophys. Res. Lett., 38, L13809, doi:10.1029/2011GL047672, 2011.

Kazil, J. and Lovejoy, E. R.: A semi-analytical method for calculating rates of new sulfate aerosol formation from the gas phase, Atmos. Chem. Phys., 7, 3447–3459, doi:10.5194/acp-7-3447-2007, 2007.

Koch, D. and Del Genio, A. D.: Black carbon semi-direct effects on cloud cover: review and synthesis, Atmos. Chem. Phys., 10, 7685–7696, doi:10.5194/acp-10-7685-2010, 2010.

Lack, D. A. and Corbett, J. J.: Black carbon from ships: a review of the effects of ship speed, fuel quality and exhaust gas scrubbing, Atmos. Chem. Phys., 12, 3985–4000, doi:10.5194/acp-12-3985-2012, 2012.

Lack, D. A., Corbett, J. J., Onasch, T., Lerner, B., Massoli, P., Quinn, P. K., Bates, T. S., Covert, D. S., Coffman, D., Sierau, B., Herndon, S., Allan, J., Baynard, T., Lovejoy, E., Ravishankara, A. R., and Williams, E.: Particulate emissions from commercial shipping: chemical, physical, and optical properties, J. Geophys. Res., 114, D00F04, doi:10.1029/2008JD011300, 2009.

Latham, J.: Control of global warming?, Nature, 347, 339–340, 1990.

Lauer, A., Eyring, V., Corbett, J. J., Wang, C., and Winebrake, J. J.: Assessment of near-future policy instruments for oceangoing shipping: impact on atmospheric aerosol burdens and the Earth's radiation budget, Environ. Sci. Technol., 43, 5592–5598, 2009.

Lerner, J., Matthews, E., and Fung, I.: Methane emission from animals: a global high-resolution database, Global Biogeochem. Cy., 2, 139–156, 1988.

Lieke, K. I., Rosenørn, T., Pedersen, J., Larsson, D., Kling J., Fuglsang, K., Bilde, M.: Micro- and Nanostructural Characteristics of Particles Before and After an Exhaust Gas Recirculation System Scrubber, Aerosol Sci. Tech., 47, 1038–1046, 2013.

Lin, H. and Leaitch, W.: Development of an in-cloud aerosol activation parameterization for climate modelling, in: Proceedings of the WMO Workshop on Measurement of Cloud Properties for Forecasts of Weather, Air Quality and Climate, Mexico City, Publisher is World Meteorological Organization (WMO), 328–335, 1997.

Lohmann, U. and Feichter, J.: Global indirect aerosol effects: a review, Atmos. Chem. Phys., 5, 715–737, doi:10.5194/acp-5-715-2005, 2005.

Lohmann, U. and Hoose, C.: Sensitivity studies of different aerosol indirect effects in mixed-phase clouds, Atmos. Chem. Phys., 9, 8917–8934, doi:10.5194/acp-9-8917-2009, 2009.

Lohmann, U., Rotstayn, L., Storelvmo, T., Jones, A., Menon, S., Quaas, J., Ekman, A. M. L., Koch, D., and Ruedy, R.: Total aerosol effect: radiative forcing or radiative flux perturbation?, Atmos. Chem. Phys., 10, 3235–3246, doi:10.5194/acp-10-3235-2010, 2010.

Löndahl, J., Swietlicki, E., Lindgren, E., and Loft, S.: Aerosol exposure versus aerosol cooling of climate: what is the optimal emission reduction strategy for human health?, Atmos. Chem. Phys., 10, 9441–9449, doi:10.5194/acp-10-9441-2010, 2010.

Luo, G. and Yu, F.: Sensitivity of global cloud condensation nuclei concentrations to primary sulfate emission parameterizations, Atmos. Chem. Phys., 11, 1949–1959, doi:10.5194/acp-11-1949-2011, 2011.

MacMartin, D. G., Keith, D. W., Kravitz, B., and Caldeira, K.: Management of trade-offs in geoengineering through optimal choice of non-uniform radiative forcing, Nat. Clim. Change, 3, 365–368, doi:10.1038/nclimate1722, 2012.

Myhre, G., Samset, B. H., Schulz, M., Balkanski, Y., Bauer, S., Berntsen, T. K., Bian, H., Bellouin, N., Chin, M., Diehl, T., Easter, R. C., Feichter, J., Ghan, S. J., Hauglustaine, D., Iversen, T., Kinne, S., Kirkevåg, A., Lamarque, J.-F., Lin, G., Liu, X., Lund, M. T., Luo, G., Ma, X., van Noije, T., Penner, J. E., Rasch, P. J., Ruiz, A., Seland, Ø., Skeie, R. B., Stier, P., Takemura, T., Tsigaridis, K., Wang, P., Wang, Z., Xu, L., Yu, H., Yu, F., Yoon, J.-H., Zhang, K., Zhang, H., and Zhou, C.: Radiative forcing of the direct aerosol effect from AeroCom Phase II simulations, Atmos. Chem. Phys., 13, 1853–1877, doi:10.5194/acp-13-1853-2013, 2013.

Ostro, B.: Outdoor air pollution: assessing the environmental burden of disease at national and local levels, WHO Environmental Burden of Disease Series, 5, Geneva, World Health Organization, 2004.

Partanen, A.-I., Kokkola, H., Romakkaniemi, S., Kerminen, V.-M., Lehtinen, K. E. J., Bergman, T., Arola, A., and Korhonen, H.: Direct and indirect effects of sea spray geoengineering and the role of injected particle size, J. Geophys. Res., 117, D02203, doi:10.1029/2011JD016428, 2012.

Peters, K., Stier, P., Quaas, J., and Graßl, H.: Aerosol indirect effects from shipping emissions: sensitivity studies with the global aerosol-climate model ECHAM-HAM, Atmos. Chem. Phys., 12, 5985–6007, doi:10.5194/acp-12-5985-2012, 2012.

Peters, K., Stier, P., Quaas, J., and Graßl, H.: Corrigendum to "Aerosol indirect effects from shipping emissions: sensitivity studies with the global aerosol-climate model ECHAM-HAM" published in Atmos. Chem. Phys., 12, 5985–6007, 2012, Atmos. Chem. Phys., 13, 6429–6430, doi:10.5194/acp-13-6429-2013, 2013.

Petzold, A., Hasselbach, J., Lauer, P., Baumann, R., Franke, K., Gurk, C., Schlager, H., and Weingartner, E.: Experimental studies on particle emissions from cruising ship, their characteristic properties, transformation and atmospheric lifetime in the marine boundary layer, Atmos. Chem. Phys., 8, 2387–2403, doi:10.5194/acp-8-2387-2008, 2008.

Pope III, C. A. and Dockery, D. W.: Health effects of fine particulate air pollution: lines that connect, J. Air Waste Manag. Assoc., 56, 709–742, 2006.

Rasch, P. J., Latham, J., and Chen, C.-C.: Geoengineering by cloud seeding: influence on sea ice and climate system, Environ. Res. Lett., 4, 045112, doi:10.1088/1748-9326/4/4/045112, 2009.

Redgwel,C.: Geoengineering the climate: techological solutions to mitigation – failure or continuing carbon addicction?, Carb. Clim. Law Rev., 2, 178–189, 2011.

Riahi, K., Grübler, A., and Nakicenovic, N.: Scenarios of long-term socio-economic and environmental development under climate stabilization, Technol. Forecast. Soc., 74, 887–935, 2007.

Riahi, K., Rao, S., Krey, V., Cho, C., Chirkov, V., Fischer, G., Kindermann, G., Nakicenovic, N., and Rafaj, P.: RCP 8.5 – a scenario of comparatively high greenhouse gas emissions, Clim. Change, 109, 33–57, 2011.

Robock, A.: 20 reasons why geoengineering may be a bad idea, Bull. Atomic Scientists, 64, 14–18, 2008.

SEDAC (NASA Socioeconomic Data and Applications Center): Gridded Population of the World, Version 3 (GPWv3): Population Count Grid, Future Estimates, Center for International Earth Science Information Network (CIESIN)/Columbia University, United Nations Food and Agriculture Programme (FAO), and Centro Internacional de Agricultura Tropical (CIAT), available at: http://sedac.ciesin.columbia.edu/data/set/gpw-v3-population-count-future-estimates, last access: 16 November 2012, 2005.

Shindell, D. T., Voulgarakis, A., Faluvegi, G., and Milly, G.: Precipitation response to regional radiative forcing, Atmos. Chem. Phys., 12, 6969–6982, doi:10.5194/acp-12-6969-2012, 2012.

Stevens, R. G., Pierce, J. R., Brock, C. A., Reed, M. K., Crawford, J. H., Holloway, J. S., Ryerson, T. B., Huey, L. G., and Nowak, J. B.: Nucleation and growth of sulfate aerosol in coal-fired power plant plumes: sensitivity to background aerosol and meteorology, Atmos. Chem. Phys., 12, 189–206, doi:10.5194/acp-12-189-2012, 2012.

Stier, P., Feichter, J., Kinne, S., Kloster, S., Vignati, E., Wilson, J., Ganzeveld, L., Tegen, I., Werner, M., Balkanski, Y., Schulz, M., Boucher, O., Minikin, A., and Petzold, A.: The aerosol-climate model ECHAM5-HAM, Atmos. Chem. Phys., 5, 1125–1156, doi:10.5194/acp-5-1125-2005, 2005.

Vignati, E., Wilson, J., and Stier, P.: M7: an efficient size-resolved aerosol microphysics module for large-scale aerosol transport models, J. Geophys. Res., 109, D22202, doi:10.1029/2003JD004485, 2004.

Wang, C., Corbett, J. J., and Firestone, J.: Improving spatial representation of global ship emissions inventories, Environ. Sci. Technol., 42, 193–199, 2008.

Winebrake, J. J., Corbett, J. J., Green, E. H., Lauer, A., and Eyring, V.: Mitigating the health impacts of pollution from oceangoing shipping: an assessment of low-sulfur fuel mandates, Environ. Sci. Technol., 43, 4776–4782, 2009.

WHO (World Health Organization): The global burden of disease: 2004 update, Geneva, 2008.

WHO (World Health Organization): Regional offices, available at: http://www.who.int/about/regions/en/index.html, last access: December 2012, 2012.

Zhang, K., O'Donnell, D., Kazil, J., Stier, P., Kinne, S., Lohmann, U., Ferrachat, S., Croft, B., Quaas, J., Wan, H., Rast, S., and Feichter, J.: The global aerosol-climate model ECHAM-HAM, version 2: sensitivity to improvements in process representations, Atmos. Chem. Phys., 12, 8911–8949, doi:10.5194/acp-12-8911-2012, 2012.

IV

Paper IV

A. Laakso, A.-I. Partanen, H. Kokkola, A. Laaksonen, K.E.J. Lehtinen and H. Korhonen, Stratospheric passenger flights are likely an inefficient geoengineering strategy. *Environ. Res. Lett.* *7*, 034021, doi:10.1088/1748-9326/7/3/034021, 2012.

OPEN ACCESS
IOP PUBLISHING
ENVIRONMENTAL RESEARCH LETTERS
Environ. Res. Lett. **7** (2012) 034021 (7pp)
doi:10.1088/1748-9326/7/3/034021

Stratospheric passenger flights are likely an inefficient geoengineering strategy

Anton Laakso[1], Antti-Ilari Partanen[1], Harri Kokkola[1], Ari Laaksonen[2,3], Kari E J Lehtinen[1,3] and Hannele Korhonen[1]

[1] Finnish Meteorological Institute, Kuopio Unit, PO Box 1627, FI-70211, Kuopio, Finland
[2] Finnish Meteorological Institute, Climate Change, PO Box 503, FI-00101, Helsinki, Finland
[3] Department of Applied Physics, University of Eastern Finland, Kuopio Campus, PO Box 1627, FI-70211, Kuopio, Finland

E-mail: Anton.Laakso@fmi.fi

Received 20 June 2012
Accepted for publication 15 August 2012
Published 4 September 2012
Online at stacks.iop.org/ERL/7/034021

Abstract
Solar radiation management with stratospheric sulfur aerosols has been proposed as a potential geoengineering strategy to reduce global warming. However, there has been very little investigation on the efficiency of specific injection methods suggested. Here, we show that using stratospheric passenger flights to inject sulfate aerosols would not cause significant forcing under realistic injection scenarios: even if all present-day intercontinental flights were lifted above the tropopause, we simulate global surface shortwave radiative forcings of -0.05 W m^{-2} and -0.10 W m^{-2} with current and five times enhanced fuel sulfur concentrations, respectively. In the highly unlikely scenario that fuel sulfur content is enhanced by a factor of 50 (i.e. ten times the current legal limit) the radiative forcing is -0.85 W m^{-2}. This is significantly lower than if the same amount of sulfur were injected over the tropics (-1.32 W m^{-2}, for 3 Tg (S) yr^{-1}) due to a faster loss rate and lower intensity of solar radiation in the northern midlatitudes where current flight paths are concentrated. We also predict lower global forcing in northern hemisphere winter than in summer due to the seasonalities of the solar radiation intensity at midlatitudes, the related OH chemistry that produces sulfate aerosol, and removal of particles.

Keywords: geoengineering, stratospheric aerosols, radiative forcing, aircraft emissions

1. Introduction

Solar radiation management (SRM) techniques aim to compensate the warming caused by increased greenhouse gas concentrations by increasing the reflectivity of the Earth. Currently the most studied, and probably the most promising, SRM method is injection of sulfur to the stratosphere (Rasch 2008). In the atmosphere, gaseous sulfur reacts to form sulfate aerosols which can reflect incoming shortwave (SW) radiation back to space and thus cool the climate. Because of the stability of the stratosphere and the relatively slow removal mechanisms for submicron aerosol, the lifetime of the sulfate aerosol can be 1–2 yr, while in the troposphere it is only from a few days to a week (Rasch 2008).

The idea of stratospheric sulfur injections goes back to the 1970s, when Budyko (1977) suggested that the emission of sulfur from the jet fuel of a civil aircraft flying in the stratosphere could increase the aerosol concentration and thus cause climate cooling. In theory, intercontinental and other long-distance flights with Concorde-type aircraft capable of operating at stratospheric altitudes could be used for this purpose. Since the 1970s, numerous other injection methods have also been proposed, including military jets, modified artillery, chimneys and high altitude balloons (The Royal

Society 2009). While the radiative and climate effects of stratospheric injections have in recent years been studied quite extensively, very few of the previous modelling studies have explicitly addressed the issue of the injection method (Rasch 2008). One exception is Pierce *et al* (2010), who studied sulfate particle formation in individual plumes of a dedicated carrier aircraft and used their results as an input to a 2D stratospheric aerosol model to calculate the radiative forcing from injections made between 30°S and 30°N latitudes. Several other studies have added sulfur into one model grid cell in the tropics (Niemeier *et al* 2011, Robock *et al* 2008, Jones *et al* 2010), implying a fairly local injection method (e.g., artillery or chimney). Such local methods would release a large amount of sulfur into a relatively small volume of air, which could enhance coagulation and thus lead to larger particles and smaller lifetime of the stratospheric aerosol (Heckendorn *et al* 2009).

Here, we revisit the idea of Budyko (1977) and investigate the cooling potential of civil aircraft in scenarios in which most long-distance flights are flown in the lower stratosphere and the jet fuel is sulfur-enhanced. One advantage of these scenarios is that the sulfate aerosol would spread over a wide area in the stratosphere, minimizing the coagulation effects predicted for local injection methods. The appeal of this method is that an already existing activity, in this case commercial air traffic, could be used for geoengineering purposes. We study several injection scenarios with the climate–aerosol model ECHAM5.5-HAM2 (Zhang *et al* 2012), making this one of the few stratospheric geoengineering studies to include an explicit treatment of sulfate aerosol microphysics.

This study is intended as a first-order estimate of the potential cooling that could theoretically be achieved utilizing civil aircraft for stratospheric geoengineering. We acknowledge that there would be several technical, financial and legal issues that would need to be solved before such a scheme could be implemented in reality. These include replacing the current commercial fleet with Concorde-type aircraft that could actually operate in the stratosphere, possible large increases in fuel consumption as flight altitudes and plane types are changed, current legal limitations of fuel sulfur content, and route restrictions for supersonic civil aircraft (currently allowed only over the oceans). There could also be significant effects on stratospheric chemistry and especially on the ozone layer, as the aircraft would also emit large amounts of NO_x which is not simulated in our model.

2. Methods

2.1. Model description

In our simulations, we have used MAECHAM5.5-HAM2, the middle atmosphere configuration of aerosol–climate model ECHAM5.5-HAM2 (Stier *et al* 2005, Zhang *et al* 2012). MAECHAM5.5 is integrated with a spectral truncation of 63 (T63), which corresponds approximately to a 1.9° × 1.9° horizontal grid, and to 47 vertical levels up to 0.01 hPa. The simulations were performed with a time step of 600 s. The aerosol module HAM2 is coupled interactively to MAECHAM5.5 and includes an explicit modal aerosol scheme M7 (Vignati *et al* 2004) describing the aerosol number and volume size distributions by a superposition of seven log-normal modes. HAM2 calculates aerosol emissions, removal, gas and liquid phase chemistry, and radiative properties for the major global aerosol compounds of sulfate, sea salt, black carbon, organic carbon and mineral dust. M7 calculates the microphysical processes of nucleation, condensation, coagulation and hydration.

For aircraft emissions, we have used the IPCC AR5 air traffic emissions for years 2000 and 2050 (Lamarque *et al* 2010). The IPCC AR5 inventory does not include SO_2 emissions for air traffic and thus we have used the NO_2 mass emissions in the database to calculate the SO_2 emissions. This was carried out based on the emission indices from the US Federal Aviation Administration's AEDT/SAGE tool (Kim *et al* 2007), which gives a global emissions index of 13.8 g kg^{-1} (fuel) for NO_2. For SO_2 we have used an emission index of 1.2 g kg^{-1} (fuel) (Barrett *et al* 2010). Based on these values, we assumed that for each kilogram of aircraft NO_2 emission, 87 g of SO_2 was simultaneously emitted.

In addition to air traffic emissions, we have included aerosol emissions from other anthropogenic sources and biomass burning as given in the AEROCOM database for the year 2000 (Dentener *et al* 2006). For sea spray emissions, we used a parameterization combining the wind-speed-dependent source functions by Monahan *et al* (1986) and Smith and Harrison (1998) (Schulz *et al* 2004). For dust emissions, we used the Tegen *et al* (2002) scheme.

The simulation was carried out with a free running setup and thus the dynamical feedback resulting from the additional heating was taken into account. However, online emissions of, e.g., sea salt and mineral dust are sensitive to wind speed at 10 m height, which can differ significantly between simulations with different aerosol fields. This can occasionally have strong local effects on the forcing. However, the effect is small when comparing the mean values of forcing in simulations of several years.

2.2. Model experiments

Nine simulations were performed in this study. Each simulation was for a five-year period from 2001 to 2005 and was preceded by a two-year spin-up period. The studied scenarios are summarized in table 1.

In the control (CTRL) run, the aircraft emissions were simulated using the flight altitudes from AEROCOM and current fuel sulfur concentration calculated as described in section 2.1. In all the other simulations, all intercontinental flights above oceans as well as the portions of flights above continents which currently take place at altitudes above 10 km were elevated about 2 km above the tropopause and spread into three model levels in the stratosphere. As a result, about half of all current aircraft emissions were emitted to the stratosphere. The SO_2 emissions from these elevated flights using year 2000 emissions are shown in figure 1(a). Due to the varying height of the tropopause, the flight altitudes need

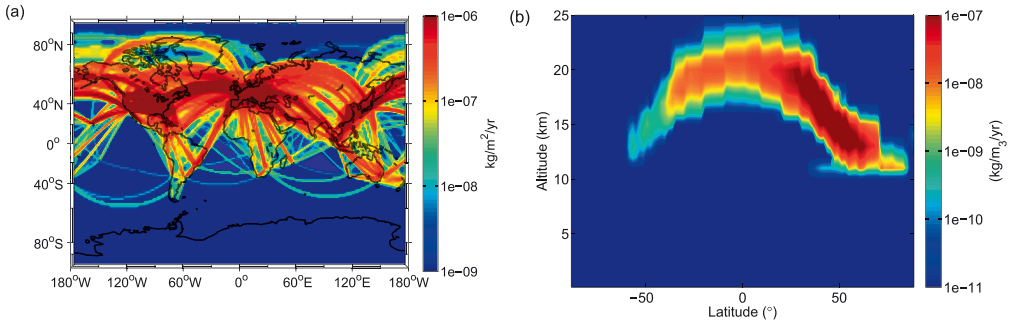

Figure 1. Column-integrated total (a) and zonal mean (b) of stratospheric SO_2 emissions in the SAT scenario.

Table 1. Summary of the model experiments. (Note: the columns list the emission index of sulfur in aircraft fuel (g (S)/kg (fuel)), the total amount of sulfur injected to the stratosphere and amounts injected to the north of 30°N, between 30°N and 30°S and to the south of 30°S. For more details on the different scenarios, see section 2.)

Scenario	EI(S) (g kg^{-1})	Stratospheric S injections (Tg yr^{-1})	Tg (S) yr^{-1} > 30 N	Tg (S) yr^{-1} tropics	Tg (S) yr^{-1} > 30 S
CTRL	0.6	0.02	0.02	—	—
SAT	0.6	0.06	0.04	0.02	0.0008
SAT × 5	3.0	0.31	0.22	0.08	0.004
SAT × 50	*30 (/0.6)*[a]	3.06	2.24	0.79	0.04
SAT × 5 2050	3.0	0.69	0.46	0.22	0.01
SAT × 5 SO4	3.0	0.31	0.22	0.08	0.004
EQ3	—	3.0	—	3.0	—
SAT × 50 H2SO4	*30 (/0.6)*[a]	3.06	2.24	0.79	0.04

[a] In the SAT × 50 and SAT × 50 H2SO4 scenarios emission index 30 is only applied in the stratosphere and index 0.6 in the troposphere.

to be increased much more in the tropics than in the mid and high latitudes (figure 1(b)).

The geoengineering simulation SAT had the same flight routes and total SO_2 emissions as the CTRL simulation, except that some of the flights were elevated to the stratosphere as described above. Scenarios SAT × 5 and SAT × 50 were as SAT, except that the current fuel sulfur content was enhanced by factors of 5 and 50, which led to injected sulfur masses of 0.3 Tg yr^{-1} and 3.0 Tg yr^{-1}, respectively (table 1). Note that the SAT × 5 scenario corresponds to the current legal limit for aircraft fuel sulfur concentration of 3 g (S)/kg (fuel) (IPCC 1999), and thus scenario SAT × 50 exceeds this limit by a factor of ten. Technically, if a 50-fold sulfur enhancement were used, the aeroplanes would probably need two separate fuel tanks: one for fuel with the current sulfur concentration to be used in lower altitudes where air pollution is an issue, and another for sulfur-enhanced fuel to be used in the stratosphere. This was taken into account in this scenario and enhanced fuel sulfur concentration was only used in the stratosphere. We assume here that the aircraft engines can be designed to sustain the increased fuel sulfur content.

The effect of future changes in air traffic volume and flight paths was investigated with scenario SAT × 5 2050, which assumes the same fuel sulfur content as SAT × 5 but uses projected flight paths for the year 2050 from the Representation Concentration Pathways scenario 8.5 (RCP8.5) of IPCC AR5. These flight paths are also elevated to be flown in the stratosphere. RCP8.5 can be viewed as the no-climate-policy scenario in which anthropogenic CO_2 emissions increase so that the warming effect of CO_2 is 8.5 W m^{-2} at the end of this century. Note that while the original RCP scenarios assume that the fuel sulfur concentration will decrease significantly in the future because of regulation, in our simulation investigating the geoengineering potential of civil aircraft we have used five times the current fuel sulfur concentration. The climate conditions and emissions other than from the air traffic were the same as in the other scenarios.

In all the simulations mentioned above, sulfur is emitted as SO_2. However, since the global climate model resolution is quite poor, we are not able to capture the high SO_2 concentrations in the aircraft plumes and thus are likely to underestimate particle formation in aircraft exhaust fumes and immediately after the emissions. Therefore, to test the sensitivity of our results, we repeated the scenario SAT × 5 assuming that 5% of sulfur emissions are emitted as primary sulfate particles with a geometric mean diameter of 50 nm (simulation SAT × 5 SO_4).

Simulation EQ3 was included as a reference case. In this model run, no stratospheric flights were simulated but instead 3 Tg yr^{-1} of sulfur was injected uniformly over the area between latitudes 20°S and 20°N at an altitude of 19–21 km. This scenario was chosen since earlier studies have shown that stratospheric sulfur injections in the tropics are the most

Table 2. Clear-sky and all-sky radiative forcing at the surface and stratospheric sulfur burden of each studied scenario.

Scenario	SW clear-sky radiative forcing (W m^{-2})	SW all-sky radiative forcing (W m^{-2})	Stratospheric sulfur burden (Tg (S))
SAT	−0.07	−0.05	0.04
SAT × 5	−0.19	−0.10	0.19
SAT × 50	−1.43	−0.85	1.63
SAT × 5 2050	−0.58	−0.38	0.44
SAT × 5 SO4	−0.21	−0.12	0.20
EQ3	−2.15	−1.32	2.40
SAT × 50 H2SO4	−1.88	−1.13	1.59

effective in terms of geoengineering (Robock *et al* 2008). Comparing the radiative forcings caused by stratospheric emissions from aircraft and emissions over the tropics allows us to evaluate the effectiveness of injection from air traffic.

Finally, we repeated simulation SAT × 50 assuming that the sulfur is injected in the form of H_2SO_4 instead of SO_2 to estimate the effect of how the form of emitted sulfur affects the forcings. It has to be noted that in our simulation H_2SO_4 is assumed to be evenly distributed within the model grid box while, in reality, gaseous H_2SO_4 would transform to particle phase very localized in aircraft plumes. Thus, this assumption of well-mixed H_2SO_4 in the grid box cannot be considered completely physical and the simulation is not directly comparable with Pierce *et al* (2010).

One limitation in the simulations described above is that we are restricted to the flight paths and total emissions of the current aircraft fleet, which are very likely not fully representative of large-scale flight operations in the stratosphere. However, more accurate estimates for the type of scenarios we are studying are currently not available. With this in mind, our results should be taken as a first-order estimate of the potential cooling from geoengineering with stratospheric civil aircraft.

3. Results

Table 2 shows the change in the global mean clear-sky and all-sky shortwave (SW) radiative forcing at the surface between the injection scenarios and the CTRL run. In all cases radiative forcing is smaller in the all-sky than in the clear-sky case because globally clouds contribute about 2/3 of the planetary albedo.

As table 2 shows, stratospheric flights without enhancement of fuel sulfur content (simulation SAT) would have an insignificant effect on the radiative forcing (−0.05 W m^{-2}). Because of this, simply operating current intercontinental civil flights in the stratosphere would likely cause negligible climate cooling. From the point of view of geoengineering, the fuel sulfur content would need to be enhanced considerably. Even if the current legal limit for aircraft fuel sulfur concentration (simulation SAT × 5) is used, the all-sky radiative forcing at the surface is only −0.10 W m^{-2}. However, by using 50 times the current sulfur concentration in aircraft fuel (simulation SAT × 50), it could be possible to considerably increase the radiative forcing of aircraft emissions. In this case, the global change in all-sky radiative forcing at the surface is −0.85 W m^{-2}, which is slightly less than one quarter of the positive forcing from doubling of CO_2 (3.7 W m^{-2}). However, we consider such a high enhancement of fuel sulfur content very unlikely.

The lifetime of stratospheric sulfur is smaller in the SAT × 50 case than in the SAT × 5 case (0.53 yr and 0.68 yr, respectively), since with larger sulfur injections the stratospheric particles grow faster which increases sedimentation (Robock *et al* 2008). This effect is also evident from the sub-linearity of the clear-sky forcing as a function of injected sulfur mass (table 2). The apparent super-linearity of all-sky forcing is caused by small differences in modelled meteorology between the simulations which have a relatively large effect in the low sulfur scenarios.

If 5% of fuel sulfur is emitted as primary SO_4 particles (run SAT × 5 SO4), the predicted aerosol radiative forcing is almost equal to the case where all sulfur is emitted as SO_2 (run SAT × 5) (table 2). In the beginning of the two-year model spin-up, simulation SAT × 5 SO4 shows more particles in the accumulation mode but this difference disappears before the end of the spin-up. There is no considerable difference in stratospheric sulfur burden between scenarios SAT × 5 and SAT × 5 SO4. Given that the timescale of SO_2 oxidation in the stratosphere is 30–40 days (McKeen and Liu 1984, Rasch 2008) and thus emitting 5% of sulfur as primary particles can be seen as a reasonable upper limit estimate of sub-grid particle formation, simulation SAT × 5 SO4 indicates that our results are not highly sensitive to the treatment of sub-grid processes when sulfur is assumed emitted as SO_2.

The predicted radiative forcing increases notably if we use estimated air traffic volumes for year 2050 instead of year 2000 (scenario SAT×5 2050). In this case, the global radiative forcing at the surface is −0.38 W m^{-2}, which is almost four times larger than the forcing in SAT × 5 (table 2). The change in the total amount of injected stratospheric sulfur by a factor of 2.25 explains this increase only partly. Figure 2 reveals that the zonal mean all-sky radiative forcing at the surface is clearly higher at all latitude bands in SAT × 5 2050 compared to SAT × 5. However, the difference is largest in the tropics roughly between latitudes 30 °S and 30 °N. Table 1 shows that the amount of sulfur injected between these latitudes is almost three times larger in simulation SAT × 5 2050 than in SAT × 5. The low latitudes receive more sunlight than the mid or high latitudes, and thus the same amount of injected sulfur has a higher geoengineering effectiveness. In addition, the lifetime of stratospheric sulfate in scenario SAT × 5 2050 is almost equal to that in scenario SAT×5 (0.65 yr and 0.68 yr, respectively), even though in the former scenario the amount of injected sulfur is twice as large as in the latter. This is because aerosol removal in the low latitudes is much slower than in the mid and high latitudes and particles in the low latitudes transport first poleward before being removed from the stratosphere.

The importance of the spatial distribution of the injections is also clearly seen if we compare scenarios SAT × 50 and EQ3, where a total of 3 Tg (S) yr^{-1} is injected to the

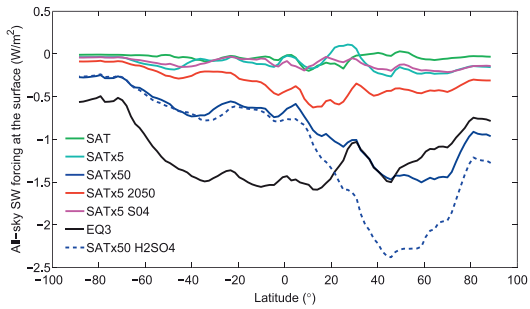

Figure 2. The 5 yr zonal means of all-sky shortwave radiative forcing for the geoengineering scenarios. The fluctuation in the curves in the figure especially between 10°N and 50°N is mostly due to the slightly different meteorology in each simulation.

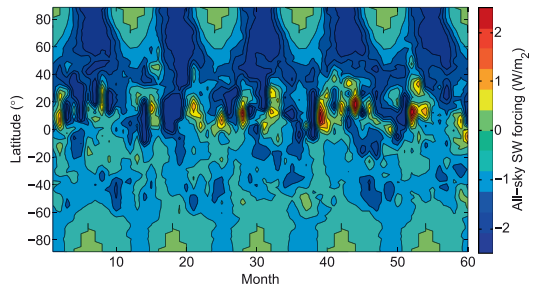

Figure 3. The seasonal variation of the zonal mean shortwave radiative forcing at the surface for the SAT × 50 scenario. Positive values of radiative forcing are from dust which results from different meteorology in the CTRL and SAT × 50 scenarios. Because of this, there is also sometimes large negative forcing between 0° and 20° latitudes.

stratosphere in both cases. The global radiative forcing is 55% larger when sulfur is injected to the tropics than when it is injected using the current flight paths predominantly in the northern midlatitudes (table 2). Figure 2 shows that, while the zonal forcings in the two scenarios are comparable in the northern mid to high latitudes, there is a large difference in favour of the EQ3 scenario in the tropics and southern midlatitudes. In scenario EQ3, the sulfur is spread more homogeneously over the globe and the lifetime of sulfate particles is longer since it takes more time for the sulfate to be transported to the mid latitudes and poles where particle deposition is faster (Hamill *et al* 1997). As a consequence, the global stratospheric sulfur burden is about 40% larger in EQ3 than in SAT × 50 (table 2). Local SO_2 concentrations are also different between the scenarios, but we expect that this will not have a significant effect on the results based on previous studies which compared the same SO_2 injection to one or multiple grid cells along the equator (Niemeier *et al* 2011).

For comparison, in SAT × 50 H2SO4 we injected sulfur as H_2SO_4 instead of SO_2. Geoengineering using H_2SO_4 injections can be anticipated to cause more cooling since it would result in higher local H_2SO_4 concentration and favour nucleation over condensation. This in turn leads overall to smaller particles and less effective coagulation (Pierce *et al* 2010, Niemeier *et al* 2011). The use of H_2SO_4 injections increases the all-sky radiative forcing at the surface to -1.13 W m^{-2}, but as we see from figure 2 the enhanced forcing takes place only in the northern hemisphere and in the south the radiative forcing is similar to the case where sulfur is injected as SO_2 (SAT × 50). This is because the local H_2SO_4 concentrations are the highest in the busiest flight routes in the northern hemisphere. In the southern hemisphere, there is clearly less flight traffic and, because of this, the local concentrations of injected sulfuric acid are so small that fast nucleation in the plume does not occur. It should be noted, however, that our model does not take account of the sub-grid particle formation in the aircraft plume, and thus our simulation with H_2SO_4 injections probably underestimates the radiative forcing to some extent.

Figure 3 depicts the seasonal variation of the zonal mean radiative forcing for the SAT × 50 scenario. There is a strong seasonal cycle in the northern mid and high latitudes with a peak forcing in summer months. Reflecting sulfate particles have concentrated to the northern mid and high latitudes and in summer time more sunlight is directed to and thus can be reflected from these latitudes. There is also some seasonal variation in SO_2 stratospheric burden (from 0.44 Tg in July to 0.65 Tg in January) due to higher summer-time concentrations of OH, which is the main oxidant of atmospheric SO_2. This means that the oxidation rate of SO_2 in the northern hemisphere is much stronger in summer than in winter. This, together with possible seasonal changes in deposition and dynamics, leads to small seasonal variation in the global stratospheric burden of sulfate particles (1.30 Tg in June–July–August and 1.12 Tg in December–January–February), which makes the seasonal variation of the radiative forcing even stronger. The respective roles of the seasonal changes in OH, deposition and dynamics are difficult to quantify from our simulations. However, a further sensitivity simulation (not shown) using the same injections as in SAT × 50 but fixing the OH concentration to summer-time values approximately halves the seasonal variation in sulfate burden compared to SAT × 50, and thus indicates that several of these factors play an important role. Overall, the global all-sky radiative forcing in northern hemisphere summer (June–July–August) is -1.07 W m^{-2} while in winter (December–January–February) it is -0.79 W m^{-2} in scenario SAT × 50.

Figure 4 shows the geographical distribution of the all-sky forcing for scenario SAT × 50. Since current air traffic is highly concentrated in the northern hemisphere, the forcing is much larger in the northern (-1.1 W m^{-2}) than in the southern hemisphere (-0.60 W m^{-2}). Since the Brewer–Dobson circulation preferentially transports air from the equator to the poles, particles released in the northern hemisphere do not spread efficiently to the southern hemisphere. If we look in detail at some specific areas, we see that this geoengineering scenario has a large effect on the radiative forcing in Europe (-1.45 W m^{-2}), North America (-1.33 W m^{-2}) and Northern Asia (-1.50 W m^{-2}), but a much smaller effect in Africa (-0.68 W m^{-2}), South America

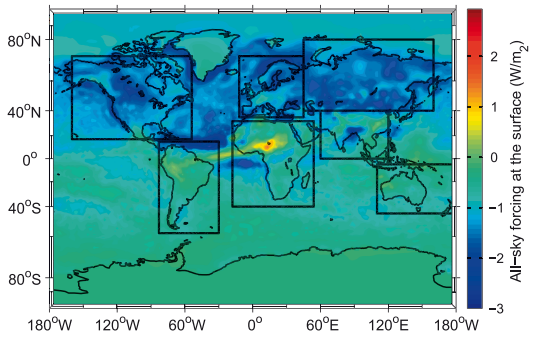

Figure 4. The 5 yr mean of all-sky radiative forcing at the surface in scenario SAT × 50. The black squares indicate the seven regions for which radiative forcings are calculated separately (see text).

(-0.65 W m^{-2}), Australia (-0.56 W m^{-2}) and in India and Southeast Asia (-0.49 W m^{-2}) (region boundaries shown in figure 4). Note that the positive forcing over and west of the Sahara is caused by a difference in dust emissions between the CTRL and SAT × 50 simulations and is due to slightly different meteorologies.

4. Discussion

It is interesting to compare our figure 4 with (b) in Ricke *et al* (2010). They studied changes in regional climates using the SRES A1B scenario for the main anthropogenic forcers and defined the 'optimal' level of globally used geoengineering as the level that in the 2070s would bring each studied region's climate back to closest to its 1990s state. They found that Europe, North America and Northern Asia would benefit from strong solar radiation management, while a much lower intensity would be more optimal for India, Africa and South America. They also suggested that non-uniform forcing could be used to produce a desirable regional temperature and precipitation effect. Using the method presented here, the forcings from our SAT × 50 scenario are directed to areas which would benefit from stronger geoengineering according to Ricke *et al* (2010). However, it is not entirely straightforward to estimate the climate effects from radiative forcing alone and further climate model studies would be needed to test the effects of non-uniform forcings.

The uneven geographical distribution of radiative forcing resulting from our scenarios could also have some other important climate consequences. The simulations imply a relatively large forcing in the northern high latitudes, where it could prevent melting of glaciers and Arctic sea ice, or release of methane from Siberia (MacCracken 2009, Westbrook *et al* 2009). Thus this geoengineering method could potentially reduce these climate feedbacks that would accelerate global warming. One undesirable effect which cannot be studied by our model is the depletion of stratospheric ozone which is predicted to result from stratospheric sulfur geoengineering (Heckendorn *et al* 2009). It is probable that this geoengineering method would cause a significant depletion in the ozone layer especially in the North Pole, where ozone depletion is a problem already.

Large enhancements in fuel sulfur content could have implications on jet engine safety as well as on planes flying in air with high sulfate aerosol concentration. However, if these challenges could be overcome, one potential advantage of using commercial aircraft for geoengineering is that it could probably be implemented relatively rapidly should the need arise as a consequence of a threat of an abrupt climate change in northern high latitudes, where commercial air traffic already flies in the stratosphere. Expanding this kind of geoengineering also to the low latitudes would cause several technical and financial challenges since one would need to reach altitudes close to 20 km. In order to obtain notable climate cooling, a significant part of global aviation traffic would have to be reorganized to serve the goal of geoengineering. Such large-scale operation in the stratosphere would require replacement of the current aircraft fleet and major changes in current flight paths to emit a sufficient amount of sulfur to stratospheric altitudes.

5. Conclusions

Our results indicate that merely elevating a large fraction of civil air traffic into the stratosphere would have a negligible radiative effect, and that in order to exploit air traffic for geoengineering, the jet fuel sulfur content would need to be increased substantially. Even if this were done, the current as well as predicted future flight paths would lead to a geographically very uneven forcing that concentrated on northern mid and high latitudes, which are not optimal for geoengineering in terms of the amount of received sunlight, conversion rate of sulfur to sulfate particles or aerosol lifetime. If a globally more uniform forcing or a forcing sufficient to counteract, e.g., doubling of CO_2 concentration were desired, some other sulfur injection method would be needed. Special aircraft dedicated to the geoengineering purpose could give more control to produce a more favourable spatial and temporal distribution of sulfur injections and thus be a much cheaper and more effective geoengineering method than using stratospheric civil flights.

Acknowledgments

This work was supported by the Academy of Finland's Research Programme on Climate Change (FICCA) (project 140867), Maj and Tor Nessling foundation (grant 2012116), and Academy of Finland's Academy Research Fellow position (decision 250348). The authors wish to thank T Bergman, U Niemeier, S Ferrachat and U Lohmann for technical assistance with the ECHAM model. The ECHAM–HAMMOZ model is developed by a consortium composed of ETHZ, Max Planck Institut für Meteorologie, Forschungszentrum Jülich, University of Oxford and the Finnish Meteorological Institute and managed by the Center for Climate Systems Modeling (C2SM) at ETHZ.

References

Barrett S R H, Britter R E and Waitz I A 2010 *Environ. Sci. Technol.* **44** 7736–42

Budyko M 1977 *Climatic Changes* (Washington, DC: American Geophysical Union)

Dentener F *et al* 2006 *Atmos. Chem. Phys.* **6** 4321–44

Hamill P, Jensen E J, Russell P B and Bauman J J 1997 *Bull. Am. Meteorol. Soc.* **78** 1395–410

Heckendorn P, Weisenstein D, Fueglistaler S, Luo B P, Rozanov E, Schraner M, Thomason L W and Peter T 2009 *Environ. Res. Lett.* **4** 045108

IPCC (Intergovernmental Panel on Climate Change) 1999 *Aviation and the Global Atmosphere* ed J E Penner, D H Lister, D J Griggs, D J Dokken and M McFarland (Cambridge: Cambridge University Press)

Jones A, Haywood J, Boucher O, Kravitz B and Robock A 2010 *Atmos. Chem. Phys. Discuss.* **10** 7421–34

Kim B Y *et al* 2007 *Transp. Res.* D **12** 325–46

Lamarque J *et al* 2010 *Atmos. Chem. Phys.* **10** 7017–39

MacCracken M C 2009 *Environ. Res. Lett.* **4** 045107

McKeen S A and Liu S C 1984 *J. Geophys. Res.* **89** 4873–81

Monahan E, Spiel D and Davidson K 1986 *Oceanic Whitecaps and their Role in Air–Sea Exchange* (Norwell, MA: Reidel) pp 167–74

Niemeier U, Schmidt H and Timmreck C 2011 *Atmos. Sci. Lett.* **12** 189–94

Pierce J R, Weisenstein D, Heckendorn P, Peter T and Keith D W 2010 *Geophys. Res. Lett.* **37** L18805

Rasch P J 2008 *Philos. Trans.* A **366** 4007–37

Ricke K, Morgan M G and Allen M R 2010 *Nature Geosci.* **3** 537–41

Robock A, Oman L and Stenchikov G L 2008 *J. Geophys. Res.* **113** D16101

Schulz M, de Leeuw G and Balkanski Y 2004 Sea-salt aerosol source functions and emissions *Emission of Atmospheric Trace Compounds* (Norwell, MA: Kluwer) pp 333–59

Smith M and Harrison N 1998 *J. Aerosol Sci.* **29** 189–90

Stier P *et al* 2005 *Atmos. Chem. Phys.* **5** 1125–56

Tegen I *et al* 2002 *J. Geophys. Res.* **107** 4576

The Royal Society 2009 *Geoengineering the Climate: Science, Governance and Uncertainty Report* (London: The Royal Society)

Vignati E, Wilson J and Stier P 2004 *J. Geophys. Res.* **109** D22202

Westbrook G K *et al* 2009 *Geophys. Res. Lett.* **36** L15608

Zhang K *et al* 2012 *Atmos. Chem. Phys. Discuss.* **12** 7545–615

V

Paper V

A. Laakso, A.-I. Partanen, U. Niemeier, C. Timmreck, H. Kokkola, K. E. J. Lehtinen, H. Hakkarainen and H. Korhonen, Effects of concurrent stratospheric sulfur geoengineering and large volcanic eruption, *Atmospheric Chemistry and Physics 16*, 305-323, doi:10.5194/acp-16-305-2016, 2016.

Atmos. Chem. Phys., 16, 305–323, 2016
www.atmos-chem-phys.net/16/305/2016/
doi:10.5194/acp-16-305-2016

Atmospheric Chemistry and Physics
Open Access
EGU

Radiative and climate impacts of a large volcanic eruption during stratospheric sulfur geoengineering

A. Laakso[1], H. Kokkola[1], A.-I. Partanen[2,3], U. Niemeier[4], C. Timmreck[4], K. E. J. Lehtinen[1,5], H. Hakkarainen[6], and H. Korhonen[2]

[1]Finnish Meteorological Institute, Atmospheric Research Centre of Eastern Finland, Kuopio, Finland
[2]Finnish Meteorological Institute, Climate Research, Helsinki, Finland
[3]Department of Geography, Planning and Environment, Concordia University, Montréal, Québec, Canada
[4]Max Planck Institute for Meteorology, Hamburg, Germany
[5]Department of Applied Physics, University of Eastern Finland, Kuopio campus, Kuopio, Finland
[6]A. I. Virtanen Institute for Molecular Sciences, University of Eastern Finland, Kuopio, Finland

Correspondence to: A. Laakso (anton.laakso@fmi.fi)

Received: 18 June 2015 – Published in Atmos. Chem. Phys. Discuss.: 12 August 2015
Revised: 21 December 2015 – Accepted: 22 December 2015 – Published: 18 January 2016

Abstract. Both explosive volcanic eruptions, which emit sulfur dioxide into the stratosphere, and stratospheric geoengineering via sulfur injections can potentially cool the climate by increasing the amount of scattering particles in the atmosphere. Here we employ a global aerosol-climate model and an Earth system model to study the radiative and climate changes occurring after an erupting volcano during solar radiation management (SRM). According to our simulations the radiative impacts of the eruption and SRM are not additive and the radiative effects and climate changes occurring after the eruption depend strongly on whether SRM is continued or suspended after the eruption. In the former case, the peak burden of the additional stratospheric sulfate as well as changes in global mean precipitation are fairly similar regardless of whether the eruption takes place in a SRM or non-SRM world. However, the maximum increase in the global mean radiative forcing caused by the eruption is approximately 21 % lower compared to a case when the eruption occurs in an unperturbed atmosphere. In addition, the recovery of the stratospheric sulfur burden and radiative forcing is significantly faster after the eruption, because the eruption during the SRM leads to a smaller number and larger sulfate particles compared to the eruption in a non-SRM world. On the other hand, if SRM is suspended immediately after the eruption, the peak increase in global forcing caused by the eruption is about 32 % lower compared to a corresponding eruption into a clean background atmosphere. In this simulation, only about one-third of the global ensemble-mean cooling occurs after the eruption, compared to that occurring after an eruption under unperturbed atmospheric conditions. Furthermore, the global cooling signal is seen only for the 12 months after the eruption in the former scenario compared to over 40 months in the latter. In terms of global precipitation rate, we obtain a 36 % smaller decrease in the first year after the eruption and again a clearly faster recovery in the concurrent eruption and SRM scenario, which is suspended after the eruption. We also found that an explosive eruption could lead to significantly different regional climate responses depending on whether it takes place during geoengineering or into an unperturbed background atmosphere. Our results imply that observations from previous large eruptions, such as Mount Pinatubo in 1991, are not directly applicable when estimating the potential consequences of a volcanic eruption during stratospheric geoengineering.

1 Introduction

Solar radiation management (SRM) by injecting sulfur to the stratosphere is one of the most discussed geoengineering methods, because it has been suggested to be affordable and effective and its impacts have been thought to be predictable based on volcanic eruptions (Crutzen, 2006; Rasch et al., 2008; Robock et al., 2009; McClellan et al., 2012).

Stratospheric sulfur injections could be seen as an analogue of explosive volcanic eruptions, during which large amounts of sulfur dioxide (SO_2) are released into the stratosphere. Once released, SO_2 oxidizes and forms aqueous sulfuric acid particles which can grow to large enough sizes (some hundreds of nanometres) to efficiently reflect incoming solar radiation back to space. In the stratosphere, the lifetime of the sulfate particles is much longer (approximately 1–2 years) than in the troposphere, and the cooling effect from sulfate aerosols may last for several years, as has been observed after large volcanic eruptions, such as Mount Pinatubo in 1991 (Hansen et al., 1992; Robock, 2000; Stenchikov et al., 2009). Stratospheric SRM would maintain a similar aerosol layer in the stratosphere continuously and could therefore be used (at least in theory) as a means to buy time for the greenhouse gas emission reductions (Keith and MacMartin, 2015).

One concern in implementing stratospheric SRM is that an explosive eruption could happen while SRM is being deployed. While it is impossible to predict the timing of such eruptions, large volcanic events are fairly frequent with three eruptions in the 20th century suggested having volcanic explosivity index (VEI) value of 6, indicating substantial stratospheric injections (Santa María in 1902, Novarupta/Katmai in 1912, and Pinatubo in 1991) (Robock, 2000). Thus it is possible that a large volcanic eruption could happen during SRM deployment, which would most likely be ongoing for decades. Should this happen, it could lead temporarily to a very strong global cooling effect when sulfate particles from both SRM and the volcanic eruption would reflect solar radiation back to space. While the climate effects of volcanic eruptions into an unperturbed atmosphere have been investigated in many previous studies (see overview papers by Robock, 2000, and Timmreck, 2012), they may be different if a volcanic eruption took place during SRM. In the unperturbed atmospheric conditions, the stratosphere is almost clean of particles, while during SRM there would already be a large amount of sulfate in the stratosphere prior to the eruption. Thus, the temporal development of the volcanic aerosol size distribution and related to this the volcanic radiative forcing under SRM conditions may behave very differently.

Here we study the effects of a volcanic eruption during SRM by using two Max Planck Institute models – i.e. the general circulation model (GCM) MAECHAM5 (Giorgetta et al., 2006) coupled to an aerosol microphysical module HAM-SALSA (Bergman et al., 2012; Kokkola et al., 2008), and the Max Planck Institute Earth System Model (MPI-ESM) (Giorgetta et al., 2013). We investigate the simulated characteristics of the stratospheric sulfur burden, radiative forcing, and global and regional climate effects.

2 Methods

2.1 Model descriptions

The simulations were performed in two steps. In the first step, we used the aerosol-climate model MAECHAM5-HAM-SALSA to define global aerosol fields in scenarios with stratospheric sulfur injections and/or a volcanic eruption. In the second step, we prescribe the simulated stratospheric aerosol fields from MAECHAM5-HAM-SALSA to MPI-ESM, similar to Timmreck et al. (2010).

2.1.1 Defining aerosol fields with MAECHAM5-HAM-SALSA

For the global aerosol simulation we use MAECHAM5-HAM-SALSA. The atmospheric model MAECHAM5 is a middle atmosphere configuration of ECHAM5, in which the atmosphere is divided into 47 height levels reaching up to ~ 80 km. MAECHAM5 is integrated with a spectral truncation of 63 (T63), which corresponds approximately to a $1.9° \times 1.9°$ horizontal grid. The simulations were performed with a time step of 600 s.

The aerosol module HAM is coupled interactively to MAECHAM5 and it calculates aerosol emissions and removal, gas and liquid phase chemistry, and radiative properties for the major global aerosol compounds of sulfate, organic carbon, black carbon, sea salt and mineral dust.

In the original ECHAM-HAM (Stier et al., 2005), the aerosol size distribution is described with seven lognormal particle modes with fixed standard deviations and is designed to represent the tropospheric aerosol conditions. Therefore, the width of the coarse mode is optimized for description of sea salt and dust particles, and it does not perform well in special cases like volcanic eruptions or SRM, when a fairly monodisperse coarse mode of sulfate particles can form in the stratosphere (Kokkola et al., 2009). Simulating stratospheric aerosols would then require narrower coarse mode (see e.g. Niemeier et al., 2009) which on the other hand is not appropriate for simulating tropospheric aerosols. Here we chose to use a sectional aerosol model SALSA (Kokkola et al., 2008), which has been previously implemented with ECHAM-HAM (Bergman et al., 2012) and is used to calculate the microphysical processes of nucleation, condensation, coagulation and hydration. SALSA does not restrict the shape of the size distribution making it possible to simulate both tropospheric and stratospheric aerosols with the same aerosol model.

The default SALSA setup divides the aerosol number and volume size distribution into 10 size sections, which are grouped into three subregions (Fig. 1, left-hand panel, distribution a). In addition, it has 10 extra size sections to describe external mixing of the particles (Fig. 1, left hand panel, distributions b and c). In order to keep the number of tracer variables to the minimum, in the third subregion (coarse par-

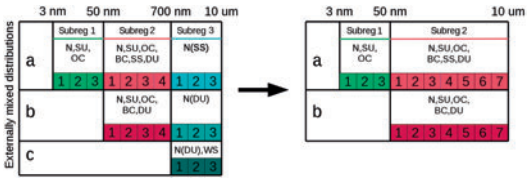

Figure 1. Particle size sections and chemical species in aerosol model SALSA. The left-hand panel illustrates the standard SALSA set-up. The rows "a", "b" and "c" denote the externally mixed particle distributions. Within each distribution and subregion, N denotes number concentration and SU, OC, BC, SS and DU respectively sulfate, organic carbon, black carbon, sea salt and dust masses, which are traced separately. Within distributions "a" and "b" in subregion 3, only particle number concentration is tracked, and all particles are assumed to be sea salt in distribution "a" (N(SS)) and dust in distribution "b" (N(DU)). In distribution "c" only number concentration (N(DU)) and water soluble fraction (WS) are traced. The numbers at the bottom of each subregion illustrate the size sections within that subregion. In our study, the third subregion is excluded and the second subregion is broadened to cover subregion 3 size sections (right-hand panel).

ticles) only a number concentration in each section is tracked and thus the particle dry size is prescribed. This means that the sulfate mass is not explicitly tracked in this region although it is allowed to change the solubility of the dust particles (distribution c in Fig. 1). In addition, there is no coagulation and condensation growth inside this third subregion, although smaller particles and gas molecules can be depleted due to collisions with particles in subregion 3. In standard tropospheric conditions, this kind of description of the coarse particles is sufficient and it saves computational time and resources. However, when studying large volcanic eruptions or stratospheric sulfur geoengineering, microphysical processing of an aerosol by a large amount of stratospheric sulfur can significantly modify also the size distribution of coarse particles during their long lifetime (Kokkola et al., 2009). With the default setup, this processing cannot be reproduced adequately. In addition, information on the sulfur mass in each size section in the coarse size range is not available in the default setup. Thus we modified the SALSA model to exclude the third subregion and broadened the second subregion to cover also the coarse-particle range, as is shown in Fig. 1 (right-hand panel). This allows a better representation of coarse particles in the stratosphere, but increases simulation time by approximately 30 % due to an increased number of the particle composition tracers.

In addition to the sulfur emissions from SRM and from volcanic eruptions (described in Sect. 2.2), the MAECHAM5-HAM-SALSA simulations include aerosol emissions from anthropogenic sources and biomass burning as given in the AEROCOM database for the year 2000 (Dentener et al., 2006). For sea spray emissions, we use a parameterization combining the wind-speed-dependent source functions by Monahan et al. (1986) and Smith and Harrison (1998) (Schulz et al., 2004). Dust emissions are calculated online as a function of wind speed and hydrological parameters according to the Tegen et al. (2002) scheme. We do not include volcanic ash emissions as it has been shown that ash sediments within a few days after the eruption from the stratosphere, and the area affected by the ash cloud is relatively small (Guo et al., 2004a). The effect of fine ash on the distribution of the volcanic cloud in the atmosphere is also relatively small (Niemeier et al., 2009).

The MAECHAM5-HAM-SALSA simulations were carried out with a free-running setup without nudging. Thus the dynamical feedback resulting from the additional heating from increased stratospheric sulfate load was taken into account. Global aerosol model studies of the Pinatubo eruption (Timmreck et al., 1999; Aquila et al., 2012) showed that the dynamic response to local aerosol heating has an important influence on the initial dispersal of the volcanic cloud. Performing non-interactive and interactive Pinatubo simulations, these studies revealed that an interactive coupling of the aerosol with the radiation scheme is necessary to adequately describe the observed transport characteristics over the first months after the eruption. Only the interactive model simulations where the volcanic aerosol is seen by the radiation scheme are able to simulate the observed initial southward cross-equatorial transport of the cloud as well as the aerosol lifting to higher altitudes. A further improvement of the interactive simulation is a reduced northward transport and an enhanced meridional transport towards the south, which is consistent with satellite observations. On the other hand, not running the model in the nudged mode means that the online emissions, of for example sea salt and mineral dust that are sensitive to wind speed at 10 m height, can differ significantly between the simulations. This can occasionally have fairly strong local effects on the aerosol radiative forcing. However, the global radiative forcing from dust is small compared to the forcing from the volcanic eruption and SRM. The radiative forcing resulting from aerosol loadings was calculated using a double call of radiation (with and without aerosols).

Because MAECHAM5-HAM-SALSA is not coupled to the ocean model, the simulations presented below have been done using fixed sea surface temperatures. All runs are preceded by a 2-year spin-up period followed by a 5-year simulation period for the baseline scenarios (defined in Sect. 2.2) and a 3-year simulation period for the sensitivity scenarios (Appendix B). Only one MAECHAM5-HAM-SALSA simulation has been performed for each of the studied scenarios to obtain the aerosol optical fields for the ESM simulations. Only for Volc we have carried out a five-member ensemble to address potential forcing uncertainties (Appendix A).

2.1.2 Determining climate effects with MPI-ESM

In the second step, simulations to quantify the global and regional climate effects of concurrent SRM and volcanic eruption are performed with the Earth system model MPI-ESM (Giorgetta et al., 2013). The model is a state-of-the-art coupled 3-dimensional atmosphere–ocean–land surface model. It includes the atmospheric component ECHAM6 (Stevens et al., 2013), which is the latest version of the atmospheric model ECHAM and whose earlier version is used in the first step of this study. The atmospheric model was coupled to the Max Planck Institute Ocean Model (MPIOM) (Jungclaus et al., 2013). MPI-ESM also includes the land model JSBACH (Reick et al., 2013) and the ocean biochemistry model HAMOCC (Ilyina et al., 2013). ECHAM6 was run with the same resolution as in the first part of this study. We did not include dynamical vegetation and carbon cycle in the simulations.

In MPI-ESM, aerosol fields are prescribed. We used the same tropospheric aerosols fields based on the Kinne et al. (2013) climatology in all scenarios. In the stratosphere, we use precalculated aerosol fields from the different simulations with MAECHAM5-HAM-SALSA. The aerosol radiative properties were calculated based on monthly mean values of the aerosol effective radius and the aerosol optical depth (AOD) at 550 nm. MPI-ESM uses a precalculated look-up table to scale AOD at 550 nm to the other radiation wavelengths based on the effective radius. Here MPI-ESM assumes the size distribution to consist of a single mode, which in most cases differs from the sectional size distribution in MAECHAM5-HAM-SALSA. This can lead to somewhat different radiative forcings between MAECHAM5-HAM-SALSA and MPI-ESM. In our study this has been seen as overestimation of both shortwave and longwave forcing. Overestimation is slightly larger in LW-radiation and thus warming effect of MPI-ESM is overestimated in MPI-ESM compared to the simulations by ECHAM-HAM. Since there is very little zonal variation in the monthly mean stratospheric aerosol fields, the zonal mean aerosol fields from MAECHAM5-HAM-SALSA are used in MPI-ESM.

The atmospheric gas concentrations were fixed to year 2010 level, in accordance with the tropospheric aerosol fields and land use maps. Year 2010 concentrations were also used for methane, chlorofluorocarbon and nitrous oxide.

Experiments with a full Earth system model require a long spin-up period as the ocean component needs centuries to stabilize. We resolved this by restarting our 105-year-long spin-ups from previously run Coupled Model Intercomparison Project Phase 5 (CMIP5) simulations ending in year 2005. Since the aerosol and atmospheric gas concentrations in our simulations differed slightly from the CMIP5 runs, the 105 years of spin-up was not enough for the model to reach a full steady state; there was a small warming ($0.3\,\mathrm{K}\,(100\,\mathrm{yr})^{-1}$) also after spin-up period in both CTRL and SRM simulations (see simulation details in Sect. 2.2). This temperature change is nevertheless so small that it does not affect our conclusions.

Since the initial state of the climate system can have a significant effect on the climate impacts resulting from forcing, we ran 10-member ensembles of 5-year duration for all baseline scenarios with a volcanic eruption. To do this, we first ran the model for 50 years after the spin-up and saved the climate state after every 5 years. We then continued the simulations from each of these saved climate states for further 5 years with a volcanic eruption taking place in these specific climate conditions. The obtained results were compared to the corresponding 5-year period in the simulations without a volcanic eruption (which were run continuously for 50 years).

2.2 Model experiments

We simulated altogether five baseline scenarios in order to investigate the radiative and climate impacts of concurrent SRM and a volcanic eruption. To better separate the effects of SRM and the eruption, these scenarios included also simulations with only SRM or only a volcanic eruption taking place. The studied scenarios are listed in Table 1, and detailed below. Three additional sensitivity simulations investigating the sensitivity of the results to the geographical location and the seasonal timing of the eruption are presented in Appendix B.

All the simulations with SRM assumed continuous injections of $8\,\mathrm{Tg\,(S)\,yr^{-1}}$ of SO_2 between 30° N and 30° S and 20–25 km in the vertical. The injection strength of $8\,\mathrm{Tg\,(S)\,yr^{-1}}$ was chosen based on previously published SRM studies and for example Niemeier et al. (2011) has shown such injection rates to lead to all-sky global shortwave radiative forcing of -3.2 to $-4.2\,\mathrm{W\,m^{-2}}$ in ECHAM5-HAM. This forcing is roughly comparable (but opposite in sign) to forcing from doubling of CO_2 from preindustrial level. Such a strong SRM forcing could be considered realistic in view of the business-as-usual scenario of the Representative Concentration Pathways (RCP8.5), which estimates that without efforts to constrain the greenhouse gas emissions the total radiative forcing from anthropogenic activities at the end of the 21st century is roughly $8.5\,\mathrm{W\,m^{-2}}$ (IPCC, 2013). All the simulations with a volcanic eruption assumed an explosive eruption releasing 8.5 Tg of sulfur to the stratosphere (Niemeier et al., 2009; Guo et al., 2004b; Read et al., 1993). This corresponds to the magnitude of the Mount Pinatubo eruption in June 1991. In all of the volcanic eruption scenarios, sulfur was injected to the height of 24 km. The eruption was always initiated on the first day of the month at 06:00 UTC and it lasted for 3 h.

The baseline scenarios summarized in Table 1 and detailed below were simulated first with MAECHAM5-HAM-SALSA, and then with MPI-ESM using the stratospheric aerosol fields from MAECHAM5-HAM-SALSA simulations. On the other hand, the sensitivity simulations in Ap-

Table 1. Studied sulfur injection and volcanic eruption scenarios.

Scenario	Description
CTRL	Control simulation with no SRM or explosive eruptions
SRM	Injections of 8 Tg (S) yr^{-1} of SO_2 between latitudes 30° N and 30° S between 20 and 25 km altitude
Volc	Volcanic eruption at the site of Mount Pinatubo (15.14° N, 120.35° E) on 1 July. 8.5 Tg of sulfur (as SO_2) injected at 24 km
SRM Volc	Volcanic eruption during SRM. SRM suspended immediately after the eruption
SRM Cont	Volcanic eruption during SRM. SRM still continued after the eruption

pendix B were run only with MAECHAM5-HAM-SALSA because of the computational expense of the MPI-ESM code.

The control (CTRL) simulation included only standard natural and anthropogenic aerosols with no SRM or explosive eruptions, while the simulation SRM included SRM on top of the background aerosol, but no volcanic eruption. All the baseline scenarios which simulated a volcanic eruption assumed a tropical eruption at the site of Mount Pinatubo (15.14° N, 120.35° E), where a real explosive eruption took place in summer 1991. We simulated a July eruption at this site both in background conditions (simulation Volc) and during SRM (simulation SRM Volc and SRM Cont). Due to safety and economic considerations, it might be that SRM is suspended at some point after the eruption. When this would happen depends on several factors (decision-making process, magnitude/timing of volcano). Here we study cases where SRM was suspended immediately after the eruption (SRM Volc) and we also simulated a scenario where SRM was continued despite the eruption (SRM Cont). The purpose of the latter simulation was also to study how additive the radiative effects of volcanic eruption and solar radiation management are. It should be noted that if the SRM injections are suspended after a volcanic eruption, the injections should be restarted after some time from the eruption to prevent abrupt warming. However, we do not simulate the restart of SRM injections in this study.

3 Results

3.1 Microphysical simulations of volcanic eruption and SRM compared to the measurements and previous studies

A comparison of the Volc simulation against observations of the Pinatubo 1991 eruption shows that the model reproduces well the temporal behaviour of particle effective radius after a tropical eruption (Fig. A1b in Appendix A). The model overestimates sulfate burden compared to those retrieved from the HIRS satellite observations (Baran and Foot, 1994) during the first 12 months after the eruption (Fig. A1 in Appendix A). There are several previous global model studies that where evolution of stratospheric aerosols following Pinatubo eruption has been investigated. Many of these shows similar sulfate burden than in the our study and overestimation of sulfate burden compared to the HIRS data (Niemeier et al., 2009; English et al., 2012; Dhomse et al., 2014; Sheng et al., 2015). This comparison between the limited set of the observational data and with other modelling studies gives us confidence that the new MAECHAM5-HAM-SALSA set-up simulates aerosol loads and properties consistent to observations under high stratospheric sulfur conditions.

We first looked at the aerosol burdens and the radiative impacts of a tropical volcanic eruption and SRM separately based on the MAECHAM5-HAM-SALSA runs (simulations Volc and SRM, respectively). The maximum stratospheric sulfate burden after the volcanic eruption (Volc) is 8.31 Tg (S). 75 % of the erupted SO_2 is oxidized during 2 months after the eruption and the global maximum of sulfate burden is reached 5 months after the eruption (Fig. 2a, black solid line). After this, the burden starts to decline rapidly, but remains above the level that was simulated prior to the eruption for approximately 4 years. On the other hand, continuous geoengineering with 8 Tg (S) yr^{-1} (SRM) leads to the global stratospheric sulfate burden of 7.8 Tg (S) with only little variation in time (Fig. 2a, dashed black line). The total sulfur amount (SO_2 and sulfate) in the stratosphere is 8.8 Tg (S) which indicates the average sulfur lifetime (sulfur burden divided by the amount of the injected sulfur) in the stratosphere to be 1.1 years. As previous studies have shown, the lifetime of sulfur is strongly dependent on the injection area and height, and the amount of injected sulfur. Some of the studies have shown a lifetime of clearly less than a year for the comparable magnitude of injected sulfur, when sulfur is injected at a lower height than in our study (Heckendorn et al., 2009; Pierce et al., 2010; Niemeier et al., 2011; English et al., 2012), slightly under a year when sulfur is injected at the same height as here (Heckendorn et al., 2009; Pierce et al., 2010), and over a year when sulfur is injected higher (Niemeier et al., 2011). Thus, overall our results are in good agreement with the previous studies.

The maximum clear-sky shortwave (SW) surface forcing in the Volc simulation reaches $-6.36\,W\,m^{-2}$ (Fig. 2b), which is close to the average global mean forcing of $-6.00\,W\,m^{-2}$

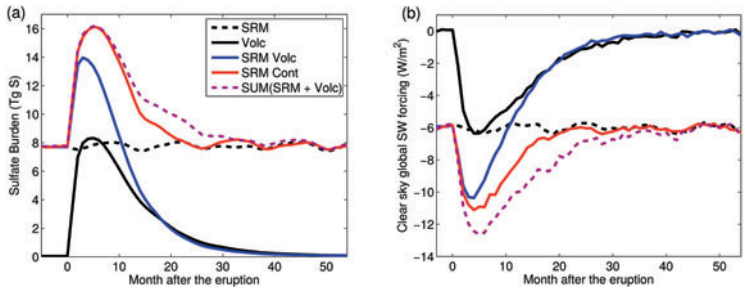

Figure 2. **(a)** Stratospheric sulfate burden and **(b)** global mean clear-sky shortwave radiative forcing at the surface in the different scenarios. In addition, the dashed purple line represents the sum of SRM and Volc runs, and is shown for comparison.

in the SRM simulation, as could be expected based on the similar maximum and steady-state sulfate burdens, respectively (Fig. 2a). In the presence of clouds, the change in SW all-sky flux in SRM is smaller ($-3.38\,\mathrm{W\,m^{-2}}$) than in clear-sky conditions. Radiative forcing from the SRM is in agreement with previous studies where the forcing effect has been studied with climate models including an explicit aerosol microphysics description. For example, Niemeier et al. (2011) showed all-sky SW radiative forcings from -3.2 to $-4.2\,\mathrm{W\,m^{-2}}$ for $8\,\mathrm{Tg\,(S)\,yr^{-1}}$ injection, and Laakso et al. (2012) a forcing of $-1.32\,\mathrm{W\,m^{-2}}$ for $3\,\mathrm{Tg\,(S)}$ injection. On the other hand, Heckendorn et al. (2009) simulated a clearly smaller radiative forcing of $-1.68\,\mathrm{W\,m^{-2}}$ for $10\,\mathrm{Tg\,(S)}$ injection.

The shortwave radiative effect ($-6.00\,\mathrm{W\,m^{-2}}$) from the sulfate particles originating from SRM is concentrated relatively uniformly between 60° N and 60° S (not shown). SRM leads also to a $0.73\,\mathrm{W\,m^{-2}}$ all-sky longwave radiative forcing which is concentrated more strongly in the Tropics than in the midlatitudes and polar regions. In the case of the volcanic eruption (Volc), forcing is distributed between 30° N and the Equator for the first 4 months after the eruption. After that, forcing is concentrated more to the midlatitudes than the low latitudes in both hemispheres. It should be noted, however, that the initial state of the atmosphere and local winds over the eruption area at the time of the eruption can have a large impact on the distribution of sulfur released from a short-duration eruption. This can be seen for example in Fig. A2, which illustrates the hemispheric sulfur burdens from five different ensemble members of the Volc simulation (see Appendix A for details). As an example, in one of the ensemble simulations, burden is concentrated much more in the Northern Hemisphere (NH) (peak value $6.7\,\mathrm{Tg\,(S)}$) than in the Southern Hemisphere (SH) ($2.2\,\mathrm{Tg\,(S)}$). This leads to northern and southern hemispheric peak values of clear-sky forcings of -8.18 and $-3.72\,\mathrm{W\,m^{-2}}$, respectively. However, in another ensemble member sulfate is distributed more uniformly between the hemispheres (4.8 and $3.7\,\mathrm{Tg\,(S)}$ in the NH and SH, respectively) resulting in clear-sky peak forcing of $-6.04\,\mathrm{W\,m^{-2}}$ in the north and $-6.35\,\mathrm{W\,m^{-2}}$ in the south. (In the analysis above (e.g. Fig. 2), we have used simulation Volc4 from Appendix A, since it resembles most closely the 5-member ensemble mean in terms how sulfate is distributed between the hemispheres.)

3.2 Burden and radiative effects of concurrent volcanic eruption and SRM – results of aerosol microphysical simulations

Next we investigated whether the radiative impacts from a volcanic eruption taking place during SRM differs from the sum of volcanic-eruption-only and SRM-only scenarios discussed in Sect. 3.1. In order to do this, we compared the SRM-only (SRM) and volcanic-eruption-only (Volc) simulations with two scenarios of concurrent eruption and SRM: SRM Volc where SRM is suspended immediately after the eruption, and SRM Cont where SRM is continued after the eruption. The magnitude, timing and location of the eruption were assumed the same as in Volc simulation.

Figure 2 shows the stratospheric sulfur burden and the global clear-sky radiative forcing from the four MAECHAM5-HAM-SALSA runs. It is evident that both the stratospheric sulfate burden and the global shortwave radiative forcing reach a maximum value and recover back to pre-eruption level clearly faster if the volcanic eruption happens during SRM than in stratospheric background conditions, as can be seen by comparing the scenario of volcanic eruption concurrent with SRM (solid blue and red lines) to the sum of eruption-only and SRM-only scenarios (dashed purple line). This is the case especially when SRM is suspended immediately after the eruption (simulation SRM Volc). In this case, in our simulation set-up, it takes only 10 months for the stratospheric sulfate burden and the global radiative effect to recover to the state before the volcanic eruption. On the other hand, if the eruption happens in stratospheric background conditions (Volc), it takes approximately 40 months before the sulfate burden and the radiative effect return to their pre-eruption values. In addition, the global SW radia-

tive forcing reaches a maximum value two months earlier in SRM Volc than in Volc (Fig. 2b). In comparison to the level before the eruption, the peak increase in radiative forcing is 32 % smaller in SRM Volc ($-4.30\,\mathrm{W\,m^{-2}}$) than in Volc ($-6.36\,\mathrm{W\,m^{-2}}$).

The first, somewhat trivial reason for lower and shorter-lasting radiative forcing in SRM Volc is that because SRM is suspended immediately after the eruption, the stratospheric sulfur load will recover from both the volcanic eruption and SRM. If the stratospheric background sulfur level is not upheld by continuous sulfur injections as before the eruption, the sulfur burden will return back to the pre-eruption conditions within less than a year after the eruption. However, the different responses to a volcanic eruption during background (Volc) and SRM (SRM Volc) conditions cannot be explained only by suspended SRM injections. This can be seen in Fig. 2a in scenario SRM Cont (solid red line) where geoengineering is continued after the volcanic eruption: also in this case the lifetime of sulfate particles is shorter than in Volc. There is a similar increase in the sulfate burden in the first 10 months after the eruption in the Volc and SRM Cont scenarios as is seen by comparing the red and purple lines in Fig. 2; here the purple dashed line shows the calculated sum of the effects from separate simulations of Volc and SRM. This scales the Volc simulation to the same start level as SRM Cont. After the first 10 months the sulfate burden starts to decrease faster in the SRM Cont scenario and is back to the level prior to the eruption after 20 months from the eruption, compared with $\sim$40 months in the Volc run. The difference between the two scenarios can be seen even more clearly in the shortwave radiative forcing (Fig. 2b). When the volcano erupts during SRM, the contribution of the eruption to the forcing is lower immediately after the eruption than after the eruption in Volc and the peak increase in global mean radiative forcing compared the pre-eruption level is 21 % lower in SRM Cont ($-5.04\,\mathrm{W\,m^{-2}}$) than in Volc ($-6.36\,\mathrm{W\,m^{-2}}$).

The reason for these findings is that the initial stratospheric aerosol load is significantly different when the volcanic eruption occurs during stratospheric sulfur geoengineering than under background conditions. If a volcano erupts concurrently with SRM, sulfur from the eruption does not only form new particles but also condenses onto pre-existing particles. Furthermore, the new small particles that are formed after the eruption coagulate effectively with the existing larger particles from the SRM injections. This means that a situation develops where there are fewer but larger particles compared to a case without SRM. The increased particle size can also be seen in Fig. 3 which shows the effective radius in the SRM injection area. These larger particles in SRM Volc and SRM Cont have higher gravitation settling velocities and sediment faster. Thus, about 30 months after the eruption the effective radius in SRM Volc becomes even smaller than in simulation Volc, when larger particles have sedimented out of the atmosphere in SRM Volc. Figure 2 indicates the impact on the radiative forcing. SW scattering gets less effective with

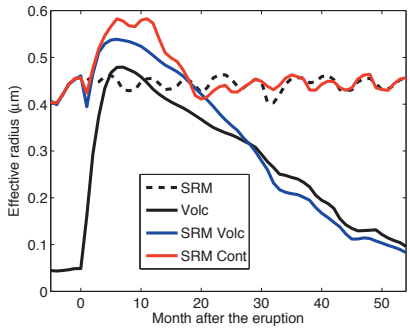

Figure 3. Mean effective radius in the different scenarios between 20° N and 20° S latitudes and between 20 and 25 km altitude levels.

increasing particle size (Pierce et al., 2010) and, although the stratospheric sulfur burden is the same in the first months after the eruption in SRM Cont and in the sum of Volc and SRM, there is a clear difference in the radiative forcing. This indicates that the number-to-mass ratio of particles is smaller in SRM Cont than in the calculated sum from Volc and SRM.

Additional sensitivity simulations with MAECHAM5-SALSA discussed in more detail in Appendix B show that the season when the tropical eruption occurs defines how sulfate from the eruption is distributed between the hemispheres. An eruption in January leads to a larger sulfur burden in the Northern Hemisphere than an eruption in July (Toohey et al., 2011; Aquila et al., 2012). This conclusion holds also if the eruption occurs during geoengineering, at least in cases where SRM is implemented evenly to both hemispheres. In the case of an eruption outside the Tropics, the season of the eruption can have a large impact on the magnitudes of both the sulfate burden and the global radiative forcing. Therefore it very likely has an impact also on the regional climates, which further defines when and where suspended stratospheric sulfur injections should be restarted. However, due to the computational expense of the fully coupled MPI-ESM, we limit our analysis of the climate impacts below only to the baseline scenarios. It should be noted that the impact after concurrent volcanic eruption and SRM may depend also on the altitude at which sulfur is released. Increasing the injection height increases the lifetime of sulfate (Niemeier and Timmreck, 2015). If sulfur from the eruption is released at the same altitude where SRM sulfur resides, it might lead to locally larger sulfur concentration and therefore to larger particles compared to a case when sulfur from the eruption is released below the SRM sulfate layer. Dependent on the geographical location this volcanic sulfur can still reach the SRM layer, e.g in the case of tropical eruption with the ascending branch of the Brewer–Dobson circulation. However, this happens on much longer timescales.

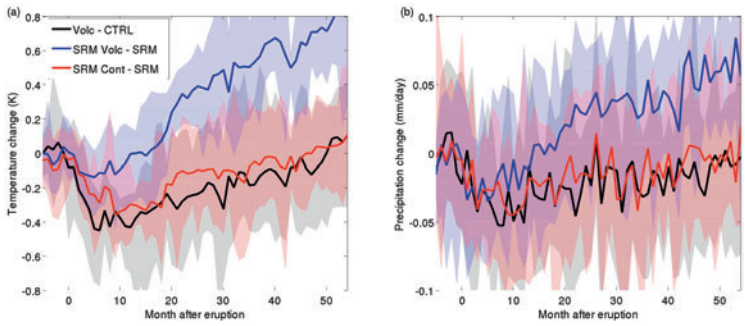

Figure 4. Global mean 2 m **(a)** temperature and **(b)** precipitation changes after the volcanic eruption compared to the background condition (black line) and during solar radiation management (blue and red lines). Solid lines are mean values of the ten members of the ensemble simulations. The maximum and minimum values of the ensemble are depicted by shaded areas.

3.3 Climate effects from concurrent volcanic eruption and SRM – results of ESM simulations

In this section we investigate how the radiative forcings simulated for the different scenarios in section 3.2 translate into global and regional climate impacts. For this purpose, we implemented the simulated AOD and effective radius of stratospheric sulfate aerosol from MAECHAM5-HAM-SALSA to MPI-ESM, similar to Timmreck et al. (2010).

Figure 4a shows the global mean temperature change compared to the pre-eruption climate. Simulation Volc (black line) leads to cooling with an ensemble mean peak value of −0.45 K reached 6 months after the eruption. On average, this cooling impact declines clearly more slowly than the radiative forcing after the eruption (shown in Fig. 2b): 1 year after the eruption the radiative forcing was 64 % of its peak value, and subsequently 17 and 8 % of the peak value 2 and 3 years after the eruption. On the other hand, the ensemble mean temperature change 1 year after the eruption is 84 % of the peak value. Subsequently, 2 and 3 years after the eruption the temperature change is still 53 and 30 % of the peak value. It should be noted, however, that the variation in temperature change is quite large between the 10 climate simulation ensemble members (±0.67 K compared the mean of the ensemble). In fact, in some of the ensemble members the pre-eruption temperature is reached already approximately 15 months after the eruption.

Figure 4a also shows that on average a volcanic eruption during continued SRM (simulation SRM Cont, red line) leads to on average 33 % smaller cooling for the next 3 years after the eruption than under unperturbed atmospheric conditions. If SRM is suspended (SRM Volc), the maximum value of the global cooling is only about one-third (i.e. less than 0.14 K at maximum for the ensemble mean) compared to an eruption to the non-geoengineered background stratosphere (simulation Volc). This is consistent with the clearly smaller radiative forcings predicted for the eruption during SRM than in the background atmospheric conditions (Fig. 2b). Similar to Volc simulation, the global mean temperature is lower compared to the pre-eruption level and even radiative forcing has levelled off. In SRM Volc scenario the global mean shortwave radiative forcing from the sulfate particles has reached the pre-eruption level after 10 months from the eruption but there would be still some global cooling after 12 months from the eruption. Our simulations indicate that if SRM is suspended but not restarted, there is fast warming compared to the pre-eruption temperature within the first 20 months after the eruption.

Figure 5 depicts the regional surface temperature changes simulated in the different scenarios. Geoengineering alone (SRM) would lead to global ensemble mean cooling of −1.35 K compared to the CTRL case. As Fig. 5a shows, cooling is clearly stronger in the Northern Hemisphere (−1.65 K) than in the Southern Hemisphere (−1.05 K). The strongest regional cooling is seen in the northern high latitudes (regional average of −2.2 K north of 50° N). The smallest cooling effect, or even slight warming, is predicted over the southern oceans. These general features are consistent with the GeoMIP multimodel intercomparison when only the impact of SRM (and not of combined SRM and CO_2 increase) is considered: Kravitz et al. (2013a) show a very similar decrease in polar temperature when subtracting temperature change under increased CO_2 from the combined SRM and CO_2 increase results.

For the three volcanic eruption scenarios we concentrate on the regional climate impacts during the first year after the eruption. Figure 5b shows the 1-year-mean temperature anomaly at the surface after a volcanic eruption into the unperturbed background stratosphere in simulation Volc. As expected, the cooling impact from the volcanic event over the first year following the eruption is clearly smaller than that from continuously deployed SRM. While there are some similar features in the temperature change patterns between Fig. 5a and b (such as more cooling in the Northern than in

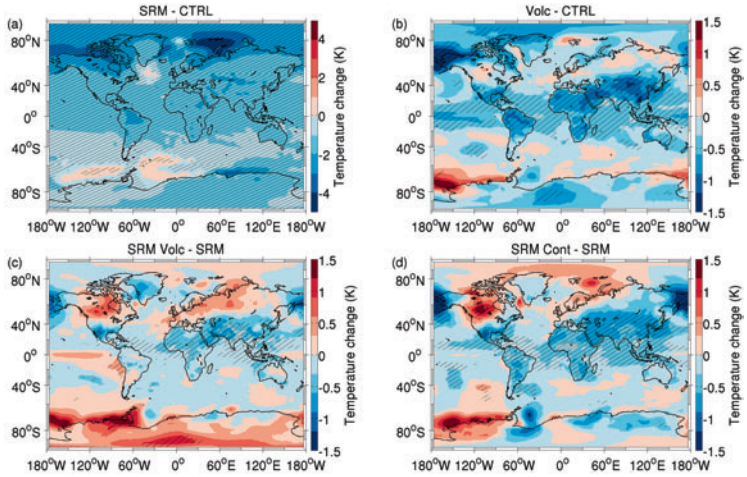

Figure 5. Ensemble mean change in annual mean 2 m temperature. **(a)** 50-year mean temperature change in SRM scenario; 1-year-mean temperature change after the volcanic eruption in **(b)** Volc, **(c)** SRM Volc and **(d)** SRM Cont compared to the pre-eruption climate (CTRL for SRM and Volc, and SRM for SRM Volc and SRM Cont). Hatching indicates a regions where the change of temperature is statistically significant at 95 % level. Significance level was estimated using Student's unpaired *t* test with a sample of 10 ensemble member means for panels **(b–d)** and a sample of 50 annual means for panel **(a)**. Note the different scale in panel **(a)**.

the Southern Hemisphere, and warming in the southern Pacific), clear differences also emerge, especially in NH mid- and high latitudes where there is less cooling, and in some regions even warming, after the eruption. During the first year after the eruption, sulfate from the tropical eruption is mainly concentrated at low latitudes where there is also strong solar intensity and thus strong radiative effect from the enhanced stratospheric aerosol layer. During the subsequent years, sulfate transport towards the poles causes stronger cooling also in the high latitudes. The global yearly mean temperature change is −0.34 K for the first year after the eruption, then decreasing to a value of −0.30 for the second year from the eruption. However, there is an increased temperature response north of 50° N from the first year mean of −0.30 K to the second year mean of −0.44 K. Even though there is larger cooling at the midlatitudes in the second year after the eruption, we see 0.06 K warming north of 75° N in the second boreal winter (December–February) after the eruption. Winter warming after a volcanic eruption has been seen also in observations (e.g. Robock and Mao, 1992; Fischer et al., 2007), though the current generation of CMIP5 models has problems to reproduce the NH post-volcanic winter warming pattern (Driscoll et al., 2012).

When the eruption takes place during geoengineering and SRM injections are suspended (SRM Volc), the global 1-year ensemble mean temperature change is only −0.09 K during the first year after the eruption (Fig. 5c). This small global impact is due to the fact that the anomaly in SW radiation after the volcanic eruption is relatively small in magnitude and only about 10 months in duration when geoengineering is suspended after the eruption (Fig. 2b). However, the regional impacts are much stronger and show distinctly different patterns from those in Volc (Fig. 5b). Volc scenario leads to 0.30 K cooling north from 50° N in the ensemble mean, while there is small warming of 0.02 K in SRM Volc after the first year from eruption. The warming is concentrated over the central areas of Canada, where the ensemble mean temperature increase is more than 1 K, and over North Eurasia, where the temperature increase is more than 0.5 K. It should be noted, however, that in most parts of these regions the warming signal is not statistically significant.

There are also differences in the southern hemispheric temperatures between the different scenarios. While Volc scenario leads to small −0.02 K mean cooling south of 50° S in the first year after the eruption, there is a warming of 0.14 K in the SRM Volc scenario. In addition, over the Pacific equatorial area the Volc scenario leads to a cooling of more than −0.5 K while SRM Volc scenario leads to a warming of more than 0.5 K. These differences between Volc and SRM Volc simulations imply that previous observations of regional climate impacts after an explosive eruption, such as Pinatubo in 1991, may not offer a reliable analogue for the impacts after an eruption during SRM. It is important to note, however, that just like there were some variations in the global mean temperature between individual ensemble members, there are also variations in regional changes between the members. Variations are the largest over high latitudes, while most of the individual ensemble members are in good

agreement at the low latitudes (hatching in Fig. 5), where the change in temperature is the largest.

The main reason for the differences between Volc and SRM Volc is that in the latter simulation the volcanic eruption is preceded by SRM injections (providing a baseline stratospheric sulfate load) which are suspended immediately after the eruption. Thus, after the eruption the baseline sulfate load starts decreasing, especially far away from the eruption site, and, therefore, during the first year after the eruption there are regions with a positive radiative forcing compared to the pre-eruption level.

We also find that there could be regional warming in some regions after the volcanic eruption even if the SRM injections were still continued (Fig. 5d, SRM Cont). This warming is concentrated in the high latitudes and areas with relatively little solar shortwave radiation but with large stratospheric particles capable of absorbing outgoing longwave radiation. The warming is strongest in the first post-eruption boreal winter when some areas over Canada, Northeast Europe and western Russia experience over 0.5 K warming (not shown). Such significant regional warming means that the ensemble mean temperature change north of 50° N during the first post-eruption winter is only −0.05 K. In some parts of the Southern Ocean a volcanic eruption could enhance the warming signal caused already by SRM (Fig. 5a).

It is also worth noting that the stratospheric sulfur geoengineering with 8 Tg (S) yr^{-1} itself leads only to −1.35 K global temperature change in our simulations. Such weak response is likely at least partly due to the radiation calculations in MPI-ESM, which assume a single modal particle size distribution (see Sect. 2.1.2 for details). Compared to a more flat size distribution simulated by the sectional approach of MAECHAM5-HAM-SALSA, this assumption leads to an overestimation longwave (LW) AOD which is calculated from 550 nm AOD. This in turn leads to an overestimation of the longwave radiative forcing (0.7 W m^{-2} for SRM) while the shortwave forcing is less affected (−0.2 W m^{-2} for SRM). However, this does not affect the conclusions of this study.

In addition to the changes in surface temperature, volcanic eruptions will also lead to changes in precipitation. Figure 4b shows the global mean precipitation change after a volcanic eruption in the three scenarios. There is a similar decrease in the precipitation in all volcanic scenarios during the first 5 months after the eruption. Thereafter there is a similar slow increase in the global mean precipitation in the simulations Volc and SRM Cont but a clearly faster increase in SRM Volc. This faster increase would also, about 1 year after the eruption, lead to a higher global ensemble mean precipitation compared to the pre-eruption climate.

The global 1-year mean precipitation change is 0.036, 0.023 and 0.031 mm day^{-1} for Volc, SRM Volc and SRM Cont respectively for the first year after the eruption. Earlier studies (Bala et al., 2008; Kravitz et al., 2013a, b; Niemeier et al., 2013) have already shown that geoengineering leads to a reduction in the global precipitation compared to the climate without geoengineering. In our SRM simulation, we obtain a precipitation reduction of 0.11 mm day^{-1} (2.8 %), which is clearly larger than the impact after the volcanic eruption.

The stratospheric sulfate affects precipitation via two climate system responses. The first one is the rapid adjustment (fast response) due to atmospheric forcing, such as change in solar irradiance, on a short timescale. The second one is the feedback response (slow response) due to temperature changes (Bony et al., 2013; Ferraro et al., 2014; Fuglestvedt et al., 2014; Kravitz et al., 2013b). The signals from both of these responses can be seen in Fig. 4b, especially in the simulation SRM Volc (blue line). During the first months after the eruption, the precipitation drops relatively rapidly which corresponds well with the rapid change in the radiative forcing (Fig. 2b); at the same time, the temperature change in SRM Volc is less steep (Fig. 4a). This implies that in the first months following the eruption, the precipitation change is more affected by the change in the radiation than the change in the temperature. On the other hand, after 2 years from the eruption there is only small SW radiative effect left from the eruption (and the SRM prior to eruption) but there is still a decrease in the global mean precipitation. During this period, precipitation is predominantly affected by the change in temperature.

Figure 6 shows the regional precipitation changes in each of the studied scenarios. The largest changes after geoengineering (SRM) are seen in the tropical convective region where SRM reduces the precipitation rate in large areas by as much as 0.5 mm day^{-1} (Fig. 6a). This is in good agreement with previous multi-model studies (Kravitz et al., 2013a). In our simulations, an increase of the same magnitude in the precipitation rate is predicted just north of Australia, which has not been seen in previous model intercomparisons (Kravitz et al., 2013a).

Although the precipitation patterns in SRM and Volc are similar in low latitudes, differences are seen especially in NH mid- and high latitudes where SRM shows clearly larger reduction in precipitation. The zonal mean value is −0.15 mm day^{-1} in both 50° north and south latitudes. In these areas, there is clearly less evaporation in the SRM scenario which is not seen in the first year after the volcanic eruption (Volc) and which would lead to different precipitation patterns. Similar to the temperature change, our simulations indicate that a tropical volcanic eruption impacts precipitation patterns differently in unperturbed and SRM conditions. In fact, a volcanic eruption during geoengineering (SRM Volc and SRM Cont) leads to an opposite precipitation change pattern than an eruption to the unperturbed atmosphere (Volc) over the tropical area in the Pacific and Atlantic (Fig. 6c and d). In these areas, a volcanic eruption during SRM leads to the increase in the evaporation flux at the surface during the first year after the eruption, whereas the evaporation flux decreases if the eruption takes place in unperturbed conditions. This is caused by different tropical tem-

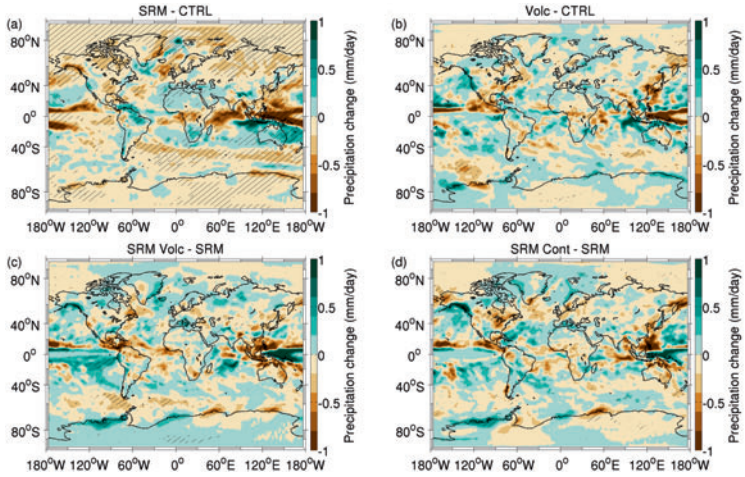

Figure 6. Ensemble-mean precipitation change in **(a)** 50-year mean precipitation change in the SRM scenario. The change in 1 year mean precipitation after the volcanic eruption in **(b)** Volc, **(c)** SRM Volc and **(d)** SRM Cont compared to the pre-eruption climate (CTRL for SRM and Volc, and SRM for SRM Volc and SRM Cont). Panels **(b–d)** show the 1-year-mean temperature after the eruption. Panel **(a)** shows the mean over the corresponding 1-year-periods as the other panels. Hatching indicates a regions where the change of precipitation is statistically significant at 95 % level. Significance level was estimated using Student's unpaired *t* test with a sample of 10 ensemble member means for panels **(b–d)** and a sample of 50 annual means for panel **(a)**.

perature responses between the simulations (Fig. 5). Compared to the pre-eruption values, in simulations SRM and Volc, equatorial sea surface temperature (SST) anomalies (latitudes 0–10° N) are relatively colder than the SST anomalies over latitudes 10–20° N. In simulation SRM, the difference in SST anomaly between these areas is −0.02 K and in simulation Volc it is −0.05 K. On the other hand, in simulations SRM Volc and SRM Cont, equatorial SST anomalies are relatively warmer than those over latitudes 10–20° N. In SRM Volc, the difference in temperature anomaly is 0.13 K and in SRM Cont it is 0.05 K. However, these changes in precipitation are not significant and a larger ensemble would be necessary for further detailed investigations. It should also be noted that here we have studied an unrealistic scenario where SRM is implemented without global warming. If warming from increased greenhouse gases had been included in the scenarios, the temperature gradient could be very different in simulation SRM which could lead to different precipitation patterns. There is also a large natural variability in the precipitation rates and as the precipitation changes after the eruption are relatively small, our results are statistically significant only in a relatively small area (hatching in Fig. 6).

4 Summary and conclusions

We have used an aerosol microphysical model coupled to an atmosphere-only GCM as well as an ESM to estimate the combined effects of stratospheric sulfur geoengineering and a large volcanic eruption. First, MAECHAM5-HAM-SALSA was used to define the stratospheric aerosol fields and optical properties in several volcanic eruption and SRM scenarios. Following the approach introduced in Timmreck et al. (2010) and Niemeier et al. (2013), these parameters were then applied in the Max Planck Institute Earth System Model (MPI-ESM) in order to study their effects on the temperature and precipitation.

According to our simulations, climate responses to be expected after a volcanic eruption during SRM depend strongly on whether SRM is continued or halted after the eruption. In the former case, the peak additional forcing is about 21 % lower and the global cooling 33 % smaller than compared to an eruption taking place in non-SRM world. However, the peak additional burden and changes in global mean precipitation are fairly similar regardless of whether the eruption takes place in a SRM or non-SRM world. On the other hand, if SRM is stopped immediately after the eruption, the peak burden is 24 % and forcing 32 % lower and reached earlier compared to the case with unperturbed atmosphere. Furthermore, the forcing from the eruption declines significantly faster, implying that if SRM was stopped after the eruption, it would need to be restarted relatively soon (in our scenario within 10 months) after the eruption to maintain the pre-eruption forcing level.

In line with the burden and forcing results, the simulated global and regional climate impacts were also distinctly different depending on whether the volcano erupts during SRM

or in the background stratospheric conditions. In the investigated scenarios, a Pinatubo-type eruption during SRM caused a maximum global ensemble-mean cooling of only 0.14 K (assuming that SRM is paused after the eruption) compared to 0.45 K in the background case. On the other hand, the ensemble-mean decline in the precipitation rate was 36 % lower for the first year after the eruption during SRM than for the eruption under unperturbed atmospheric conditions. Both the global mean temperature and the precipitation rate recovered to the pre-eruption level in about 1 year, compared to approximately 40 months in the background case. If SRM was continued despite the large volcanic eruption, the global ensemble mean cooling was averagely −0.19 K (−(0.31–0.02) K in individual ensemble member) for 3 subsequent years after the eruption. This is only 67 % of 3 subsequent years cooling after the eruption in normal unperturbed atmospheric conditions, when global ensemble mean cooling was −0.28 K (−(0.49–0.15) K).

In terms of the regional climate impacts, we found cooling throughout most of the Tropics regardless of whether the eruption took place during SRM or in the background conditions, but a clear warming signal (up to 1° C) in large parts of the mid- and high latitudes in the former scenario. While it should be noted that the regional temperature changes were statistically significant mostly only in the Tropics, the declining stratospheric aerosol load compared to the pre-eruption level (as a result of switching off SRM after the eruption) offers a plausible physical mechanism for the simulated warming signal in the mid- and high latitudes. On the other hand, the largest regional precipitation responses were seen in the Tropics. Interestingly, the sign of the precipitation change was opposite in SRM Volc and SRM Cont than in the Volc and SRM in large parts of the tropical Pacific. We attribute this difference to a clearly weaker tropical cooling, or in some areas even a slight warming, in the former scenario leading to an increased evaporation in the first year following the eruption.

Based on both the simulated global and regional responses, we conclude that previous observations of explosive volcanic eruptions in stratospheric background conditions, such as the Mount Pinatubo eruption in 1991, are likely not directly applicable to estimating the radiative and climate impacts of an eruption during stratospheric geoengineering. The global mean temperature and precipitation decline from the eruption can be significantly alleviated if the SRM is switched off after the eruption; however, large regional impacts could still be expected during the first year following the eruption.

Appendix A: Evaluation of the model: Pinatubo eruption 1991, comparison between model and measurements

This is the first study where ECHAM5-HAM-SALSA has been used to simulate aerosol processes in the stratosphere. To ensure that the model can be applied for simulation of high aerosol load in the stratosphere, we evaluated the model's ability to reproduce the response of the stratospheric aerosol layer to the Mount Pinatubo eruption in 1991. We simulated the Pinatubo eruption with MAECHAM5-HAM-SALSA making a five-member ensemble initiated on 1 July (see simulation Volc in Sect. 2.2 for details). In these simulations, we first used the same 2-year spin-up for all ensemble members. After the spin-up, the model was slightly perturbed by a very small change in a model tuning parameter and then run freely for 6 months, in order to create different atmospheric states for the volcano to erupt into. Only after this was the volcanic eruption triggered in the model. Simulated sulfur burdens and particle effective radii were compared against observations from satellite (HIRS) (Baran and Foot, 1994) and lidar measurements (Ansmann et al., 1997), respectively.

Figure A1 shows that the model results are in general in good agreement with the observations. For example, the model correctly indicates that the oxidation of SO_2 and formation of sulfate particles is very fast right after the eruption. However, the simulated sulfate burden peaks at higher values than the observations after which sulfur burden decreases below observed values approximately 1 year after the eruption. This has been seen also in previous studies (e.g. English et al., 2013, and Niemeier et al., 2009). English et al. (2013) suggest that this might be because aerosol heating was not included their model. Our model includes the aerosol heating effect and still underestimates the burden. This might be due to poleward transport at the stratosphere which is overestimated in the model (Niemeier et al., 2009).

In all of the ensemble members the effective radius is generally overestimated during months 3–8 after the eruption, although there is also large variation in the measured values (Fig. A1b). The simulated maximum value for the effective radius is reached 3–4 months earlier than in observations. After 8 months from the eruption results from all the model simulations are in good agreement with observations.

One possible explanation for the larger burden and effective radius in the model could be that the amount of erupted sulfur is overestimated in the model compared to the real Pinatubo eruption. Recent global stratospheric aerosol studies indicate a much better agreement with observations if they assume a smaller amount of the volcanic SO_2 emission of 5 to 7 Tg (S) (Dhomse et al., 2014; Sheng et al., 2015). Another possible explanation is that a larger proportion of sulfur was removed from the stratosphere during the first months after the eruption due the cross-tropopause transport out of the stratosphere or the enhanced removal with ash and ice cloud (Dhomse et al., 2014). Unfortunately, there is only a limited amount of observations after the eruption of Pinatubo which makes comparison between model results and observations difficult. However, our results here are similar to the previous model studies (Niemeier et al., 2009; English et al., 2012; Dhomse et al., 2014; Sheng et al., 2015).

There is some variation in the predicted peak burden and effective radii between the five members of the ensemble simulation (Fig. A1). This indicates that the results are dependent on the local stratospheric conditions at the time of the eruption. Depending on meridional wind patterns during and after the eruption, the released sulfur can be distributed in very different ways between the hemispheres. This can be seen in Fig. A2 which shows the sulfate burdens after the eruption separately in the northern and southern hemispheres. As the figure shows, in simulation Volc1 over 70 % of the sulfate from the eruption is distributed to the Northern Hemisphere, whereas in Volc5 simulation it is distributed quite evenly to both hemispheres. These very different spatial distributions of sulfate lead to the aerosol optical depth (AOD) fields illustrated in Fig. A3. The AOD in the Northern Hemisphere is clearly higher in the Volc1 simulation (panel a) than in the Volc5 simulation (panel b) for about 18 months after the eruption, whereas the opposite is true for the Southern Hemisphere for approximately the first 2 years following the eruption. These results highlight that when investigating the climate effects of a volcanic eruption during SRM, an ensemble approach is necessary.

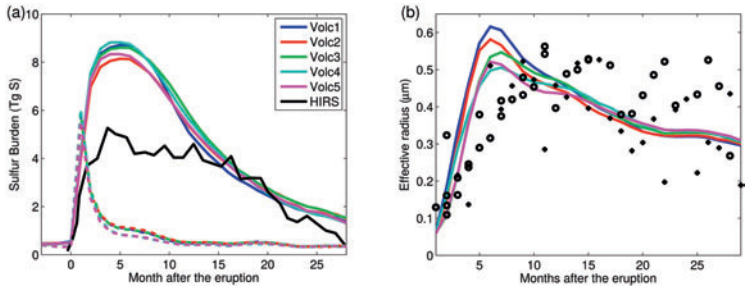

Figure A1. **(a)** Global SO_2 (dashed lines) and particulate sulfate (solid lines) burdens after a simulated volcanic eruption in July compared to sulfate observations from HIRS satellite after the 1991 Pinatubo eruption (black). **(b)** Zonal mean effective radius at 53° N latitude after the simulated July eruption compared to lidar measurements at Laramie 41° N (dots) and Geesthacht 53° N (crosses) after the Pinatubo eruption (Ansmann et al., 1997). In both panels the results are shown for altitude range 16–20 km. The different coloured lines show results from the five members of the simulated ensemble (simulations Volc1, . . . , Volc5).

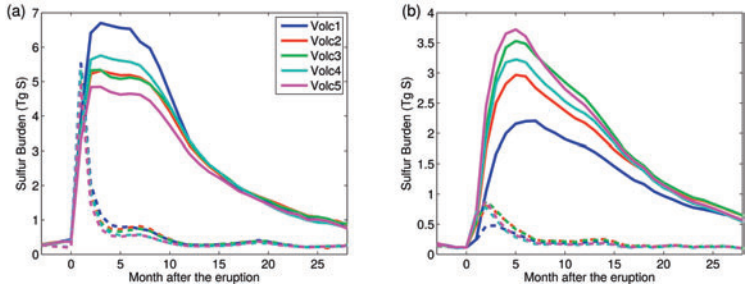

Figure A2. SO_2 (dashed lines) and sulfate (solid lines) burden after the eruption on **(a)** Northern Hemisphere and **(b)** Southern Hemisphere. Note different the scales on the *y* axes.

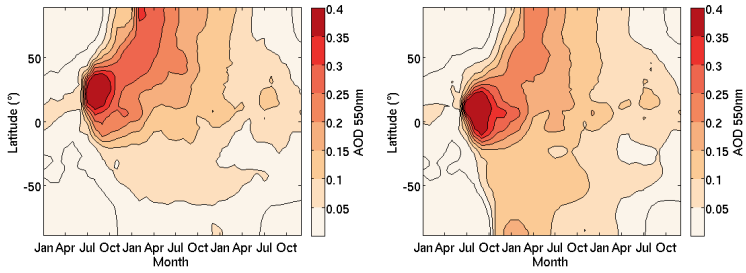

Figure A3. Zonal and monthly mean 550 nm aerosol optical depth after volcanic eruption in **(a)** Volc1 simulation and **(b)** Volc5 simulation.

Appendix B: Sensitivity simulations: location and season of the eruption

B1 Description of sensitivity runs

We also performed a set of sensitivity simulations to investigate how the season and location of the volcanic eruption during SRM impacts the global sulfate burden and radiative forcing. The baseline scenario SRM Volc was compared with three new simulations summarized in Table B1 and detailed below. These sensitivity runs were performed only using MAECHAM5-HAM-SALSA due to the high computational cost of the full ESM, and are therefore limited to analysis of sulfur burdens and radiative forcings.

In the baseline simulations the eruption took place in the Tropics. Because the predominant meridional transport in the stratosphere is from the Tropics towards the poles, sulfur released in the Tropics is expected to spread throughout most of the stratosphere. On the other hand, sulfate released in the mid- or high latitudes will spread less effectively to the lower latitudes, and an eruption at mid- or high latitudes will therefore lead to more local effects in only one hemisphere. Therefore we conducted a sensitivity run simulating a July eruption during SRM at Mount Katmai (Novarupta) (58.2° N, 155° W) where a real eruption took place near the northern arctic area in year 1912 (simulation SRM Arc July).

The local stratospheric circulation patterns over the eruption site will also affect how the released sulfur will be transported. Furthermore, stratospheric circulation patterns are dependent on the season and thus sulfur transport and subsequent climate effects can be dependent on the time of the year when the eruption occurs. For example, the meridional transport toward the poles is much stronger in the winter than in the summer hemisphere (Fig. B1). For this reason, we repeated both the tropical and the Arctic volcanic eruption scenarios assuming that the eruption took place in January instead of July (SRM Volc Jan and SRM Arc Jan, respectively).

B2 Results from sensitivity simulations

Figure B2 shows that the season of the tropical eruption does not significantly affect the stratospheric sulfate burden or the global mean clear-sky radiative forcing (simulations SRM Volc and SRM Volc Jan). The difference in peak burden values between the simulations with January and July eruptions is under 1 % (0.11 Tg (S)) and in peak clear-sky forcing about 1 %. Although the timing of the eruption does not have a large impact on the global mean values, there is some asymmetry between the hemispheres as peak value of additional sulfate from the eruption is 54 % larger after the tropical NH eruption in July (boreal summer) than in January (boreal winter) (not shown). This is because the predominant meridional wind direction is towards the south in July and towards the north in January (Fig. B1). Our results are consistent with previous studies (Toohey et al., 2011; Aquila et al., 2012)

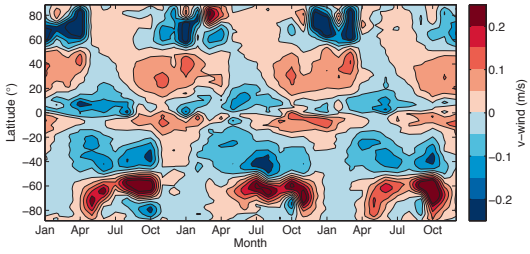

Figure B1. Meridional wind components (positive values from south to north) at 25 km altitude in CTRL simulation with MAECHAM5-HAM-SALSA.

which showed that a Pinatubo type tropical eruption in April would lead to an even increase in AOD in both hemispheres, while a volcanic eruption during other seasons will lead to more asymmetric hemispheric forcings. We show that these results hold also if the eruption takes place during SRM.

On the other hand, if the eruption takes place in the Arctic, the season of the eruption becomes important. Figure B2a shows that a summertime Arctic eruption (SRM Arc July) leads to similar global stratospheric peak sulfate burden as the tropical eruptions (SRM Volc Jan and SRM Volc), although the burden declines much faster after the Arctic eruption. However, an Arctic eruption in January (SRM Arc Jan) leads to a global stratospheric sulfate burden peak value that is only ∼ 82 % of the July eruption value. The peak value is also reached 2 months later in the January eruption. Regarding the global forcing (Fig. B2b), an Arctic winter-time eruption (SRM Arc Jan) leads to a very similar peak forcing than the tropical eruptions, while the additional peak forcing (compared to the pre-eruption level) is 38 % lower if the Arctic eruption takes place in July.

It is interesting to note that in the case of the Arctic volcano, a July eruption leads to a clearly higher stratospheric sulfate peak burden than the January eruption, but the opposite is true for global peak forcing (Fig. B2). A major reason for this is the strong seasonal variation in available solar radiation and subsequent hydroxyl radical (OH) concentration in the high latitudes. OH is the main oxidant that converts SO_2 to sulfuric acid (H_2SO_4). Due to the rising OH concentrations in the Arctic spring, the peak in sulfur burden in the January eruption is reached during the Arctic summer when there is highest amount of sunlight available to be reflected back to space. However, when the eruption takes place in July, the peak burden is reached already in October due to high OH concentrations, and thus much faster compared to the winter-time eruption. However, when the peak value is reached, the intensity of solar radiation has already dramatically decreased, and thus the peak radiative forcing from the eruption remains small. The fast conversion of SO_2 to sulfate also leads to larger particles than after the winter eruption

Table B1. Sensitivity scenarios run only with MAECHAM5-HAM-SALSA. Here Jan refers to a volcanic eruption in January and Arc to an Arctic eruption at the site of Katmai.

Scenario	Timing of eruption	Eruption site	SRM
SRM Volc Jan	1 January	Pinatubo (15° N, 120° E)	suspended
SRM Arc Jan	1 January	Katmai (58° N, 155° W)	suspended
SRM Arc July	1 July	Katmai (58° N, 155° W)	suspended

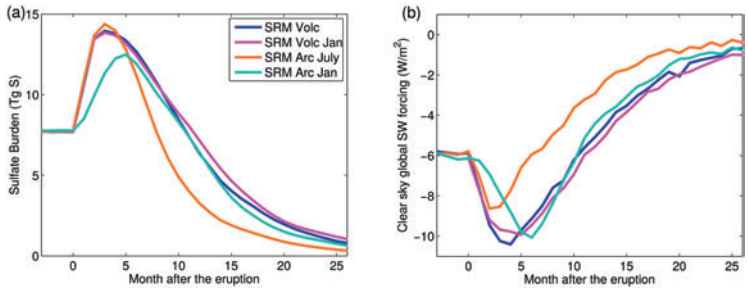

Figure B2. (a) Stratospheric sulfate burden and **(b)** global mean clear-sky shortwave radiative forcing after the eruption in January (blue line) and July (magenta line) and Arctic eruption in January (cyan line) and July (orange line).

and consequently to faster sedimentation and shorter lifetime (Fig. B2a).

Another main factor that has impact on the climate effects of an Arctic eruption is the stratospheric circulation. Concurrent circulation patterns can influence the sulfate lifetime and radiative effects. As Fig. B1 shows, there is a strong seasonal cycle in the Arctic meridional winds. If an Arctic volcano erupts in January, strong zonal polar vortex winds block poleward transport of released sulfur and it can spread towards midlatitudes. In contrast, in July the atmospheric flow is towards the north at the northern high latitudes (Fig. B1) and the sulfur stays in the Arctic. At the same time seasonality of subtropical barrier affects how sulfate is transported to the Tropics. As Fig. B1 shows, winds in the northern border of the Tropics are towards the south only between April and July and sulfur is transported to the Tropics only during this time period. There is clearly more sulfate at the northern border of the Tropics during these months after the Arctic eruption in January, while most of the sulfate is already removed from the atmosphere if the volcano erupted in July. Thus 6 months after the Arctic eruption, the stratospheric sulfur burden in the Tropics between 30° N and 30° S is 3.1 Tg (S) for a July eruption but 4.2 Tg (S) for a January eruption. Since the Tropics have much more solar radiation for the sulfate particles to scatter than the higher latitudes, part of the stronger radiative forcing in the SRM Arc Jan simulation compared to SRM Arc July (Fig. B2b) arises from this difference in transport to the Tropics. Furthermore, since the lifetime of sulfur is longer in the low than in the high latitudes, this leads to a longer average sulfur lifetime in the SRM Arc Jan simulation (Fig. B2a).

Acknowledgements. This work was supported by the Academy of Finland's Research Programme on Climate Change (FICCA) (project 140867), Academy of Finland's Centre of Excellence Programme (decision 272041), Maj and Tor Nessling Foundation (grant 2012116), and the Academy of Finland's Academy Research Fellow position (decision 250348). The authors wish to thank T. Bergman and S. Rast for technical assistance with the models, A. Karpecho for helpful discussions related to stratospheric dynamics and T. Kühn for discussions related to using coupled models and A. Baran for comments concerning about HIRS data. The ECHAM–HAMMOZ model is developed by a consortium composed of ETHZ, Max Planck Institut für Meteorologie, Forschungszentrum Jülich, University of Oxford and the Finnish Meteorological Institute and managed by the Center of Climate Systems Modeling (C2SM) at ETHZ.

Edited by: J.-U. Grooß

References

Ansmann, A., Mattis, I., Wandinger, U., Wagner, F., Reichardt, J., and Deshler, T.: Evolution of the pinatubo aerosol: raman lidar observations of particle optical depth, effective radius, mass, and surface area over central europe at 53.4° N, J. Atmos. Sci., 54, 2630–2641, doi:10.1175/1520-0469(1997)054<2630:EOTPAR>2.0.CO;2, 1997.

Aquila, V., Oman, L. S., Stolarski, R. S., Colarco, P. R., and Newman, P. A.: Dispersion of the volcanic sulfate cloud from a Mount Pinatubo–like eruption, J. Geophys. Res., 117, D06216, doi:10.1029/2011JD016968, 2012.

Bala, G., Duffy, P. B., and Taylor, K. E.: Impact of geoengineering schemes on the global hydrological cycle, P. Natl. Acad. Sci. USA, 105, 7664–7669, doi:10.1073/pnas.0711648105, 2008.

Baran, A. J. and Foot, J. S.: New application of the operational sounder HIRS in determining a climatology of sulphuric acid aerosol from the Pinatubo eruption, J. Geophys. Res.-Atmos., 99, 25673–25679, 1994.

Bergman, T., Kerminen, V.-M., Korhonen, H., Lehtinen, K. J., Makkonen, R., Arola, A., Mielonen, T., Romakkaniemi, S., Kulmala, M., and Kokkola, H.: Evaluation of the sectional aerosol microphysics module SALSA implementation in ECHAM5-HAM aerosol-climate model, Geosci. Model Dev., 5, 845–868, doi:10.5194/gmd-5-845-2012, 2012.

Bony, S., Bellon, G., Klocke, D., Sherwood, S., Fermepin, S., and Denvil, S.: Robust direct effect of carbon dioxide on tropical circulation and regional precipitation, Nat. Geosci., 6, 447–451, 2013.

Crutzen, P. J.: Albedo enhancement by stratospheric sulphur injections: A contribution to resolve a policy dilemma?, Climatic Change, 77, 211–219, 2006.

Dentener, F., Kinne, S., Bond, T., Boucher, O., Cofala, J., Generoso, S., Ginoux, P., Gong, S., Hoelzemann, J. J., Ito, A., Marelli, L., Penner, J. E., Putaud, J.-P., Textor, C., Schulz, M., van der Werf, G. R., and Wilson, J.: Emissions of primary aerosol and precursor gases in the years 2000 and 1750 prescribed data-sets for AeroCom, Atmos. Chem. Phys., 6, 4321–4344, doi:10.5194/acp-6-4321-2006, 2006.

Dhomse, S. S., Emmerson, K. M., Mann, G. W., Bellouin, N., Carslaw, K. S., Chipperfield, M. P., Hommel, R., Abraham, N. L., Telford, P., Braesicke, P., Dalvi, M., Johnson, C. E., O'Connor, F., Morgenstern, O., Pyle, J. A., Deshler, T., Zawodny, J. M., and Thomason, L. W.: Aerosol microphysics simulations of the Mt. Pinatubo eruption with the UM-UKCA composition-climate model, Atmos. Chem. Phys., 14, 11221–11246, doi:10.5194/acp-14-11221-2014, 2014.

Driscoll, S., Bozzo, A., Gray, L. J., Robock, A., and Stenchikov, G.: Coupled Model Intercomparison Project 5 (CMIP5) simulations of climate following volcanic eruptions, J. Geophys. Res., 117, D17105, doi:10.1029/2012JD017607, 2012.

English, J. M., Toon, O. B., and Mills, M. J.: Microphysical simulations of sulfur burdens from stratospheric sulfur geoengineering, Atmos. Chem. Phys., 12, 4775–4793, doi:10.5194/acp-12-4775-2012, 2012.

English, J. M., Toon, O. J., and Mills, M. J.: Microphysical simulations of large volcanic eruptions: Pinatubo and Toba, J. Geophys. Res.-Atmos., 118, 1880–1895, doi:10.1002/jgrd.50196, 2013.

Ferraro, A. J., Highwood, E. J., and Charlton-Perez, A. J.: Weakened tropical circulation and reduced precipitation in response to geoengineering, Environ. Res. Lett., 9, 014001, doi:10.1088/1748-9326/9/1/014001, 2014.

Fischer, E., Luterbacher, J., Zorita, E., Tett, S. F. B., Casty, C., and Wanner, H.: European climate response to tropical volcanic eruptions over the last half millennium, Geophys. Res. Lett., 34, L05707, doi:10.1029/2006GL027992, 2007.

Fuglestvedt, J. S., Samset, B. J., and Shine, K. P.: Counteracting the climate effects of volcanic eruptions using short-lived greenhouse gases, Geophys. Res. Lett., 41, 8627–8635, doi:10.1002/2014GL061886, 2014.

Giorgetta, M. A., Manzini, E., Roeckner, E., Esch, M., and Bengtsson, L.: Climatology and forcing of the quasi-biennial oscillation in the MAECHAM5 model, J. Climate, 19, 3882–3901, 2006.

Giorgetta, M. A., Jungclaus, J., Reick, C. H., Legutke, S., Bader, J., Böttinger, M., Brovkin, V.,Crueger, T., Esch, M., Fieg, K., Glushak, K., Gayler, V., Haak, H., Hollweg, H.-D., Ilyina, T.,Kinne, S., Kornblueh, L., Matei, D., Mauritsen, T., Mikolajewicz, U., Mueller, W., Notz, D., F., Raddatz, T., Rast, S., Redler, R., Roeckner, E., Schmidt, H., Schnur, R., Segschneider, J., Six, K. D., Stockhause, M., Timmreck, C., Wegner, J., Widmann, H., Wieners, K.-H., Claussen, M., Marotzke, J., and Stevens, B.:Climate and carbon cycle changes from 1850 to 2100 in MPI-ESM simulations for the coupled model intercomparison project phase 5, J. Adv. Model. Earth Syst., 5, 572–597, doi:10.1002/jame.20038, 2013.

Guo, S., Rose, W. I., Bluth, G. J. S., and Watson, I. M.: Particles in the great Pinatubo volcanic cloud of June 1991: The role of ice, Geochem. Geophy. Geosy., 5, Q05003, doi:10.1029/2003GC000655, 2004a.

Guo, S., Bluth, G. J. S., Rose, W. I., Watson, I. M., and Prata, A. J.: Re-evaluation of SO_2 release of the 15 June 1991 Pinatubo eruption using ultraviolet and infrared satellite sensors, Geochem. Geophy. Geosy., 5, Q04001, doi:10.1029/2003GC000654, 2004b.

Hansen, J., Lacis, A., Ruedy, R., and Sato, M.: Potential climate impact of Mount-Pinatubo eruption, Geophys. Res. Lett., 19, 215–218, doi:10.1029/91GL02788, 1992.

Heckendorn, P., Weisenstein, D., Fueglistaler, S., Luo, B. P., Rozanov, E., Schraner, M., Thomason, L. W., and Peter, T.: The impact of geoengineering aerosols on stratospheric temperature and ozone, Environ. Res. Lett. 4, 045108, doi:10.1088/1748-9326/4/4/045108, 2009.

Ilyina, T., Six, K. D., Segschneider, J., Maier-Reimer, E., Li, H., and Nunez-Riboni, I.: Global ocean biogeochemistry model HAMOCC: Model architecture and performance as component of the MPI-Earth System Model in different CMIP5 experimental realizations, J. Adv. Model. Earth Syst., 5, 287–315, doi:10.1029/2012MS000178, 2013.

IPCC: Climate Change 2013: The Physical Science Basis. Contribution of Working Group I to the Fifth Assessment Report of the Intergovernmental Panel on Climate Change, edited by: Stocker, T. F., Qin, D., Plattner, G.-K., Tignor, M., Allen, S. K., Boschung, J., Nauels, A., Xia, Y., Bex, V., and Midgley, P. M., Cambridge University Press, Cambridge, UK and New York, NY, USA, 1535 pp., doi:10.1017/CBO9781107415324, 2013.

Jungclaus, J. H., Fischer, N., Haak, H., Lohmann, K., Marotzke, J., Matei, D., Mikolajewicz, U., Notz, D., and von Storch, J.-S.: Characteristics of the ocean simulations in MPIOM, the ocean component of the MPI Earth System Model, J. Adv. Model. Earth Syst., 5, 422–446, doi:10.1002/jame.20023, 2013.

Keith, D. W. and MacMartin, D. G.: A temporary, moderate and responsive scenario for solar geoengineering, Nature Clim. Change, 5, 201–206, doi:10.1038/NCLIMATE2493, 2015.

Kinne, S., O'Donnell, D., Stier, P., Kloster, S., Zhang, K., Schmidt, H., Rast, S., Giorgetta, M., Eck, T. F., and Stevens, B.: MAC-v1: A new global aerosol climatology for climate studies, J. Adv. Model. Earth Syst., 5, 704–740, doi:10.1002/jame.20035, 2013.

Kokkola, H., Korhonen, H., Lehtinen, K. E. J., Makkonen, R., Asmi, A., Järvenoja, S., Anttila, T., Partanen, A.-I., Kulmala, M., Järvinen, H., Laaksonen, A., and Kerminen, V.-M.: SALSA – a Sectional Aerosol module for Large Scale Applications, Atmos. Chem. Phys., 8, 2469–2483, doi:10.5194/acp-8-2469-2008, 2008.

Kokkola, H., Hommel, R., Kazil, J., Niemeier, U., Partanen, A.-I., Feichter, J., and Timmreck, C.: Aerosol microphysics modules in the framework of the ECHAM5 climate model – intercomparison under stratospheric conditions, Geosci. Model Dev., 2, 97–112, doi:10.5194/gmd-2-97-2009, 2009.

Kravitz, B., Caldeira, K., Boucher, O., Robock, A., Rasch, P. J., Alterskjær, K., Karam, D., B., Cole, J. N. S., Curry, C. L., Haywood, J. M., Irvine, P. J., Ji, D., Jones, A., Kristjánsson, J. E., Lunt, D. J., Moore, J. C., Niemeier, U., Schmidt, H., Schulz, M., Singh, B., Tilmes, S., Watanabe, S., Yang, S., and Yoon, J.-H.: Climate model response from the Geoengineering Model Intercomparison Project (GeoMIP), J. Geophys. Res.-Atmos., 118, 8320–8332, doi:10.1002/jgrd.50646, 2013a.

Kravitz, B., Rasch, P. J., Forster, P. M., Andrews, T., Cole, J. N. S., Irvine, P. J., Ji, D., Kristjánsson, J. E., Moore, J. C., Muri, H., Niemeier, U., Robock, A., Singh, B., Tilmes, S., Watanabe, S., and Yoon, J.-H.: An energetic perspective on hydrological cycle changes in the Geoengineering Model Intercomparison Project, J. Geophys. Res.-Atmos., 118, 13087–13102, doi:10.1002/2013JD020502, 2013b.

Laakso, A., Partanen, A.-I., Kokkola, H., Laaksonen, A., Lehtinen, K. E. J., and Korhonen, H.: Stratospheric passenger flights are likely an ineffcient geoengineering strategy, Environ. Res. Lett., 7, 034021, doi:10.1088/1748-9326/7/3/034021, 2012.

McClellan, J., Keith, D. W., and Apt, J.: Cost analysis of stratospheric albedo modification delivery systems, Environ. Res. Lett., 7, 034019, doi:10.1088/1748-9326/7/3/034019, 2012.

Monahan, E., Spiel, D., and Davidson, K.: Oceanic whitecaps and their role in air-sea exchange, D. Reidel, Norwell, Mass., USA, 167–174, 1986.

Niemeier, U. and Timmreck, C.: What is the limit of climate engineering by stratospheric injection of SO_2?, Atmos. Chem. Phys., 15, 9129–9141, doi:10.5194/acp-15-9129-2015, 2015.

Niemeier, U., Timmreck, C., Graf, H.-F., Kinne, S., Rast, S., and Self, S.: Initial fate of fine ash and sulfur from large volcanic eruptions, Atmos. Chem. Phys., 9, 9043–9057, doi:10.5194/acp-9-9043-2009, 2009.

Niemeier, U., Schmidt, H., and Timmreck, C.: The dependency of geoengineered sulfate aerosol on the emission strategy, Atmos. Sci. Lett. 12, 189–194, 2011.

Niemeier, U., Schmidt, H., Alterskjær, K., and Kristjánsson, J. E.: Solar irradiance reduction via climate engineering: Impact of different techniques on the energy balance and the hydrological cycle, J. Geophys. Res., 118, 12195–12206, 2013.

Pierce, J. R., Weisenstein, D., Heckendorn, P., Peter, T., and Keith D. W.: Efficient formation of stratospheric aerosol for climate engineering by emission of condensible vapor from aircraft, Geophys. Res. Lett., 37, L18805, doi:10.1029/2010GL043975, 2010.

Rasch, P. J., Tilmes, S., Turco, R. P., Robock, A., Oman, L., Chen, C.-C., Stenchikov, G. L., and Garcia, R.: An overview of geoengineering of climate using stratospheric sulphate aerosols, Phil. T. R. Soc. A, 366, 4007–4037, 2008.

Read, W. G., Froidevaux, L., and Waters, J. W.: Microwave limb sounder measurements of stratospheric SO_2 from the Mt. Pinatubo volcano, Geophys. Res. Lett., 20, 1299–1302, 1993.

Reick, C., Raddatz, T., Brovkin, V., and Gayler, V.: The representation of natural and anthropogenic land cover change in MPI-ESM, J. Adv. Model. Earth Syst., 5, 459–482, doi:10.1002/jame.20022, 2013.

Robock, A.: Volcanic eruptions and climate, Rev. Geophys., 38, 191–219, doi:10.1029/1998RG000054, 2000.

Robock, A. and Mao, J.: Winter warming from large volcanic eruptions, Geophys. Res. Lett., 19, 2405–2408, 1992.

Robock, A., Marquardt, A., Kravitz, B., and Stenchikov, G.: Benefits, risks, and costs of stratospheric geoengineering, Geophys. Res. Lett., 36, L19703, doi:10.1029/2009GL039209, 2009.

Schulz, M., de Leeuw, G., and Balkanski, Y.: Sea-salt aerosol source functions and emissions, in: Emission of Atmospheric Trace Compounds, Kluwer Acad., Norwell, Mass., USA, 333–359, 2004.

Sheng, J.-X., Weisenstein, D. K., Luo, B.-P., Rozanov, E., Arfeuille, F., and Peter, T.: A perturbed parameter model ensemble to investigate Mt. Pinatubo's 1991 initial sulfur mass emission, Atmos. Chem. Phys., 15, 11501–11512, doi:10.5194/acp-15-11501-2015, 2015.

Smith, M. and Harrison, N.: The sea spray generation function. J. Aerosol Sci., 29, 189–190, 1998.

Stenchikov, G., Delworth, T. L., Ramaswamy, V., Stouffer, R. J., Wittenberg, A., and Zeng, F.: Volcanic signals in oceans, J. Geophys. Res., 114, D16104, doi:10.1029/2008JD011673, 2009.

Stevens, B., Giorgetta, M., Esch, M., Mauritsen, T., Crueger, T., Rast, S., Salzmann, M., Schmidt, H., Bader, J., Block, K., Brokopf, R., Fast, I., Kinne, S., Kornblueh, L., Lohmann, U., Pincus, R., Reichler, T., and Roeckner, E.: The atmospheric component of the MPI-M Earth System Model: ECHAM6, J. Adv. Model. Earth Syst., 5, 1–27, doi:10.1002/jame.20015, 2013.

Stier, P., Feichter, J., Kinne, S., Kloster, S., Vignati, E., Wilson, J., Ganzeveld, L., Tegen, I., Werner, M., Balkanski, Y., Schulz, M., Boucher, O., Minikin, A., and Petzold, A.: The aerosol-climate model ECHAM5-HAM, Atmos. Chem. Phys., 5, 1125–1156, doi:10.5194/acp-5-1125-2005, 2005.

Tegen, I., Harrison, S. P., Kohfeld, K., Prentice, I. C., Coe, M., and Heimann, M.: Impact of vegetation and preferential source areas on global dust aerosol: Results from a model study, J. Geophys. Res., 107, 4576, doi:10.1029/2001JD000963, 2002.

Timmreck, C.: Modeling the climatic effects of volcanic eruptions, Wiley Interdisciplinary Reviews: Climate Change, 3, 545–564, doi:10.1002/wcc.192, 2012.

Timmreck, C., Graf, H.-F., and Kirchner, I.: A one and a half year interactive simulation of Mt. Pinatubo aerosol, J. Geophys. Res., 104, 9337–9360, 1999.

Timmreck, C., Graf, H.-F., Lorenz, S. J., Niemeier, U., Zanchettin, D., Matei, D., Jungclaus, J. H., and Crowley T. J.: Aerosol size confines climate response to volcanic super-eruptions (2010), Geophys. Res. Lett., 37, L24705, doi:10.1029/2010GL045464, 2010.

Toohey, M., Krüger, K., Niemeier, U., and Timmreck, C.: The influence of eruption season on the global aerosol evolution and radiative impact of tropical volcanic eruptions, Atmos. Chem. Phys., 11, 12351–12367, doi:10.5194/acp-11-12351-2011, 2011.

FINNISH METEOROLOGICAL INSTITUTE
Erik Palménin aukio 1
P.O.Box 503
FI-00101 HELSINKI
tel. +358 29 539 1000
WWW.FMI.FI

FINNISH METEOROLOGICAL INSTITUTE
CONTRIBUTIONS No. 119
ISBN 978-951-697-870-6 (paperback)
ISSN 0782-6117
Erweko
Helsinki 2016

ISBN 978-951-697-871-3 (pdf)
http://epublications.uef.fi
UEF Electronic Publications
Kuopio 2016